Sedimentary evolution of a high-energy, low-accumulation shelf system during the late Quaternary (NW Iberia)

Dissertation
zur Erlangung des Doktorgrades der Naturwissenschaften
am Fachbereich Geowissenschaften
der Universität Bremen

vorgelegt von
Hendrik Lantzsch
Bremen, September 2009

Gutachter:
Prof. Dr. Rüdiger Henrich
Prof. Dr. Sebastian Krastel-Gudegast

Table of contents

Appendix 1: **A Late Quaternary sedimentary shelf system under hyperarid conditions: Unravelling climatic, oceanographic and sea-level controls (Golfe d'Arguin, Mauritania, NW Africa).** Till J.J. Hanebuth, Hendrik Lantzsch, *Marine Geology, 2008, 256, 77–89*

Appendix 2: **Mud depocentres on continental shelves – a classification.** Till J.J. Hanebuth, Hendrik Lantzsch, Jean Nizou, s*ubmitted to Earth Science Reviews*

Appendix 3: **Results of microscopic component counting and fuzzy c-means cluster analysis**

Acknowledgements

Abstract

Continental shelf systems are the major marine storage area for terrigenous material and feature highest organic production rates in, for instance, upwelling areas. Moreover, these systems were strongly affected by past sea-level changes and, consequently, experienced major shifts in the interface between marine and terrestrial environments. However, the large variability of shelves in terms of, for example, morphologies, sedimentary constructions, hydrodynamic regimes, and tectonic settings is contrasted by limited scientific knowledge on the sedimentary development of these systems.

The major aim of this thesis is to reconstruct the late-Quaternary sedimentary evolution of the NW Iberian shelf system as a case study of a high-energy, low-accumulation shelf regime which represents the dominant shelf type in the modern situation and, most probably, in geological history as well. Moreover, this thesis aims at revealing the factors and processes which control the local, spatial and temporal sediment distribution in the NW Iberian shelf regime to contribute to the general understanding of such systems.

The NW Iberian shelf is characterised by a narrow and steep geometry. Basement outcrops fringe parts of the outer shelf and dominate the inner shelf. Three confined mud depocentres are located in mid-shelf position. The general late-Quaternary architecture of this shelf system was reconstructed for the first time on the base of extensive seismo-acoustic profiles. The results reveal three stratigraphic units above the basement, which are separated by strong reflectors. These data were combined with a large set of 47 sediment cores and 61 radiocarbon dates to establish the stratigraphic framework of the NW Iberian shelf. A detailed visual core description, grain-size analysis, X-ray diffraction measurement, and statistical calculation on the results of microscopic component counting display the spatial and temporal evolution of four main sedimentary facies types within this framework.

A Gravel Facies, mirrored by the two strong reflectors in the Boomer profiles, consists of coarse-grained beds of either shell-fragment gravel or siliceous coarse sands, which represent tempestites and shoreface deposits. These beds initially developed during the last sea-level lowstand and show a time-transgressive evolution. A homogenous Glaucony-Sand Facies and a Mixed-Sand Facies developed mostly under moderate hydrodynamic conditions during the last deglacial sea-level rise. The major portion of the Glaucony-Sand Facies stems from reworking of older deposits and authigenic mineral formation. The time-transgressive Mixed-Sand Facies is characterised by a mixture of fluvial-derived terrigenous and reworked sands as well as marine biogenic carbonate. A Mud Facies is mainly restricted to Holocene mud depocentres in mid-shelf position. The spatial and temporal evolution of these main facies types reveals how the local balance of hydrodynamic conditions and morphology enables or prevents deposition, and how the type of sediment supply (terrigenous supply, biogenic production, sediment recycling) influences the individual composition of sediments within the framework of sea-level changes. For example, morphological features may offer protection against erosion by strong hydrodynamic conditions, but may also deflect and focus shelf currents leading to enhanced erosion and off-shelf export of sediments.

Besides the substantial corroboration of previous ideas such as (1) shelf exposure, large-scale erosion, and enhanced outer-shelf deposition during the last-glacial sea-level

lowstand, (2) ravinement processes and landward shift of facies belts in the run of the last deglacial sea-level rise, and (3) mid-shelf mud deposition during the Holocene sea-level highstand, the detailed investigations of this thesis contradict some common assumptions on the evolution of high-energy, low-accumulation shelf systems.

First, the landward shift of facies belts during deglacial sea-level rise may have been hindered by insufficient specific sediment supply. Thus, facies types may have showed a stationary position as is the case for glaucony-containing deposits on the outer shelf.

Second, previous shelf studies often revealed condensed deposits related to strong erosion during the deglacial sea-level rise and comparatively thicker deposits developed during sea-level highstand due to an increased accommodation space. However, these findings do not necessarily represent a general pattern in high-energy, low-accumulation shelf settings. The reversed situation is observed on the NW Iberian shelf. The deposition during sea-level rise was not only restricted to a thin transgressive lag deposit but up to 15-m thick deposits developed above a transgressive ravinement surface. This significant material deposition and the general absence of river incisions indicate large-scale reworking and recycling of older deposits. In contrast, the deposition of major mud deposits during the Holocene sea-level highstand was suppressed by the overall low terrigenous sediment supply related to the large distance to the sediment source. Consequently, such deposits have formed but show a maximum thickness of only 4 m.

Third, Holocene mid-shelf fine depocentres do not necessarily expand linear from the source of terrigenous supply. This thesis represents the first comprehensive study on the initial emplacement and further expansion of shelf mud depocentres and reveals differentiated mechanisms controlling initiation and further formation. On one hand, even in high-energy, low-accumulation systems, mud depocentres may be fully connected to the sediment source due to the protection by morphological features. On the other hand, such depocentres may have initially started to form in a confined centre detached from the sediment source due to the wave regime and expanded afterwards into specific directions. These observed dynamics could be a general mechanism for the development of mid-shelf mud depocentres and the results draw attention to this previously unobserved field. A conceptual subdivision is proposed displaying the individual degree of influence of availability of sediment input and the interplay of hydrodynamic conditions and morphological features on the emplacement and evolution of such depocentres. Thus, the results of this thesis improve our understanding of the particular controls on the sediment distribution under a changing shelf configuration.

Kurzfassung

Kontinentale Schelfsysteme sind das marine Hauptablagerungsgebiet von terrigenem Material und zeigen höchste organische Produktionsraten z. B. in Auftriebsgebieten. Diese Systeme wurden stark von früheren Meeresspiegelschwankungen beeinflusst, die zu einer wesentlichen Verlagerung der Schnittstelle zwischen marinem und terrestrischem Ablagerungsraum führten. Die große Variabilität von Schelfsystemen bezüglich Morphologie, sedimentärer Konstruktion, hydrodynamischem Regime und tektonischem Milieu, spiegelt sich im begrenzten wissenschaftlichen Kenntnisstand zur sedimentären Entwicklung dieser Systeme wieder.

Das Hauptziel der vorliegenden Dissertation ist die Rekonstruktion der spätquartären sedimentären Entwicklung des NW-Iberischen Schelfsystems als Fallstudie für hochenergetische, niedrig-akkumulierende Schelfregimes. Schelfe dieser Charakteristik sind der dominante Typus im gegenwärtigen System und waren es höchstwahrscheinlich auch in der geologischen Vergangenheit. Ein weiteres Ziel besteht darin, die dominierenden Kontrollfaktoren der räumlichen und zeitlichen Sedimentverteilung im NW-Iberischen Schelfsystem aufzuzeigen und damit das generelle Verständnis der Ablagerungsprozesse zu erweitern.

Der NW-Iberische Schelf ist durch eine schmale und steile Geometrie charakterisiert. Felsaufragungen kennzeichnen Teile des äußeren Schelfs und dominieren den inneren Schelf. Der mittlere Schelf zeigt drei räumlich begrenzte Schlammdepozentren. Die generelle spätquartäre Architektur dieses Schelfsystems wurde nun erstmals anhand umfangreicher seismo-akustischer Profile rekonstruiert. Die Ergebnisse zeigen drei stratigraphische Einheiten, die von ausgeprägten Reflektoren begrenzt sind. Um den stratigraphischen Rahmen des NW-Iberischen Schelfs zu etablieren, wurden diese Daten mit den Untersuchungen an 47 Sedimentkernen und Ergebnissen von 61 Radiokarbondatierungen kombiniert. Detaillierte Kernbeschreibungen, Korngrößenanalysen, Röntgendiffraktionsmessungen und statistische Berechnungen an den Ergebnissen einer mikroskopischen Komponentenzählung zeigen innerhalb dieses Rahmens die räumliche und zeitliche Entwicklung von vier Haupt-Faziestypen.

Eine Kies-Fazies verursacht zwei ausgeprägte Reflektoren in den Boomerprofilen. Dieser Faziestyp besteht aus groben Lagen biogener Karbonatfragmente oder siliziklastischer Grobsande und repräsentiert Tempestite und küstennahe Ablagerungen. Diese Ablagerungen bildeten sich erstmals während des letzten Meeresspiegelniedrigstands und zeigen eine anschließende zeit-transgressive Entwicklung. Eine homogene Glaukonit-Sand-Fazies und eine Misch-Sand-Fazies entwickelten sich größtenteils unter moderaten hydrodynamischen Bedingungen während des letzten deglazialen Meeresspiegelanstiegs. Der überwiegende Teil des Glaukonits stammt aus der Aufarbeitung älterer Ablagerungen und authigener Mineralbildung. Die zeit-transgressive Misch-Sand-Fazies beinhaltet eine Mischung aus fluvialem Sedimenteintrag, aufgearbeiteten terrigenen Sanden und marinen biogenen Karbonatpartikeln. Die Verbreitung einer Schlamm-Fazies beschränkt sich hingegen hauptsächlich auf holozäne Schlammdepozentren auf dem mittleren Schelf. Die räumlich und zeitliche Entwicklung dieser Hauptfaziestypen zeigt, wie das lokale Zusammenwirken von Hydrodynamik und Morphologie die Sedimentation begünstigen oder verhindern kann und wie im Rahmen von Meeresspiegelschwankungen die Art des Sedimenteintrags (terri-

gener Eintrag, biogene Produktion, Sedimentaufarbeitung) die individuelle Zusammensetzung der Ablagerungen beeinflusst. So können morphologische Aufragungen Schutz vor hydrodynamisch-bedingter Erosion bieten. Andererseits ist eine Umleitung und Fokussierung von Strömungen entlang dieser Felsaufschlüsse auf dem Schelf möglich, was zu verstärkter Erosion und erhöhtem Sedimentexport führten kann.

Die Ergebnisse dieser Studie belegen in umfassender Weise frühere Vorstellungen, wie z.B. (1) Schelfexposition, weiträumige Erosion, und erhöhte Sedimentablagerung auf dem äußeren Schelf während des letzten glazialen Meeresspiegelniedrigstandes, (2) „Ravinement"-Prozesse und landwärts gerichtete Verlagerungen von Faziesgürteln im Verlauf des deglazialen Meeresspiegelanstiegs und (3) Schlammablagerungen auf dem mittleren Schelf während des holozänen Meeresspiegelhochstands.

Dennoch stehen einige Ergebnisse der detailierten Untersuchungen dieser Studie im Kontrast zu allgemeinen Annahmen zur Entwicklung hochenergetischer, niedrig-akkumulierender Schelfsysteme. So kann etwa die eigentlich landwärts gerichtete Verlagerung von Faziesgürteln während des deglazialen Meeresspiegelanstiegs durch unzureichenden Sedimenteintrag verhindert werden. Demzufolge können Faziestypen eine stationäre Position zeigen, wie es auch bei glaukonithaltigen Ablagerungen am äußeren Schelf der Fall ist.

Weiterhin zeigten frühere Schelfstudien häufig kondensierte Ablagerungen, die mit starker Erosion im Zuge des deglazialen Meeresspiegelanstiegs im Zusammenhang stehen. Diese sind normalerweise von vergleichsweise mächtigen Ablagerungen bedeckt, die während des Meeresspiegelhochstands aufgrund des vergrößerten Akkommodationsraums entstanden. Diese Beobachtungen repräsentieren jedoch nicht zwangsläufig ein generelles Muster in hochenergetischen, niedrig-akkumulierenden Schelfmilieus. Die entgegengesetzte Situation ist auf dem NW-Iberischen Schelf zu beobachten. Hier ist die Ablagerung während des Meeresspiegelanstiegs nicht auf eine dünne transgressive Rückstandslage beschränkt, sondern es entstanden bis zu 15 m dicke Ablagerungen über einer trangressiven „Ravinement"-Oberfläche. Diese signifikanten Materialablagerungen und die generelle Abwesenheit älterer Flusseinschnitte auf dem Schelf weisen auf eine großräumige Aufarbeitung und anschließende Wiederablagerung älterer Sedimente hin. Im Gegensatz dazu wurde die Ablagerung mächtigerer Schlammablagerungen während des holozänen Meeresspiegelhochstands durch den generell niedrigen terrigenen Sedimenteintrag unterdrückt, der durch die große Distanz zur Sedimentquelle erklärt werden kann. Infolgedessen haben sich zwar holozäne Ablagerungen gebildet, sie erreichen allerdings nur eine maximale Mächtigkeit von etwa 4 m.

Ein weiterer Punkt ist, dass feinkörnige holozäne Ablagerungszentren auf dem mittleren Schelf nicht unbedingt eine lineare Ausdehnung zeigen, die von der Quelle des terrigenen Eintrags ausgeht. Die vorliegende Studie untersucht erstmals umfassend die initiale Phase und die anschließende Weiterentwicklung von Schelf-Schlammdepozentren und zeigt differenzierte Mechanismen, die die Initiierung und weitere Ausbreitung bestimmen. Einerseits können Schlammdepozentren aufgrund des Schutzes durch morphologische Merkmale sogar in hochenergetischen, niedrig-akkumulierenden Systemen eine Verbindung zur Sedimentquelle zeigen. Andererseits können sich diese feinkörnigen Ablagerungen aufgrund des Wellenregimes losgelöst von der Sedimentquelle bilden und sich später in verschiedene Richtungen ausbreiten. Diese bislang unerforschte Dynamik könnte einen

generellen Mechanismus für die Entwicklung von Schlammablagerungszentren auf dem mittleren Schelf darstellen.

Es wird weiterhin eine konzeptionelle Unterteilung vorgeschlagen, die den Einfluss der Verfügbarkeit von Sedimenteintrag und die Wechselwirkung von Hydrodynamik und Morphologie auf die Platznahme und Entwicklung solcher Depozentren verdeutlicht. Somit erweitern die Ergebnisse dieser Studie substantiell das Verständnis der Kontrollfaktoren der Sedimentverteilung unter einer sich verändernden Schelfkonfiguration.

1. Introduction

1.1. Continental shelf systems – a brief overview

Continental shelves are defined as the area between shoreline and continental slope (e.g., Johnson and Baldwin, 1996). The shelf break forms the border between continental shelf and slope, and occurs usually in a water depth of 150–200 m (Einsele, 2000) with a maximum depth of about 400 m in case of the Antarctic and Namibian shelf (Bremner and Willis, 1993; Yoon et al., 2002). The worldwide average depth of shelves was calculated to be 132 m and the shelf width averages to 75 km (Shepard and Moore, 1963) but extreme values of up to 1500 km are reached on the Siberian shelf (Murdmaa et al., 2006; Fig. 1.1).

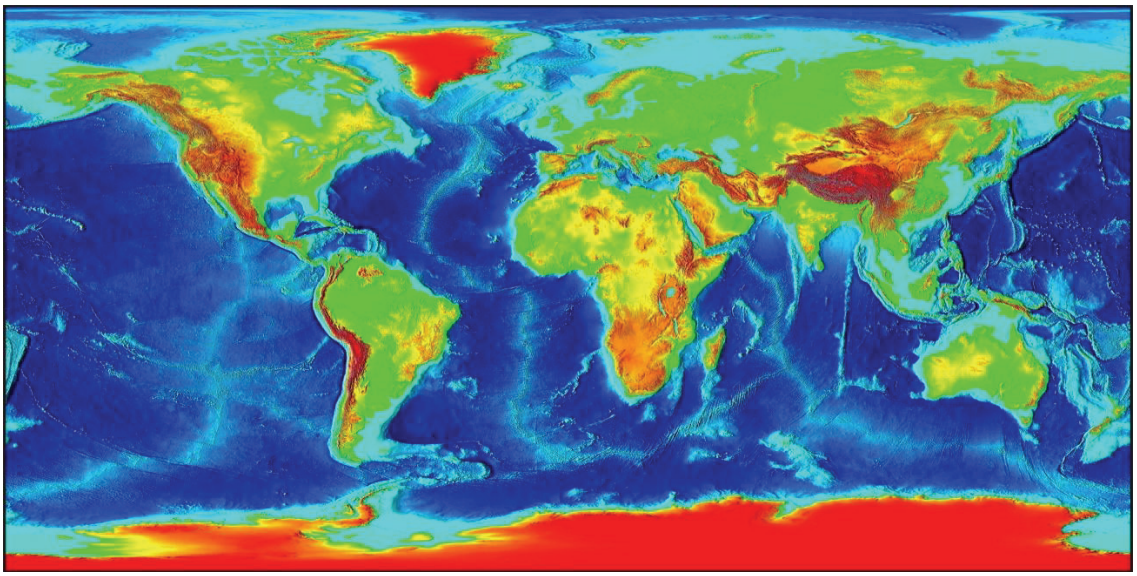

Fig. 1.1. General bathymetry of the Earth, shelves are displayed in light blue (from www.ngdc.noaa.gov).

The large variability of shelf systems in terms of, for example, shapes, tectonic settings, sediment distribution patterns, and hydrodynamic conditions is mirrored by the number of classification attempts. Differences in shelf morphology, for instance, allowed the subdivision into narrow and steep pericontinental shelves (e.g., West- and East-African shelves), and wide and shallow epicontinental shelves (e.g., Siberian shelf and Sunda shelf; Johnson and Baldwin, 1996; Einsele, 2000). Classifications based on the tectonic settings distinguished between shelves related to convergent margins (e.g., western South America), passive margins (Atlantic Coast), and foreland basins (e.g., Persian Gulf; Swift and Thorne, 1991). Moreover, various studies focussed on differences related to sediment supply (Emery, 1968; Swift, 1974; Mount, 1984; Swift and Thorne, 1991). These studies were mainly based on

(1) the source of sediment supply (autochtonous VS. allochtonous shelves; Swift, 1974),

(2) the interplay of available sediment supply and accommodation space (supply-dominated/high-accumulation shelves and accommodation-dominated/low-accumulation shelves; Swift and Thorne, 1991; Fig. 1.2; Table 1.1),

(3) the type of sediment supply (e.g., siliciclastic, carbonate, and mixed carbonate-siliciclastic shelf systems; Mount, 1984), or

(4) type and volume of sediment supply (detrital, biogenic, residual, authigenic, volcanic, and relict shelves; Emery, 1968).

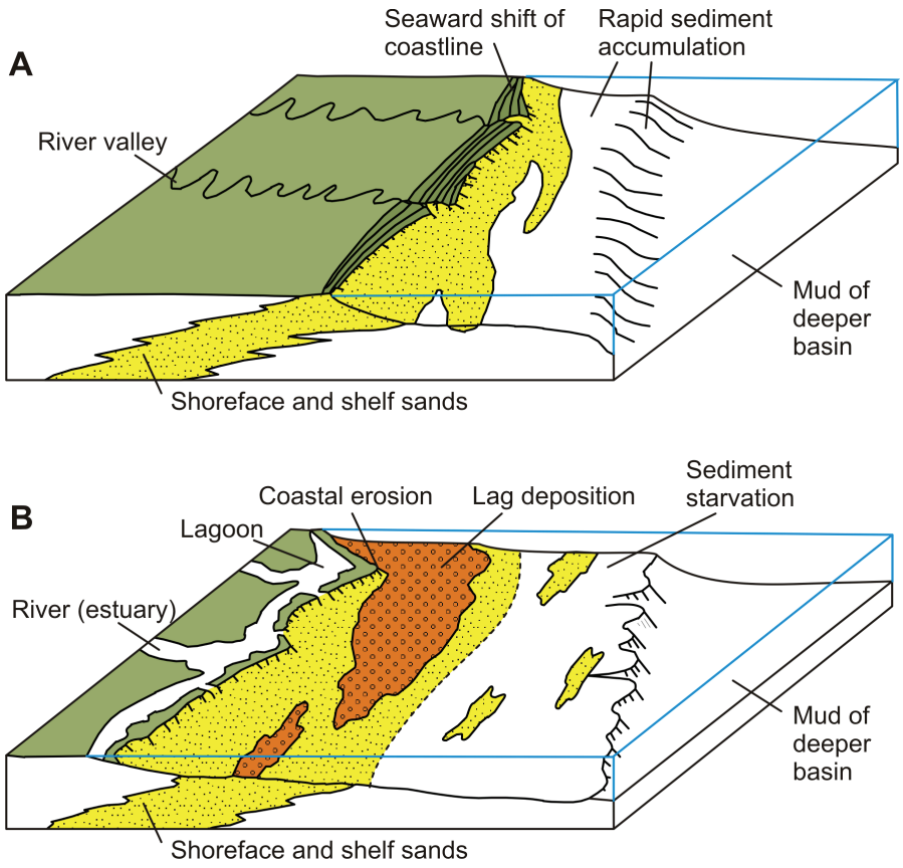

Fig. 1.2. Sedimentary regimes of the shelf: (A) high-accumulation (supply-dominated) shelf where fluvial-derived sediments spread rapidly across the shelf; (B) starved to low-accumulation (accommodation-dominated) regime characterised by low terrigenous sediment supply, erosional shoreface retreat and intensive marine erosion (redrawn from Swift et al., 1987).

Besides these supply-related subdivisions, a classification based on climate zones was proposed by Vanney and Stanley (1983). These authors differentiated between polar, glaciated, non-glaciated, mid-latitude, and tropical shelves. Finally, based on the hydrodynamic conditions, shelves were subdivided into storm-/wave-dominated, tide-dominated, and oceanic-current-dominated (Swift et al., 1986). Storm- and wave-dominated siliciclastic shelf systems such as the NW Iberian shelf system represent about 80% of the worldwide modern margins (Swift et al., 1986) and are suggested to have been the most abundant type over the geological record (e.g., Brenchley, 1985; Duke, 1985).

Table 1.1. Definitions of selected terms mentioned in the introduction.

Term	Definition
Accommodation space	The space in which sediment may accumulate
Base level	Surface of equilibrium between erosion and deposition (Cross, 1991)
Suspension threshold	Below this limit the turbulence intensity is no longer holding particles up (McCave, 2008)
Viscous sublayer	Very thin layer of laminar flow directly above the seafloor (McCave, 2008)
Macroforms	Sediment bodies of metre-scale height to hundreds-of-metres width (Catuneanu, 2002)
Progradation	Lateral buildup of deposits in direction of the sediment transport (Catuneanu et al., 2009)
Aggradation	Continuous up-building of deposits (Catuneanu et al., 2009)
Transgressive lag	Coarse-grained bed as a result of shoreface erosion and winnowing during base-level rise (Posamentier and Allen, 1999)
Transgressive ravinement surface	Erosional surface that form by means of wave or tidal scouring during transgression in coastal to upper shoreface settings (Catuneanu et al., 2009)
Sediment partitioning	The differential redistribution of sediments forming individual sedimentary environments
Shelf transformation	Changes within the sedimentary shelf configuration

1.2. Quaternary sea-level changes

Sea-level changes were common phenomena in Earth's history (Hallam, 1989). They are subdivided into relative (regional) and eustatic (global) changes (Posamentier et al., 1988). Whereas eustatic sea-level changes describe the movement of the sea surface within a fixed reference frame, relative sea-level changes are a function of movements of both sea surface and seafloor/coastline (Posamentier et al., 1988). The forces which cause sea-level changes occur on a variety of scales. Long-term processes include sea-level changes due to, for instance, major climatic changes, vertical movement of the seafloor by subsidence, uplift, and tectonic processes, and variations in shape or volume of oceans by mantle dynamic processes (Warrick et al., 1993; Fleming et al., 1998). Examples for short-term processes range from seasonal changes like enhanced river discharge, to daily and hourly changes due to tides, prevailing wind directions, and catastrophic events such as tsunamis (Warrick et al., 1993).

The Quaternary epoch was characterised by large-scale eustatic sea-level changes (Fig. 1.3) which were related to the waxing and waning of ice sheets due to climate fluctuations (Imbrie et al., 1992). The main mechanisms for these glacial-interglacial cycles are proposed to be related to variations in the Earth's orbit and axis orientation (Imbrie et al., 1992). These changes in orbital eccentricity, obliquity and precession were originally elaborated by Milutin Milankovitch in the 1920's and various studies provided evidence that the interaction of these orbital parameters are even able to cause rhythmic sedimentation patterns in, for instance, coral reef sequences (Aharon, 1984), lake sediments (Trauth et al., 2001), loess profiles (Sun et al., 2006), and shelf deposits (Rabineau et al., 2006).

However, besides these rhythmic patterns in high-resolution sedimentary records, eustatic sea-level variations also strongly influence the general type of sediment deposition in siliciclastic shelves. In these systems, the lowering of base level (Table 1.1) due to a fall in sea level, for instance, may result in enhanced erosion of mainland and shoreface, and increased sediment export towards continental slope and deep sea, whereas an initial sea-level rise might lead to substantial accumulation of marine and fluvial sediments on the shelf due to increased accommodation space (Posamentier et al., 1988; Einsele, 1996; Catuneanu, 2002). Another example for the influence of the sea-level position on the sedimentary system is provided by excessive carbonate production on flat-topped carbonate platforms during sea-level highstands and related enhanced sediment export known as "highstand shedding" (Mullins et al., 1984; Schlager et al., 1994). As the influence of sea-level changes on the sedimentary construction of high-energy, low-accumulation siliciclastic shelves is an important part of this thesis, it will be further specified in Chapter 1.3.3.

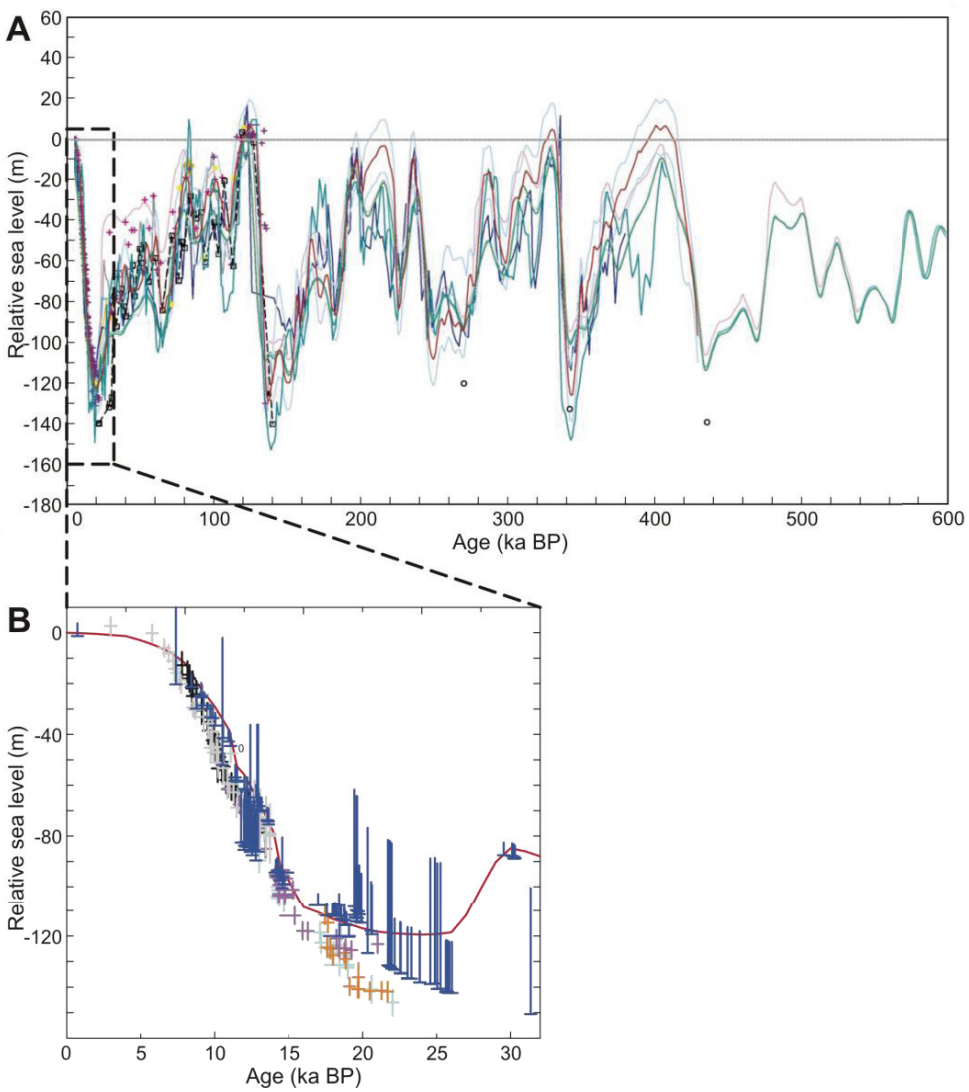

Fig. 1.3. Sea-level curves displaying fluctuations of the sea surface relative to the modern highstand. (A) Synthesis of published Quaternary sea-level curves (modified from Rabineau et al., 2006); (B) Summary of existing data of the latest-Quaternary sea-level change (modified from Peltier and Fairbanks, 2006). Full references for the data are provided in the respective publications.

During the past decades, reconstructions of the latest-Quaternary sea-level change have become of major interest due to its strong impact on the modern sedimentary configuration such as the development of coastal areas and material distribution budgets in shelf systems (e.g., Kaplin and Selivanov, 1995; Barrie and Conway, 2002; Schimanski and Stattegger, 2005; Grossman et al., 2006; Moura et al., 2007). Furthermore, observations of the latest-Quaternary sea-level change provide a base for the prediction and modelling of the future sea-level development (Pirazzoli et al., 1989; Lambeck, 1990; Mörner, 2004). Serious attempts to reconstruct latest-Quaternary sea-level changes were based on U/Th- and radiocarbon dating of corals (Chappell and Polach, 1991; Bard et al., 1996; Peltier and Fairbanks, 2006), and radiocarbon measurement on material from siliciclastic systems (Hanebuth et al., 2000, 2009). Observations of these authors reveal that the sea-level development from the last-glacial sea-level lowstand towards the modern highstand was far away from showing a uniform rate of rise. During the Last Glacial Maximum (LGM) from 21–19 calibrated kiloyears before present (ka BP in the following), sea level was at its lowstand around 123 metres below modern sea-level (mbsl; Hanebuth et al., 2009). However, modelled sea-level history suggests an initial high-glacial lowstand a few thousand years prior to this stage (26–21 ka BP; Peltier and Fairbanks, 2006; Fig. 1.3). A comparably rapid sea-level rise of about 1.25 m per 100 years was observed between 19.6 and 18.8 ka BP (Hanebuth et al., 2009), the terminal phase of the LGM. Afterwards, sea-level rose moderately to 96 mbsl at 14.6 ka BP at a rate of 0.41 m per 100 years (Hanebuth et al., 2000). Then, between 14.6 and 14.3 ka BP, the time of the meltwater pulse 1A, sea level rose rapidly from 96 to 80 mbsl at an rate of 5.33 m per 100 years (Hanebuth et al., 2000). The following stage until 7.5 ka BP was characterised by a more gradual sea-level rise to 10 mbsl at a rate of about 1.2 m per 100 years (Peltier and Fairbanks, 2006; Fig. 1.3), but interrupted by a rapid rise during meltwater pulse 1B (58–45 m, 11.5–11.2 ka BP; Fairbanks, 1989; Bard et al., 1990). Finally, a strong decrease in the rate of eustatic sea-level rise was observed until the modern sea level was reached at around 5 ka BP (Peltier and Fairbanks, 2006).

1.3. Sedimentary dynamics in high-energy, low-accumulation siliciclastic shelf regimes

1.3.1. Material source and contribution to the shelf

In siliciclastic shelf systems, two main mechanisms provide material – erosion of older deposits and biogenic production (Einsele, 2000). Three principal source areas provide material by erosion. First, erosion of the hinterland results in delivery of terrigenous material to the shelf by alluvial systems, wind, and ice transport (Swift and Thorne, 1991; Reading and Collinson, 1996; Einsele, 2000). The global fluvial supply of sediments was calculated to be $15 \cdot 10^9$ tons per year (Milliman and Meade, 1983). Even in low-accumulation systems the terrigenous input may be the dominant type of supply (e.g., Dias et al., 2002b; Lobo et al., 2005; Hill et al., 2007), and high rates of terrigenous fluvial supply occur usually during river floods (Fan et al., 2004; Guillén et al., 2006; Ulses et al., 2008). Second, erosion of the shoreface by wave effects, coastal currents, and catastrophic events such as large storms and tsunami waves may supply major amounts of material to the shelf (Kennett, 1982; Morton et al., 1995; Reading and Collinson, 1996; Abrantes et al., 2005; Noda et al., 2007). Third, recycling of older shelf material is a widespread phenome-

non on high-energy, low-accumulation shelf regimes due to, for instance, the frequent impact of storms (Fan et al., 2004; Ferré et al., 2005; Guillén et al., 2006). These high-energy events may cause significant sediment remobilsation even in water depths below 200 m (Huthnance et al., 2002). Other catastrophic events, such as mass wasting and volcanic eruptions are usually of minor importance but may lead to large-scale sediment redistribution and enhanced supply to the shelf (e.g., Glade, 2003; Schmincke, 2004).

The second important material source is the biogenic production. The biogenic contribution to siliciclastic shelves in form of carbonate, siliceous material, and phosphates is especially enhanced in upwelling zones due to the availability of nutrient-rich waters and a related high organic productivity (e.g., Abrantes and Moita, 1999; De Haas et al., 2002). However, intensive biogenic carbonate production in these shelf settings is usually suppressed by the inhibiting effect of siliciclastic material on carbonate-secreting organisms (Mount, 1984) in contrast to extensive shallow-water carbonate production rates in tropical and subtropical shelves (e.g., Milliman, 1974; Schlager and Ginsburg, 1981) as well as moderate carbonate production in temperate to polar shelf areas (e.g., Shepard, 1977; Henrich et al., 1995; Freiwald and Roberts, 2005).

The material contribution to siliciclastic shelf systems by authigenic mineral formation plays a minor role but may be important in, for instance, outer shelf settings where glaucony might be enriched (Logvinenko, 1982; Odin and Lamboy, 1988; Demirpolat, 1991; Gonzalez et al., 2004). However, factors which influence the volume of general sediment supply to the shelf are complex. Main factors are long time-scale processes such as tectonic movements of the hinterland, variations of the sea-level, climatic fluctuations, and changes in upwelling intensity to short-term influences such as storm events and mass wasting which are able to remobilise major amounts of sediments within few hours and minutes, respectively.

1.3.2. Transport dynamics on the shelf

A pioneering study on transport dynamics in shelf environments was published by Curray (1965). This author concluded that sediments are transported either as bedload or in suspension. Sands and coarser materials are mainly transported as bedload, which is supposed to remain retained on the inner shelf and near the shoreline due to the "littoral energy fence" (Allen, 1970). The basic assumption of this model is that shoaling and breaking waves create a mean landward-directed bottom stress and, therefore, mean sediment movement towards the shore (Allen, 1970; Fig. 1.4). Hence, sands and coarser material tend to be transported parallel to the coastline by longshore currents rather than offshore. However, the littoral energy fence can be bypassed by larger amounts of material during (1) shoreface erosion by wave/storm processes, (2) ebb-tide enhanced currents, and (3) river floods (Allen, 1970; Swift, 1976).

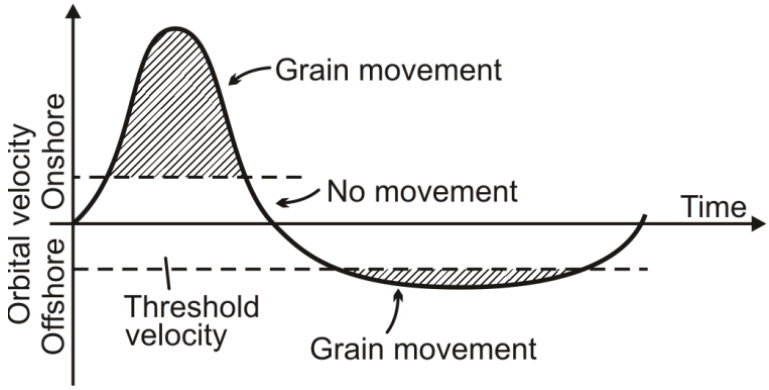

Fig. 1.4. Time-velocity record of bottom flow during the passage of a shoaling wave. A higher velocity flow during the landward stroke compared to the return stroke results in a mean sediment onshore transport (redrawn from Swift and Thorne, 1991).

Fine-grained sediments (silt, clay) are supplied to the shelf by river or wind transport. Although wind transport is often of minor importance, it can be the dominant supply mode for fines in areas lacking major rivers such as, for instance, off NW Africa (Koopmann et al., 1979; DeMenocal et al., 2000). Fines which are contributed by rivers reach the shelf in suspension as buoyant plumes (Curray, 1965; Hill et al., 2007; Fig. 1.5). The further transport dynamics of these fines have been of major interest for several decades (e.g., Curray, 1965; Moore, 1969; Swift, 1970; McCave, 1972) and a review of the major processes leading to the shelf dispersal of fine sediments was recently presented by Hill et al. (2007; Fig. 1.5). Three conceptional models were proposed to explain the across-margin transport. Fines are delivered to the mid-shelf by either (1) diffusion due to the impact of storms (Swift, 1970; Fig. 1.5A), (2) advection by currents (McCave, 1972; Fig. 1.5B), or (3) transport in dense suspension flows driven by gravity (Moore, 1969; Fig. 1.5C). However, the particular importance of these mechanisms is still matter of debate. Hill et al. (2007) stated, for example, that the transport as near-bottom fluid-mud layer was largely underestimated in the past and represents an important process on the Eel shelf (northern California). This shelf is one of the two study sites of the STRATAFORM project (Nittrouer et al., 2007) and represents, therefore, one of the most intensively investigated margins in terms of sediment dynamics. A conceptual sedimentation model for this shelf was summarised by Guillén et al. (2006). Following this study, the sediment is supplied by rivers and forms an ephemeral deposit of fines on the inner shelf. This layer becomes resuspended during major storms and is subsequently transported to the mid-shelf via a near-bottom fluid mud layer. There, the material either forms a mid-shelf mud deposit or experiences further resuspension by high-energy storms and is transported towards the outer shelf or off-shelf. The importance of storm-impact on the sediment transport was also highlighted by studies on various other shelves (e.g., off northern Portugal – Vitorino et al., 2002; off northern California – Fan et al., 2004; in the Gulf of Lions – Ferré et al., 2005).

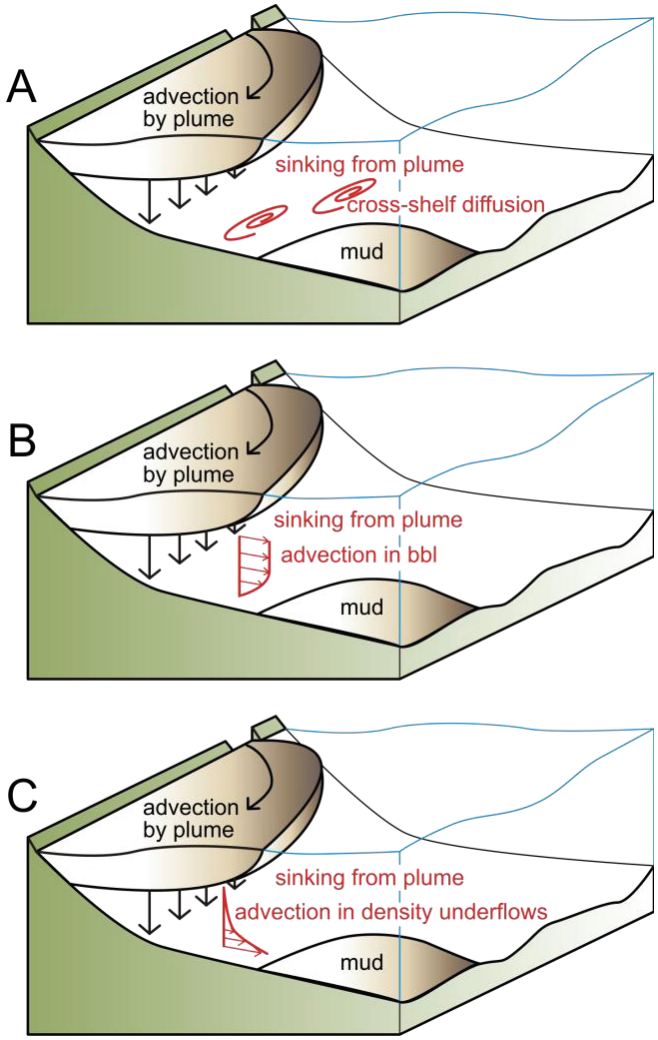

Fig. 1.5. Scheme of shelf-mud transport (redrawn from Hill et al., 2007). Mud is supplied to the shelf by advective buoyant plumes. Three conceptual models propose mechanisms for seaward transport of muds: (A) by wave-generated diffusion (Swift, 1970); (B) by advection due to oceanographic currents (McCave, 1972); (C) seaward transport occurs in wave-supported, gravity-driven underflows (Moore, 1969); bbl = bottom boundary layer.

Off-shelf export of suspended particles mainly occurs by transport within nepheloid layers (Van Weering et al., 2002; McPhee-Shaw et al., 2004). Those layers are characterised by high concentration of suspended material relative to the surrounding waters and occur (1) associated with the biologically active surface mixed layer as "surface nepheloid layer", (2) related to strong density gradients of water masses as "intermediate nepheloid layer", and (3) in the lowermost part of the water column as "bottom nepheloid layer" (McCave, 1984; Oliveira et al., 2002a; Inthorn et al., 2006). Whereas transport of organic matter occurs more or less in all three nepheloid layers, intermediate and bottom nepheloid layers are of higher importance for the off-shelf transport of inorganic sediments (Van Weering et al., 2002). Additionally, upwelling and downwelling may enhance transport in surface and bottom nepheloid layer, respectively (Oliveira et al., 2002a; Vitorino et al., 2002), and shelf incisions such as large canyon systems might act as efficient conduits for the bottom nepheloid layer (Van Weering et al., 2002).

1.3.3. Material deposition and its main controls

The deposition of bedload material occurs rather abruptly when the shear stress is slightly lower than the critical erosion stress (McCave, 2008). In contrast to this rapid deposition of bedload, suspended fines tend to form flocs and aggregates and sink to the near-bed region if the shear stress is below the suspension threshold (Table 1.1; McCave, 2008). In the near-bed region, deposition is strongly depending on the settling velocity of these particles and such material with insufficient settling velocity is again ejected from the viscous sublayer (Table 1.1). This selective deposition of material leads to increased sediment sorting (McCave, 2008).

In a broader context, the deposition of material on the shelf depends on a number of interacting external forces and internal processes such as tectonics, climate, sea-level changes, type and availability of sediment input, hydrodynamics (waves and currents), morphology, and biogenic production. Generally, sediment deposition is determined by the presence of (1) sufficient accommodation space determined by the position of the base level, (2) adequate sediment supply and (3) favourable hydrodynamic conditions. An important external force controlling these three factors is the position of the sea level.

The response of sedimentation patterns to base-level variations due to relative sea-level changes is a topic of the broad field of sequence stratigraphy. Comprehensive overviews on sequence stratigraphy are provided by, for instance, Van Wagoner et al. (1988), Catuneanu (2002, 2006) and Emery and Myers (2003). This introduction will focus in the following on the basic sedimentary response of siliciclastic shelf systems to the position and movement of the global sea-level.

An eustatic sea-level fall causes a significant lowering of base level. Thus, substantial erosion of alluvial and coastal systems is initiated (Fig. 1.6A; Van Wagoner et al., 1988; Catuneanu, 2002). The deposition in the water-covered part of the shelf depends largely on the position of base level in relation to the shelf break. If the base level remains above the shelf break, shoreface lobes and shelf macroforms (Table 1.1) may develop as well as deep-sea fans (Catuneanu, 2002). In contrast, a fall of base level below the shelf break results in shelf-edge delta progradation (Table 1.1) on the uppermost continental slope if sufficient sediment supply is available (Hernández-Molina et al., 1994; Catuneanu, 2002). Exposed parts of the shelf are characterised by intensive erosion and formation of river incisions during base-level fall (Fig. 1.6A; Van Wagoner et al., 1988). Although deposits related to a falling sea level may dominate the buildup of high-accumulation shelves (Posamentier et al., 1988; Hanebuth and Stattegger, 2004), these deposits are characterised by a low preservation potential in high-energy, low-accumulation shelf systems due to intensive reworking in the run of ongoing sea-level lowering (Catuneanu, 2002; Emery and Myers, 2003).

During a stage of eustatic sea-level lowstand, large areas of the shelf are exposed and the sediment off-shelf export continues as indicated by highest sedimentation rates in sediment cores of the continental slope during glacial stages (Schönfeld and Kudrass, 1993; Baas et al., 1997; Steinke et al., 2003; Henrich et al., in press). Observations of enhanced turbidite activity during this stage (Sarnthein and Diester-Haass, 1977; Shanmugam and Moiola, 1982; Stow et al., 1985) also corroborate with the idea of intensified sediment buildup on shelf break and uppermost continental slope which favours sediment instability and related event-like mass transport.

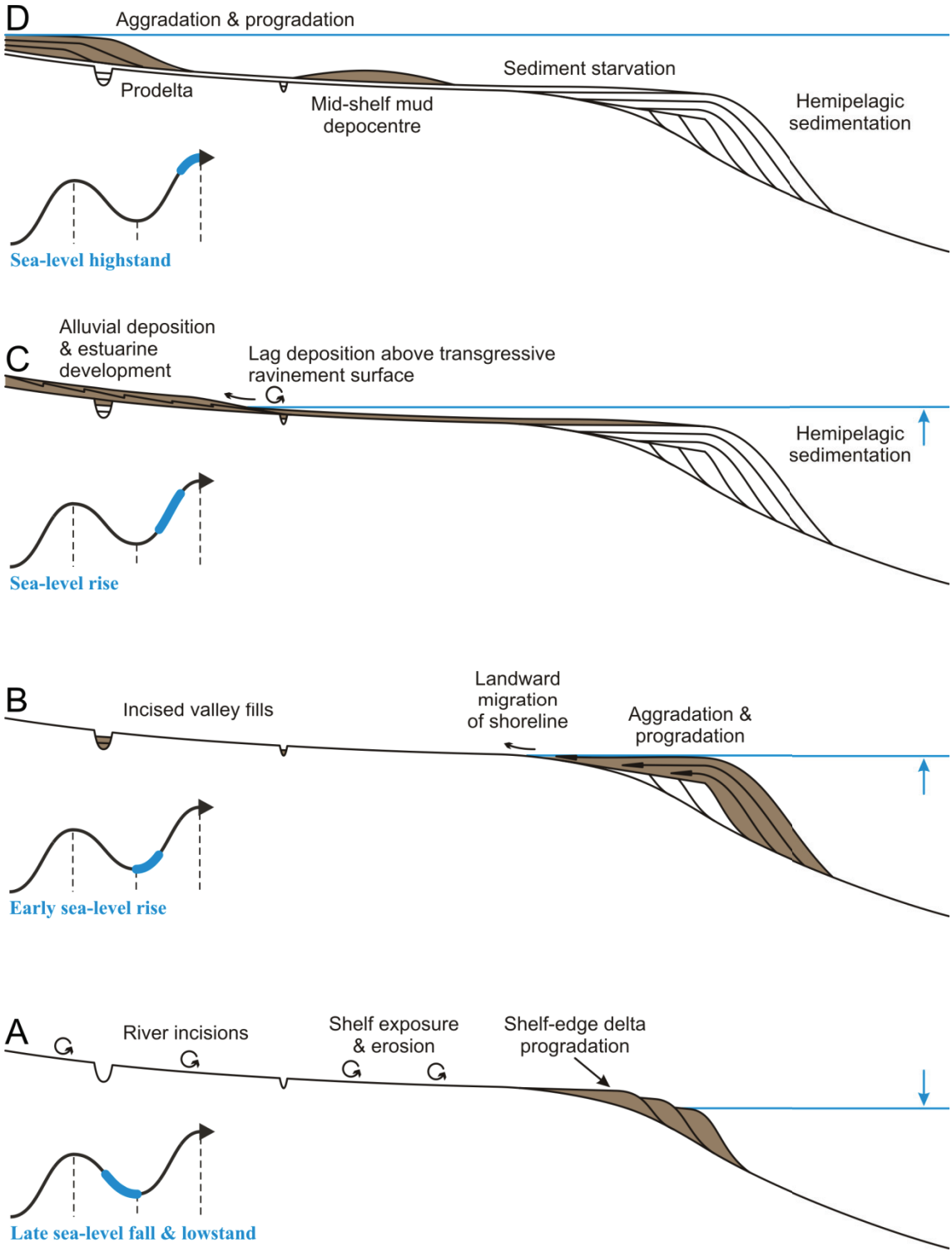

Fig. 1.6. Simplified model of sedimentary changes in a high-energy, low-accumulation shelf system in response to sea-level variations: (A) late sea-level fall and lowstand; (B) early sea-level rise; (C) further sea-level rise; (D) sea-level highstand (based on Posamentier et al., 1988; Hernández-Molina et al., 1994; Catuneanu, 2002; Emery and Myers, 2003).

During initial sea-level rise, the rate of base-level rise is not yet able to keep pace with the sedimentation rate (Catuneanu, 2002). Therefore, marine and coastal deposits are still characterised by aggradational to progradational sequences (Table 1.1; Posamentier and Allen, 1999). Incised valley fills and amalgamated fluvial channel sediments are typical deposits in non-marine successions of the shelf (Fig. 1.6B; Posamentier and Allen, 1999). During the following sea-level rise, the sedimentation rate is outpaced by base-level rise (Curray, 1965; Catuneanu, 2002). Marine sections show a development of transgressive lag deposits above a major transgressive ravinement surface (Table 1.1), and hemipelagic sedimentation offshore (Fig. 1.6C; Galloway, 1989). In contrast, the coastal zone is characterised by the landward migration of the shoreline and estuarine development due to the flooding of river valleys, and the formation of barrier-island systems (Curray, 1965; Catuneanu, 2002).

The sedimentation rate becomes again the determinant factor due to the sea-level stabilisation in the stage of sea-level highstand (Catuneanu, 2002). The terrigenous supply to the shelf starts to increase due to the progressive filling of the accommodation space within river basins (Dabrio et al., 2000; Boski et al., 2002; Vis et al., 2008). Shelf deposits which developed during the sea-level highstand are usually characterised by a low preservation potential in the run of sea-level cycles due to intensive erosion during the succeeding sea-level fall and lowstand (Catuneanu, 2002). However, the modern sea-level highstand enables detailed observations on the sediment deposition pattern during such a stage. In non-marine sections, amalgamated channel and meander systems as well as floodplain deposits may develop during the late highstand (Shanley and McCabe, 1993). Marine highstand sediments show aggradational to progradational accumulation patterns depending on the individually available accommodation space (Fig. 1.6D; Van Wagoner et al., 1988; Catuneanu, 2002). Highstand sedimentation of sands in high-energy, low-accumulation shelf systems is usually restricted to the littoral zone, whereas large areas of the outer shelf are characterised by sediment starvation (Emery, 1952). The deposition of fines is often restricted to confined areas on the shelf such as to mid-shelf mud depocentres (Fig. 1.6D). These depocentres of fines seem to be a common feature in shelf systems and the first attempt of a classification based on the distribution patterns in relation to hydrodynamic conditions was made by McCave (1972; Fig. 1.7). Later studies revealed that the influences on the formation of these bodies are more complex. The location of such mud depocentres can be related to, for instance, oceanic current boundaries (Castaing et al., 1999; Lobo et al., 2004) or morphological steps (Hanebuth and Lantzsch, 2008; Appendix 1). However, the restricted knowledge of the mud-depocentre formation history and their controls led to confusion in the determination of these deposits (Hanebuth, 2009). The Shandong mud deposit in the Yellow Sea, for instance, was determined as “mud wedge” (Liu et al., 2002) and “mud clinoform as distal part of a tidal depositional system” (Liu et al., 2007). Other sediment bodies which show a roughly comparable geometry were inconsistently described in literature as “subaqueous clinoform” (Nittrouer et al., 1986), “prograding wedge” (Lobo et al., 2004), and “shallow-water contourite drift” (Verdicchio et al., 2008). First comprehensive attempts to clarify the general confusion concerning the classification of mud depocentres are provided by the reviews of Walsh and Nittrouer (2009) with regard to the processes controlling the sediment deposition and of Hanebuth et al. (submitted; Appendix 2) dealing with the formation history of such deposits.

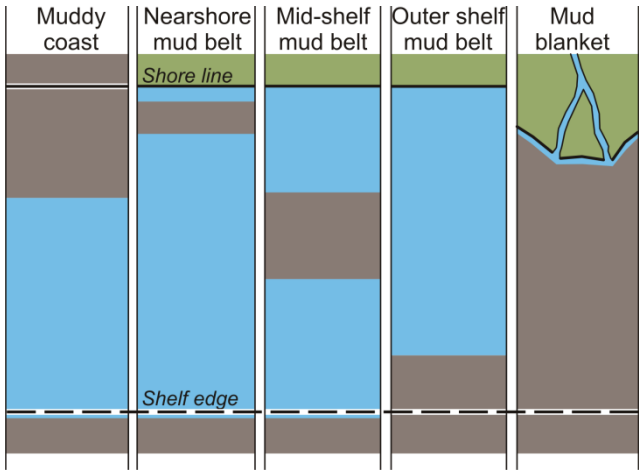

Fig. 1.7. Loci of major mud deposition on coast, shelf, and upper slope (redrawn from McCave, 1972).

1.4. The NW Iberian shelf system: regional settings & previous studies

1.4.1. Morphology and geology

This study was conducted on the NW Iberian continental shelf system between 41°30'N and 43°10'N (Fig. 1.8). The NW Iberian shelf shows a steep and narrow morphology varying in width between 25 km in the northern study area and up to 40 km in front of the Minho river mouth (Fig. 1.8). The shelf break occurs in water depths between 160 and 180 m (Dias et al., 2002b) and is not dissected by submarine canyons as is the case for the Portuguese continental shelf south of the study area (Dias et al., 2002a; Fig. 1.9). Prominent morphological elevations are present on the inner shelf and, south of 42°N, on the outer shelf. These rocky outcrops comprise Palaeozoic plutonic and metamorphic rocks on the inner shelf as well as Late Cretaceous to Pleistocene limestones and sandstones on the outer shelf (Rey Salgado, 1993; Dias et al., 2002b; Cascalho and Fradique, 2007).

The rough morphology of the Spanish coast is characterised by the occurrence of the Rías Baixas (Ría de Muros, Arosa, Pontevedra, and Vigo; Fig. 1.8). These represent the remains of Tertiary river systems which drowned during the deglacial sea-level rise. The Rías are up to 50 m deep and act as sediment traps during the modern sea-level highstand (Rey Salgado, 1993; Dias et al., 2002b). The smoothed Portuguese coastline features three main river estuaries within the study area, the Minho, Lima, and Cávado River. The larger Douro River is situated 40 km southward of the study area (Fig. 1.9). The catchment area of this river covers 97,700 km^2 and represents the largest drainage basin in Spain Fig.(Oliveira et al., 2002b; Santisteban and Schulte, 2007; Fig. 1.10). The annual mean discharge of the Douro River amounts to $8.2 \cdot 10^9$ m^3 and it is considered as the main supplier of modern terrigenous material to the shelf (Araújo et al., 2002; Dias et al., 2002a,b; Oliveira et al., 2002b; Fig. 1.9).

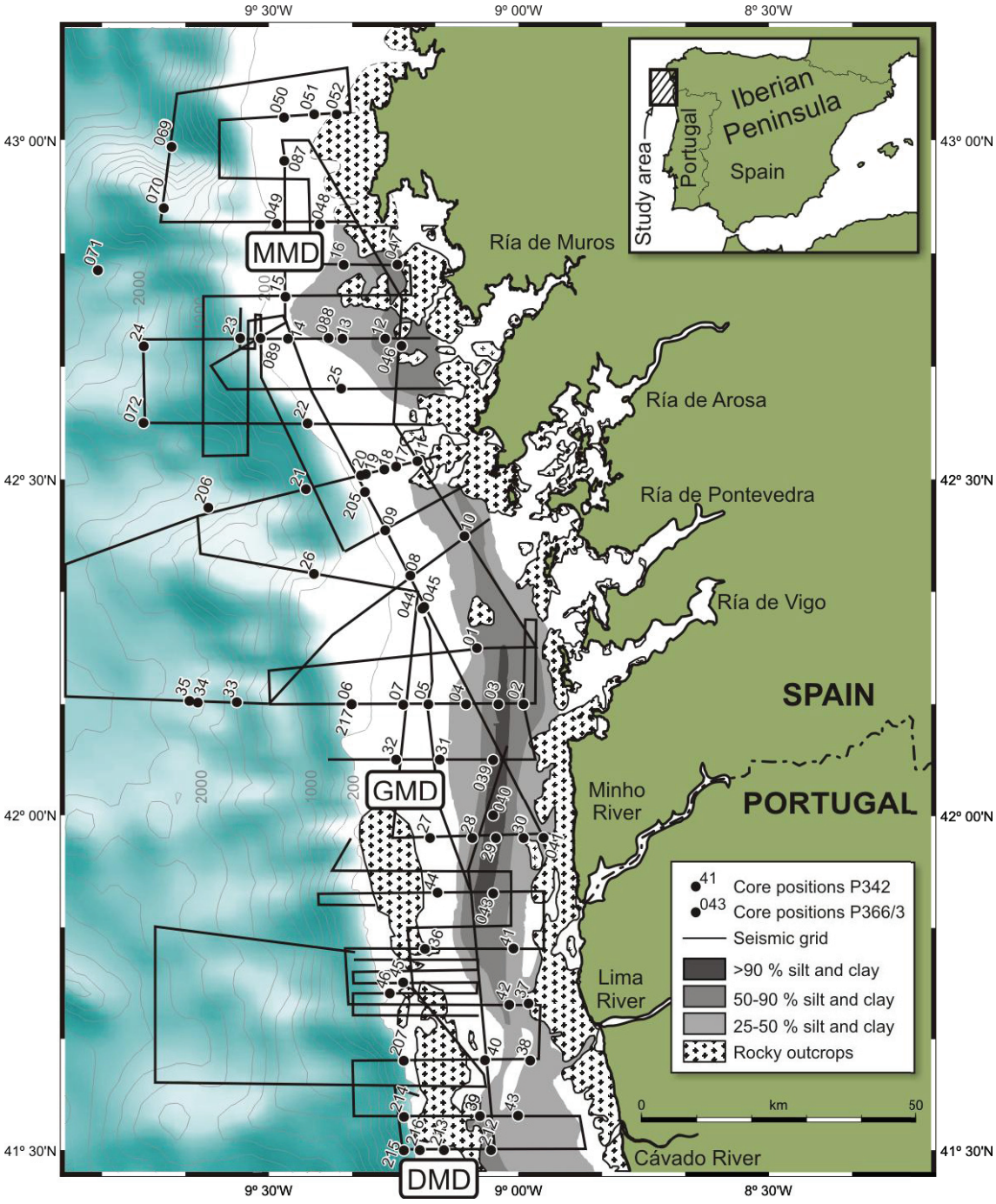

Fig. 1.8. Map of the study area. Core positions of cruises P342 and P366/3 are marked by black dots. Cores used in this study are displayed in short form with, for instance, 11002-3 and 11038-2 being positions 02 and 38 (P342), and 13089-2 and 130207-3 being positions 089 and 207 (P366/3). The surface geology was adapted from Dias et al. (2002a). Mud depocentres are displayed in grey. MMD = Muros Mud Depocentre; GMD = Galicia Mud Depocentre; DMD = Douro Mud Depocentre.

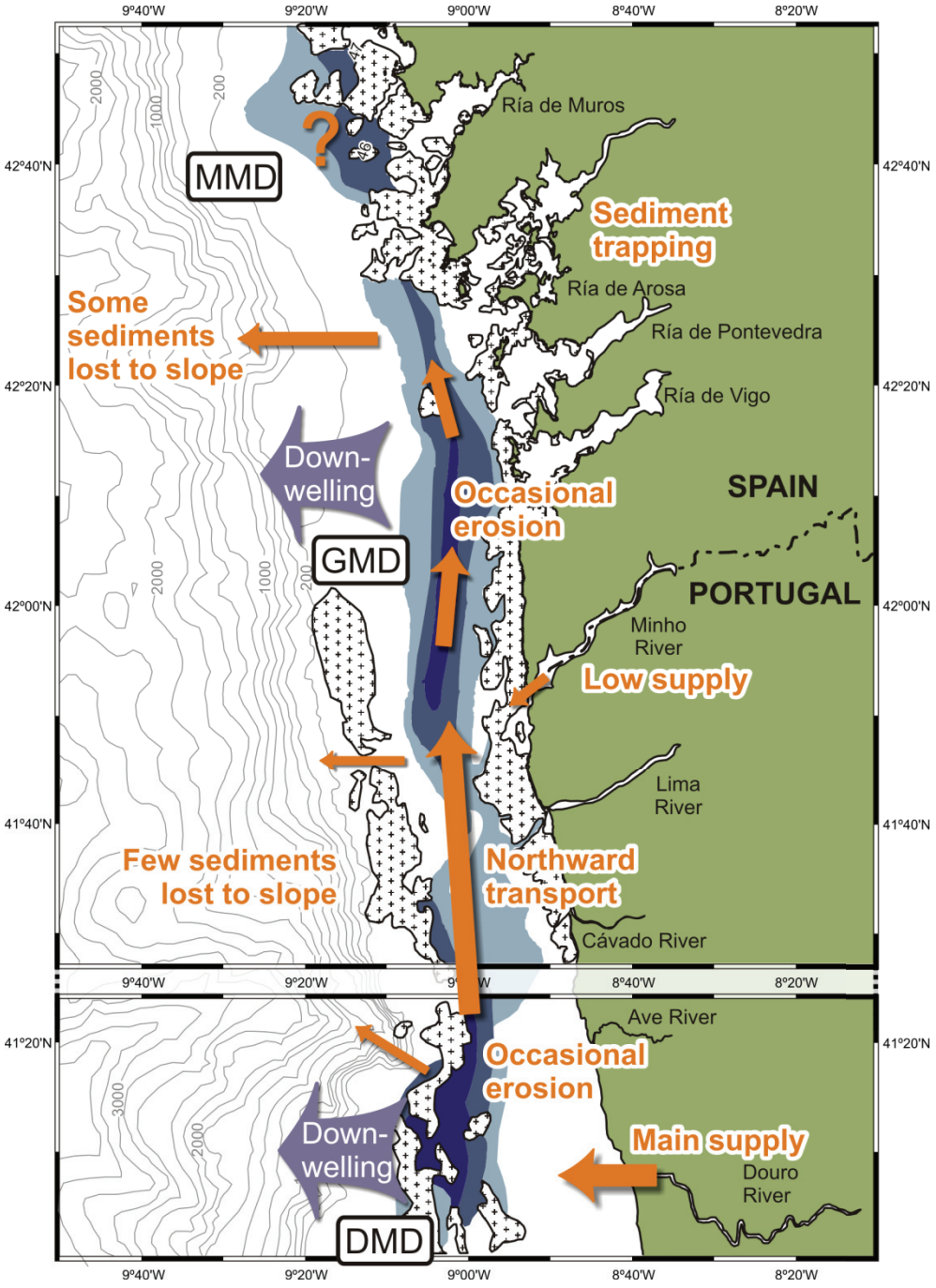

Fig. 1.9. Conceptual model for the modern transport of fines within study area and adjacent southern part of the NW Iberian shelf (based on Drago et al., 1998; Araújo et al., 2002; Dias et al., 2002b). Terrigenous fines are mainly supplied by the Douro River, and form the Douro Mud Depocentre in mid-shelf position where rocky outcrops tend to trap sediments. During the high-energy winter conditions, these deposits are frequently resuspended and transported to the north by a poleward shelf current where they are redeposited and form the Galicia Mud depocentre. Wind-induced downwelling favours seaward transport and off-shelf export of fines. MMD = Muros Mud Depocentre; GMD = Galicia Mud Depocentre; DMD = Douro Mud Depocentre.

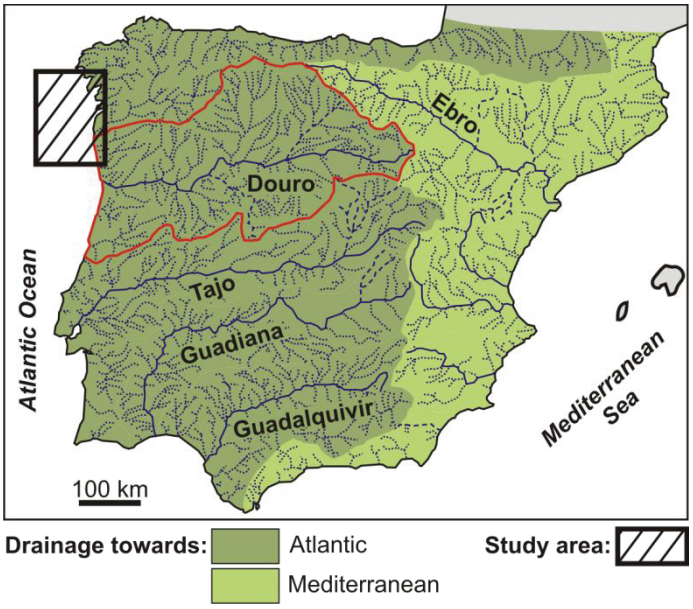

Fig. 1.10. The Iberian drainage network (modified from Santisteban and Schulte, 2007). The Douro drainage area is marked in red.

The geology of the NW Iberian drainage basins is mainly characterised by Precambrian and Palaeozoic igneous and metamorphic rocks, and, to a minor account, by Mesozoic to Tertiary sedimentary rocks and Quaternary sediments (Cascalho and Fradique, 2007). On the shelf, the Quaternary sedimentary cover was described to consist of up to 6-m thick sandy and muddy sediments in a wedge-shaped layer, thinning to the outer shelf (Rey Salgado, 1993). Other stratigraphic studies on the NW Iberian shelf were conducted by Muñoz et al. (2003) and Ferrín (2005). Muñoz et al. (2003) concentrated on tectonic deformations during the Neogene and assigned five seismic units above a Palaeozoic basement. One unit was suggested to be of Cretaceous age. The age of the other units was "tentatively assigned" and ranges from middle Tertiary to Holocene. Ferrín (2005) described the late-Quaternary seismic stratigraphy. This author recognized four seismic units which are separated by erosive unconformity surfaces. The three lower units were suggested to be sediments of Pleistocene sea-level highstands contrasting the common assumption of a low preservation potential of these deposits in siliciclastic systems (Catuneanu, 2002). The uppermost seismic unit is interpreted to consist of deposits related to the last sea-level rise and modern highstand. Moreover, major storms were assumed to export large volumes of sediments off-shelf forming clinoforms at the uppermost continental slope. The general late-Quaternary shelf setting was characterised as starved. However, the stratigraphic observations of Ferrín (2005) are based on a debatable correlation of shallow-seismic profiles with a single dated sediment vibrocore from the inner shelf. In summary, the stratigraphy of the NW Iberian shelf is mainly based on suggestions and can be considered as sparsely known.

1.4.2. Oceanographic setting and sedimentary dynamics

The modern oceanographic setting of the NW Iberian shelf and its influence on the surface sediment distribution was intensively studied during the Ocean Margin Exchange-II project (OMEX II; Van Weering and McCave, 2002). Following these studies, the NW Iberian continental shelf circulation is strongly driven by local meteorological forcing and shows, therefore, a strong seasonality (Fig. 1.11). During summer (April–October; Fig. 1.11A), the Azores High is located over the central North Atlantic, offshore of the Iberian Peninsula, and the Iceland Low is weak. The pressure gradient between the two systems results in

(1) northerly/north-westerly prevailing winds,
(2) low-energy wave conditions with significant wave heights less than 2 m,
(3) wind-induced upwelling of cold and nutrient-rich Eastern North Atlantic Central Water,
(4) equatorward surface shelf flow, and
(5) increased offshore transport of particulate matter via a surface nepheloid layer (Wooster et al., 1976; Fiuza et al., 1982; Prego and Bao, 1997; Vitorino et al., 2002).

In contrast, during winter (October–April; Fig. 1.11B), the Azores High is displaced to its most southern position near the northwest African coast and the Iceland Low is strengthened and centred over Iceland (Fig. 1.11). The pressure gradient results in

(1) prevailing southerly/south-westerly winds,
(2) high-energy wave conditions with significant wave heights exceeding 5 m during storms,
(3) the establishment of a downwelling regime,
(4) high river runoff due to increased precipitation,
(5) persistent poleward current flow at all depths of the shelf, and
(6) increased sediment offshore transport in the bottom nepheloid layer (Wooster et al., 1976; Fiuza et al., 1982; Vitorino et al., 2002).

The sedimentary cover of the NW Iberian shelf is generally sandy, but two well-defined muddy areas were observed in surface samples of the mid-shelf – the Douro and Galicia mud patches (Dias et al., 2002a; Fig. 1.8). However, the interpretive description as "mud patch" requires detailed knowledge of 3d-structures of these depocentres. Therefore, the descriptive term "mud deposit" is used in this introduction and interpretive terms are provided in Chapters 2–4. Whereas the northern branch of the Douro Mud Deposit (DMD) is situated in the southernmost part of the study area, the Galicia Mud Deposit (GMD) comprises major parts of the mid shelf. An additional mid-shelf mud deposit in front of the Ría de Muros was mapped (Dias et al., 2002a) but not further described. However, the mud deposits experience the highest sedimentation rates of all shelf deposits in the region ranging from 0.05 to 0.40 cm yr^{-1} (Jouanneau et al., 2002).

The main fluvial source of terrigenous material supply for both DMD and GMD is the Douro River (Araújo et al., 2002; Fig. 1.9). Highest rates of fluvial sediment supply are reached in winter, especially during river floods after storms coupled with enhanced precipitation (Dias et al., 2002b). The distribution and deposition of sediments is then strongly controlled by the oceanographic setting. Sandy material is usually carried southward by littoral drift (Dias and Nittrouer, 1984). In contrast, fine sediments are transported seaward

through nepheloid layers (Oliveira et al., 2002a). The relatively quiet hydrodynamic regime in mid-shelf position favours the deposition of fines (McCave, 1972). Nevertheless, strong winter storms are able to resuspend these previously deposited fine sediments and generate bottom nepheloid layers which extend a few meters above the bottom (Oliveira et al., 2002a, 2002b). The off-shelf transport might be blocked by rocky outcrops on the outer shelf (Jouanneau et al., 2002; Van Weering et al., 2002). Consequently, the resuspended material is mainly transported to the north via a poleward-flowing shelf current prevailing in winter where it might be deposited again in mid-shelf position (Drago et al., 1998; Fig. 1.9).

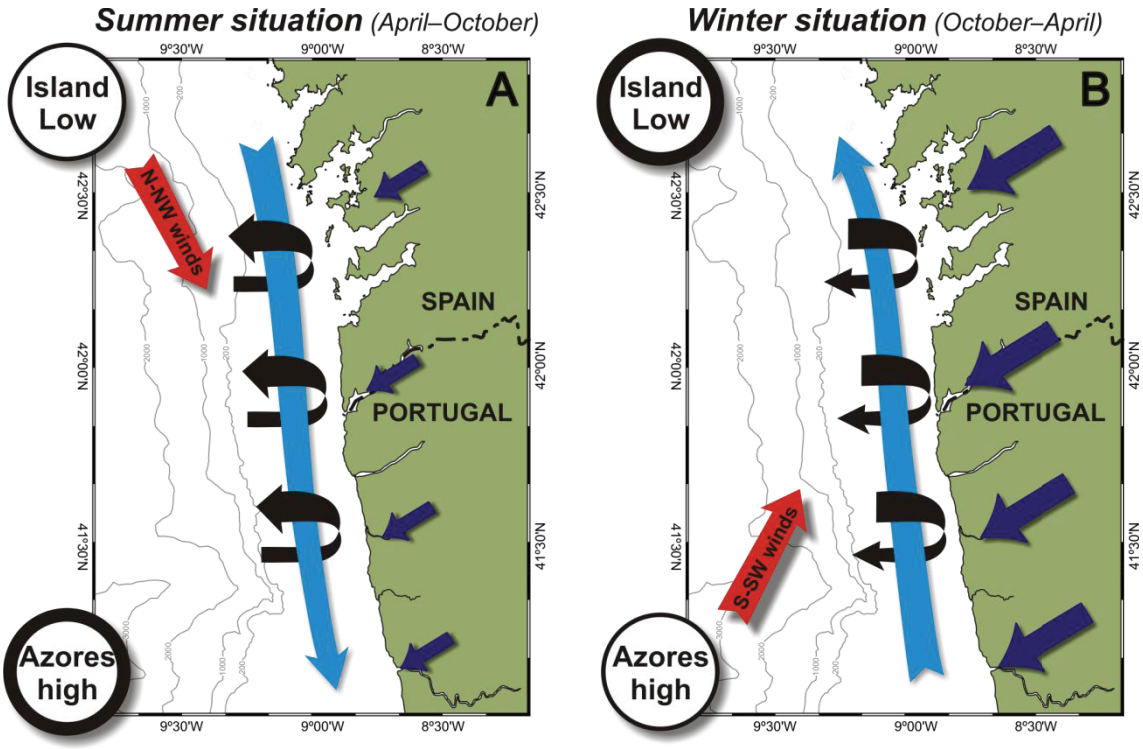

Fig. 1.11. General meteorological forcing and oceanographic setting of the NW Iberian shelf during (A) summer situation and (B) high-energy winter conditions. Red arrow = prevailing wind direction; light-blue arrow = wind-induced seasonal shelf current; black arrows = upwelling/downwelling; dark-blue arrows = relative amount of fluvial discharge.

The general oceanographic configuration of the NW Iberian shelf is thought to have been persistent over the past 5 ka BP (Bernárdez et al., 2008a). Nevertheless, minor variations occurred in, for instance, upwelling intensity, climate, and degree of fluvial discharge (e.g., González-Álvarez et al., 2005; Martins et al., 2007; Bernárdez et al., 2008b, 2008b). A compilation of such studies on Holocene climatic fluctuations and precipitation variations was provided by Bernárdez et al. (2008b) but the results are often divergent or even contrary. However, in contrast to these Holocene studies, the pre-Holocene oceanographic and sedimentary systems, and the impact of sea-level variations on the sedimentary construction of the NW Iberian shelf remained fully unknown prior to this study.

1.5. Motivation and main objectives

Although continental shelves comprise a rather small part of the Earth's ocean surface (<8%) they represent the most important marine sink for terrigenous material (Milliman, 1991; Wollast, 1991; Gebhardt et al., 2005). Only 7–10% of the fluvial input is proposed to reach the deep sea (Eisma et al., 1985). Besides this importance as sediment storage environment, the ecological and economical relevance of shelf systems are undisputable. These systems feature highest primary production, especially in areas of enhanced upwelling (De Haas et al., 2002) and represent, consequently, an important habitat of the biosphere. Additionally, the economical value of shelves is exploited by, for instance, fishery industry and explorations of hydrocarbon and mineral resources. Nevertheless, the scientific knowledge on shelf systems is still very limited.

In the past decades, shelf systems became of increasing interest for the scientific community due to their role as important part of the sediment pathway from the coast to the deep sea, which, for example, provided the chance to calculate sediment budgets (Milliman and Syvitski, 1992; Hovius, 1998; Syvitski et al., 2003). The modern processes controlling the surface sediment distribution on shelves are partly well investigated (e.g., Dias and Nittrouer, 1984; Demirpolat, 1991; Brooks et al., 2003). Nevertheless, comprehensive sedimentary studies concerning (1) the evolution of sediment partitioning (Table 1.1) as well as (2) the spatial and temporal transformation (Table 1.1) of shelf systems are still a rare case. There are two main reasons for these gaps of knowledge. First, a sufficient quantity of sediment cores is necessary to conduct comprehensive sedimentary studies. Second, the challenging coring process requires specialised equipment due to the abundance of sand and gravel deposits.

This PhD thesis is an outcome of the MARUM project C6 "Sediment partitioning and transformation on the shelf". Two of the main targets of this project are to reveal the factors and processes which govern the partitioning of shelf sediments, and to display the response of these forces to contrasting shelf configurations. This thesis aims at reaching these targets by reconstructing the architecture as well as the sediment distribution and -partitioning patterns in the NW Iberian sedimentary shelf system. The main approaches to achieve these objectives are:

(1) the observation and interpretation of the Late-Pleistocene to Holocene stratigraphy and sedimentary construction of the NW Iberian shelf system,

(2) the reconstruction of the late-Quaternary sedimentary facies evolution and major forces controlling the distribution of facies types, and

(3) the detailed analysis of the Holocene mud-depocentre developments and of the main controls on the spatial and temporal distribution of these deposits.

The NW Iberian shelf was chosen as representative example of a high-energy, low-accumulation shelf system. The modern oceanographical situation and surface geology of this shelf system were intensively investigated during the OMEX II project (Van Weering and McCave, 2002). The ancient situation, however, remained largely unknown. Studies dealing with the geological history of the NW Iberian shelf were restricted to somewhat questionable interpretations of surface features (Rodrigues et al., 1991; Dias et al., 2000), two arguable seismic studies (Muñoz et al., 2003; Ferrín, 2005), and few studies on single cores focussing on the analysis of Holocene climatic variations (González-Álvarez et al.,

2005; Martins et al., 2007; Bernárdez et al., 2008a, 2008b). Thus, an extensive seismic survey together with the retrieval of numerous sediment cores and a large set of radiocarbon dates was conducted to provide a comprehensive base for sedimentary studies in the NW Iberian shelf system. These studies of a typical high-energy, low-accumulation shelf should significantly increase our understanding on the sedimentary evolution of the most-common type of shelf systems and should provide a new view on the forces controlling the sedimentary construction of these environments.

1.6. Materials and methods

1.6.1. Geophysical profiling

In total, about 1900 km of seismic lines were collected during the first GALIOMAR (Galician Ocean Margin) cruise in 2006 onboard the German research vessel Poseidon (Cruise P342; Fig. 1.8) in order to reveal the stratigraphic framework of the shelf and to provide a basis for the localisation of sediment core positions. The system setup during this cruise is displayed in Fig. 1.12.

Seismic data were obtained by a high-resolution multichannel system during Cruise P342. A Mini-Generator-Injector (GI)-Airgun with reduced chamber volume (2 x 0.25 l) and a main frequency of ~300 Hz was used as seismic source. The signals were received by a 100-m long 16-channel streamer. A Marine Multi-Channel Acquisition System (MaMuCS; developed by the working group Marine Technology/Environmental Research, University of Bremen) was used for data recording.

Acoustic-reflection data were collected by means of a Boomer system. The frequency band of the UWAK-05 transducer was between 300 Hz and 20 kHz with a pulse length of 0.6 µs. The boomer was shot on the shelf every second with a 2 second break after 6 shots for firing the Mini-GI-Gun of the multichannel seismic system. The signals were received by a 3-m long Mini-Streamer and subsequently amplified and filtered by an ORE Geopulse receiver 5210a. The output signals were recorded by a Paradigma unit (Fig. 1.12).

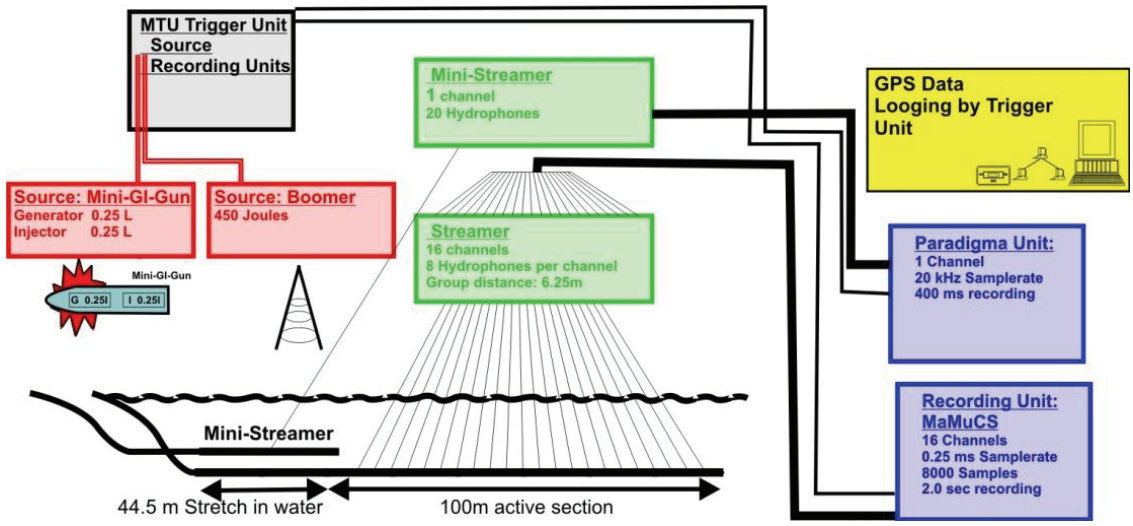

Fig. 1.12. Geophysical system setup during Cruise P342 (from Hanebuth et al., 2007).

1.6.2. Coring devices

All coring devices were applied during both GALIOMAR cruises in 2006 (P342) and 2008 (P366/3). A giant box corer was used at every core location (Figs. 1.8 and 1.13A). The maximum penetration depth of the device is 50 cm. Depending on the recovered grain size, a vibrocorer or gravity corer was chosen. A vibrocorer was used in case of sandy sediments and a gravity corer was selected for sediments characterised by high mud contents. Additionally, the giant box corer recovers an undisturbed surface which was used for the measurements of the modern situation.

A vibrocorer (Fig. 1.13B) was used to retrieve sediments down to 250 m water depth. The maximum core recovery of the vibrocorer system is 5 m and the retrieved sediment cores have a diameter of 10 cm. A gravity corer (Fig. 1.13C) was mainly used where the water depth exceeds the limit of the vibrocorer and at some stations within mud depocentres on the shelf. A 3-m long barrel was used to retrieve slightly sandy seafloor material and a 6-m long version was applied for the recovery of finer and softer sediments. The sediment cores have a diameter of 12 cm.

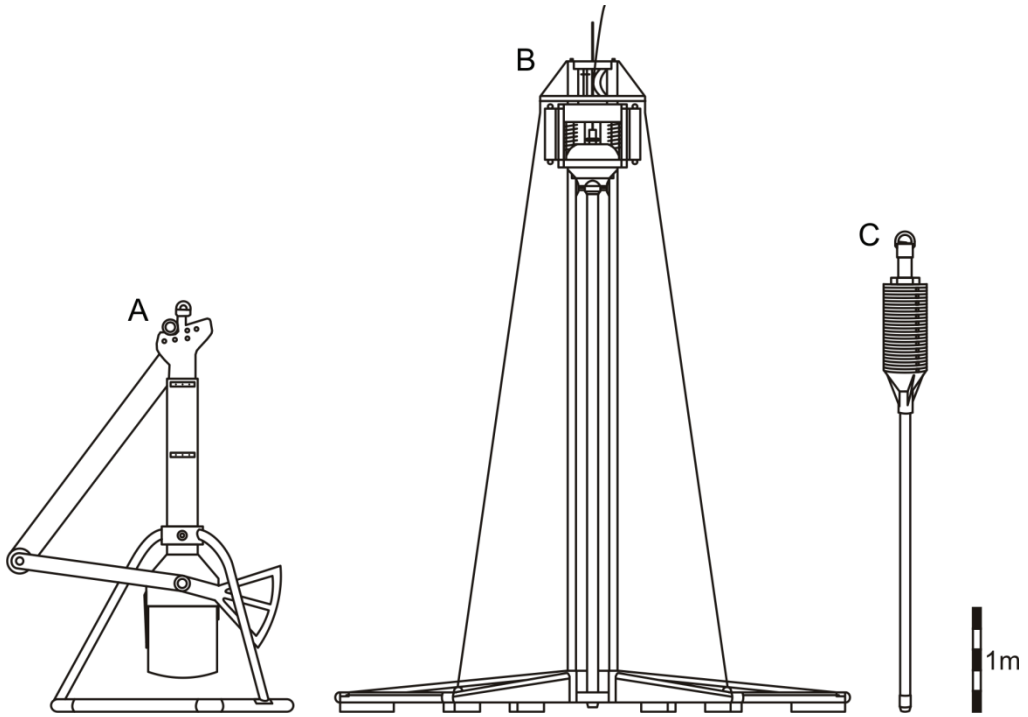

Fig. 1.13. Coring devices used during Cruises P342 and P366/3: (A) giant box corer; (B) vibrocorer (redrawn from manual); (C) gravity corer.

1.6.3. Laboratory analyses & statistics

The recovered sediment cores were cut into 1-m segments and split into archive and work half. The archive half was photographed and used for detailed visual core description. Sediment samples were taken from the work half part in intervals of 20 cm in sandy sections and in a distance of 5 cm in muddy fine sands and mud (Fig. 1.14). Samples were split into A and B subsamples for grain-size analysis and X-ray diffraction measurements, respectively. Samples were dried with respect to their mud contents. Samples with considerable contents of the fine fraction were freeze-dried and pure fine sands were oven-dried.

Subsamples for grain-size analysis were wet sieved into coarse (>63 μm) and fine fraction (<63 μm, Fig. 1.14). After oven-drying, the fine fraction was stored and coarse fraction was sonic sifting using sieve mesh widths of 63–125, 125–250, 250–500, 500–1000, and >1000 μm. The grain-size distribution was calculated from the individual weight of the grain-size fractions. The sediments have been classified according to the grain-size scheme of Blair and McPherson (1999) and the obtained grain-size distributions were used to corroborate the initial visual core description.

X-ray diffraction analysis was applied to the bulk of selected samples (Fig. 1.14). Those samples were chosen by visual core description in order to represent the broad compositional range of sand and mud deposits of the NW Iberian shelf. After careful grinding, the samples were measured with a Philips X'Pert Pro multipurpose diffractometer (Cu-K-α 1.541Å, 45 kV, 40 mA, fixed divergence slit 1/4°). The measurements were performed using a 2-θ angle between 3° and 85° and a step size of 0.016°. The Philips software "X'Pert HighScore" was used for mineral identification and provides semi-quantitative estimates.

Accelerator mass spectrometry (AMS) radiocarbon dating was used for age control. The measurements were carried out by the Leibniz Laboratory in Kiel (Germany), and the Poznań Radiocarbon Laboratory (Poland). Dates with conventional ages <22 ka were corrected for a standard marine reservoir effect of 400 years and converted into 1-σ calibrated ages using the program Calib 5.0.1 (Stuiver et al., 1998). Older dates were calibrated based on the function of Bard et al. (1998).

A microscopic component analysis was used to reveal characteristic compositional differences between samples (Appendix 3). At least 300 grains of sand fraction 250–500 μm were determined under a binocular microscope to provide sufficient statistical relevance. Samples for component analysis were chosen by visual core description and analysis was applied on at least two samples in homogenous sections. Where considerable differences in the component distribution occurred, subsamples were selected within this interval.

Statistical analysis was performed on the results of the microscopic component analysis using the MATLAB (R2007a) software package. Fuzzy c-means cluster analysis (FCM) provides a powerful tool to unravel the similarities and dissimilarities of different samples by a given cluster solution (Bedzek et al., 1984). In this thesis, FCM was used to quantify the complex relationships among individual sample compositions of the microscopic component analysis (Appendix 3). Samples with a high degree of similarity plot as clusters within the multidimensional measurement space. The composition of the central point within a cluster represents its characteristic component distribution. However, the treatment of compositional data requires special care. In contrast to "open" data sets where the components range from $-\infty$ to $+\infty$, compositional data sets contain only relative information and are, therefore "closed", i.e. they sum to a constant such as 100%. If one component increases within such data sets, others must decrease. Hence, the components are linked and results of standard statistical analysis are, therefore, influenced by spurious effects (Pawlowsky-Glahn and Egozcue, 2006). The centred-log-ratio transformation was applied to the data before the calculation of the FCM solution in order to minimize the influence of such artefacts (Aitchison et al., 2000; Pawlowsky-Glahn and Egozcue, 2006). Additionally, the non-linear mapping dimension reducing technique (NLM; Sammon, 1969) was used in combination with the FCM to display the validity of a given cluster solution (Vriend et al.,

1988; Dekkers et al., 1994). The obtained statistical results were used in combination with the observations of visual core description, grain-size analysis, and X-ray diffraction to define sediment facies types on the NW Iberian shelf.

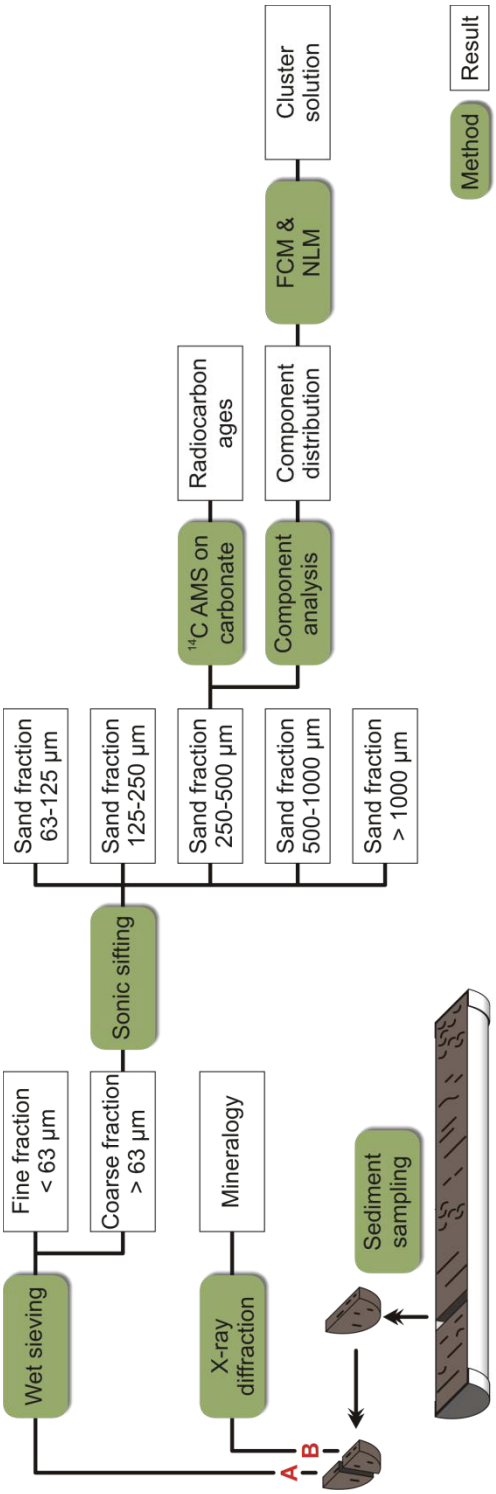

Fig. 1.14. Flow chart of the laboratory methods and statistics used in this study; AMS = accelerator mass spectrometry; FCM = fuzzy c-means cluster analysis; NLM = non-linear mapping technique.

1.7. References

Abrantes, F., Moita, M.T., 1999. Water column and recent sediment data on diatoms and coccolithophorids, off Portugal, confirm sediment record of upwelling events. Oceanologica Acta 22 (1), 67-84.

Abrantes, F., Lebreiro, S., Rodrigues, T., Gil, I., Bartels-Jónsdóttir, H., Oliveira, P., Kissel, C., Grimalt, J.O., 2005. Shallow-marine sediment cores record climate variability and earthquake activity off Lisbon (Portugal) for the last 2000 years. Quaternary Science Reviews 24 (23-24), 2477-2494.

Aharon, P., 1984. Implications of the coral reef record from New Guinea concerning the astronomical theory of climate change. In: Berger, A., Imbrie, J., Kukla, G., Saltzman, B. (Eds.), Milankovitch and Climate. Reidel, Dordrecht, pp. 379-390.

Aitchison, J., Barceló-Vidal, C., Martín-Fernández, J.A., Pawlowsky-Glahn, V., 2000. Logratio analysis and compositional distance. Mathematical Geology 32 (3), 271-275.

Allen, J.R.L., 1970. Physical processes of sedimenation. Elsevier, New York.

Araújo, M.F., Jouanneau, J.M., Valério, P., Barbosa, T., Gouveia, A., Weber, O., Oliveira, A., Rodrigues, A., Dias, J.M.A., 2002. Geochemical tracers of northern Portuguese estuarine sediments on the shelf. Progress in Oceanography 52 (2-4), 277-297.

Baas, J.H., Mienert, J., Abrantes, F., Prins, M.A., 1997. Late Quaternary sedimentation on the Portuguese continental margin: climate-related processes and products. Palaeogeography, Palaeoclimatology, Palaeoecology 130 (1-4), 1-23.

Bard, E., Hamelin, B., Fairbanks, R.G., Zindler, A., 1990. Calibration of the C-14 timescale over the past 30,000 years using mass-spectrometric U-Th ages from Barbados corals. Nature 345 (6274), 405-410.

Bard, E., Arnold, M., Hamelin, B., Tisnerat-Laborde, N., Cabioch, G., 1998. Radiocarbon calibration by means of mass spectrometric Th-230/U-234 and C-14 ages of corals: an updated database including samples from Barbados, Mururoa and Tahiti. Radiocarbon 40 (3), 1085-1092.

Bard, E., Hamelin, B., Arnold, M., Montaggioni, L., Cabioch, G., Faure, G., Rougerie, F., 1996. Deglacial sea-level record from Tahiti corals and the timing of global meltwater discharge. Nature 382 (6588), 241-244.

Barrie, J.V., Conway, K.W., 2002. Rapid sea-level change and coastal evolution on the Pacific margin of Canada. Sedimentary Geology 150 (1-2), 171-183.

Bedzek, J.C., Ehrlich, R., Full, W., 1984. The fuzzy c-means clustering algorithm. Computers & Geoscience 10, 191-203.

Bernárdez, P., González-Álvarez, R., Francés, G., Prego, R., Bárcena, M.A., Romero, O.E., 2008a. Paleoproductivity changes and upwelling variability in the Galicia Mud Patch during the last 5000 years: geochemical and microfloral evidence. Holocene 18 (8), 1207-1218.

Bernárdez, P., González-Álvarez, R., Francés, G., Prego, R., Bárcena, M.A., Romero, O.E., 2008b. Late Holocene history of the rainfall in the NW Iberian peninsula – evidence from a marine record. Journal of Marine Systems 72 (1-4), 366-382.

Blair, T.C., McPherson, J.G., 1999. Grain-size and textural classification of coarse sedimentary particles. Journal of Sedimentary Research 69 (1), 6-19.

Boski, T., Moura, D., Veiga-Pires, C., Camacho, S., Duarte, D., Scott, D.B., Fernandes, S.G., 2002. Post-glacial sea-level rise and sedimentary response in the Guadiana Estuary, Portugal/Spain border. Sedimentary Geology 150 (1-2), 103-122.

Bremner, J.M., Willis, J.P., 1993. Mineralogy and geochemistry of the clay fraction of sediments from the Namibian continental margin and the adjacent hinterland. Marine Geology 115 (1-2), 85-116.

Brenchley, P.J., 1985. Storm influenced sandstone beds: Modern Geology. Modern Geology 9, 369-396.

Brooks, G.R., Doyle, L.J., Davis, R.A., DeWitt, N.T., Suthard, B.C., 2003. Patterns and controls of surface sediment distribution: west-central Florida inner shelf. Marine Geology 200 (1-4), 307-324.

Cascalho, J., Fradique, C., 2007. The sources and hydraulic sorting of heavy minerals on the northern portuguese continental margin. Developments in Sedimentology 58, 75-110.

Castaing, P., Froidefond, J.M., Lazure, P., Weber, O., Prud'homme, R., Jouanneau, J.M., 1999. Relationship between hydrology and seasonal distribution of suspended sediments on the continental shelf of the Bay of Biscay. Deep Sea Research Part II: Topical Studies in Oceanography 46 (10), 1979-2001.

Catuneanu, O., 2002. Sequence stratigraphy of clastic systems: concepts, merits, and pitfalls. Journal of African Earth Sciences 35 (1), 1-43.

Catuneanu, O., 2006. Principles of Sequence Stratigraphy. Elsevier, Amsterdam, Oxford.

Catuneanu, O., Abreu, V., Bhattacharya, J.P., Blum, M.D., Dalrymple, R.W., Eriksson, P.G., Fielding, C.R., Fisher, W.L., Galloway, W.E., Gibling, M.R., Giles, K.A., Holbrook, J.M., Jordan, R., Kendall, C.G.S.C., Macurda, B., Martinsen, O.J., Miall, A.D., Neal, J.E., Nummedal, D., Pomar, L., Posamentier, H.W., Pratt, B.R., Sarg, J.F., Shanley, K.W., Steel, R.J., Strasser, A., Tucker, M.E., Winker, C., 2009. Towards the standardization of sequence stratigraphy. Earth-Science Reviews 92 (1-2), 1-33.

Chappell, J., Polach, H., 1991. Postglacial sea-level rise from a coral record at Huon Peninsula, Papua-New-Guinea. Nature 349 (6305), 147-149.

Cross, T.A., 1991. High-resolution stratigraphic correlation from the perspectives of base-level cycles and sediment accommodation. In: Dolson, J. (Ed.) Unconformity Related Hydrocarbon Exploration and Accumulation in Clastic and Carbonate Settings, short course notes. Rocky Mountain Association of Geologists, pp. 28–41.

Curray, J.R., 1965. Late Quaternary history – continental shelves of the United States. In: Wright, H.E., Frey, D.G. (Eds.), The Quaternary of the United States. Princeton University Press, Princeton.

Dabrio, C.J., Zazo, C., Goy, J.L., Sierro, F.J., Borja, F., Lario, J., González, J.A., Flores, J.A., 2000. Depositional history of estuarine infill during the last post-

glacial transgression (Gulf of Cadiz, Southern Spain). Marine Geology 162 (2-4), 381-404.

De Haas, H., Van Weering, T.C.E., De Stigter, H., 2002. Organic carbon in shelf seas: sinks or sources, processes and products. Continental Shelf Research 22 (5), 691-717.

Dekkers, M.J., Langereis, C.G., Vriend, S.P., Van Santvoort, P.J.M., De Lange, G.J., 1994. Fuzzy c-means cluster analysis of early diagenetic effects on natural remanent magnetisation acquisition in a 1.1 Myr piston core from the Central Mediterranean. Physics of the Earth and Planetary Interiors 85, 155-171.

DeMenocal, P., Ortiz, J., Guilderson, T., Adkins, J., Sarthein, M., Baker, L., Yarusinsky, M., 2000. Abrupt onset and termination of the African Humid Period: rapid climate responses to gradual insolation forcing. Quaternary Science Reviews 19, 347–361.

Demirpolat, S., 1991. Surface and near-surface sediments from the continental shelf off the Russian River, Northern California. Marine Geology 99 (1-2), 163-173.

Dias, J.M.A., Nittrouer, C.A., 1984. Continental shelf sediments of northern Portugal. Continental Shelf Research 3 (2), 147-165.

Dias, J.M.A., Boski, T., Rodrigues, A., Magalhães, F., 2000. Coast line evolution in Portugal since the Last Glacial Maximum until present – a synthesis. Marine Geology 170 (1-2), 177-186.

Dias, J.M.A., Gonzalez, R., Garcia, C., Diaz-del-Rio, V., 2002a. Sediment distribution patterns on the Galicia-Minho continental shelf. Progress in Oceanography 52 (2-4), 215-231.

Dias, J.M.A., Jouanneau, J.M., Gonzalez, R., Araújo, M.F., Drago, T., Garcia, C., Oliveira, A., Rodrigues, A., Vitorino, J., Weber, O., 2002b. Present day sedimentary processes on the northern Iberian shelf. Progress in Oceanography 52 (2-4), 249-259.

Drago, T., Oliveira, A., Magalhães, F., Cascalho, J., Jouanneau, J.M., Vitorino, J., 1998. Some evidences of northward fine sediment transport in the northern Portuguese continental shelf. Oceanologica Acta 21 (2), 223-231.

Duke, W.L., 1985. Hummocky cross-stratification, tropical hurricanes, and intense winter storms. Sedimentology 32 (2), 167-194.

Einsele, G., 1996. Event deposits: the role of sediment supply and relative sea-level changes--overview. Sedimentary Geology 104 (1-4), 11-37.

Einsele, G., 2000. Sedimentary basins: evolution, facies, and sediment budget. Springer, Berlin.

Eisma, D., Bernard, P., Boon, J.J., Van Grieken, R., Kalf, J., Mook, W.G., 1985. Loss of particulater organic matter in estuaries as exemplified by the Ems and Gironde estuaries. In: Degens, E.T., Kempe, S., Herrera, R. (Eds.), Transport of Carbon and Minerals in Major World Rivers. SCOPE/UNEP Special Issue 58, University of Hamburg, pp. 397-412.

Emery, D., Myers, K., 2003. Sequence stratigraphy. Blackwell Science, Malden.

Emery, K.O., 1952. Continental shelf sediments off southern California. Geological Society of America Bulletin 63, 1105-1108.

Emery, K.O., 1968. Relict sediments on continental shelves of world. AAPG Bulletin 52 (3), 445-464.

Fairbanks, R.G., 1989. A 17,000-year glacio-eustatic sea level record: influence of glacial melting rates on the Younger Dryas event and deep-ocean circulation. Nature 342 (6250), 637-642.

Fan, S.J., Swift, D.J.P., Traykovski, P., Bentley, S., Borgeld, J.C., Reed, C.W., Niedoroda, A.W., 2004. River flooding, storm resuspension, and event stratigraphy on the northern California shelf: observations compared with simulations. Marine Geology 210 (1-4), 17-41.

Ferré, B., Guizien, K., Durrieu de Madron, X., Palanques, A., Guillén, J., Grémare, A., 2005. Fine-grained sediment dynamics during a strong storm event in the inner-shelf of the Gulf of Lion (NW Mediterranean). Continental Shelf Research 25 (19-20), 2410-2427.

Ferrín, A., 2005. Cenozoic seismic stratigraphy of the SW Galician continental shelf. Comparative study with the Canterbury shelf (SE New Zealand) during the Quaternary. Ph.D. thesis, Facultad de Ciencas del Mar, Departmento de Geociencias Marinas y Ordenación del Territorio, Universidad de Vigo, Spain.

Fiuza, A.F.D., Demacedo, M.E., Guerreiro, M.R., 1982. Climatological space and time variation of the Portuguese coastal upwelling. Oceanologica Acta 5 (1), 31-40.

Fleming, K., Johnston, P., Zwartz, D., Yokoyama, Y., Lambeck, K., Chappell, J., 1998. Refining the eustatic sea-level curve since the Last Glacial Maximum using far- and intermediate-field sites. Earth and Planetary Science Letters 163 (1-4), 327-342.

Freiwald, A., Roberts, J.M., 2005. Cold-water corals and ecosystems. Springer, Berlin, Heidelberg, New York.

Galloway, W.E., 1989. Genetic stratigraphic sequences in basin analysis – part I: architecture and genesis of flooding-surface bounded depositional units. American Association of Petroleum Geologists Bulletin 73, 125-142.

Gebhardt, A.C., Gaye-Haake, B., Unger, D., Lahajnar, N., Ittekkot, V., 2005. A contemporary sediment and organic carbon budget for the Kara Sea shelf (Siberia). Marine Geology 220 (1-4), 83-100.

Glade, T., 2003. Landslide occurrence as a response to land use change: a review of evidence from New Zealand. CATENA 51 (3-4), 297-314.

González-Álvarez, R., Bernárdez, P., Pena, L.D., Francés, G., Prego, R., Diz, P., Vilas, F., 2005. Paleoclimatic evolution of the Galician continental shelf (NW of Spain) during the last 3000 years: from a storm regime to present conditions. Journal of Marine Systems 54 (1-4), 245-260.

Gonzalez, R., Dias, J.M.A., Lobo, F., Mendes, I., 2004. Sedimentological and paleoenvironmental characterisation of transgressive sediments on the Guadiana Shelf (Northern Gulf of Cadiz, SW Iberia). Quaternary International 120 (1), 133-144.

Grossman, E.E., Eittreim, S.L., Field, M.E., Wong, F.L., 2006. Shallow stratigraphy and sedimentation history during high-frequency sea-level changes on the central California shelf. Continental Shelf Research 26 (10), 1217-1239.

Guillén, J., Bourrin, F., Palanques, A., Durrieu de Madron, X., Puig, P., Buscail, R., 2006. Sediment

dynamics during wet and dry storm events on the Tet inner shelf (SW Gulf of Lions). Marine Geology 234 (1-4), 129-142.

Hallam, A., 1989. The case of sea-level change as a dominant factor in mass extinctions of marine invertebrates. Philosophical Transactions of the Royal Society, Series B 325, 437-455.

Hanebuth, T., Stattegger, K., Grootes, P.M., 2000. Rapid flooding of the Sunda Shelf: a late-glacial sea-level record. Science 288 (5468), 1033-1035.

Hanebuth, T., Bender, V., Bujan, S., Elvert, M., Frederichs, T., Kockisch, B., Krastel-Gudegast, S., Lantzsch, H., Mena Rodríguez, Á., Schmidt, F., Strozyk, F., Wagner Friedrichs, M., 2007. Report and first results of the Poseidon cruise P342 GALIOMAR, Vigo–Lisboa (Portugal), August 19th–September 06th, 2006. Distribution pattern, residence times and export of sediments on the Pleistocene/Holocene Galician Shelf (NW Iberian Peninsula). Berichte, Fachbereich Geowissenschaften, University of Bremen 255, 203 pp.

Hanebuth, T.J.J., 2009. Clastic continental shelves as environmental archives along the sedimentary pathway over Late Quaternary times. Habilitationsschrift, Faculty of Geosciences, University of Bremen, 102.

Hanebuth, T.J.J., Stattegger, K., 2004. Depositional sequences on a late Pleistocene-Holocene tropical siliciclastic shelf (Sunda Shelf, southeast Asia). Journal of Asian Earth Sciences 23 (1), 113-126.

Hanebuth, T.J.J., Lantzsch, H., 2008. A Late Quaternary sedimentary shelf system under hyperarid conditions: unravelling climatic, oceanographic and sea-level controls (Golfe d'Arguin, Mauritania, NW Africa). Marine Geology 256 (1-4), 77-89.

Hanebuth, T.J.J., Stattegger, K., Bojanowski, A., 2009. Termination of the Last Glacial Maximum sea-level lowstand: The Sunda-Shelf data revisited. Global and Planetary Change 66 (1-2), 76-84.

Hanebuth, T.J.J., Lantzsch, H., Nizou, J., submitted. Mud depocentres on continental shelves – a classification. Earth Science Reviews.

Henrich, R., Hanebuth, T.J.J., Cherubini, Y., Krastel, S., Pierau, R., Zühlsdorff, C., in press. Climate-induced turbidity current activity in NW-African canyon systems. In: Mosher, D. (Ed.) Submarine mass movements and their consequences, Advances in Natural and Technological Hazards Research 28. Springer

Henrich, R., Freiwald, A., Betzler, C., Bader, B., Schäfer, P., Samtleben, C., Brachert, T., Wehrmann, A., Zankl, H., Kühlmann, D., 1995. Controls on modern carbonate sedimentation on warm-temperate to arctic coasts, shelves and seamounts in the Northern Hemisphere: Implications for fossil counterparts. Facies 32 (1), 71-108.

Hernández-Molina, F.J., Somoza, L., Rey, J., Pomar, L., 1994. Late Pleistocene-Holocene sediments on the Spanish continental shelves: model for very high resolution sequence stratigraphy. Marine Geology 120 (3-4), 129-174.

Hill, P.S., Fox, J.M., Crockett, J.S., Curran, K.J., Friedrichs, C.T., Rockwell Geyer, W., Milligan, T.G., Ogston, A.S., Puig, P., Scully, M.E., Traykovski, P.A., Wheatcroft, R.A., 2007. Sediment delivery to the seabed on continental margins. In: Nittrouer, C.A., Austin, J.A., Field, M.E., Kravitz, J.H., Syvitski, J.P.M., Wiberg, P.L. (Eds.), Continental margin sedimentation - from sediment transport to sequence stratigraphy, International Association of Sedimentologists Special Publication 37. Blackwell, Malden, Oxford, Carlton, pp. 49-98.

Hovius, N., 1998. Controls on sediment supply by large rivers. In: Shanley, K.W., McCabe, P.J. (Eds.), Relative role of eustasy, climate and tectonism in continental rocks Society of Economic Paleontologists and Mineralogists Special Publication, Tulsa, pp. 3-16.

Huthnance, J.M., Humphery, J.D., Knight, P.J., Chatwin, P.G., Thomsen, L., White, M., 2002. Near-bed turbulence measurements, stress estimates and sediment mobility at the continental shelf edge. Progress in Oceanography 52 (2-4), 171-194.

Imbrie, J., Boyle, E.A., Clemens, S.C., Duffy, A., Howard, W.R., Kukla, G., Kutzbach, J., Martinson, D.G., McIntyre, A., Mix, A.C., Molfino, B., Morley, J.J., Peterson, L.C., Pisias, N.G., Prell, W.L., Raymo, M.E., Shackleton, N.J., Toggweiler, J.R., 1992. On the Structure and Origin of Major Glaciation Cycles – Linear Responses to Milankovitch Forcing. Paleoceanography 7, 701–738.

Inthorn, M., Mohrholz, V., Zabel, M., 2006. Nepheloid layer distribution in the Benguela upwelling area offshore Namibia. Deep Sea Research Part I: Oceanographic Research Papers 53 (8), 1423-1438.

Johnson, H.D., Baldwin, C.T., 1996. Shallow clastic seas. In: Reading, H.G. (Ed.) Sedimentary environments: processes, facies and stratigraphy. Blackwell, Malden, Oxford, Carlton, pp. 232-280.

Jouanneau, J.M., Weber, O., Drago, T., Rodrigues, A., Oliveira, A., Dias, J.M.A., Garcia, C., Schmidt, S., Reyss, J.L., 2002. Recent sedimentation and sedimentary budgets on the western Iberian shelf. Progress in Oceanography 52 (2-4), 261-275.

Kaplin, P.A., Selivanov, A.O., 1995. Recent coastal evolution of the Caspian sea as a natural model for coastal responses to the possible acceleration of global sea-level rise. Marine Geology 124 (1-4), 161-175.

Kennett, J.P., 1982. Marine Geology. Prentice Hall, New Jersey.

Koopmann, B., Lees, A., Piessens, P., Sarthein, M., 1979. Skeletal carbonate sands and wind-derived silty-marls off the Saharan coast: Baie du Lévrier, Arguin Platform, Mauritania. Meteor Forschungs Ergebnisse C30, 15-57.

Lambeck, K., 1990. Late pleistocene, holocene and present sea-levels: constraints on future change. Global and Planetary Change 3 (3), 205-217.

Liu, J., Saito, Y., Wang, H., Yang, Z.G., Nakashima, R., 2007. Sedimentary evolution of the Holocene subaqueous clinoform off the Shandong Peninsula in the Yellow Sea. Marine Geology 236 (3-4), 165-187.

Liu, J.P., Milliman, J.D., Gao, S., 2002. The Shandong mud wedge and post-glacial sediment accumulation in the Yellow Sea. Geo-Marine Letters 21 (4), 212-218.

Lobo, F.J., Fernández-Salas, L.M., Hernández-Molina, F.J., González, R., Dias, J.M.A., del Río, V.D., Somoza, L., 2005. Holocene highstand deposits in the

Gulf of Cádiz, SW Iberian Peninsula: a high-resolution record of hierarchical environmental changes. Marine Geology 219 (2-3), 109-131.

Lobo, F.J., Sánchez, R., González, R., Dias, J.M.A., Hernández-Molina, F.J., Fernández-Salas, L.M., Díaz del Río, V., Mendes, I., 2004. Contrasting styles of the Holocene highstand sedimentation and sediment dispersal systems in the northern shelf of the Gulf of Cadiz. Continental Shelf Research 24 (4-5), 461-482.

Logvinenko, N.V., 1982. Origin of glauconite in the recent bottom sediments of the ocean. Sedimentary Geology 31 (1), 43-48.

Martins, V., Dubert, J., Jouanneau, J.-M., Weber, O., da Silva, E.F., Patinha, C., Alveirinho Dias, J.M., Rocha, F., 2007. A multiproxy approach of the Holocene evolution of shelf-slope circulation on the NW Iberian Continental Shelf. Marine Geology 239 (1-2), 1-18.

McCave, I.N., 1972. Transport and escape of fine-grained sediment from shelf areas. In: Swift, D.J.P., Duane, D.B., Pilkey, O.H. (Eds.), Shelf sediment transport: process and pattern. Dowden, Hutchinson and Ross, Inc., Stroudsburg, pp. 225-244.

McCave, I.N., 1984. Mechanics of deposition of fine-grained sediments from nepheloid layers. Geo-Marine Letters 4 (3-4), 243-245.

McCave, I.N., 2008. Size sorting during transport and deposition of fine sediments: sortable silt and flow speed. Developments in Sedimentology 60, 121-142.

McPhee-Shaw, E.E., Sternberg, R.W., Mullenbach, B., Ogston, A.S., 2004. Observations of intermediate nepheloid layers on the northern California continental margin. Continental Shelf Research 24 (6), 693-720.

Milliman, J.D., 1974. Marine Carbonates. Springer, Berlin, Heidelberg, New York.

Milliman, J.D., 1991. Flux and fate of fluvial sediment and water in coastal seas. In: Mantoura, R.F.C., Martin, J.-M., Wollast, R. (Eds.), Ocean Margin Processes in Global Change. Wiley, New York, pp. 69-89.

Milliman, J.D., Meade, R.H., 1983. World-Wide Delivery of River Sediment to the Oceans. The Journal of Geology 91 (1), 1-21.

Milliman, J.D., Syvitski, J.P.M., 1992. Geomorphic/Tectonic Control of Sediment Discharge to the Ocean: The Importance of Small Mountainous Rivers. The Journal of Geology 100 (5), 525-544.

Moore, D.G., 1969. Reflection profiling studies of the california continental borderland: structure and Quaternary turbidite basins Geological Society of America Special Papers 107, 142 pp.

Mörner, N.-A., 2004. Estimating future sea level changes from past records. Global and Planetary Change 40 (1-2), 49-54.

Morton, R.A., Gibeaut, J.C., Paine, J.G., 1995. Meso-scale transfer of sand during and after storms: implications for prediction of shoreline movement. Marine Geology 126 (1-4), 161-179.

Mount, J.F., 1984. Mixing of siliciclastic and carbonate sediments in shallow shelf environments. Geology 12 (7), 432-435.

Moura, D., Veiga-Pires, C., Albardeiro, L., Boski, T., Rodrigues, A.L., Tareco, H., 2007. Holocene sea level fluctuations and coastal evolution in the central Algarve (southern Portugal). Marine Geology 237 (3-4), 127-142.

Mullins, H.T., Heath, K.C., van Buren, M., Newton, C.R., 1984. Anatomy of a modern open-ocean carbonate slope; northern Little Bahama Bank. Sedimentology 31 (2), 141-168.

Muñoz, A., Acosta, J., Uchupi, E., 2003. Cenozoic tectonics on the Galicia margin, northwest Spain. Geo-Marine Letters 23 (1), 72-80.

Murdmaa, I., Ivanova, E., Duplessy, J.-C., Levitan, M., Khusid, T., Bourtman, M., Alekhina, G., Alekseeva, T., Belousov, M., Serova, V., 2006. Facies system of the Eastern Barents Sea since the last glaciation to present. Marine Geology 230 (3-4), 275-303.

Nittrouer, C.A., Kuehl, S.A., Demaster, D.J., Kowsmann, R.O., 1986. The deltaic nature of Amazon shelf sedimentation. Geological Society of America Bulletin 97 (4), 444-458.

Nittrouer, C.A., Austin, J.A., Field, M.E., Kravitz, J.H., Syvitski, J.P.M., Wiberg, P.L., 2007. Continental margin sedimentation – from sediment transport to sequence stratigraphy, International Association of Sedimentologists Special Publication 37. Blackwell, Malden, Oxford, Carlton.

Noda, A., Katayama, H., Sagayama, T., Suga, K., Uchida, Y., Satake, K., Abe, K., Okamura, Y., 2007. Evaluation of tsunami impacts on shallow marine sediments: an example from the tsunami caused by the 2003 Tokachi-oki earthquake, northern Japan. Sedimentary Geology 200 (3-4), 314-327.

Odin, G.S., Lamboy, M., 1988. Glaucony from the Margin off Northwestern Spain. In: Odin, G.S. (Ed.) Green Marine Clays. Developments in Sedimentology 45, Elsevier, Amsterdam, Oxford, New York, pp. 249-275.

Oliveira, A., Vitorino, J., Rodrigues, A., Jouanneau, J.M., Dias, J.A., Weber, O., 2002a. Nepheloid layer dynamics in the northern Portuguese shelf. Progress in Oceanography 52 (2-4), 195-213.

Oliveira, A., Rocha, F., Rodrigues, A., Jouanneau, J., Dias, A., Weber, O., Gomes, C., 2002b. Clay minerals from the sedimentary cover from the Northwest Iberian shelf. Progress in Oceanography 52 (2-4), 233-247.

Pawlowsky-Glahn, V., Egozcue, J.J., 2006. Compositional data and their analysis: an introduction. Geological Society, London, Special Publications 264 (1), 1-10.

Peltier, W.R., Fairbanks, R.G., 2006. Global glacial ice volume and Last Glacial Maximum duration from an extended Barbados sea level record. Quaternary Science Reviews 25 (23-24), 3322-3337.

Pirazzoli, P.A., Grant, D.R., Woodworth, P., 1989. Trends of relative sea-level change: Past, present and future. Quaternary International 2, 63-71.

Posamentier, H.W., Allen, G.P., 1999. Siliciclastic sequence stratigraphy: concepts and applications. Society of Economic Paleontologists and Mineralogists, Concepts in Sedimentology and Paleontology 7, Tulsa.

Posamentier, H.W., Jervey, M.T., Vail, P.R., 1988. Eustatic controls on clastic deposition – part I: conceptual framework. In: Wilgus, C.K., Hastings, B.S.,

Kendall, C.G.S.C., Posamentier, H.W., Ross, C.A., van Wagoner, J.C. (Eds.), Sea level changes - an integrated approach Society of Economic Paleontologists and Mineralogists Special Publications 42, Tulsa, pp. 110-124.

Prego, R., Bao, R., 1997. Upwelling influence on the Galician coast: silicate in shelf water and underlying surface sediments. Continental Shelf Research 17 (3), 307-318.

Rabineau, M., Berné, S., Olivet, J.-L., Aslanian, D., Guillocheau, F., Joseph, P., 2006. Paleo sea levels reconsidered from direct observation of paleoshoreline position during Glacial Maxima (for the last 500,000 yr). Earth and Planetary Science Letters 252 (1-2), 119-137.

Reading, H.G., Collinson, J.D., 1996. Clastic coasts. In: Reading, H.G. (Ed.) Sedimentary environments: processes, facies and stratigraphy. Blackwell, Malden, Oxford, Carlton, pp. 154-231.

Rey Salgado, J., 1993. Relación morfosedimentaria entre la plataforma continental de Galicia y las Rías Bajas y su evolución durante el Cuaternario. Publicaciones Especiales, Instituto Español de Oceanografía 17, 1-233.

Rodrigues, A., Magalhães, F., Dias, J.A., 1991. Evolution of the North Portuguese coast in the last 18,000 years. Quaternary International 9, 67-74.

Sammon, J.W., 1969. A non-linear mapping for data structure analysis. IEEE Transactions on Computers C18, 401-409.

Santisteban, J.I., Schulte, L., 2007. Fluvial networks of the Iberian Peninsula: a chronological framework. Quaternary Science Reviews 26 (22-24), 2738-2757.

Sarnthein, M., Diester-Haass, L., 1977. Eolian-sand turbidites. Journal of Sedimentary Petrology 47, 868-890.

Schimanski, A., Stattegger, K., 2005. Deglacial and Holocene evolution of the Vietnam shelf: stratigraphy, sediments and sea-level change. Marine Geology 214 (4), 365-387.

Schlager, W., Ginsburg, R.N., 1981. Bahama carbonate platform – the deep and the past. Marine Geology 44 (1-2), 1-24.

Schlager, W., Reijmer, J.J.G., Droxler, A., 1994. Highstand shedding of carbonate platforms. Journal of Sedimentary Research 64 (3), 270–281.

Schmincke, H.-U., 2004. Volcanism. Springer, Berlin, Heidelberg, New York.

Schönfeld, J., Kudrass, H.-R., 1993. Hemipelagic Sediment Accumulation Rates in the South China Sea Related to Late Quaternary Sea-Level Changes. Quaternary Research 40 (3), 368-379.

Shanley, K.W., McCabe, P.J., 1993. Alluvial architecture in a sequence stratigraphic framework: a case history from the Upper Cretaceous of southern Utah, USA. In: Flint, S., Bryant, I. (Eds.), Quantitative Modeling of Clastic Hydrocarbon Reservoirs and Outcrop Analogues, International Association of Sedimentologists Special Publication 15. Blackwell, Malden, Oxford, Carlton, pp. 21-55.

Shanmugam, G., Moiola, R.J., 1982. Eustatic control of turbidites and winnowed turbidites. Geology 10 (5), 231-235.

Shepard, F.P., 1977. Geological oceanography: evolution of coasts, continental margins, and the deep-sea floor. Crane, Russak & Company, New York.

Shepard, F.P., Moore, D.G., 1963. Submarine Geology. Harper and Row, New York.

Steinke, S., Kienast, M., Hanebuth, T., 2003. On the significance of sea-level variations and shelf paleomorphology in governing sedimentation in the southern South China Sea during the last deglaciation. Marine Geology 201 (1-3), 179-206.

Stow, D.A.V., Howell, D.G., Nelson, C.H., 1985. Sedimentary, tectonic, and sea-level controls. In: Bouma, A.H., Normark, W.R., Barnes, N.E. (Eds.), Submarine fans and related turbidite systems. Springer, Berlin, pp. 15-22.

Stuiver, M., Reimer, P.J., Bard, E., Beck, J.W., Burr, G.S., Hughen, K.A., Kromer, B., McCormac, G., Van der Plicht, J., Spurk, M., 1998. INTCAL98 radiocarbon age calibration, 24,000–0 cal BP. Radiocarbon 40 (3), 1041-1083.

Sun, Y., Clemens, S.C., An, Z., Yu, Z., 2006. Astronomical timescale and palaeoclimatic implication of stacked 3.6-Myr monsoon records from the Chinese Loess Plateau. Quaternary Science Reviews 25 (1-2), 33-48.

Swift, D.J.P., 1970. Quaternary shelves and the return to grade. Marine Geology 8 (1), 5-30.

Swift, D.J.P., 1974. Continental shelf sedimentation. In: Burk, C.A., Drake, C.L. (Eds.), The geology of continental margins. Springer, Berlin, pp. 117-135.

Swift, D.J.P., 1976. Coastal shelf sedimentation. In: Stanley, D.J., Swift, D.J.P. (Eds.), Marine sediment transport and environmental management. Wiley, New York, pp. 255-311.

Swift, D.J.P., Thorne, J.A., 1991. Sedimentation on continental margins, I: a general model for shelf sedimentation. In: Swift, D.J.P., Oertel, G.F., Tillman, R.W., Thorne, J.A. (Eds.), Shelf sand and sandstone bodies, geometry, facies and sequence stratigraphy - International Association of Sedimentologists Special Publication 14. Blackwell, Oxford, pp. 3-31.

Swift, D.J.P., Han, G., Vincent, C.E., 1986. Fluid processes and sea-floor response on a modern storm-dominated shelf: middle Atlantic Shelf of North America. Part I: the storm current regime. In: Knight, R.J., McLean, J.R. (Eds.), Shelf sands and sandstones. Canadian Society of Petroleum Geologists, Memoir 11, Calgary, pp. 99-119.

Swift, D.J.P., Hudelson, P.M., Brenner, R.L., Thompson, P., 1987. Shelf construction in a foreland basin: storm beds, shelf sandbodies, and shelf-slope depositional sequences in the Upper Cretaceous Mesaverde Group, Book Cliffs, Utah. Sedimentology 34 (3), 423-457.

Syvitski, J.P.M., Peckham, S.D., Hilberman, R., Mulder, T., 2003. Predicting the terrestrial flux of sediment to the global ocean: a planetary perspective. Sedimentary Geology 162 (1-2), 5-24.

Trauth, M.H., Deino, A., Strecker, M.R., 2001. Response of the East African climate to orbital forcing during the last interglacial (130-117 ka) and the

early last glacial (117-60 ka). Geology 29 (6), 499-502.

Ulses, C., Estournel, C., Durrieu de Madron, X., Palanques, A., 2008. Suspended sediment transport in the Gulf of Lions (NW Mediterranean): impact of extreme storms and floods. Continental Shelf Research 28 (15), 2048-2070.

Van Wagoner, J.C., Posamentier, H.W., Mitchum, H.W., Vail, P.R., Sarg, J.F., Loutit, T.S., J, H., 1988. An overview of sequence stratigraphy and key definitions. In: Wilgus, C.K., Hastings, B.S., Kendall, C.G.S.C., Posamentier, H.W., Ross, C.A., van Wagoner, J.C. (Eds.), Sea level changes - an integrated approach Society of Economic Paleontologists and Mineralogists Special Publications 42, Tulsa, pp. 110-124.

Van Weering, T.C.E., McCave, I.N., 2002. Benthic processes and dynamics at the NW Iberian margin: an introduction. Progress in Oceanography 52 (2-4), 123-128.

Van Weering, T.C.E., de Stigter, H.C., Boer, W., de Haas, H., 2002. Recent sediment transport and accumulation on the NW Iberian margin. Progress in Oceanography 52 (2-4), 349-371.

Vanney, J.R., Stanley, D.J., 1983. Shelfbreak physiography: an overview. In: Stanley, D.J., Moore, G.T. (Eds.), The shelfbreak: critical interface on continental margins, Society of Economic Palaeontologists and Mineralogists Special Publication 33 pp. 1-24.

Verdicchio, G., Trincardi, F., Rebesco, M., Camerlenghi, A., 2008. Shallow-water contourites. In: Rebesco, M., Camerlenghi, A. (Eds.), Developments in Sedimentology 60. Elsevier, Amsterdam, Oxford, pp. 409-433.

Vis, G.-J., Kasse, C., Vandenberghe, J., 2008. Late Pleistocene and Holocene palaeogeography of the Lower Tagus Valley (Portugal): effects of relative sea level, valley morphology and sediment supply. Quaternary Science Reviews 27 (17-18), 1682-1709.

Vitorino, J., Oliveira, A., Jouanneau, J.M., Drago, T., 2002. Winter dynamics on the northern Portuguese shelf. Part 2: bottom boundary layers and sediment dispersal. Progress in Oceanography 52 (2-4), 155-170.

Vriend, S.P., van Gaans, P.F.M., Middelburg, J., de Nijs, A., 1988. The application of fuzzy c-means cluster analysis and non-linear mapping to geochemical datasets: examples from Portugal. Applied Geochemistry 3 (2), 213-224.

Walsh, J.P., Nittrouer, C.A., 2009. Understanding fine-grained river-sediment dispersal on continental margins. Marine Geology 263 (1-4), 34-45.

Warrick, R.A., Barrrow, E.M., Wigley, T.M.L., 1993. Climate and sea level change – observations, projections and implications. Cambridge University Press, Cambridge.

Wollast, R., 1991. The coastal organic carbon cycle: fluxes, sources, and sinks. In: Mantoura, R.F.C., Martin, J.-M., Wollast, R. (Eds.), Ocean Margin Processes in Global Change. Wiley, New York, pp. 365-381.

Wooster, W.S., Bakun, A., McLain, D.R., 1976. Seasonal upwelling cycle along the eastern boundary of the North Atlantic. Journal of Marine Research 34 (2), 131-141.

Yoon, H.I., Park, B.-K., Kim, Y., Kang, C.Y., 2002. Glaciomarine sedimentation and its paleoclimatic implications on the Antarctic Peninsula shelf over the last 15[punctuation space]000 years. Palaeogeography, Palaeoclimatology, Palaeoecology 185 (3-4), 235-254.

2. Sedimentary architecture of a low-accumulation shelf since the Late Pleistocene (NW Iberia)

Hendrik Lantzsch, Till J.J. Hanebuth, Vera B. Bender, Sebastian Krastel

Marine Geology, 2009, 259, 47–58

Marine Geology 259 (2009) 47–58

Contents lists available at ScienceDirect

Marine Geology

journal homepage: www.elsevier.com/locate/margeo

Sedimentary architecture of a low-accumulation shelf since the Late Pleistocene (NW Iberia)

Hendrik Lantzsch *, Till J.J. Hanebuth, Vera B. Bender, Sebastian Krastel [1]

MARUM — Center for Marine Environmental Sciences, and Faculty of Geosciences, University of Bremen, Klagenfurter Strasse, 28359 Bremen, Germany

ARTICLE INFO

Article history:
Received 27 June 2008
Received in revised form 10 December 2008
Accepted 29 December 2008

Keywords:
Late Quaternary
siliciclastic shelves
stratigraphy
Atlantic Ocean
mud belt
sea-level change

ABSTRACT

Continental shelves represent areas of highest economical and ecological importance. Nevertheless, these sedimentary systems remain poorly understood due to a complex interplay of various factors and processes which results in highly individual construction schemes. Previous studies of sedimentary shelf systems have mainly focused on a limited number of cores, retrieved from Holocene fine-grained depocentres. As such, the relation between shelf architecture and sedimentary history remains largely obscure. Here, we present new data from the NW Iberian shelf comprising shallow-seismic profiles, a large number of sediment cores, and an extended set of radiocarbon dates to reveal the Late Quaternary evolution of a low-accumulation shelf system in detail.

On the NW Iberian shelf, three main seismic units are identified. These overly a prominent erosional unconformity on top of the basement. The lowermost Unit 1 is composed of maximal 75-m thick, Late Tertiary to Pleistocene deposits. The youngest sediments of this unit are related to the last glacial sea-level fall. Unit 2 was controlled by the deglacial sea-level rise and shows a maximum thickness of 15 m. Finally, Unit 3 comprises deposits related to the late stage of sea-level rise and the modern sea-level highstand with a thickness of 4 m in mid-shelf position. Two pronounced seismic reflectors separate these main units from each other. Their origin is related to (1) exposure and ravinement processes during lower sea level, and (2) to reworking and re-deposition of coarse sediments during subsequent sea-level rise.

According to the sediment core ground-truthing, sediments of the Late Tertiary to Pleistocene unit predominantly display homogenous fine sands with exceptional occurrences of palaeosols that indicate an ancient exposure surface. Fine sands which were deposited in the run of the last sea-level rise show a time-transgressive retrogradational development. The seismic reflectors, bounding the individual units, appear in the cores as 0.1 to 1-m thick deposits consisting either of shell gravels or siliceous coarse sands with gravels. The modern sea-level highstand stage is characterised by zonal deposition of mud forming a mud belt in mid-shelf position, and sediment starvation on outer shelf zones. Radiocarbon ages indicate that this mud belt was the main depocentre for river-supplied fine material on the NW Iberian shelf at least over the past 5.32 ka BP. The initial onset of this depocentre is proposed to be related to a shift in the balance between rate of sea-level rise and amount of terrigenous sediment supply.

Various other stratigraphical shelf reconstructions reveal analogies in architecture which indicate that timing and shaping of the individual units on low-accumulation shelves is fundamentally controlled by eustatic sea-level changes. Other factors of local importance such as differential elevation of the basement and the presence of morphological barriers formed by rocky outcrops on the seafloor have additionally modifying influence on the sedimentary processes.

1. Introduction

Shelf systems represent a major sink for terrestrial and marine sediments. Nevertheless, the understanding of these environments remains restricted due to the complex interplay of various factors such as changes in sea level, tectonics, morphology and oceanographic conditions. Within this framework, sedimentary processes that control supply, sorting, selective deposition, bypassing, winnowing, and re-mobilization of materials have major influence on the sediment distribution pattern. Tracing the fate of sediments on their paths between land and deep-sea basin helps us to increase the understanding of shelf sediment dynamics in general and provides a better insight into the interaction mechanisms of forcing factors and controlling processes.

During the past decades numerous studies have been carried out regarding the shelf water masses as well as surface sediments off NW Iberia in order to understand the present-day situation (OMEX II; van Weering and McCave, 2002). However, almost no downcore studies

* Corresponding author. Tel.: +49 421 218 65193; fax: +49 421 218 65219.
E-mail address: lantzsch@uni-bremen.de (H. Lantzsch).
[1] Present address: Cluster of Excellence: The Future Ocean, University of Kiel, Leibniz Institute of Marine Sciences (IFM-GEOMAR), Wischhofstr. 1-3, 24148 Kiel, Germany.

0025-3227/$ – see front matter © 2009 Elsevier B.V. All rights reserved.
doi:10.1016/j.margeo.2008.12.008

have been achieved to reveal the Late Quaternary shelf history. For instance, the first four radiocarbon ages from the Galician continental shelf were published by González-Álvarez et al. (2005) and only 14 additional dates were applied by Ferrín (2005), Martins et al. (2007) and Bernárdez et al. (2008). The first major studies concerning the stratigraphy of the NW Iberian shelf were achieved by Rey Salgado (1993) and Ferrín (2005). Nevertheless, their interpretations were mainly restricted to seismic data because core recovery in coarse deposition regimes on low-accumulation shelf systems presents significant challenges. Hence, the majority of shelf studies have focused mainly on muddy depocentres related to the present sea-level highstand, and the Late Quaternary sedimentary evolution remains scarcely known. With consideration of this gap of knowledge, we present new data from the NW Iberian shelf including a grid of shallow-seismic profiles and 18 well-dated sediment cores.

This study (1) reconstructs in a comprehensive manner the spatial and temporal architectural development of a low-accumulation shelf in relation to fluctuations in sea level, (2) describes the resulting depositional pattern, and (3) particularly elucidates the evolution of a major highstand depocentre.

2. Regional settings

2.1. Morphology and geology

The NW Iberian shelf is relatively narrow in the Spanish sector (~30 km), slightly broadening to the north and south with a maximum extension of about 40 km in front of the Minho River mouth (Fig. 1). The shelf break generally occurs in water depths of 160 to 180 m (Dias et al., 2002a). The break is obviously not cut by submarine canyons as is the case for the northern Portuguese continental shelf south of the Cávado River.

Prominent features on the NW Iberian shelf are rocky outcrops on the outer and inner shelf (Fig. 1; Rey Salgado, 1993; Dias et al., 2002a; Oliveira et al., 2002). Outcrops on the outer shelf consist of Mesozoic and Cenozoic rocks. On the inner shelf, rocks are described as plutonic and metamorphic bedrock.

The coastline along the Portuguese and the Spanish sectors shows notable morphological differences. The Spanish coast is comparably rough, characterised by a rocky topography and the four deep Rías Baixas which represent Tertiary river valleys, drowned during the last deglacial sea-level rise (Rey Salgado, 1993; Oliveira et al., 2002). In contrast, the Portuguese coastline in the south of the study area is smoother and characterised by the main estuaries of the Minho, Lima and Cávado River (Fig. 1). The large Douro River is situated 40 km southward of the study area.

2.2. Oceanography and sea-level history

The region of the NW Iberian shelf is characterised by strong seasonal variations in the water column and shows considerable changes in wind regime and oceanography between the winter and summer seasons (Fiuza et al., 1982; Drago et al., 1998). Several authors (Drago et al., 1998; Dias et al., 2002b; Vitorino et al., 2002) pointed out

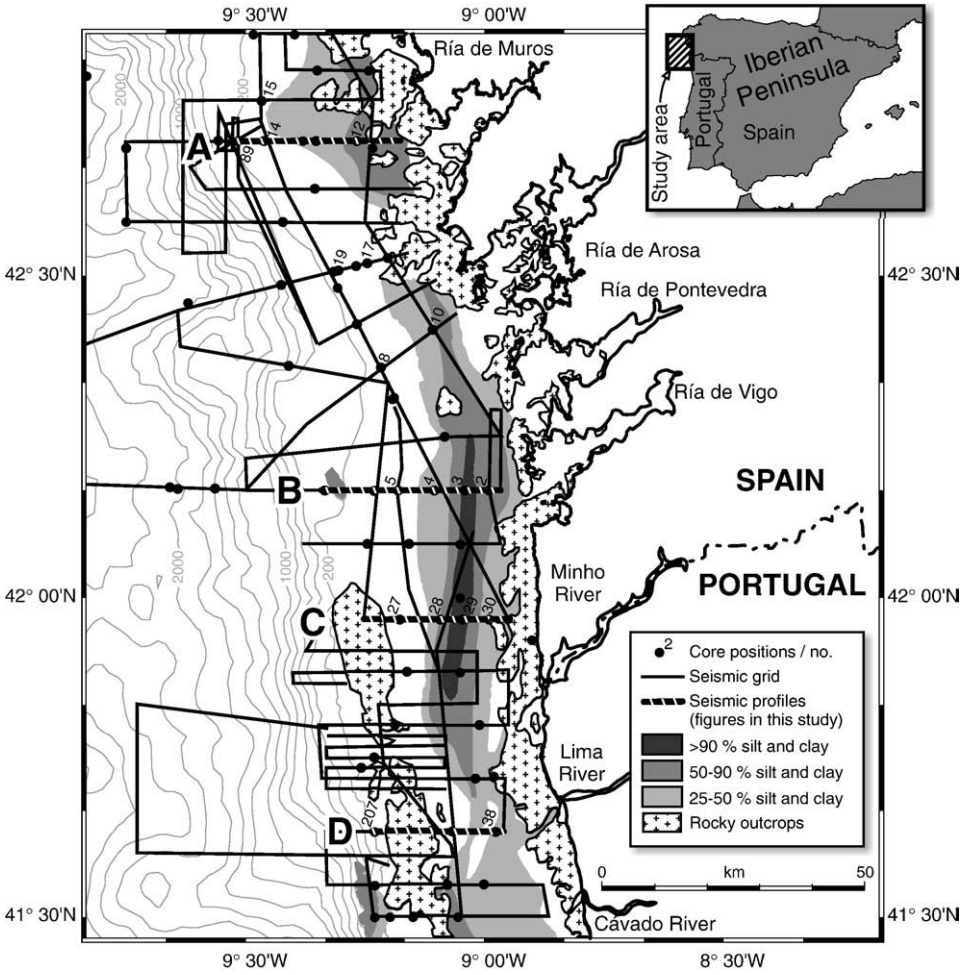

Fig. 1. Map of the study area, core positions and seismic profiles. Surface geology after Dias et al. (2002a). The Galicia Mud Belt is displayed in grey. Core positions of cruises P342 and P366 are marked by black dots. Cores used in this study are labelled in short form with e.g. 11*002*-3 and 11*038*-2 being positions 2 and 38 (P342), and 13*089*-2 and 13*0207*-3 being positions 89 and 207 (P366). Characters A to D represent seismic profiles shown in Figs. 2, 3 and 5.

Table 1
List of the *GALIOMAR* and GALIOMAR II sediment vibrocores of this study

Core no. (GeoB)	Latitude (N)	Longitude (W)	Water depth (m)	Recovery (m)
11002-3	42°10.00	8°59.24	111	4.34
11003-3	42°10.00	9°02.24	129	4.54
11004-2	42°10.00	9°06.17	141	3.78
11005-2	42°10.00	9°10.50	161	3.21
11008-2	42°21.29	9°13.00	157	3.77
11010-2	42°25.00	9°06.28	119	4.10
11012-2	42°42.29	9°16.00	119	4.28
11014-2	42°42.29	9°27.39	153	4.50
11015-2	42°46.11	9°27.58	159	4.94
11017-2	42°31.10	9°14.40	120	4.88
11019-2	42°30.28	9°18.16	149	4.92
11027-2	41°57.59	9°10.34	136	4.54
11028-2	41°57.59	9°05.29	127	4.59
11029-2	41°57.59	9°02.42	114	4.88
11030-2	41°58.00	8°59.24	94	4.60
11038-2	41°38.03	8°58.27	78	4.88
13089-2	42°42.48	9°31.00	190	4.90
130207-3	41°38.01	9°13.70	146	4.94

that the highly energetic regime and prevailing southerly winds during winter season result in (1) a poleward directed current on the mid-shelf, (2) a shelf-wide downwelling cell, and (3) intensified river runoff due to both increased overall precipitation and episodic river floods after storms. These conditions have been suggested to essentially control the modern sediment distribution on the shelf. In contrast, prevailing northerly winds in summer cause an equatorward directed along-shelf current and low-energy conditions, and favour temporal upwelling. These conditions are assumed to be of minor influence on the sedimentation pattern.

For the Late Quaternary time interval, the only available regional sea-level curve for the NW Iberian shelf was constructed by Dias (1985; later in Dias et al., 2000). However, this curve covering the past 20 ka (and frequently cited in the regional literature) does not fulfill the modern criteria of a sea-level curve. The reason is that pioneer-reconstructions from another continent from the 1960s were combined with undated morphological features of the NW Iberian shelf and were supported by only two radiocarbon dates. Therefore, we follow instead the latest eustatic sea-level reconstruction of Peltier and Fairbanks (2006) for a sound interpretation although we are aware that regional effects could have modified this global signal.

2.3. Sediment input, transport and deposition

The fluvial sediment supply to the NW Iberian shelf has been calculated to be approximately $2.25 \cdot 10^6$ t a^{-1} (Oliveira et al., 1982). The Douro River alone is assumed to contribute between 79 and 87% of this supply and is, therefore, the main source of fine sediments (Araújo et al., 2002; Dias et al., 2002a,b). In contrast, the Rías Baixas seem to play a minor role and mostly act as sediment traps (Rey Salgado, 1993).

Although the NW Iberian shelf is generally characterised by a sand cover, well defined areas of mud deposition are developed (Oliveira et al., 2002). Fine-grained fluviogenic sediments are frequently re-suspended by winter storms and transported to the north by the poleward flowing bottom current (Dias et al., 2000, 2002a). This input of fine sediments leads to the development of two confined muddy deposits in 110 to 120 m water depth on the NW Iberian shelf (Dias et al., 2002b).

Of these, the Galicia Mud Patch is a central feature in the study area (Fig. 1) whereas the Douro Mud Patch is situated further southward. Modern-day accumulation rates in these muddy areas range between 0.05 and 0.40 cm ka^{-1}. These rates are comparable to those of the mud

Table 2
Radiocarbon measurements and age calibration

Lab no.	Core no. (GeoB)	Depth in core (cm)	Material	^{14}C ages [a BP]	1σ calibrated [cal a BP][a]	Intercept [cal ka BP]	Stratigraphic position
KIA 33665	11002-3	250	bF	2715±35	2342–2455	2.40±0.06	U3
KIA 33664	11002-3	435	bF, bv pieces, gp	4955±45	5249–5388	5.32±0.07	U3
Poz-24670	11003-3	240	bF	7840±50	8259–8371	8.32±0.06	U3
Poz-22923	11003-3	360	bF	10,770±50	12,101–12,321	12.21±0.11	U3
Poz-24771	11003-3	399	bF	13,080±70	14,814–15,107	14.96±0.15	U2
KIA 33668	11004-2	277	bv piece	14,660±100	16,793–17,297	17.05±0.25	R1
Poz-22944	11005-2	250	*E. crispum*	18,470±100	21,160–21,689	21.42±0.26	R1
Poz-22945	11005-2	300	bF, bv pieces	46,000±3000	48,878–54,952[b]	51.91±3.04	U1
Poz-22946	11010-2	377	*E. crispum*	15,540±80	18,220–18,690	18.46±0.24	R1
Poz-22925	11012-2	100	bF	3995±35	3949–4068	4.01±0.06	U3
Poz-22948	11012-2	320	*E. crispum*	14,820±80	17,073–17,554	17.31±0.24	R1
KIA 33675	11014-2	441	bF, bv pieces	>42,580	uncalibrated	>42.58	U1
KIA 33692	11015-2	430	bF, bv pieces	30,710±670	35,016–36,496[b]	35.76±0.74	U1
KIA 33781	11015-2	448	Plant debris, char coal	49,140±2930	52,154–57,976[b]	55.07±2.91	U1
KIA 33683	11017-2	247	*E. crispum*	28,520±480	32,787–33,860[b]	33.32±0.54	U1
KIA 33684	11017-2	417	*E. crispum*	>42,090	uncalibrated	>42.09	U1
KIA 33685	11017-2	486	bF	>44,990	uncalibrated	>44.99	U1
KIA 33699	11027-2	49	*E. crispum*	17,040±130	19,567–19,900	19.74±0.17	U2
KIA 33700	11027-2	454	*E. crispum*	19,120±160	22,141–22,419	22.28±0.14	U2
Poz-21470	11028-2	140	bF	2555±30	2184–2290	2.24±0.05	U3
Poz-21471	11028-2	416	*E. crispum*	16,780±80	19,444–19,756	19.60±0.16	U2
Poz-22950	11028-2	429	*E. crispum*	17,310±190	19,862–20,243	20.05±0.19	R1
KIA 33687	11029-2	103	bF	850±30	458–503	0.48±0.02	U3
Poz-24772	11029-2	360	bF	2910±35	2669–2737	2.70±0.03	U3
KIA 33689	11029-2	488	Echinoderm pieces	12,740±80	14,082–14,475	14.28±0.20	U2
Poz-21472	11030-2	220	bF	2940±35	2693–2749	2.72±0.03	U3
Poz-21473	11030-2	460	bF, bv	10,740±50	12,035–12,255	12.15±0.11	U2
Poz-22951	11038-2	120	bF	3165±35	2888–3013	2.95±0.06	U3
Poz-22952	11038-2	460	bF, gp	16,880±90	19,501–19,793	19.65±0.15	U2
Poz-26862	13089-2	489	*E. crispum*	17,850±100	20,414–20,742	20.58±0.16	U2
Poz-26864	130207-3	430	bF	18,280±110	20,900–21,338	21.12±0.22	U2

[a] For reservoir correction, the conventional age of 400 years is applied using CALIB 5.0.1. (Stuiver et al., 1998).
[b] Reservoir correction based on the function of Bard et al. (1998).
bF = benthic foraminifers; *E. crispum* = *Elphidium crispum* (monospecific sample); bv = bivalve; gp = gastropod.

centres in the Bay of Biscay and on the Tagus Shelf (Jouanneau et al., 2002). Due to these relatively low accumulation rates and shelf-wide sand draping we consider the NW Iberian shelf as being controlled by a low-accumulation sedimentation regime.

The surface distribution of the Galicia Mud Patch was compiled by Dias et al. (2002a). Fig. 1 displays the present-day extent of this depocentre, defined by a mud content of more than 25%. Here, we introduce the term "Galicia Mud Belt" instead of "Galicia Mud Patch" due to its elongated shape running contour-parallel in mid-shelf position.

3. Materials and methods

3.1. Geophysical methods

Seismic data were collected by means of a Boomer and a high-resolution multichannel system running simultaneously during the *GALIOMAR* (Galician Ocean Margin) cruise in 2006 onboard the German research vessel *Poseidon* (P342). In total, about 1900 km of seismic lines were collected. The frequency band of the Boomer was between 500 Hz and 10 kHz with a main frequency of around 2–3 kHz. The Boomer was shot every second with a two second break every six shots for firing an airgun. The multichannel seismic data were obtained using a Mini-Generator–Injector-Airgun (main frequency ~300 Hz) and a 100-m long 16 channel streamer with a group distance of 6.25 m.

The Boomer data are used in this study to establish the Late Quaternary shelf stratigraphy. Where the penetration depth of the shallow-acoustic Boomer system was insufficient to get the exact position of the basement, the measurements of the high-resolution multichannel system were integrated.

3.2. Coring devices

In total, 66 sediment cores (up to 5-m long) were recovered on the NW Iberian shelf and at the continental slope during the *GALIOMAR* cruise (P342) in 2006 and GALIOMAR II expedition in 2008 (part of PERGAMOM cruise P366; Fig. 1 and Table 1). A vibrocorer was used down

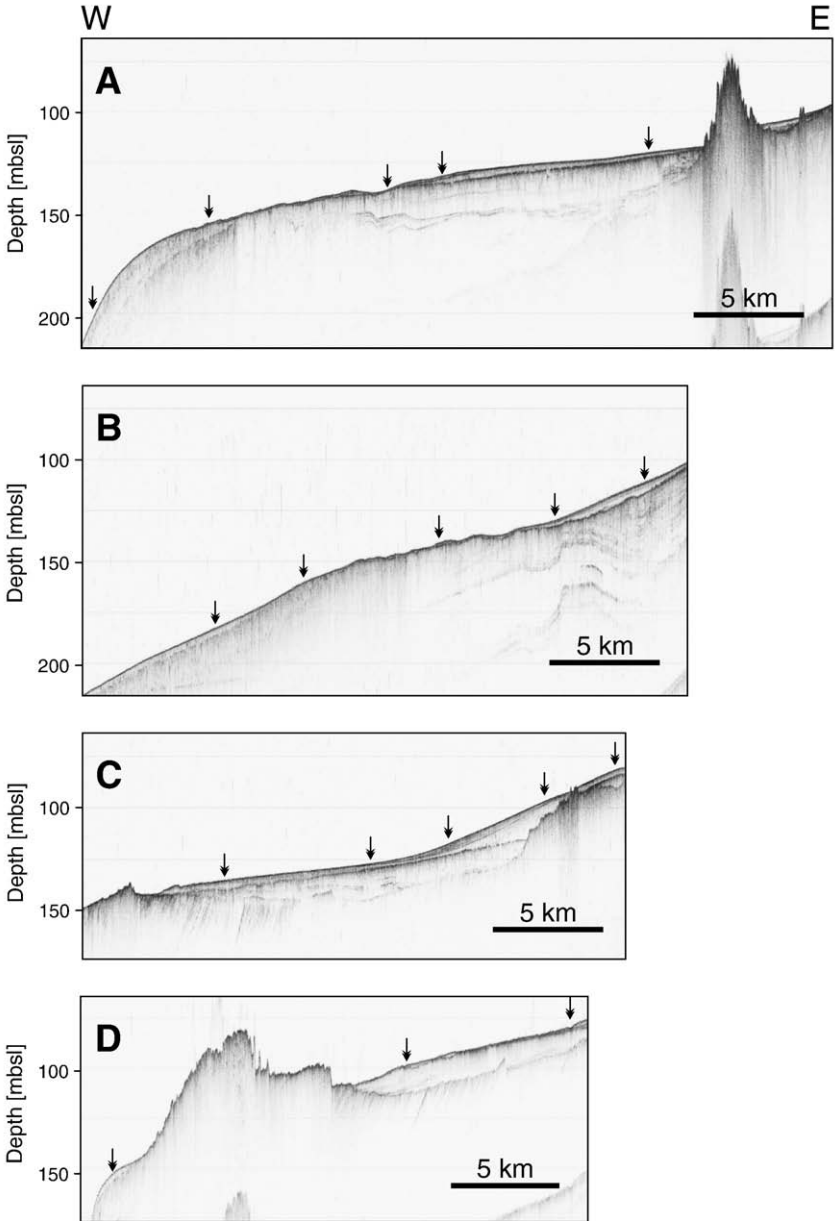

Fig. 2. Boomer profiles of the respective seismic Profiles A to D shown in Fig. 1 and interpreted shelf architecture. B: basement; EU: erosional unconformity; U1, U2, U3: main seismic units; R1, R2: seismic reflectors separating the units. Black arrows indicate sediment core positions. Boxes in the interpretation display magnifications shown in Fig. 3. Depth on *y*-axis is given in metres below modern sea level (mbsl).

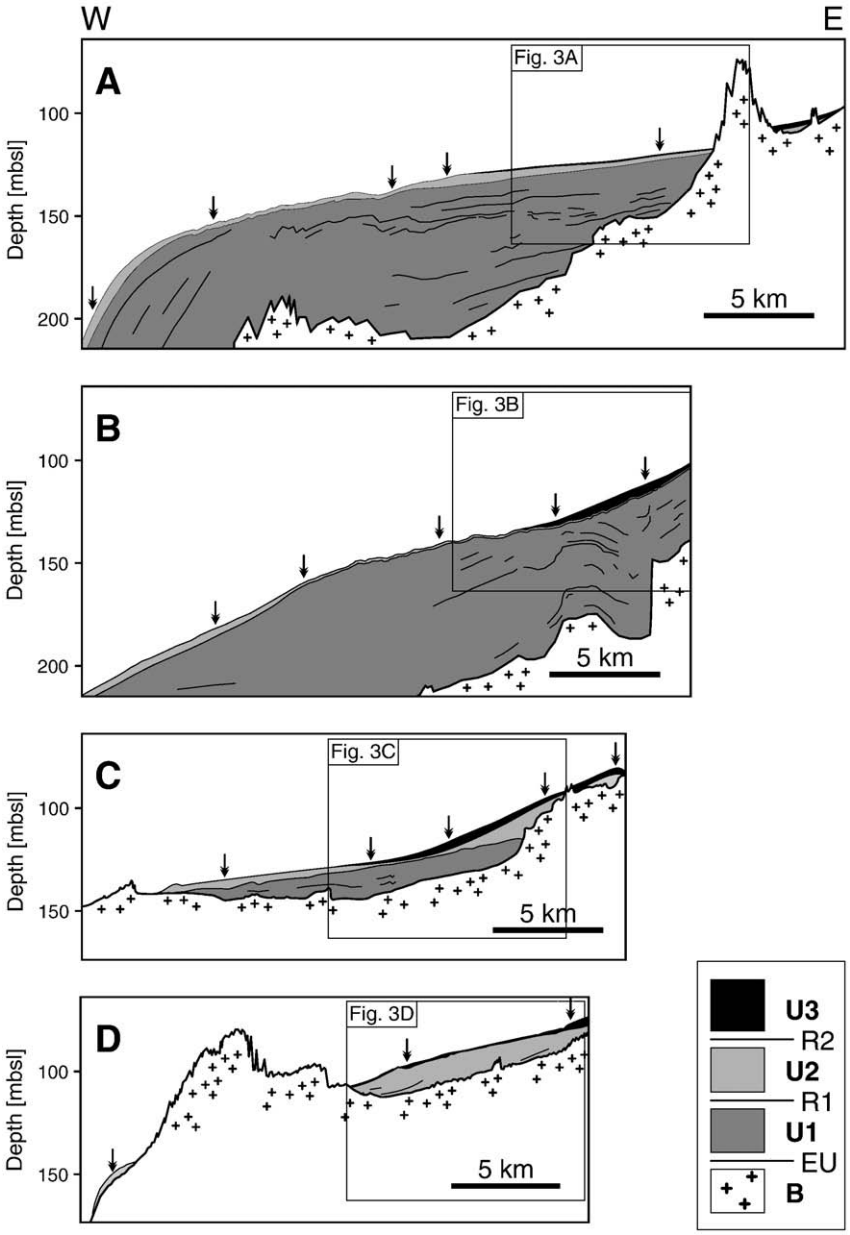

Fig. 2 (*continued*).

to 230 m water depth in places where the sediment was too coarse to retrieve material by gravity coring. Giant box cores were taken at every core location to sample the modern surface. In this study, the sedimentary reconstruction of the shelf architecture is based on the analysis of 18 vibrocores, which represent the range of sediments on the NW Iberian shelf.

3.3. Analyses in the lab

After detailed lithological description and photography, samples were taken at 20-cm intervals. These samples were split into fine and coarse fractions (<63 and >63 μm) by wet sieving. Afterwards, the coarse fraction was sonic-sifted into the grain-size subfractions 63–125 μm, 125–250 μm, 250–500 μm, 500–1000 μm and >1000 μm to obtain the grain-size distribution of the coarse fraction. The classification scheme of Blair and McPherson (1999) was used to determine the different grain-size classes from clay to gravel and the data obtained by grain-size measurement were used to corroborate the visual core description.

The selection of shelf material for radiocarbon dating is a complex issue. Age reversals might occur due to re-deposition of older material. In order to avoid age biasing, only delicate material of fresh preservation was carefully handpicked. Wherever applicable, monospecific samples were selected. However, due to the lack of such a material in some samples, a selection of benthic foraminifers and mollusc shells was necessary. Nevertheless, we found that also such material was of fresh condition and reliable for measurement. As a result, 31 radiocarbon dates on 16 analysed cores are displayed in this study (Table 2). The measurement was carried out by the Leibniz Laboratory in Kiel (Germany), and the Poznań Radiocarbon Laboratory (Poland). All radiocarbon dates are given in calibrated kiloyears before present (ka BP). They are corrected for a standard marine reservoir effect of 400 years and converted into 1-sigma calibrated ages using the program Calib 5.0.1 (Stuiver et al., 1998). Dates with a conventional age >22 ka are calibrated based on the function of Bard et al. (1998). The stratigraphic correlation was applied by combining the interpreted Boomer profiles, lithological facies analysis, and radiocarbon dating.

4. Results

4.1. Shelf architecture

Three main seismic units overly the basement (B) and define the architecture of the NW Iberian shelf (Fig. 2). The basement itself is characterised by a strong tectonic influence (Dias et al., 2002a; Muñoz et al., 2003) as can, for instance, be seen in the western part of Fig. 2C where tilted rocks are exposed on the outer shelf. These rocky outcrops are only present in the southern part of the study area (Fig. 2C, D). In contrast, outcrops on the inner shelf extend parallel to the coastline and are, for example, observed in the eastern parts of the Boomer Profiles A and C (Fig. 2A, C).

A major erosional unconformity surface (EU) separates the tilted basement from the overlying sediments of Units 1 to 3. The lowermost seismic Unit 1 (U1) is characterised by a transparent to semi-transparent seismic facies in the Boomer profiles with minor internal reflections showing an onlap pattern (Fig. 2A, B, C). These internal reflectors are often deformed by folding and follow elevations of tilted basement blocks (see eastern part of Fig. 2B). They appear frequently as local features in the Boomer profiles but also extend, in some cases, across wide parts of the shelf (Fig. 2A). However, the multichannel seismic data suggest that this variation in extension might be due to depth limitations of the Boomer system. The thickness of U1 is highly variable with a maximum thickness of about 75 m in the northernmost part (Fig. 2A) decreasing to the south and being absent south of the Minho River mouth (Fig. 2D).

Seismic Unit 2 (U2) is separated from U1 by a continuous high-amplitude reflector (R1), which can be traced across major parts of the shelf (Fig. 2A, B, C). With increasing water depths, the amplitude of R1 becomes weaker (western part of Fig. 2A, B). U2 is mainly transparent with only scarce internal reflection (Fig. 2D). A maximum thickness of 15 m is observed in the southernmost part of the study area (Fig. 2D). Northern parts of the shelf are characterised by a decreasing sediment thickness, usually to less than 5 m (Fig. 2A, B). However, U2 deposits are not restricted to the mid-shelf but up to 4-m thick deposits are found either beyond (Fig. 2A, B) or directly at the shelf break (Fig. 2D).

The uppermost unit, seismic Unit 3 (U3), is separated from U2 by a weak but continuous reflector (R2; Fig. 2). U3 shows a maximum thickness of about 4 m between the Minho River mouth and the Rías Baixas, representing the central part of this unit (Figs. 1 and 2B, C). A wedge-shaped appearance of U3 and distinct internal stratification are also restricted to this area of maximum thickness (Fig. 2B, C). In contrast, U3 forms a 1-m thin sheet in the northern part of the study area and no internal stratification can be observed within the resolution of the Boomer data, here (Fig. 2A). The latter is also the case for most parts of the southern study area, where the sheet-like U3 reaches a maximum thickness of approximately 3 m (Fig. 2D). Furthermore, U3 displays a gradual thinning in offshore as well as onshore direction. This is most obviously displayed by the lateral pinching out in Profiles B and C, but can also be detected in Profile A (Fig. 2A). The exception to this pattern is visible in the easternmost part of Profile C where sediments between rocky outcrops form an up to 3-m thick sediment

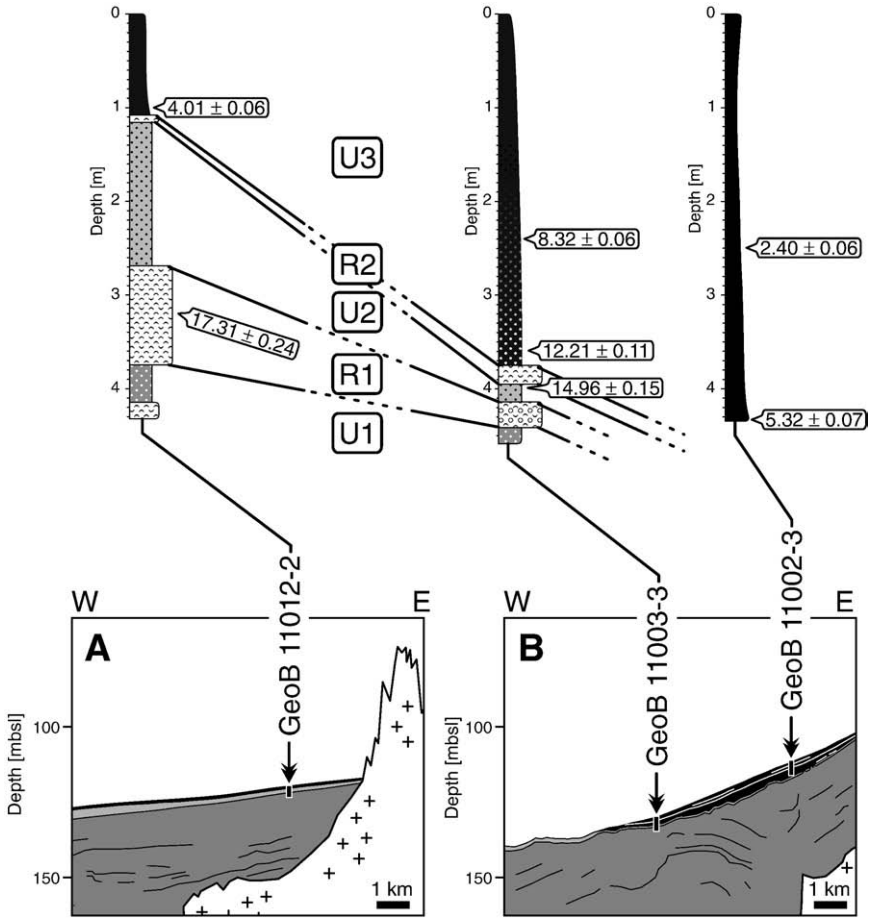

Fig. 3. Interpretations of the Boomer Profiles A to D and respective columns of sediment cores. Boxes display magnifications marked in Fig. 2. Core lithology, grain size and radiocarbon ages are shown in core columns above. All seismic units of the Boomer profiles are found in the sediment cores. U1 and U2 are mainly composed of fine sands and U3 is characterised by mud to muddy fine sands. Reflectors R1 and R2 extend across the shelf as gravel layers. Boomer interpretation, core lithology and radiocarbon measurements enable the correlation between single cores. Position of Profiles A–D is shown in Fig. 1.

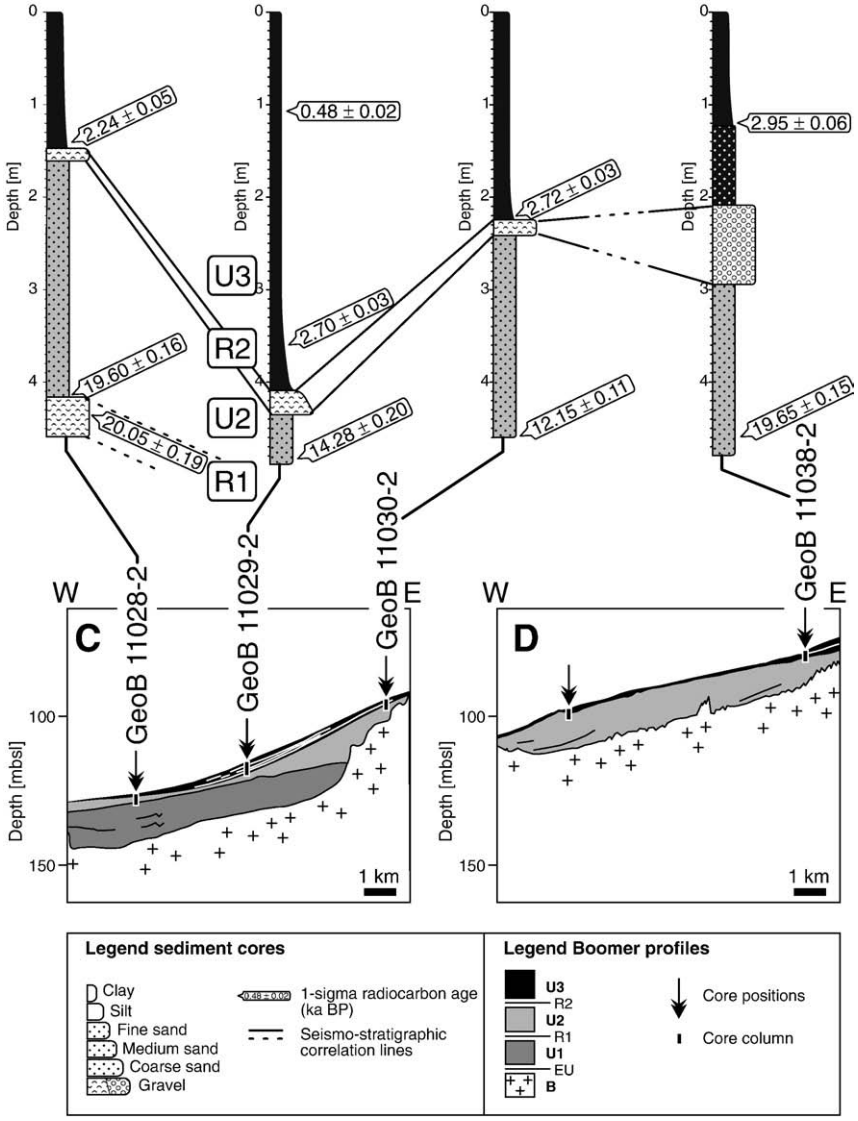

Fig. 3 (*continued*).

body on the inner shelf (Fig. 2C), and in Profile A where a 2-m thick layer deposited next to rocky outcrops in front of the Ría de Muros (Fig. 2A).

4.2. Sedimentary characteristics of the stratigraphical units

Sediment cores were retrieved at selected positions along the Boomer profiles to get insight into the sedimentary characteristics of these individual seismic units (Table 1). The sediments are mainly composed of either homogenous fine sands or homogenous mud, and show only subordinate variations in grain size (Fig. 3). These monotonous deposits are usually several metres thick. However, they are intersected by 0.1 to 1-m thick, coarse-sandy to gravelly beds which are composed of either shell fragments or siliceous gravel. Those drastic grain-size changes are observed in almost all of the cores (Fig. 3). These coarse beds are mirrored in the Boomer profiles by the above mentioned strong reflectors and can be used as stratigraphical marker horizons across the whole shelf. Consequently, the correlation between individual cores is done by combining the sedimentary facies characteristics and the stratigraphical interpretation of the Boomer profiles (Fig. 3). The results are then corroborated by radiocarbon age control (chapter 4.3).

Sediments from all three units overlying the basement were retrieved by coring. U1 is present in a number of cores, for instance in the lower part of Core 11012-2 in Profile A and of Core 11003-3 in Profile B (Fig. 3A, B). The sediments of U1 are mainly composed of grey homogenous fine sands (Fig. 4A) consisting of a mixture of siliciclastic and biogenous material of marine and terrigenous origin. Nevertheless, lateral variations of this facies are found, as documented, for instance, in the lower parts of Cores 11005-2 and 11008-2 (positions 5 and 8 in Fig. 1), where the homogenous fine sands of U1 are dominated by glauconite (Fig. 4B). Another prominent feature of U1 is rigid, yellowish brown to grey sediment with intercalations of clay and mica-rich silt and abundant organic material. These deposits occur in water depths lower than 150 m and a thickness of up to 90 cm was recovered at the bottom of Cores 11015-2 and 11019-2 (15 and 19 in Fig. 1; Fig. 4C).

The bed associated with R1, separating U1 and U2, was retrieved in the lower parts of the selected Cores 11012-2, 11003-3 and 11028-2 (Fig. 3A, B, C). These sediments consist mainly of coarse sands to gravel composed of shell fragments and complete valves (Fig. 4D). Bivalves are very common constituents. To a minor degree, also gastropods, scaphopods, serpulids are present, in complete preservation or fragmented.

U2 is present in all sediment cores of the profiles displayed in Fig. 3 (except for Core 11002-3 in Profile B), and is characterised by homogenous

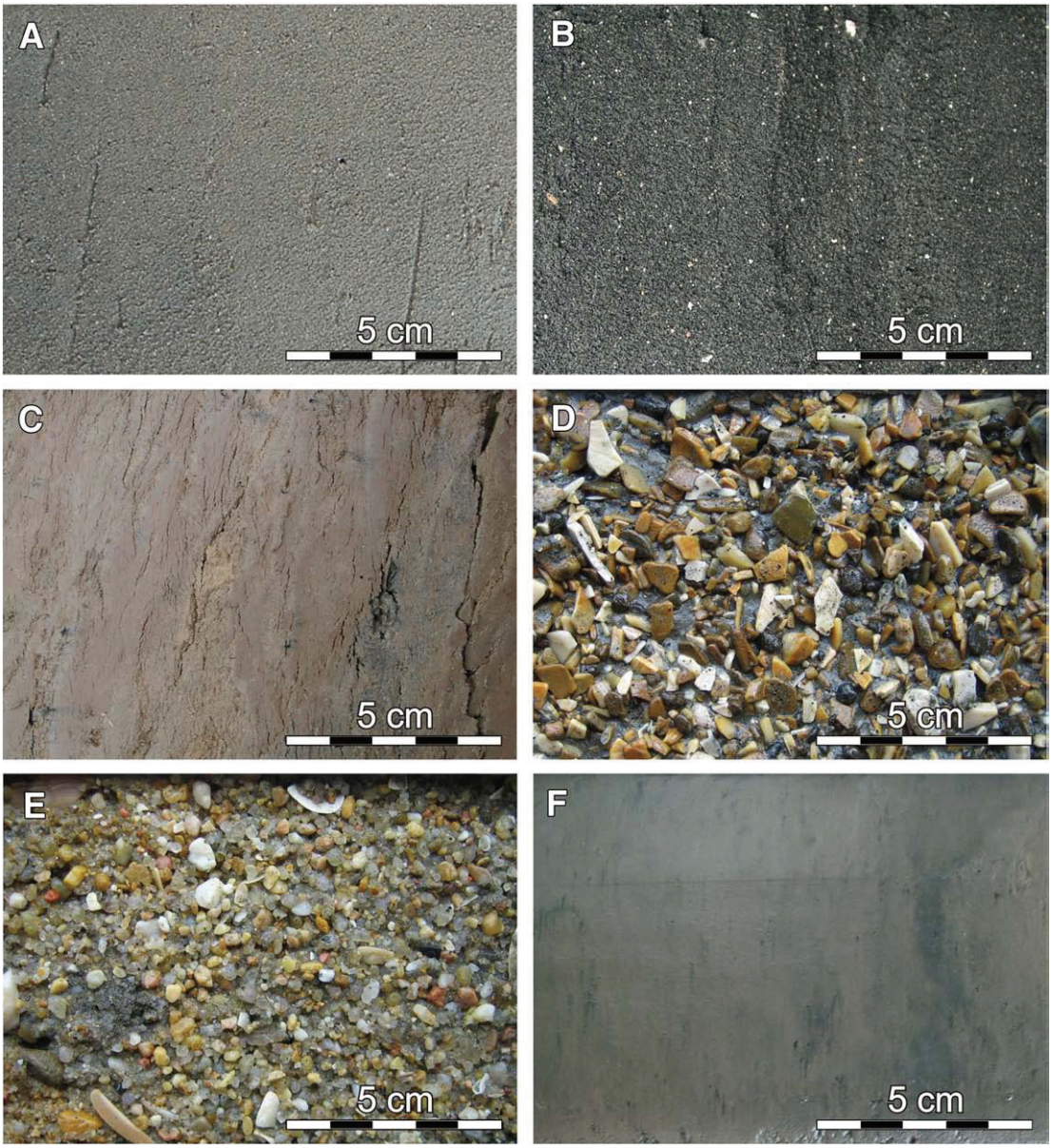

Fig. 4. Core images representing the variety of sediments deposited on the NW Iberian shelf. (A) Homogenous fine sand (exemplarily shown by Core 11027-2; 432–444 cm; U2; interpreted as regressive facies of U1 or transgressive deposits of U2); (B) glauconite-rich fine sand (11008-2; 230–242 cm; U1; outer shelf palimpsest facies); (C) overconsolidated clay (11015-2; 449–461 cm; U1; palaeosol facies); (D) shell fragment gravel (11028-2; 435–447 cm; R1; lag deposit); (E) siliceous gravel (11038-2; 279–291 cm; R2; shoreface deposit); and (F) mud (11029-2; 181–193 cm; U3; mud-belt facies). Core tops are directed to the left, core bottoms to the right.

fine sands that are comparable to the fine sands of U1 in terms of grain size and composition. Grey homogenous sands occur as well as dark greenish fine sands, which are dominated by glauconite (Fig. 4A, B).

A prominent gravel layer separates U2 and U3. These coarse deposits cause the seismic Reflector R2. Again, all sediment cores in the profiles displayed (Fig. 3; except for Core 11002-3) show this abrupt recurrence of a gravel bed, which again consists of shell fragments (Fig. 4D). Quartz is generally a minor component in this bed but can be the dominant constituent. This is the case in Core 11038-2 in the westernmost part of Profile D (Fig. 3D) in which coarse-grained, subangular to sub-rounded quartz makes up more than 70% of the bulk sediment (Fig. 4E).

Sediments of U3 are overlying the deposits of R2 in almost all displayed cores (Fig. 3). Only Core 11002-3 is entirely composed of U3 sediments (Fig. 3B). Generally, U3 can be subdivided into two sedimentary units, a lower unit composed of fine sands with less than 10% of fine material ($U3_s$) and an upper unit characterised by a mud content of more than 25% ($U3_m$). The fine-sandy sediments of $U3_s$ were observed in Cores 11003-3 and 11038-2 (Fig. 3B, D), whereas the muddy deposits of $U3_m$ are present in all displayed cores of Fig. 3. Three modes of the initial onset of $U3_m$ were observed: (1) a continuous fining upward from $U3_s$ towards $U3_m$ in Core 11003-3 (Fig. 3B), (2) the deposition of mud above an erosional unconformity, separating $U3_s$ and $U3_m$ in Core 11038-2 (Fig. 3D), and (3) an absence of $U3_s$ and a deposition of $U3_m$ above the coarse sediments of R2 (e.g. Fig. 3C). The spatial distribution of $U3_m$ deposits in the Boomer profiles correlates well with the present-day mud belt as mapped by Dias et al. (2002a; Fig. 1). Hence, sediments of $U3_m$ represent the mud-belt body in depth.

The thickness of this Galicia Mud Belt is highly variable. As demonstrated in Fig. 3, variations in mud-belt thickness are not only visualised in the Boomer profiles but are recorded in the cores. In Profile C (Fig. 3C), for instance, Core 11029-2 was retrieved from the central part of the mud belt and shows an increased thickness of about 4 m, whereas Cores 11028-2 and 11030-2 document marginal

parts of the mud belt, which is described by a decreasing thickness. Moreover, mud-belt sediments show a clear fining-upward trend in lower parts. Additionally, the Galicia Mud Belt shows a slight coarsening to silt or muddy fine sand in offshore as well as onshore directions. These trends are shown in Profile C (Fig. 3C). Core 11029-2 shows muddy sediments and the marginal Cores 11028-2 and 11030-2 consist mainly of silt to muddy fine sands. This coarsening also occurs towards the north and south of the main mud-belt centre, which is displayed by the occurrence of muddy fine sands in Cores 11012-2 and 11038-2 (Fig. 3A, D).

4.3. Age determination of the units

The uppermost part of U1 was dated in seven sediment cores (Table 2). Of these, five radiocarbon ages are older than 42 ka BP, i.e. beyond the measurement limitations of the radiocarbon method (Table 2). The youngest ages of U1 are 35.76±0.74 ka BP and 33.32±0.54 ka BP (Table 2).

The bed representing reflector R1, separating U1 and U2, was retrieved in 15 cores. Within this reflector, five radiocarbon samples were taken and show ages between 21.42±0.26 ka BP and 17.05±0.25 ka BP (Table 2).

U2 was dated in various cores of Profiles C and D (Fig. 3C, D). The radiocarbon ages measured display a range from 22.28±0.14 ka BP to 12.15±0.11 ka BP (Table 2). Thereof, the oldest radiocarbon ages of U2 were measured in outer-shelf cores (positions 27, 89 and 207 in Fig. 1) and the youngest ages were observed in mid-shelf position (3 and 29 in Fig. 1).

In contrast, the bed representing reflector R2, bordering U2 and U3, was not directly dated due to absence of freshly preserved carbonate material. Nevertheless, two radiocarbon dates, taken below and above R2 in Core 11003-3 (Fig. 3B), indicate that the bed formation at this core position must have taken place within the time interval after 14.96±0.15 ka BP and prior to 12.21±0.11 ka BP (Table 2).

The oldest age of U3 was measured within the $U3_s$ sediments of Core 11003-3 (12.21±0.11 ka BP; Fig. 3B) whereas the youngest age in this lower, sandy part of U3 dates at 8.32±0.06 ka BP. A date in Core 11002-3 shows that the transition from the fine-sandy $U3_s$ sediments to deposits of the Galicia Mud Belt ($U3_m$) already took place prior to 5.32±0.07 ka BP (Fig. 3B). Moreover, seven further measurements on the Galicia Mud Belt show a range between 4.01±0.06 ka BP and 0.48±0.02 ka BP (Table 2).

5. Discussion

There are few indications for the age of the basement (B) and for sediments of U1 in literature. Following the work of Rey Salgado (1993) and Dias et al. (2002a) the basement is of Precambrian to Cenozoic age.

U1 overlies the basement over wide parts of the study area. Succeeding internal reflectors within U1 show mainly a progradational to aggradational pattern. The timing and origin of these internal reflectors, however, remains speculative and depends on the stratigraphic interpretation of U1. According to the interpretation of Muñoz et al. (2003) sediments of U1 comprise Late Tertiary to Late Pleistocene sediments and were deformed by mainly normal faulting during the Neogene Betic Orogeny. Ferrín (2005), in contrast, suggested that U1 is composed of Upper Cretaceous to Upper Pliocene deposits. Hence, internal reflectors of U1 are most probably related to prominent sedimentary changes during Tertiary and Pleistocene times. However, these interpretations are almost exclusively based on seismic data and remain speculative. Radiocarbon ages of our study show that the youngest sediments of U1 have been deposited during the last glacial sea-level fall prior to the sea-level lowstand of the Last Glacial Maximum (LGM).

An ancient exposure surface within U1 is indicated by the occurrence of very stiff, yellowish brown to grey intercalations of clay and mica-rich silt in water depths of 150 to 160 m. Following the definition of Rohrlich et al. (1995) these deposits can be considered as overconsolidated and are interpreted as palaeosols. Two alternatives of exposure are conceivable: (1) these soils have developed during the LGM sea-level lowstand, when the eustatic sea-level was located at around 130 m below modern sea level (mbsl; Peltier and Fairbanks, 2006). Consequently, the position of this exposure surface would require an additional local shelf subsidence of about 30 m over the past 20 ka. (2) Alternatively, these palaeosols have originated during low sea levels in earlier Pleistocene times.

Generally, the local thickness of U1 seems to be largely controlled by differential elevation of the basement due to tectonic displacement, and erosion related to sea-level fluctuations. For instance, U1 is absent in the southern part of the study area (Fig. 2D). The local elevation of the basement here might have led to enhanced erosion during succeeding sea-level lowstands. In contrast, the northern part of the study area displays up to 75-m thick deposits of U1 (Fig. 2A, B). The deeper-situated basement surface in this region, thus, has probably caused the preservation of such U1 sediments.

Reflector R1, separating U1 from U2, with ages between 21 and 17 ka BP, is related to the LGM sea-level lowstand and earliest deglacial sea-level rise, respectively (Fig. 5A). The lower boundary of this bed represents, in fact, an erosional surface which probably originated during the last sea-level fall between 33 ka BP, the youngest age of U1, and the LGM. The deposition of coarse R1 sediments was then related to the LGM sea-level lowstand as well as to an early sea-level rise. These data show that the last sea-level lowstand was not only characterised by exposure surfaces and suggested lowstand deposits beyond the shelf break (as stated by Ferrín, 2005). Rather, this interval is documented by sedimentation on the shelf itself. Taking into account the significant deposition of coarse material, as observed in our records, the simplified interpretation as an erosional surface alone, as described by Rodrigues et al. (1991) and Ferrín (2005), is no longer suitable. Furthermore, the age range of R1 between 21 and 17 ka BP indicates that this reflector does not represent a single-event bed but that its formation as lag deposit was largely controlled by a long-lasting development. In this context, sea level and shelf bathymetry have strongly influenced the position of the particular shoreline, which must be considered as the main source of such coarse and shell-rich sediments. Additionally, the re-deposition of coarse material was most probably enhanced by the stronger impact of wave activity in this shallow-water zone.

Other examples of such reflectors, separating deposits of the last sea-level rise from older sediments, have been reported, for instance, from the Mersin Bay shelf, (NE Mediterranean Sea; Ergin et al., 1992; Okyar et al., 2005), the New Jersey continental shelf (Duncan et al., 2000) and the Californian shelf (Slater et al., 2002; Crockett and Nittrouer, 2004; Grossman et al., 2006). These reflectors are usually considered as indicating either a pre-Holocene erosional surface (Ergin et al., 1992; Slater et al., 2002) or a "Late Pleistocene–Early Holocene erosional–depositional surface" (Okyar et al., 2005; Grossman et al., 2006). In contrast, Duncan et al. (2000) suggested for the New Jersey continental shelf that this prominent reflector represents the ravinement surface of the Late Pleistocene regression (120 to 25 ka BP). Our radiocarbon dates of R1 show that the formation of the R1 bed in association with this phase of sea-level fall can be excluded on the NW Iberian shelf. The occurrence of reflectors comparable to R1 on various other shelves might suggest a similar mechanism of formation. It is, however, unlikely that all shelves have experienced changes in oceanography, tectonics, morphology and sedimentary processes in the same way. Therefore, eustatic sea-level fluctuations would be the force of equivalent global effect on the buildup of these extensive reflectors on the different shelves.

The timing of the emplacement of U2 is well documented by radiocarbon dating indicating that the initial onset of this unit had already taken place during the LGM, right after the formation of R1 (Fig. 3C; Table 2). Other radiocarbon ages measured in U2 indicate that

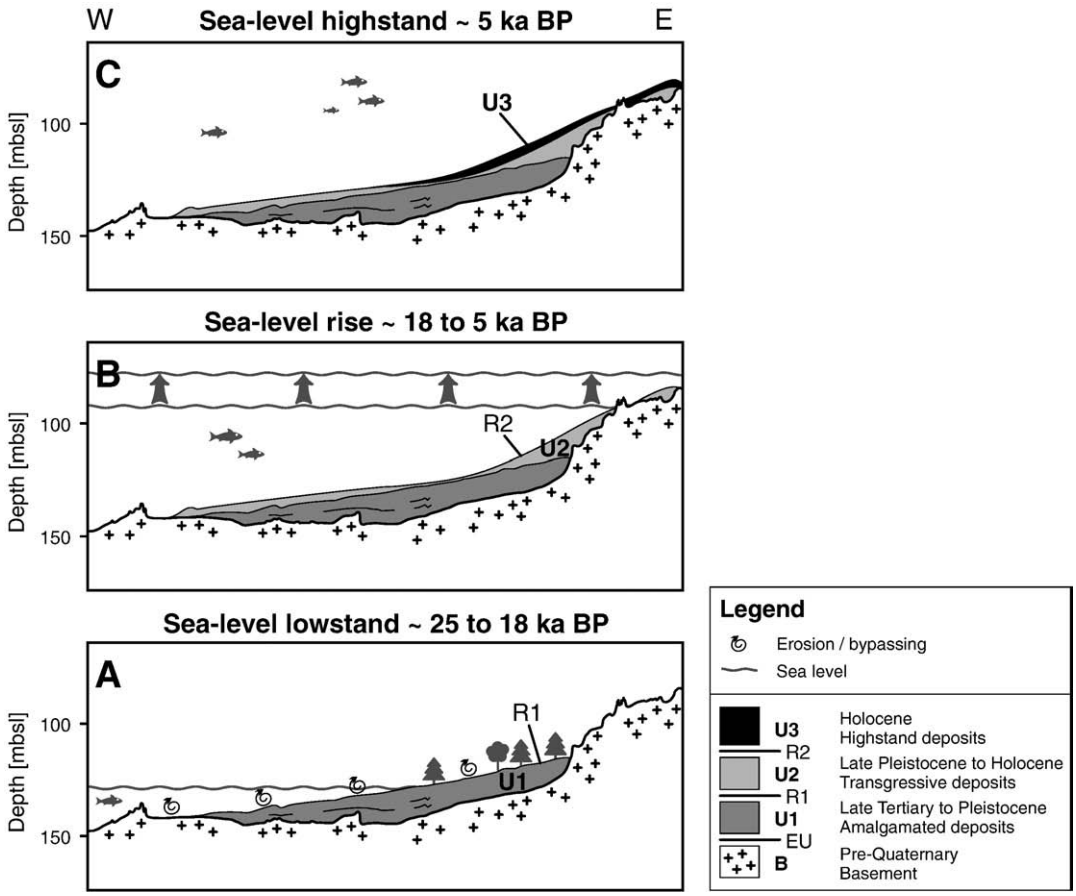

Fig. 5. Scheme of the Late Pleistocene–Holocene shelf evolution related to the superordinated sea-level history along Profile C. The development of seismic reflector R1 during the last sea-level lowstand and early sea-level rise is followed by the deposition of U2 sediments and the formation of reflector R2. (U3) represents the main depocentre during the modern sea-level highstand.

this unit was mainly built up during the time of deglacial sea-level rise (Figs. 3C; 5B). Consequently, a time-transgressive trend can be observed in Profile C with the oldest age occurring on the outer shelf in a water depth of 127 mbsl (19 ka BP) getting younger in landward direction to 14 ka BP in 114 mbsl and to 12 ka BP in 94 mbsl in mid-shelf position (Fig. 3C). This landward shift implies that the development of U2 was largely controlled by the respective position of the sea level (Fig. 5B). However, the irregular thickness distribution of U2 shows that the sea level was not the exclusive factor controlling the architectural development of the sedimentary shelf system. Instead, the increasing thickness of U2 in the southern part of the study area (Fig. 2D) is probably related either to shelf morphology or to sediment input. The pronounced shape of rocky outcrops on the outer shelf has most likely sheltered mid-shelf deposits against stronger wave and current impacts during sea-level rise. An alternative explanation for thicker deposits in the southern sector would be a higher sediment input. Rodrigues et al. (1991) and Dias et al. (2000) proposed a large fluvial palaeo-drainage system south of the Minho River mouth aligned in a SSE–NNW direction. This system could have delivered large amounts of sediments. However, we have to state that not any incision or other remnants of a drowned fluvial system are observed in our study area.

The deposits of U2 predominantly consist of homogenous fine sands that were deposited, respectively re-deposited in the run of the sea-level rise. The coast was retreating landward and the lower wave base during times of lower sea level led to reworking of shelf deposits and winnowing of fines. Additionally, sediment contribution by rivers was probable higher and sandy material was exported to the shelf prior to the flooding of the estuaries during late sea-level rise.

Reflector R2 separates seismic Units 2 and 3 from each other (Fig. 5B). Radiocarbon ages below and above R2 in 129 m water depth define a time span of formation between 14.9 and 12.2 ka BP (Fig. 3B). In contrast, an age of 12.1 ka BP, measured within the underlying U2 in 94 m water depth, indicates again a time-transgressive evolution of R2. Therefore, the time interval between 14.9 and 12.2 ka BP was characterised by both, R2 deposition on the outer part of the shelf, and simultaneous U2 sedimentation on the inner shelf. Necessary transport energy of the coarse R2 deposits suggests a high-energy environment and the time-transgressive trend points again to the rising sea level as driving force. Peltier and Fairbanks (2006) and Hanebuth et al. (2000) described a rapidly rising sea level from 100 mbsl at 15 ka BP to 50 mbsl at 12 ka BP. It is conceivable that the depocentre of coarse material shifted towards the inner shelf during this time.

Erosional surfaces and coarse layers, comparable to R2, were described by several authors e.g. from the New Jersey continental shelf and the Californian shelf (Duncan et al., 2000; Grossman et al., 2006). However, the interpretations vary largely. Grossman et al. (2006) relate a lithological transition from transgressive sands and gravels towards massive silt drape at about 11.5 ka BP to the Melt-Water Pulse 1B event. Duncan et al. (2000) described a seismic reflector between 12.3 and 10.5 ka BP and interpret this feature as a flooding surface internal to a transgressive systems tract. On the NW Iberian continental shelf, Ferrín (2005) proposed a regressive nature of a coarse deposit but without a confirmation by radiocarbon dating. In contrast, González-Álvarez et al. (2005), García-García et al. (2005) and Durán et al. (2007) related a basal coarse layer, respectively an erosional surface to the age interval of the Younger Dryas (11 to 10 ka BP; YD). Our study shows, in contrast, that deposition of R2 material was not confined to the YD time interval. The retrogradational shift of R2, as well as of U2, shows that the occurrence of main sedimentary units on low-accumulation shelves is not necessarily restricted to a certain time interval. Rather, one unit can

record a longer time interval, such as initial deposition during a sea-level lowstand and subsequent sedimentation during a succeeding sea-level rise. Therefore, correlation between a series of cores does not necessarily reveal contemporaneous deposition, but links shifting zones of deposition, which are characterised by a similar genetic background, for instance a formation during the rising sea-level.

Generally, the entire U3 is interpreted to include sediments of both, the late sea-level rise ($U3_s$) and the modern sea-level highstand ($U3_m$; Fig. 5C). However, U3 is not distributed equally over the shelf. On outer parts of the shelf, the deposition of U3 is restricted to low marine background sedimentation (mainly planktonic and benthic foraminifera) on fine-sandy palimpsest deposits, as described by Dias and Nittrouer (1984) for this region. In contrast, the Galicia Mud Belt in mid-shelf position and inner parts of the shelf show a higher thickness of U3 sediments. This is, for instance, the case in the easternmost part of Profile C where sediments are trapped between rocky outcrops on the inner shelf and form an up to 3-m thick sediment body (Fig. 2C). Profile A shows a comparable feature but the sedimentary setting is different. There, a 2-m thick layer is deposited next to rocky outcrops but its increased thickness seems to be related to local sediment input from the Ría de Muros (Fig. 2A). Therefore, the U3 thickness in these inner-shelf areas is controlled by a combination of sediment input and shelf morphology.

The fine-sandy deposits of $U3_s$ document the time interval between R2 deposition and the initial formation of the Galicia Mud Belt ($U3_m$; Fig. 3B). However, in most of the cores either non-deposition or subsequent erosion occurred in this time interval. Depositional remnants of $U3_s$ are only observed in Profiles C and D (Fig. 3C, D).

The oldest measured age of $U3_m$ indicates that the transition from $U3_s$ to $U3_m$ had already taken place in the time interval between 8.3 and 5.3 ka BP (Fig. 3B). Hence, the initial onset of the Galicia Mud Belt is displayed by a gradual development from fine sands towards mud deposition and is presumed to have taken place in the region of Profile B (Fig. 3B).

The sea-level curve of Peltier and Fairbanks (2006) indicates that the modern sea level was established at around 5 ka BP. Radiocarbon dates, taken directly from the base of the Galicia Mud Belt ($U3_m$), mostly record ages between 5.3 and 2.2 ka BP. Therefore, this depocentre has formed during the modern sea-level highstand. Furthermore, radiocarbon ages of our study indicate that the Galicia Mud Belt has been the main depocentre for fluvially supplied fine material on the NW Iberian shelf not only since 2.8 ka BP, as proposed by González-Álvarez et al. (2005), or 4.8 ka, as shown by Martins et al. (2007) and Bernárdez et al. (2008), but at least since 5.3 ka BP.

The initial onset of the Galicia Mud Belt was most probably related to a shift in the balance between sea-level rise and sediment supply. This balance is probably of major influence on the rate of fluvial sediment export towards the shelf. Generally, Long (2001) stated that between 7.8 and 4.4 ka BP the available accommodation space within estuaries was largely filled by very rapid sedimentation due to the early Holocene deceleration in the rate of sea-level rise. This proposed time interval is in agreement with studies of the Gulf of Cadiz (Dabrio et al., 2000) and Tagus River valley (Vis et al., 2008). In addition, Sommerfield and Wheatcroft (2007) proposed a Holocene transition from estuary- to shelf-centred mud accumulation at the northern California shelf. Since the Douro River is considered as the main source for mud-belt sediments, the initiation of the Galicia Mud Belt should be related to the evolution of this river. A change from a continental sedimentary facies towards marine conditions inside the Douro River valley related to the early Holocene flooding of this estuary was observed from 9.8 to about 6 ka BP (Drago et al., 2006). Afterwards, a gradual filling of the estuary and the evolution of a gravel barrier is documented by Drago et al. (2006) and Naughton et al. (2007), indicating a transition from sediment trapping inside the inundated estuary towards sediment export to the shelf. Hence, this transition and the timing of the first onset of the Galicia Mud Belt indicates that the balance between rate of sea-level rise and sediment supply, and the decreasing accommodation space within the estuary were the key factors for initial mud-belt deposition on the NW Iberian shelf. This accumulation of mud was confined to structural lows on the middle shelf (Fig. 3B), that have sheltered these sediments against the erosion by currents and waves.

6. Conclusions

The NW Iberian shelf provides a well-suited example for the stratigraphic construction of a low-accumulation sedimentary shelf system. Three main stratigraphical units are identified on top of a basal unconformity. The lowermost Unit 1 is considered to represent stacked Late Tertiary to Pleistocene deposits, including sediments related to the last glacial sea-level fall. Unit 2 is related to the LGM sea-level lowstand and early deglacial sea-level rise. Unit 3 comprises deposits of the late deglacial sea-level rise and Holocene sea-level highstand. These individual units are separated by strong seismic reflectors that are related to the last glacial sea-level lowstand and late deglacial transgression.

Sediments from all of these units are recovered by coring. Pre-Holocene sediments are predominately composed of homogenous fine sands controlled by the position of sea level and wave base. Also, palaeosols are recovered for the first time on the NW Iberian shelf indicating an ancient exposure of large areas of the shelf. Strong reflectors, bounding the individual units, represent not only erosional surfaces but consist of considerable coarse-grained beds. Sedimentation during the Late Holocene sea-level highstand is mainly restricted to mud deposition in mid-shelf position, forming a mud belt. The Galicia Mud Belt was the main depocentre over at least the past 5.32 ka BP. Its initial formation was related to a shift in the balance between sea-level rise and sediment supply.

This study shows that sea-level changes represent the major force controlling the stratigraphic framework on low-accumulation shelves. Sediment input and other forcing factors such as the morphologic influence of rocky barriers and tectonically induced differences in the elevation of the basement strongly influence the sediment distribution within such a framework. Further work should focus on spatial and temporal variations in sediment composition on local scale to reveal the impact of individual external forces and internal processes on both, sediment distribution pattern as well as material residence times and shelf storage capacities, respectively.

Acknowledgements

Special thanks go to Hannes Riepshoff for his contribution to this project. We also wish to thank Captain Michael Schneider and his complete crew on *RV Poseidon* for their outstanding support, and two anonymous reviewers for constructive comments. We are thankful to Prof. Rüdiger Henrich for providing the laboratory facilities. Furthermore, BSH (Bundesanstalt für Seeschifffahrt und Hydrographie) is acknowledged for providing the Boomer system. This work was funded through DFG-Research Center / Excellence Cluster "The Ocean in the Earth System".

References

Araújo, M.F., Jouanneau, J.M., Valério, P., Barbosa, T., Gouveia, A., Weber, O., Oliveira, A., Rodrigues, A., Dias, J.M.A., 2002. Geochemical tracers of northern Portuguese estuarine sediments on the shelf. Prog. Oceanogr. 52 (2–4), 277–297.

Bard, E., Arnold, M., Hamelin, B., Tisnerat-Laborde, N., Cabioch, G., 1998. Radiocarbon calibration by means of mass spectrometric Th-230/U-234 and C-14 ages of corals: an updated database including samples from Barbados, Mururoa and Tahiti. Radiocarbon 40 (3), 1085–1092.

Bernárdez, P., González-Álvarez, R., Francés, G., Prego, R., Bárcena, M.A., Romero, O.E., 2008. Late Holocene history of the rainfall in the NW Iberian peninsula—evidence from a marine record. J. Mar. Syst. 72 (1–4), 366–382.

Blair, T.C., McPherson, J.G., 1999. Grain-size and textural classification of coarse sedimentary particles. J. Sediment. Res. 69 (1), 6–19.

Crockett, J.S., Nittrouer, C.A., 2004. The sandy inner shelf as a repository for muddy sediment: an example from Northern California. Cont. Shelf Res. 24 (1), 55–73.
Dabrio, C.J., Zazo, C., Goy, J.L., Sierro, F.J., Borja, F., Lario, J., González, J.A., Flores, J.A., 2000. Depositional history of estuarine infill during the last postglacial transgression (Gulf of Cadiz, Southern Spain). Mar. Geol. 162 (2–4), 381–404.
Dias, J.M.A., 1985. Registos da migração da linha de costa nos últimos 18.000 anos na plataforma continental portuguesa setentrional. 1a. Reun. Quat. Ibérico 1, 281–285.
Dias, J.M.A., Nittrouer, C.A., 1984. Continental shelf sediments of northern Portugal. Cont. Shelf Res. 3 (2), 147–165.
Dias, J.M.A., Boski, T., Rodrigues, A., Magalhães, F., 2000. Coast line evolution in Portugal since the Last Glacial Maximum until present—a synthesis. Mar. Geol. 170 (1–2), 177–186.
Dias, J.M.A., Gonzalez, R., Garcia, C., Diaz-del-Rio, V., 2002a. Sediment distribution patterns on the Galicia-Minho continental shelf. Prog. Oceanogr. 52 (2–4), 215–231.
Dias, J.M.A., Jouanneau, J.M., Gonzalez, R., Araújo, M.F., Drago, T., Garcia, C., Oliveira, A., Rodrigues, A., Vitorino, J., Weber, O., 2002b. Present day sedimentary processes on the northern Iberian shelf. Prog. Oceanogr. 52 (2–4), 249–259.
Drago, T., Oliveira, A., Magalhães, F., Cascalho, J., Jouanneau, J.M., Vitorino, J., 1998. Some evidences of northward fine sediment transport in the northern Portuguese continental shelf. Oceanol. Acta 21 (2), 223–231.
Drago, T., Freitas, C., Rocha, F., Moreno, J., Cachao, M., Naughton, F., Fradique, C., Araujo, F., Silveira, T., Oliveira, A., Cascalho, J., Fatela, F., 2006. Paleoenvironmental evolution of estuarine systems during the last 14,000 years—the case of Douro estuary (NW Portugal). J. Coast. Res. 1, 186–192.
Duncan, C.S., Goff, J.A., Austin, J.A., Fulthorpe, C.S., 2000. Tracking the last sea-level cycle: seafloor morphology and shallow stratigraphy of the latest Quaternary New Jersey middle continental shelf. Mar. Geol. 170 (3–4), 395–421.
Durán, R., García-Gil, S., Diez, R., Vilas, F., 2007. Stratigraphic framework of gas accumulations in the Ría de Pontevedra (NW Spain). Geo Mar. Lett. 27 (2–4), 77–88.
Ergin, M., Okyar, M., Timur, K., 1992. Seismic stratigraphy and late quaternary sediments in inner and mid-shelf areas of eastern Mersin Bay, northeastern Mediterranean Sea. Mar. Geol. 104 (1–4), 73–91.
Ferrín, A., 2005. Cenozoic Seismic Stratigraphy of the SW Galician Continental Shelf. Comparative Study With the Canterbury Shelf (SE New Zealand) During the Quaternary. Ph.D. thesis, Facultad de Ciencas del Mar, Departmento de Geociencias Marinas y Ordenación del Territorio, Universidad de Vigo, Spain.
Fiuza, A.F.D., Demacedo, M.E., Guerreiro, M.R., 1982. Climatological space and time variation of the Portuguese coastal upwelling. Oceanol. Acta 5 (1), 31–40.
García-García, A., García-Gil, S., Vilas, F., 2005. Quaternary evolution of the Ría de Vigo, Spain. Mar. Geol. 220 (1–4), 153–179.
González-Álvarez, R., Bernárdez, P., Pena, L.D., Francés, G., Prego, R., Diz, P., Vilas, F., 2005. Paleoclimatic evolution of the Galician continental shelf (NW of Spain) during the last 3000 years: from a storm regime to present conditions. J. Mar. Syst. 54 (1–4), 245–260.
Grossman, E.E., Eittreim, S.L., Field, M.E., Wong, F.L., 2006. Shallow stratigraphy and sedimentation history during high-frequency sea-level changes on the central California shelf. Cont. Shelf Res. 26 (10), 1217–1239.
Hanebuth, T., Stattegger, K., Grootes, P.M., 2000. Rapid flooding of the Sunda Shelf: a late-glacial sea-level record. Science 288 (5468), 1033–1035.
Jouanneau, J.M., Weber, O., Drago, T., Rodrigues, A., Oliveira, A., Dias, J.M.A., Garcia, C., Schmidt, S., Reyss, J.L., 2002. Recent sedimentation and sedimentary budgets on the western Iberian shelf. Prog. Oceanogr. 52 (2–4), 261–275.
Long, A., 2001. Mid-Holocene sea-level change and coastal evolution. Prog. Phys. Geogr. 25 (3), 399–408.
Martins, V., Dubert, J., Jouanneau, J.-M., Weber, O., da Silva, E.F., Patinha, C., Alveirinho Dias, J.M., Rocha, F., 2007. A multiproxy approach of the Holocene evolution of shelf-slope circulation on the NW Iberian Continental Shelf. Mar. Geol. 239 (1–2), 1–18.
Muñoz, A., Acosta, J., Uchupi, E., 2003. Cenozoic tectonics on the Galicia margin, northwest Spain. Geo Mar. Lett. 23 (1), 72–80.
Naughton, F., Goñi, M.F.S., Drago, T., Freitas, M.C., Oliveira, A., 2007. Holocene changes in the Douro estuary (Northwestern Iberia). J. Coast. Res. 23 (3), 711–720.
Okyar, M., Ergin, M., Evans, G., 2005. Seismic stratigraphy of Late Quaternary sediments of western Mersin Bay shelf, (NE Mediterranean Sea). Mar. Geol. 220 (1–4), 113–130.
Oliveira, I., Valle, A., Miranda, F., 1982. Litoral problems in the portuguese west coast. Proc. 18th Coastal Eng. Conf. 3, 1951–1969.
Oliveira, A., Rocha, F., Rodrigues, A., Jouanneau, J., Dias, A., Weber, O., Gomes, C., 2002. Clay minerals from the sedimentary cover from the Northwest Iberian shelf. Prog. Oceanogr. 52 (2–4), 233–247.
Peltier, W.R., Fairbanks, R.G., 2006. Global glacial ice volume and Last Glacial Maximum duration from an extended Barbados sea level record. Quat. Sci. Rev. 25 (23–24), 3322–3337.
Rey Salgado, J., 1993. Relacion morphose dimentaria entre la platforma continental de Galicia y las Rias bajas y su evolucion durante el Cuaternario. Publ. Espec.-Inst. Oceanogr. 17, 1–233.
Rodrigues, A., Magalhães, F., Dias, J.A., 1991. Evolution of the North Portuguese coast in the last 18,000 years. Quat. Int. 9, 67–74.
Rohrlich, V., Wiseman, G., Komornik, A., 1995. Overconsolidated clays from the Israeli Mediterranean coast and inner shore. Eng. Geol. 39 (1–2), 87–94.
Slater, R.A., Gorsline, D.S., Kolpack, R.L., Shiller, G.I., 2002. Post-glacial sediments of the Californian shelf from Cape San Martin to the US–Mexico border. Quat. Int. 92 (1), 45–61.
Sommerfield, C.K., Wheatcroft, R.A., 2007. Late Holocene sediment accumulation on the northern California shelf: oceanic, fluvial, and anthropogenic influences. Geol. Soc. Amer. Bull. 119 (9–10), 1120–1134.
Stuiver, M., Reimer, P.J., Bard, E., Beck, J.W., Burr, G.S., Hughen, K.A., Kromer, B., McCormac, G., Van der Plicht, J., Spurk, M., 1998. INTCAL98 radiocarbon age calibration, 24,000-0 cal BP. Radiocarbon 40 (3), 1041–1083.
van Weering, T.C.E., McCave, I.N., 2002. Benthic processes and dynamics at the NW Iberian margin: an introduction. Prog. Oceanogr. 52 (2–4), 123–128.
Vis, G.-J., Kasse, C., Vandenberghe, J., 2008. Late Pleistocene and Holocene palaeogeography of the Lower Tagus Valley (Portugal): effects of relative sea level, valley morphology and sediment supply. Quat. Sci. Rev. 27 (17–18), 1682–1709.
Vitorino, J., Oliveira, A., Jouanneau, J.M., Drago, T., 2002. Winter dynamics on the northern Portuguese shelf. Part 1: physical processes. Prog. Oceanogr. 52 (2–4), 129–153.

3. Reconfiguration of a high-energy, low-accumulation sedimentary shelf system since the Last Glacial Maximum (NW Iberia)

Hendrik Lantzsch, Till J.J. Hanebuth , Rüdiger Henrich

Manuscript, ready for submission to Continental Shelf Research

Reconfiguration of a high-energy, low-accumulation sedimentary shelf system since the Last Glacial Maximum (NW Iberia)

Hendrik Lantzsch[1], Till J.J. Hanebuth[1], Rüdiger Henrich[1]

[1] *MARUM – Center for Marine Environmental Sciences and Faculty of Geosciences, University of Bremen, P.O. Box 330 440, 28334 Bremen, Germany.*

Manuscript, ready for submission to Continental Shelf Research

Abstract

Based on a well-established stratigraphic framework and 47 AMS-^{14}C dated sediment cores the distribution of facies types on the NW Iberian margin is analysed in its spatial and temporal context in response to the last deglacial sea-level rise, thus providing a case study on the sedimentary evolution of a high-energy, low-accumulation shelf system.

Altogether, four main types of sedimentary facies are defined. (1) A gravel-dominated facies occurs mostly as time-transgressive ravinement bed, which initially developed as shoreface and storm deposits in shallow waters on the outer shelf during the last sea-level lowstand; (2) A widespread, time-transgressive, mixed siliceous/biogenic-carbonaceous sand facies indicates areas of moderate hydrodynamic regimes, high contribution of reworked shelf material, and fluvial supply to the shelf; (3) A glaucony-containing sand facies in a stationary position on the outer shelf formed mostly during the last-glacial sea-level rise, and the glaucony stems from reworking of older deposits and authigenic mineral formation; (4) A mud facies is mostly restricted to confined Holocene fine-grained depocentres, which are strictly located in mid-shelf position.

The observed spatial and temporal distribution of these facies types on the high-energy, low-accumulation NW Iberian shelf was essentially controlled by the local interplay of sediment supply, shelf morphology, and strength of the hydrodynamic system. These patterns are in contrast to high-accumulation systems where extensive sediment supply is the dominant factor on the facies distribution.

This study emphasises the importance of large-scale erosion and material recycling on the sedimentary shelf buildup during the deglacial sea-level rise. Up to 15-m thick transgressive deposits above a transgressive lag horizon contradict the common assumption of low sediment accumulation on high-energy shelf systems during deglacial sea-level rise. Additionally, maximal 4-m thin Holocene mud deposits are in contrast to thicker highstand units in other shelf systems. The restricted formation of mud depocentres was related to the combination of (1) frequently occurring high-energy hydrodynamic conditions, (2) low overall terrigenous input by the adjacent rivers, and (3) the large distance of the Galicia Mud Belt to its main sediment supplier.

Keywords: Late Quaternary, siliciclastic shelves, NW Iberia, sedimentary facies, continental shelf processes, shelf sedimentation

3.1. Introduction

Continental shelf systems are of highest economical and ecological importance and represent the major sink for sediments on the sediment pathway from the coast to the deep sea. Nevertheless, the scientific knowledge on the sedimentary shelf evolution is still limited due to the complex buildup of these systems as a result of the interplay of various forces which control distribution and deposition of sediments.

During the past decades, several studies aimed at explaining the sedimentary construction of shelf systems and their material distribution patterns. On the one hand, pure geophysical approaches were used to illustrate general aspects of shelf-strata development. These studies were characterised by a general lack of sedimentary ground-truthing and sufficient age control. Studies corroborating such seismic interpretations by a comprehensive sediment coring program are still a rare case (e.g., Bahr et al., 2005; Okyar et al., 2005; Grossman et al., 2006). On the other hand, studies dealing with the sediment distribution patterns were often restricted to the modern surface situation (e.g., Ogston et al., 2000; Dias et al., 2002; Brooks et al., 2003) or few sediment cores (e.g., Maldonado et al., 1983; Díaz et al., 1990; Buck et al., 1999) which might not adequately represent the complexity of shelf environments. Additionally, several of these studies focussed on Holocene fine-grained depocentres due to their role as high-resolution environmental archives (e.g., Abrantes et al., 2005; Bartels-Jónsdóttir et al., 2006; Naughton et al., 2007). Coarser sediments surrounding or underlying these mud deposits were mainly oversimplified as "relict sands" providing no further information on the sedimentary mechanisms. Hence, the spatial and temporal sedimentary evolution of shelf systems remained often unclear. This is in particular the case for environments under high-energy, low-accumulation regimes such as the NW Iberian shelf system where coring is challenging due to frequently occurring coarse-grained material.

In this study, we use (1) detailed visual core description, (2) microscopic component counting combined with fuzzy c-means cluster analysis, (3) X-ray diffraction measurements, and (4) grain-size analysis to reveal the detailed spatial and temporal sedimentary facies evolution of the NW Iberian shelf system as well as to unravel the dominant processes controlling this facies distribution.

3.2. Regional Settings

3.2.1. Morphology, geological framework, and oceanography of the study area

The NW Iberian continental shelf is generally narrow, varying in width between 25 and 40 km (Fig. 3.1). The shelf break occurs in water depths of 160 to 180 m (Dias et al., 2002). Outcrops of Palaeozoic plutonic and metamorphic rocks appear along the entire inner shelf extending down to water depths of 70 m (Dias et al., 2002). On the outer shelf, a chain of rocky elevations comprised of Late Cretaceous to Pleistocene limestones and sandstones is located south of 42°00'N (Fig. 3.1; Rey Salgado, 1993; Dias et al., 2002; Oliveira et al., 2002). These outcrops on inner and outer shelf are bare of recent sediments (Oliveira et al., 2002).

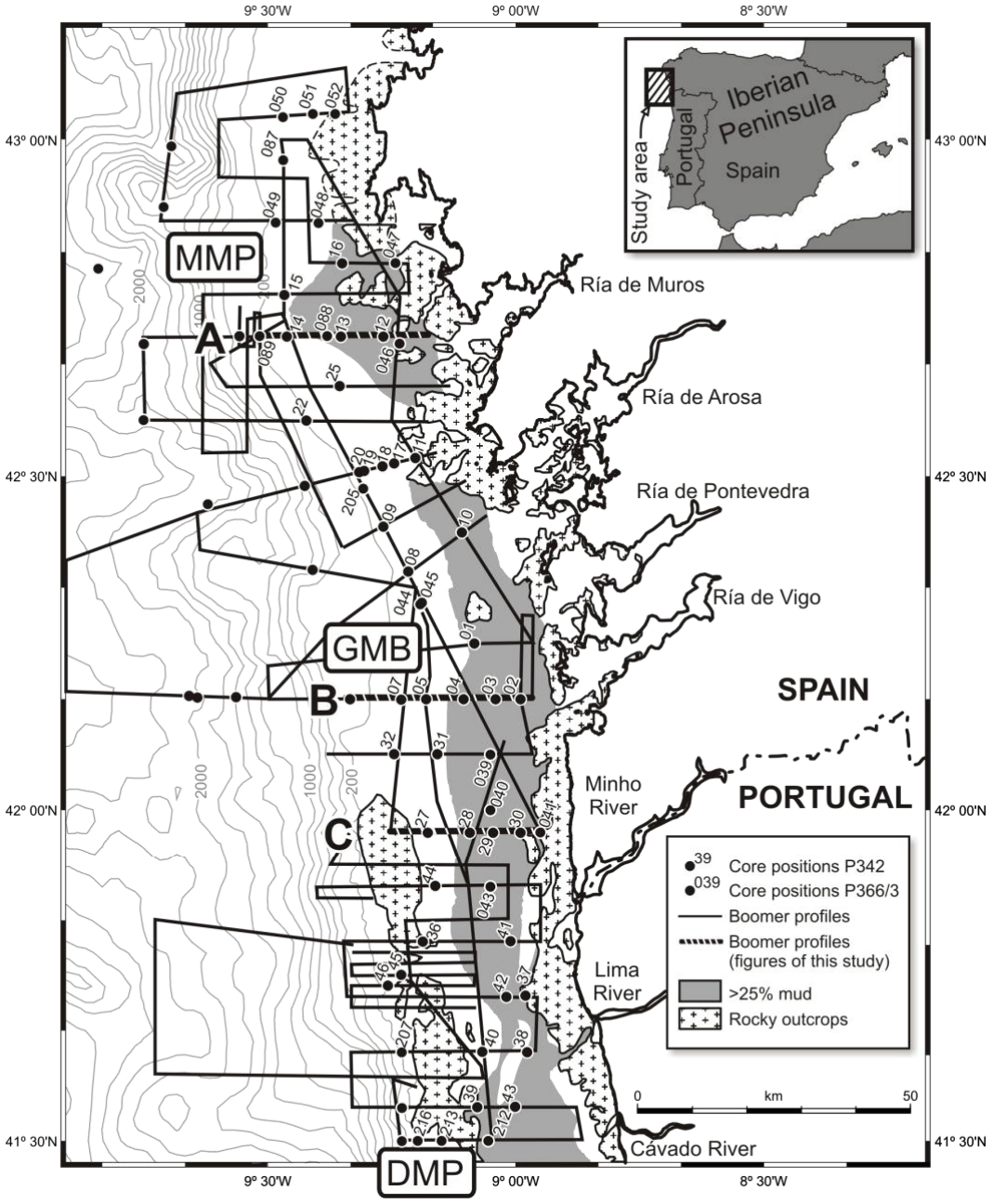

Fig. 3.1. Map of the study area. The surface geology was adapted from Dias et al. (2002). Mud depocentres are displayed in grey. MMP = Muros Mud Patch; GMB = Galicia Mud Belt; DMP = Douro Mud Patch. Core positions of cruises P342 and P366/3 are marked by black dots. Cores used in this study are displayed in short form with, for instance, 11002-3 and 11038-2 being positions 02 and 38 (P342), and 13089-2 and 130207-3 being positions 089 and 207 (P366/3). Characters A to C represent Boomer profiles shown in Fig. 3.3.

Five major river estuaries discharge along the Portuguese coastline – the Minho, Lima, Cávado, Ave and Douro (Fig. 3.1). The rough and irregular coastline in the northern part of the study area is characterised by the four up to 50-m deep Rías Baixas (Muros,

Arosa, Pontevedra, Vigo). These Rías represent Tertiary river valleys, which became drowned during the last deglacial sea-level rise (Rey Salgado, 1993; Oliveira et al., 2002).

The NW Iberian margin is characterised by strong seasonal oceanographic variations (Dias et al., 2002; Vitorino et al., 2002b). The high-energy winter situation is characterised by (1) occasional wind-driven downwelling, (2) a poleward mid-shelf current, and (3) intensified river runoff (Vitorino et al., 2002b). In contrast, the summer regime shows less energetic conditions, wind-related upwelling events, and an equatorward directed shelf current. These general oceanographic patterns were probably persistent over the past five thousand calibrated years before present (cal yr BP in the following; Bernárdez et al., 2008).

3.2.2. Shelf stratigraphy and sedimentary system

The late-Quaternary stratigraphy of the NW Iberian shelf system was studied in detail by Lantzsch et al. (2009) refining earlier studies (Muñoz et al., 2003; Ferrín, 2005). Three main seismic units were identified that overly a prominent erosional unconformity on top of a tilted basement (Fig. 3.2). The lowermost Unit 1 (U1) is mainly composed of Late-Tertiary to Pleistocene fine sands and the youngest part of this unit was related to the regressional dynamic of the last glacial sea-level fall. Unit 2 (U2) was built up by homogenous fine sands of the Last Glacial Maximum (LGM) and the following deglacial sea-level rise. Finally, Unit 3 (U3) comprises mainly muddy fine sands to mud which formed during the late stage of sea-level rise and during the modern sea-level highstand.

These three stratigraphic units are strictly separated from each other by two pronounced reflectors in the Boomer profiles (R1 and R2; Fig. 3.2) which are mirrored in the sediment cores by coarse-sand to gravel beds. The origin of R1 was related to the enrichment of such coarse material during the last-glacial sea-level lowstand and during the subsequent sea-level rise (Lantzsch et al., 2009). The coarse deposition of R2 was restricted to the late stage of deglacial sea-level rise.

In contrast to the pre-Holocene sedimentary system, the modern system was intensively investigated by various authors (e.g., Dias et al., 2002; Oliveira et al., 2002; Vitorino et al., 2002a; Lantzsch et al., in press). The fluvial sediment supply to the NW Iberian shelf amounts to approximately $2.25 \cdot 10^6$ t a^{-1} (Oliveira et al., 1982). Estuaries are the main suppliers of terrigenous material to the NW Iberian shelf with the Douro River being the main source for fine sediments (Dias et al., 2002). In contrast, the Rías Baixas are expected to act mainly as sediment traps (Oliveira et al., 2002) but an exceptional occurrence of fine deposits was observed in front of the Ría de Muros (Lantzsch et al., in press).

The sediment surface situation on the NW Iberian shelf is generally characterised by sand draping (Oliveira et al., 2002). Nevertheless, three defined mud depocentres are present in mid-shelf position, the northern branch of the Douro Mud Patch (DMP), the Galicia Mud Belt (GMB) and the Muros Mud Patch (MMP; Dias et al., 2002; Oliveira et al., 2002; Lantzsch et al., in press). The surface extent of these mud depocentres was compiled by Dias et al. (2002). Fig. 3.1 shows the surface shaping of the northern part of the DMP as well as the distribution of GMB and MMP, defined by a mud content of more than 25%. According to Jouanneau et al. (2002), these mud depocentres show sedimentation rates between 0.05 to 0.40 cm ka^{-1}. The sedimentary composition of these mud deposits was described by Corredeira et al. (2005) and Martins et al. (2007), as a product of terrigenous supply of fines in combination with marine biogenic sedimentation.

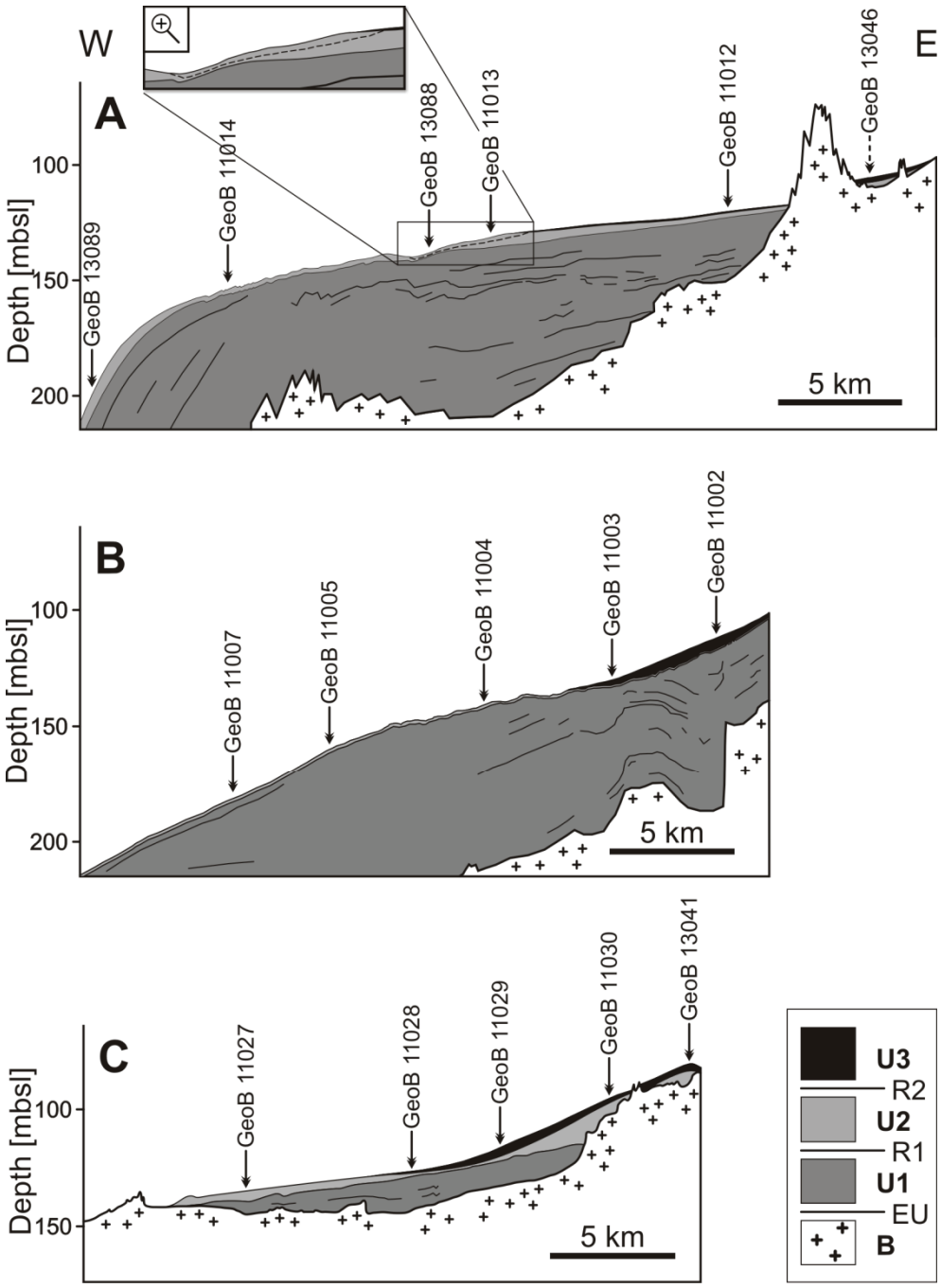

Fig. 3.2. Late-Quaternary stratigraphic interpretation of the Profiles A to C in Fig. 3.1 (modified from Lantzsch et al., 2009). B = basement; EU = erosional unconformity; U1, U2, U3 = main stratigraphic units; R1, R2: seismic reflectors separating the units. Magnification of Profile A displays an internal reflector within U2 (marked by dashed line). Sediment core positions are indicated by black arrows. Depth on y-axis is given in metres below modern sea level (mbsl).

The high-energy hydrodynamic winter conditions were proposed as being responsible for the modern sediment distribution patterns on the shelf (Dias et al., 2002; Vitorino et al., 2002b). In case of the GMB, fine sediments are introduced by the Douro River, occasion-

ally resuspended by winter storms and transported to the north by the poleward shelf current (Drago et al., 1998). In front of Ría de Muros, fines are directly deposited between local basement elevations which provide protection against current- and wave effects (Lantzsch et al., in press).

3.3. Materials and methods

3.3.1. Sediment coring

During the two GALIOMAR (*Galician Ocean Margin Expedition*) cruises with the German research vessel Poseidon (P342 and P366/3) in 2006 and 2008, a total of 66 sediment cores was collected from the NW Iberian shelf and, to a minor extent, from the continental slope (Fig. 3.1; Table 3.1). A vibrocorer was used to recover sandy sediments from water depths of less than 230 m and the core recovery was up to 5 m. In greater water depths, sediment was retrieved using a 6-m gravity corer. A giant box corer was additionally assembled at each core location to sample the modern sediment surface. This study is based on 47 sediment vibrocores as well as 57 surface samples. The subdivision of sediment core sections into stratigraphic units U1–3, R1, and R2 follows the late-Quaternary subdivision of the NW Iberian stratigraphic shelf architecture as recently established by Lantzsch et al. (2009; Chapter 3.2.2).

Table 3.1. Position of sediment vibrocores and surface samples of this study.

Core pos. (GeoB)	Latitude (N)	Longitude (W)	Water depth [m]	Recovery [m][a]	Core pos. (GeoB)	Latitude (N)	Longitude (W)	Water depth [m]	Recovery [m][a]
11001-3	42°15.00	9°05.01	136	1.14	11037-2	41°43.09	8°58.48	80	2.70
11002-3	42°10.00	8°59.24	111	4.34	11038-2	41°38.03	8°58.27	78	4.88
11003-3	42°10.00	9°02.24	129	4.54	11039-2	41°33.03	9°04.38	99	4.28
11004-2	42°10.00	9°06.17	141	3.78	11040-2	41°38.04	9°04.02	98	4.90
11005-2	42°10.00	9°10.50	161	3.21	11041-2	41°48.05	9°00.37	93	4.79
11007-2	42°10.00	9°13.49	183	3.20	11042-2	41°43.04	9°01.07	96	4.51
11008-2	42°21.29	9°13.00	157	3.77	11043-2	41°33.05	9°00.03	84	4.51
11009-2	42°25.29	9°16.00	166	1.67	11044-1	41°53.06	9°09.42	126	Ss
11010-2	42°25.00	9°06.28	119	4.10	11045-1	41°45.02	9°13.51	129	Ss
11011-2	42°31.38	9°12.07	100	4.85	11046-1	41°44.04	9°15.27	142	Ss
11012-2	42°42.29	9°16.00	119	4.28	13039-5	42°05.00	9°02.98	123	Ss
11013-2	42°42.29	9°21.07	129	4.30	13041-2	41°57.98	8°57.00	76	3.13
11014-2	42°42.29	9°27.39	153	4.50	13043-1	41°52.98	9°03.01	105	ss
11015-2	42°46.11	9°27.58	159	4.94	13045-1	42°18.72	9°11.31	148	ss
11016-2	42°49.00	9°21.00	132	4.56	13046-2	42°41.80	9°14.00	106	2.41
11017-2	42°31.10	9°14.40	120	4.88	13047-2	42°49.00	9°14.47	94	4.85
11018-2	42°30.54	9°16.04	125	4.00	13048-2	42°52.68	9°23.78	146	3.78
11019-2	42°30.28	9°18.16	149	4.92	13049-2	42°52.68	9°28.96	170	2.39
11020-2	42°30.23	9°18.53	154	3.95	13050-2	43°01.98	9°28.21	164	1.88
11022-1	42°35.00	9°25.17	289	ss	13051-2	43°02.29	9°24.49	134	3.66
11025-2	42°38.04	9°21.19	131	4.88	13052-2	43°02.30	9°21.79	109	4.52
11027-2	41°57.59	9°10.34	136	4.54	13088-2	42°42.51	9°22.78	132	2.44
11028-2	41°57.59	9°05.29	127	4.59	13089-2	42°42.48	9°31.00	190	4.90
11029-2	41°57.59	9°02.42	114	4.88	130205-2	42°28.91	9°18.37	171	4.96
11030-2	41°58.00	8°59.24	94	4.60	130207-3	41°38.01	9°13.70	146	4.94
11031-3	42°05.04	9°09.25	148	1.96	130212-2	41°29.98	9°03.30	89	4.34
11032-1	42°05.06	9°14.43	166	ss	130213-2	41°29.99	9°08.89	111	4.35
11036-2	41°48.03	9°11.15	125	3.35	130216-2	41°29.99	9°11.84	141	4.85

[a] A surface sample was taken on every core position; ss = surface-sample only.

3.3.2. Laboratory analyses

Core samples from muddy sections were investigated in 10-cm intervals. Samples from homogenous fine sands were taken in 20-cm intervals. The coarse fraction (>63 µm) was separated from the fine fraction (<63 µm) by wet sieving. Grain-size distribution of the coarse fraction was determined by sonic-sifting with sieve mesh widths of 63–125, 125–250, 250–500, 500–1000, and >1000 µm. The sediments were classified using the grain-size scheme of Blair and McPherson (1999) and the results of the grain-size analysis were used to corroborate the initial visual core description.

A binocular component analysis was performed on the grain-size fraction 250–500 µm on 325 samples (full dataset available at www.pangaea.de). At least 300 grains were examined for being statistically relevant. In homogenous sections, at least two samples were selected for analysis. If considerable differences in the component distribution occurred, subsamples were selected within this interval. An additional conversion of the derived component distribution (grain-size fraction 250–500 µm) into weight percentages with respect to the bulk sample was applied to test if significant differences in the statistical analysis occur (Chapter 3.4.3).

X-ray diffraction (XRD) was used on 18 representative samples to analyse the mineralogy of the bulk sediment. The samples were chosen from mud deposits as well as from fine sands in the northern, middle, and southern parts of the study area. After careful grinding the samples were measured with a Philips X'Pert Pro multipurpose diffractometer with Cu-tube (k-α 1.541 Å) and fixed divergence slit (1/4°). A 2-θ angle between 3° and 85° with a step size of 0.016° was chosen and the measurements were performed at 45 kV and 40 mA. Mineral identification was done by using the Philips software "X'Pert HighScore", which provides additionally semi-quantitative estimates.

Radiocarbon dating was carried out by the Leibniz Laboratory in Kiel (Germany), and the Poznań Radiocarbon Laboratory (Poland). All dates were calibrated with the Calib 5.0.1 software (Stuiver et al., 1998) using the standard marine reservoir effect of 400 years. A calibrated age range within 1-σ confidence limits was obtained. Dates with a conventional age older than 22 ka were calibrated with the function of Bard et al. (1998). 61 radiocarbon dates on 28 cores are displayed in this study (Table 3.2).

Table 3.2. Radiocarbon dates and age calibration.

Lab No.[a]	Core No. (GeoB)	Depth in core (cm)	Material[b]	Age (^{14}C yr BP)	Age (cal yr BP, 1σ)[c]	Intercept (cal kyr BP)	Strat. class.	In Fig. 3.3
KIA 33666	11002-3	98	bF, pF, bv pieces	2500 ± 35	2111-2241	2.18 ± 0.07	U3	x
KIA 33665	11002-3	250	bF	2715 ± 35	2342-2455	2.40 ± 0.06	U3	x
KIA 33664	11002-3	435	bF, bv pieces, gp	4955 ± 45	5249-5388	5.32 ± 0.07	U3	x
Poz-24670	11003-3	240	bF	7840 ± 50	8259-8371	8.32 ± 0.06	U3	x
Poz-22923	11003-3	360	bF	10,770 ± 50	12,101-12,321	12.21 ± 0.11	U3	x
Poz-24771	11003-3	399	bF	13,080 ± 70	14,814-15,107	14.96 ± 0.15	U2	x
Poz-21469	11004-2	60	bF, bv	14,900 ± 70	17,219-17,692	17.46 ± 0.24	U2	x
KIA 33669	11004-2	155	*E. crispum*	16,430 ± 120	19,062-19,335	19.20 ± 0.14	U2	x
KIA 33668	11004-2	277	bv piece	14,660 ± 100	16,793-17,297	17.05 ± 0.25	R1	x
Poz-22944	11005-2	250	*E. crispum*	18,470 ± 100	21,160-21,689	21.42 ± 0.26	R1	x
Poz-22945	11005-2	300	bF, bv pieces	>42,000	uncalibrated	>42	U1	x
KIA 33670	11007-2	144	bF, bv pieces, gp	11,740 ± 70	13,149-13,270	13.21 ± 0.06	U2	x
Poz-22946	11010-2	377	*E. crispum*	15,540 ± 80	18,220-18,690	18.46 ± 0.24	R1	
Poz-22925	11012-2	100	bF	3995 ± 35	3949-4068	4.01 ± 0.06	U3	x
Poz-22948	11012-2	320	*E. crispum*	14,820 ± 80	17,073-17,554	17.31 ± 0.24	R1	x
KIA 33671	11013-2	85	bF	18,320 ± 160	20,881-21,461	21.17 ± 0.29	U2	x
KIA 33672	11013-2	234	*E. crispum*	14,960 ± 120	17,308-17,866	17.59 ± 0.28	U2	x
Poz-22949	11013-2	423	*E. crispum*	15,750 ± 80	18,652-18,786	18.72 ± 0.07	U2	x
KIA 33673	11014-2	188	bF, pF, bv pieces	13,420 ± 100	15,181-15,552	15.37 ± 0.19	U2	x
KIA 33675	11014-2	441	bF, bv pieces	>42,000	uncalibrated	>42	U1	x
KIA 33692	11015-2	430	bF, bv pieces	30,710 ± 670	35,016-36,496*	35.76 ± 0.74	U1	
KIA 33781	11015-2	448	plant debris, cc	>42,000	uncalibrated	>42	U1	
KIA 33676	11016-2	439	bF	17,560 ± 130	20,120-20,425	20.27 ± 0.15	U2	
KIA 33677	11017-2	130	*E. crispum*	21,390 ± 200	24,912-25,542	25.23 ± 0.32	U2	
KIA 33683	11017-2	247	*E. crispum*	28,520 ± 480	32,787-33,860*	33.32 ± 0.54	U1	
KIA 33684	11017-2	417	*E. crispum*	>42,000	uncalibrated	>42	U1	
KIA 33685	11017-2	486	bF	>42,000	uncalibrated	>42	U1	
KIA 33693	11018-2	153	*E. crispum*	20,420 ± 230	23,688-24,278	23.99 ± 0.30	U2	
KIA 33695	11018-2	400	*E. crispum*	22,030 ± 220	25,688-26,197*	25.94 ± 0.25	U2	
KIA 33696	11020-2	60	*E. crispum*	17,190 ± 130	19,814-20,103	19.96 ± 0.15	U2	
Poz-22926	11020-2	135	*E. crispum*	16,880 ± 290	19,365-19,922	19.64 ± 0.28	U2	
KIA 33697	11020-2	367	*E. crispum*	20,020 ± 230	22,995-23,780	23.39 ± 0.39	U2	
KIA 33699	11027-2	49	*E. crispum*	17,040 ± 130	19,567-19,900	19.74 ± 0.17	U2	x
KIA 33700	11027-2	454	*E. crispum*	19,120 ± 160	22,141-22,419	22.28 ± 0.14	U2	x
Poz-21470	11028-2	140	bF	2555 ± 30	2184-2290	2.24 ± 0.05	U3	x
Poz-21471	11028-2	416	*E. crispum*	16,780 ± 80	19,444-19,756	19.60 ± 0.16	U2	x
Poz-22950	11028-2	429	*E. crispum*	17,310 ± 190	19,862-20,243	20.05 ± 0.19	R1	x
KIA 33687	11029-2	103	bF	850 ± 30	458-503	0.48 ± 0.02	U3	x
Poz-27846	11029-2	159	bF	1750 ± 30	1268-1326	1.30 ± 0.03	U3	x
Poz-27922	11029-2	245	bF, pF, bv pieces	2100 ± 30	1619-1723	1.67 ± 0.05	U3	x
KIA 33688	11029-2	326	bF, bv pieces	2830 ± 35	2533-2676	2.61 ± 0.07	U3	x
Poz-24772	11029-2	360	bF	2910 ± 35	2669-2737	2.70 ± 0.03	U3	x
Poz-27847	11029-2	400	bF	4300 ± 35	4385-4490	4.44 ± 0.05	U3	x
KIA 33689	11029-2	488	ec pieces	12,740 ± 80	14,082-14,475	14.28 ± 0.20	U2	x
Poz-21472	11030-2	220	bF	2940 ± 35	2693-2749	2.72 ± 0.03	U3	x
Poz-21473	11030-2	460	bF, bv	10,740 ± 50	12,035-12,255	12.15 ± 0.11	U2	x
Poz-22951	11038-2	120	bF	3165 ± 35	2888-3013	2.95 ± 0.06	U3	
Poz-22952	11038-2	460	bF, gp	16,880 ± 90	19,501-19,793	19.65 ± 0.15	U2	
Poz-26860	13041-2	250	bF	8570 ± 50	9127-9293	9.21 ± 0.08	U3	x
Poz-26858	13046-2	135	bF	4135 ± 35	4135-4260	4.20 ± 0.06	U3	x
Poz-26856	13046-2	210	bF	8750 ± 50	9386-9483	9.43 ± 0.05	U3	x
Poz-26859	13047-2	136	bF, gp	4900 ± 40	5135-5297	5.22 ± 0.08	U3	
Poz-26861	13051-2	278	bF	15,350 ± 80	18,054-18,486	18.27 ± 0.22	U2	
Poz-26865	13052-2	447	bF	11,420 ± 60	12,879-12,991	12.94 ± 0.06	U2	

Table 3.2 *(continued)*.

Lab No.[a]	Core No. (GeoB)	Depth in core (cm)	Material[b]	Age (^{14}C yr BP)	Age (cal yr BP, 1σ)[c]	Intercept (cal kyr BP)	Strat. class.	In Fig. 3.3
Poz-26862	13089-2	489	*E. crispum*	17,850 ± 100	20,414-20,742	20.58 ± 0.16	U2	x
Poz-28832	130205-2	35	bF, pF	18,550 ± 100	21,354-21,858	21.61 ± 0.25	U2	
Poz-26863	130205-2	269	bF, pF, bv pieces	18,970 ± 110	22,054-22,276	22.17 ± 0.11	U2	
Poz-26864	130207-3	430	bF	18,280 ± 110	20,900-21,338	21.12 ± 0.22	U2	
Poz-26873	130213-2	70	bF, pF, bv, ec	11,780 ± 60	13,191-13,296	13.24 ± 0.05	U2	
Poz-26870	130213-2	300	bF, pF, bv, ec	13,120 ± 70	14,890-15,153	15.02 ± 0.13	U2	
Poz-26871	130213-2	442	bF, bv	20,460 ± 130	23,842-24,195	24.02 ± 0.18	U2	

[a] Radiocarbon laboratory: KIA = Leibniz Laboratory in Kiel (Germany); Poz = Poznań Radiocarbon Laboratory (Poland).
[b] Material: bF = benthic foraminifers; *E. crispum* = *Elphidium crispum* (monospecific sample); bv = bivalve; gp = gastropod; cc = char coal; ec = echinoderm pieces.
[c] For reservoir correction, the conventional age of 400 years is applied using CALIB 5.0.1. (Stuiver et al., 1998).
* Age calibration is based on the function of Bard et al. (1998).

3.3.3. Fuzzy c-means cluster analysis and non-linear mapping

Fuzzy c-means cluster analysis (FCM; Bedzek et al., 1984) and the non-linear mapping dimension reducing technique (NLM; Sammon, 1969) were applied to the results of the microscopic component analysis in order to aid the identification of major relationships amongst the samples (full dataset available at www.pangaea.de). Due to the "closed" nature of the data sets the centred-log-ratio transformation was applied before processing to avoid spurious statistical effects (Aitchison et al., 2000; Pawlowsky-Glahn and Egozcue, 2006). The characteristic component distribution of a certain cluster is displayed by the composition of the related cluster centre. All samples belonging to a cluster will plot around this centre in the multidimensional measurement space. NLM has been used in combination with the FCM to confirm the validity of a given cluster solution (Vriend et al., 1988; Dekkers et al., 1994).

3.4. Characterisation of sedimentary facies types and age control

3.4.1. Grain size and sediment composition

Visual core description and grain-size measurements on the sediment cores and surface samples reveal predominately homogenous fine sands with low mud contents (Figs. 3.3 and 3.4A). These fine sands consist of variable contents of terrigenous particles as well as marine carbonate shells and their fragments. Glaucony *sensu* Odin and Matter (1981; see chapter 3.4.2) may occur in larger amounts in dark-green to black homogenous fine sands (Fig. 3.4B). In contrast, the highest mud contents were recovered within U3 from the Galicia Mud Belt (GMB; Fig. 3.4C) and the Muros Mud Patch (MMP) ranging from 25% mud in distal parts (e.g., Cores 11028-2 and 11030-2; Fig. 3.3C) to more than 90% in the central part of the Galicia Mud Belt (Cores 11002-3 and 11029-2; Fig. 3.3B, C). Furthermore, distinct layers of siliceous or shell-fragment gravel are present in almost all cores and intersect finer sections (Figs. 3.3 and 3.5).

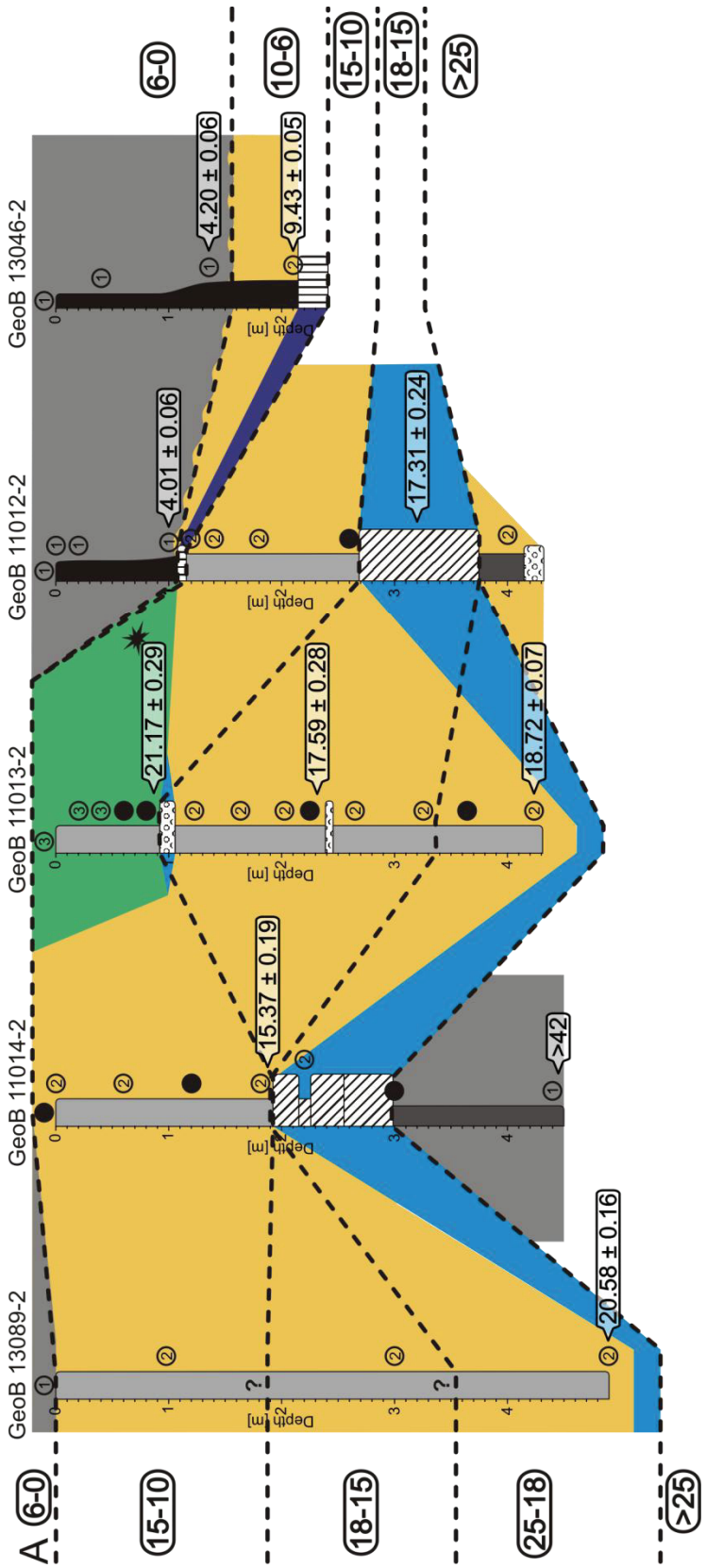

Fig. 3.3. Sediment core columns displaying grain-size, stratigraphic units. Samples for microscopic component counting are marked by cluster numbers derived from fuzzy c-means cluster analysis. Facies types are displayed by background colours. Positions of time-slices are marked by dashed lines. Correlations See Fig. 3.2 for respective Boomer profiles.

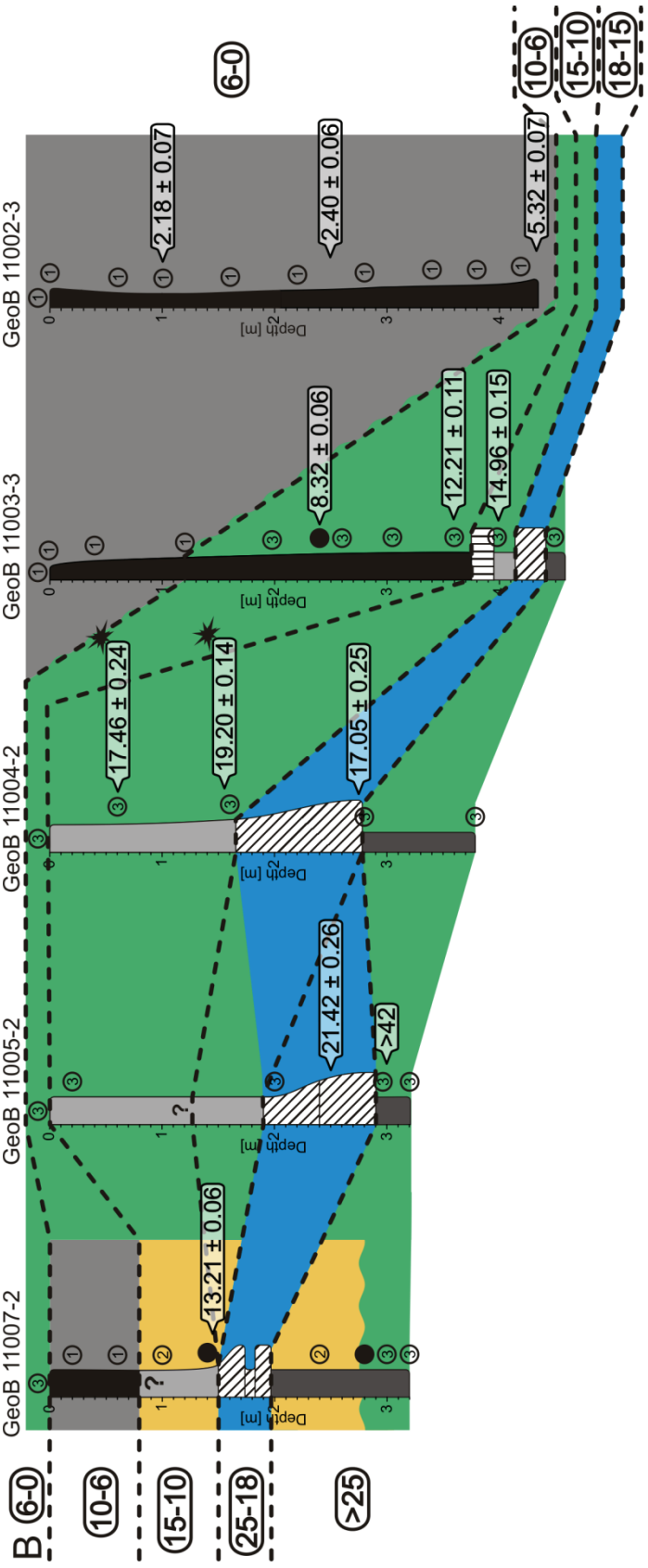

Fig. 3.3 *(continued)*.

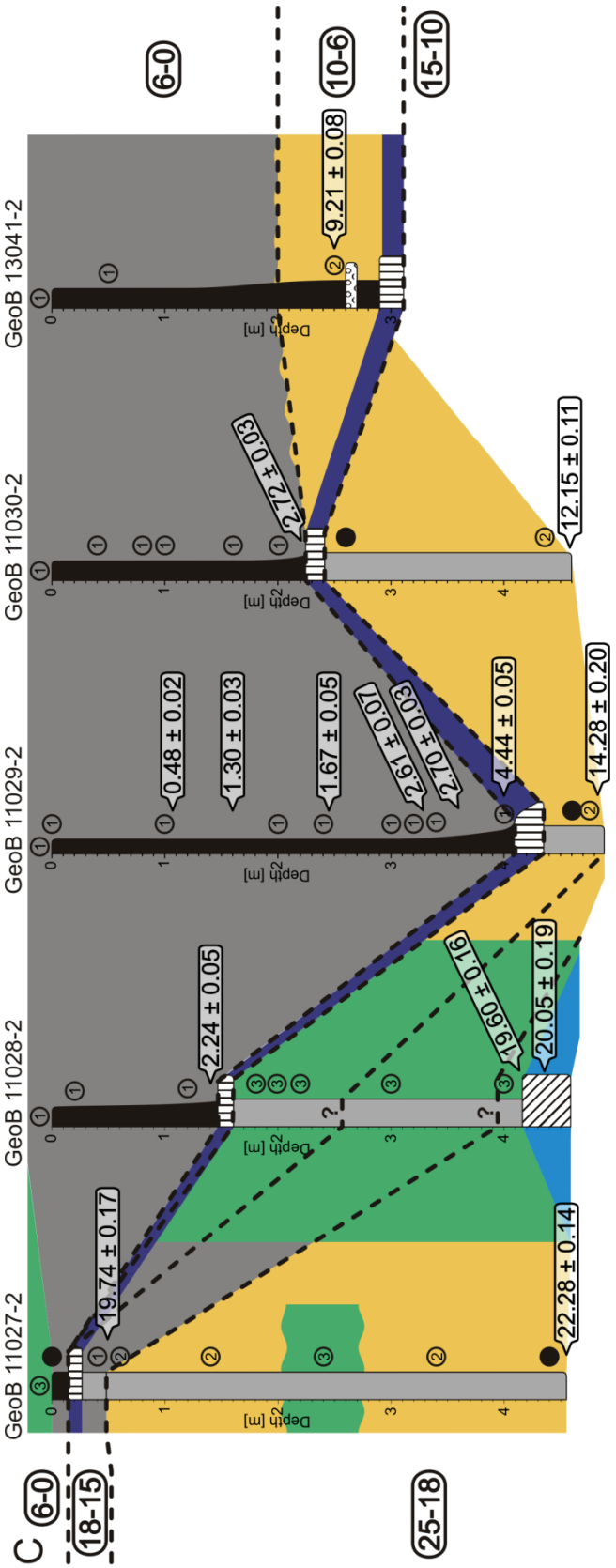

Fig. 3.3 *(continued)*.

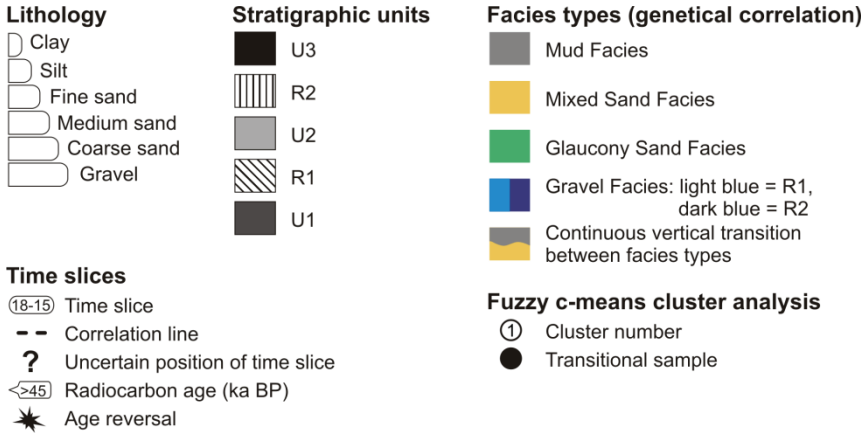

Fig. 3.3 *(continued)*.

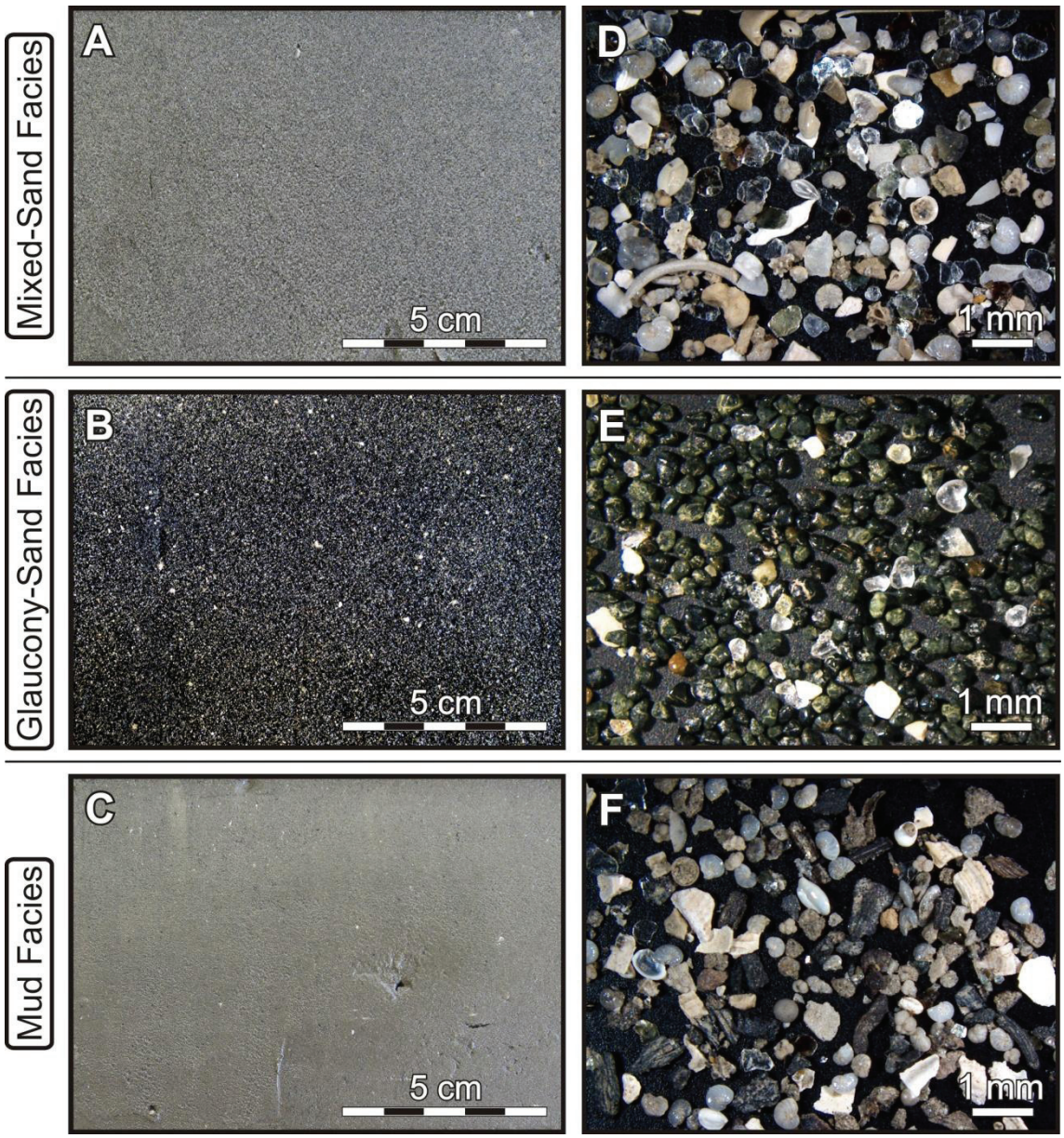

Fig. 3.4. Core pictures (left) and microscopic photos (right) of the Mud Facies (A, B), Mixed-Sand Facies (C, D), and Glaucony-Sand Facies (E, F).

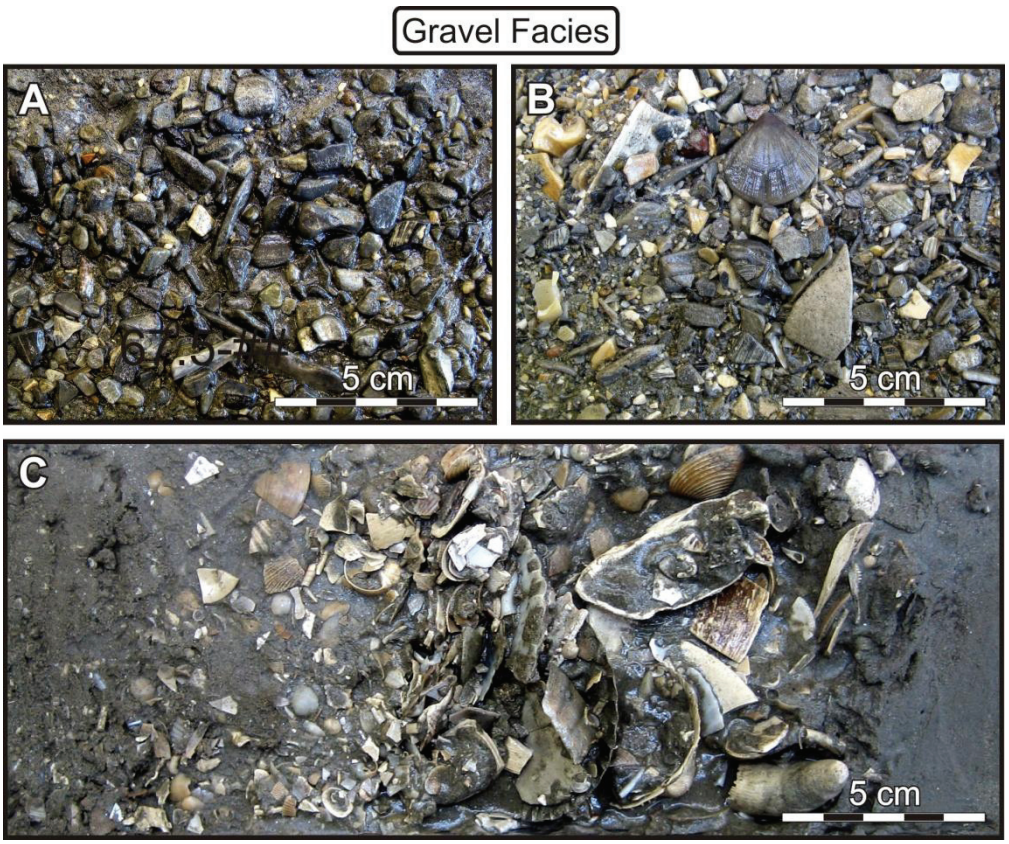

Fig. 3.5. Core pictures of the Gravel Facies; A = shoreface deposit; B = event bed; C = fining upward event bed.

XRD measurements on selected samples within mud and fine sands show generally a more or less similar composition (Fig. 3.6). All samples contain quartz and to a minor degree feldspars, micas and illite. These main components generally add to >60%. Minor components are carbonate, kaolinite, chlorite, serpentinite, heavy minerals, expandable clay minerals, and palygorskite.

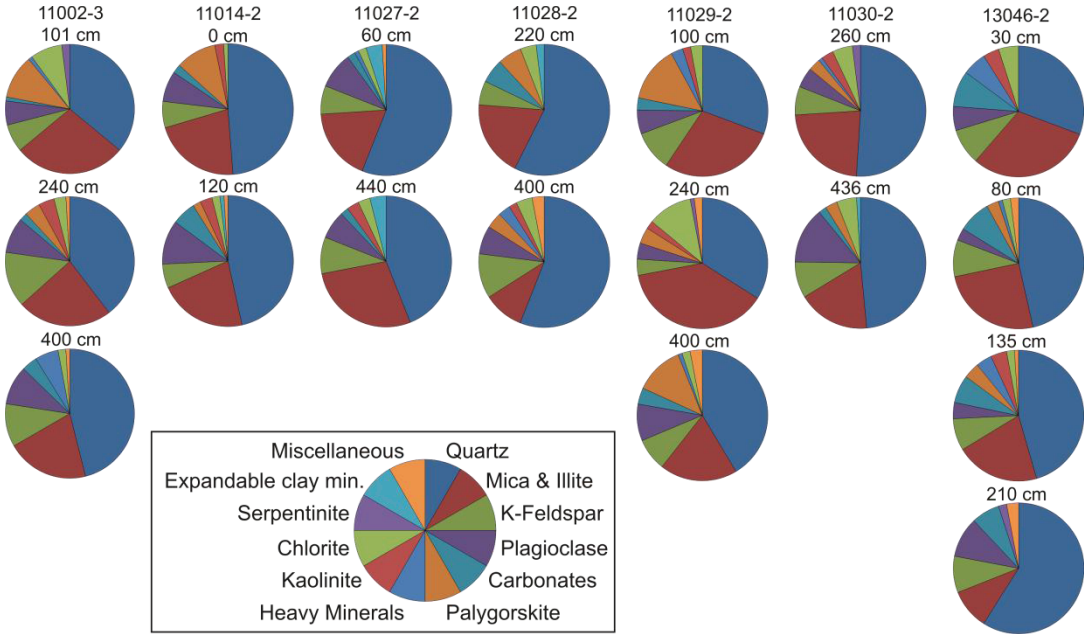

Fig. 3.6. Results of the X-ray diffractometry measurements.

3.4.2. Microscopic component analysis on grain-size fraction 250–500 µm

The microscopic analysis on the grain-size fraction 250–500 µm on muddy and sandy sediments reveals six main component groups. The first group, *biogenic carbonate*, contains mainly planktonic and benthic foraminifers, and to a minor degree mollusc shells and ostracods. Biogenic carbonate particles with less than 50% estimated preservation were assigned to the second group *carbonate fragments*. Fragments of echinoderms, bryozoans and crustaceans were also placed in this group. In general, carbonate particles show the whole range from white delicate tests in complete preservation to orange-brown and heavily-worn fragments which were characterised as older, reworked components (Dias and Nittrouer, 1984). The third component group consists of mainly well-rounded dark-green to greenish black grains. Other shapes like book-sheets and foraminiferal test fillings occur occasionally. These particles are considered as *glaucony sensu* Odin and Matter (1981) representing a group of minerals with highly variable morphology and physicochemical properties which are often confusingly denominated by the mineralogical term glauconite. *Quartz* represents the fourth main component. The quartz grains are usually hyaline and sub-angular to sub-rounded. A few frosted, orange, iron-stained quartz grains may appear indicating older incorporated material (Dias and Nittrouer, 1984). The fifth group, *plant fibres*, comprises brown to dark brown, fibrous plant fragments, and to a minor degree black charcoal pieces. The sixth main component group, *mica*, mainly consists of single lucent platelets. Packages of mica are only scarcely present. Moreover, remains of sponges, fishes, rocks, pyrite, pellets, and further, undefined components were assigned into a seventh group – *others* – due to their scarce appearance. These particles mostly sum up to less than 5% of the relative component distribution.

3.4.3. Facies types

Although XRD measurements reveal comparable bulk compositions, the results of visual core description, grain-size analysis, and microscopic component analysis show considerable differences between sediment samples and allow the definition of main facies types. The microscopic component analysis on grain-size fraction 250–500 µm was found to effectively display the general differences, which were observed by visual core description. Although this fraction is not the dominant fraction, glaucony-containing sands, for instance, are mirrored by higher glaucony contents in the microscopic component analysis, whereas muddy sediments are characterised by higher contents of plant fibres. Therefore, fuzzy c-means cluster analysis (FCM) and non-linear mapping (NLM) were applied on the results of the microscopic component analysis in order to corroborate the definition of facies types and to provide better assignment of ambiguous samples. As a result, a three cluster solution is proposed as being adequate to explain the variations in the component distribution (Table 3.3). This observation is corroborated by the well-defined separation of the clusters in the NLM (Fig. 3.7). When a four-cluster solution was calculated it showed no significant improvement over the three-cluster solution, with Cluster 1 being separated into a sub-cluster containing slightly more quartz and a sub-cluster containing higher contents of plant fibres. Furthermore, the conversion of the component-distribution (grain-size fraction 250–500 µm) into weight percentages in relation to the bulk sediment (Table 3.4) reveals no significant improvement for the cluster-centre calculation. Although the percentage values of the cluster-centre compositions are much lower due to the underrepresentation of fraction

250–500 µm, the general trends are similar (Table 3.4). Therefore, this study concentrates on the description of the particular component distribution percentages of this fraction.

Table 3.3. Cluster-centre compositions as result of the fuzzy c-means cluster analysis. Bold numbers represent the main components of the three clusters. mF = Mud Facies; sF_{mixed} = Mixed-Sand Facies; sF_{glauc} = Glaucony-Sand Facies; carb. fragm. = carbonate fragments; biog. carb. = biogenic carbonate.

Components (%):	**Glau-cony**	**Carb. fragm.**	**Quartz**	**Mica**	**Plant fibres**	**Biog. carb.**	**Others**	**Average mud content (%)**
Cluster 1 (mF)	0	**25**	1	**25**	**18**	**28**	2	62
Cluster 2 (sF_{mixed})	3	**45**	**16**	**28**	0	6	0	8
Cluster 3 (sF_{glauc})	**54**	**20**	**20**	2	0	4	0	15

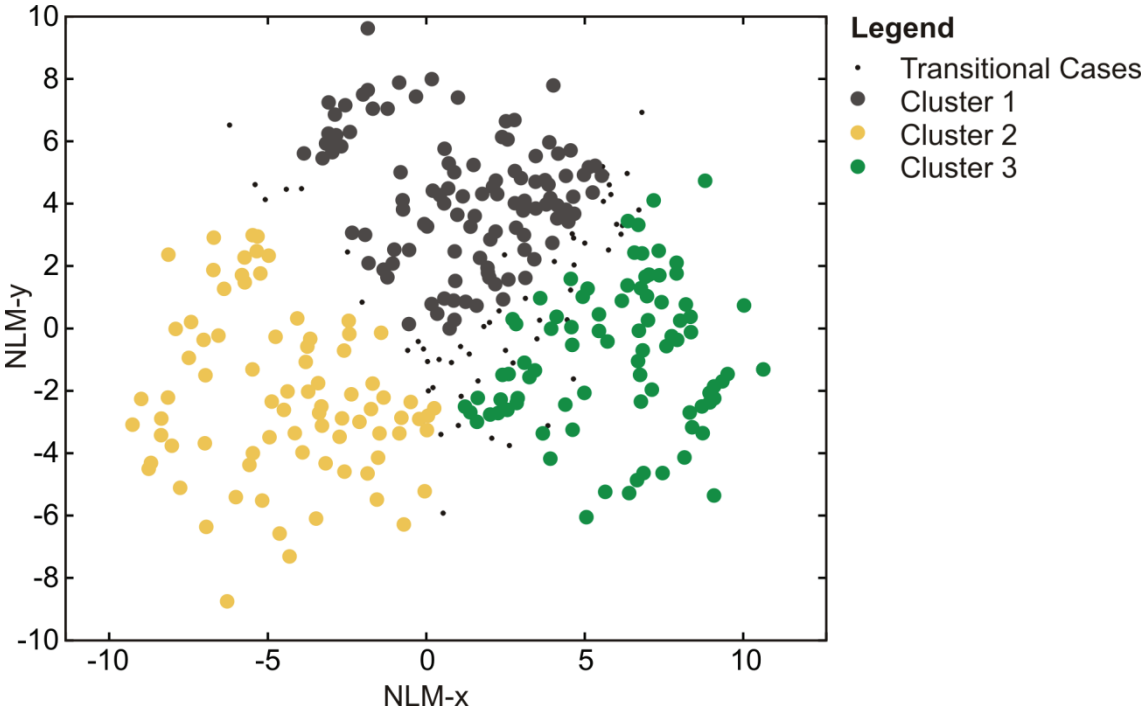

Fig. 3.7. Non-linear map of the three-cluster solution displaying a low-dimensional representation of the results of the fuzzy c-means cluster analysis. Individual samples are marked with dots. The colour of these points depends on the assignment to the clusters centre. Transitional cases are marked with small black dots. The axes on the NLM are arbitrary.

Table 3.4. Cluster-centre compositions with respect to the bulk sample. Bold numbers represent the main components of the respective cluster. mF = Mud Facies; sF_{mixed} = Mixed-Sand Facies; sF_{glauc} = Glaucony-Sand Facies; carb. fragm. = carbonate fragments; biog. carb. = biogenic carbonate.

Components (%):	**Glau-cony**	**Carb. fragm.**	**Quartz**	**Mica**	**Plant fibres**	**Biog. carb.**	**Others**	**Other fractions**
Cluster 1 (mF)	0.01	**0.11**	0.01	**0.08**	**0.07**	**0.18**	0.01	99.51
Cluster 2 (sF_{mixed})	0.07	**0.39**	**0.15**	**0.34**	0.01	0.05	0.01	98.98
Cluster 3 (sF_{glauc})	**3.84**	**0.91**	**1.23**	0.06	0.02	0.22	0.02	93.70

For the three-cluster solution of the FCM, each cluster represents one main facies type (Table 3.3). These three clusters are named Mud Facies (Cluster 1), Mixed-Sand Facies (Cluster 2), and Glaucony-Sand facies (Cluster 3) according to the following description of their typical appearance in the cores, their cluster properties and the mean grain size of the related samples. The characteristic components of fraction 250–500 µm are displayed by the particular cluster-centre composition, i.e. the composition of a theoretical centre calculated from all individual samples of a cluster in the measurement space.

The *Mud Facies* (mF; Cluster 1) comprises 80 samples. The characteristic sand components of this facies type are biogenic carbonate (28%), mica (25%), carbonate fragments (25%), and plant fibres (18%). The average content of the fine fraction (<63 µm) was determined by grain-size analysis and shows with a mean of 62% the highest mud content of the three clusters (Table 3.3). Figs. 3.4C and F illustrate the typical appearance of the mF within the sediment cores and its characteristic components of the microscopic analysis on grain-size fraction 250–500 µm, respectively. The occurrence of the mF is mainly restricted to U3 (Fig. 3.3).

In contrast to the mF, the average fine-fraction content of samples belonging to the *Mixed-Sand Facies* (sF_{mixed}; Cluster 2) is only 8%. Most of the samples contain pure fine sands (Fig. 3.4A). The majority of the sediment samples (108 samples) belong to this facies type. The characteristic main components of this cluster are carbonate fragments (45%), mica (28%), and quartz (16%; Fig. 3.4D). Almost all cores contain deposits of the sF_{mixed} (Fig. 3.3). Nevertheless, the majority of the samples belonging to the sF_{mixed} can be found in U2 and to a minor degree in U1.

The most characteristic main component of the *Glaucony-Sand Facies* (sF_{glauc}; Cluster 3; Fig. 3.4B) is glaucony (54%). Minor components are quartz (20%) and carbonate fragments (20%; Fig. 3.4E). This facies type shows low average contents of the fine fraction (15%). The samples belonging to this facies type are mainly restricted to U1 and U2 (Fig. 3.3).

Transitional cases (Fig. 3.7) represent samples which cannot be assigned by FCM to a certain cluster and represent, therefore an intermediate of the three defined clusters. They are characterised by strongly varying contents of the main components. In total, 54 samples are assigned to be transitional.

One additional facies type was defined by visual core description and grain-size analysis – the *Gravel Facies* (gF; Fig. 3.5). These coarse-sandy to gravelly deposits represent obviously an own facies type and are mainly restricted to R1 and R2 beds associated with the stratigraphic borders of the three units U1–3 (Fig. 3.3). The characteristic components of the gF vary strongly. Carbonate material shows the whole range from heavily altered mollusc fragments to freshly preserved bivalves, gastropods, and scaphopods. Furthermore, these beds may contain strongly variable amounts of quartz and some rock fragments. Quartz represents in some cases the main constituent. Usually, the thickness of the gF deposits ranges between few cm and 1 m, but an exceptional thickness of 2.7 m is reached at site 37 (Fig. 3.1).

The gF can be subdivided into two end-members, shoreface deposits and event beds (Fig. 3.5). Typical shoreface deposits are characterised by massive, well-sorted beds of carbonate shell fragments and/or siliceous particles (Fig. 3.5A). In contrast, typical event beds consist predominantly of carbonate shell fragments, and show chaotic or fining-

upward structures (Figs. 3.5B, C). A poor sorting and the particle angularity indicate remobilisation and rapid deposition by short-lasting high-energy events.

3.4.4. Age control

61 radiocarbon measurements were applied to the sediment cores to provide a robust age control. The results are very reliable and fit the stratigraphic interpretation of the NW Iberian shelf by Lantzsch et al. (2009). Two radiocarbon dates on U1 sediments show ages of 35.76 and 33.32 ka BP (Table 3.2). Five further measurements within U1 are older than 42 ka BP and lie, therefore, beyond the limitations of the radiocarbon method. Five radiocarbon dates of R1 reveal ages between 21.42 and 17.05 ka BP, and 30 radiocarbon measurements on U2 sediments display ages between 25.94 and 12.15 ka BP. R2 was not dated due to insufficient amounts of fresh carbonate but 19 measurements on U3 range between 12.21 and 0.48 ka BP.

However, although only very delicate and unaltered carbonate was used for radiocarbon measurements in order to avoid dating of reworked material and to display the last time of deposition, age reversals occur in three core sections (11004-2 and 11013-2 in Figs. 3.3A, B; 11020-2 at site 20 in Fig. 3.1). All these reversals occur in sF_{glauc} sections in the upper half of the cores. In case of Core 11013-2, the core position displays an internal reflector in the Boomer profile bordering the sF_{glauc} section at the upper quarter of the core from underlying deposits (see magnification in Fig. 3.2A). Possible reasons are given in Chapter 3.5.3.

3.5. Late-Quaternary sedimentary shelf development

The extended dating program and the late-Quaternary shelf stratigraphy of the NW Iberian shelf as recently established by Lantzsch et al. (2009) allow the definition of time slices. These time slices represent stages of the global sea-level. The time slice pre-LGM (>25 ka BP) comprises all deposits of former sea-level cycles and of the pre-LGM sea-level fall. The further slices describe the stages of last-glacial sea-level lowstand (25–18 ka BP), early deglacial sea-level rise (18–15 ka BP), further sea-level rise of the late deglaciation (15–10 ka BP), early-Holocene decrease in sea-level rise (10–6 ka BP), and late-Holocene sea-level stabilisation (6–0 ka BP).

Stratigraphic units and borders of the individual time slices are displayed in Fig. 3.3 by the colour of the core columns and dashed lines, respectively. However, it has to be noted that the stratigraphic units (U1–3, R1–2) are not restricted to one of the defined time slices but may show time-transgressive developments. Deposits belonging to U2, for instance, show an initial formation in cores from the outer shelf during the LGM time slice (Core 11027-2 in Fig. 3.3C) and later expansion towards the mid-shelf during the late deglaciation (Cores 11029-2 and 11030-2 in Fig. 3.3C). Due to this time-transgressive evolution the definition of time slices is essential to display snapshots of the sedimentary shelf configuration. The spatial and temporal development of investigated facies types provides an insight into the late-Quaternary shelf evolution and illustrates the factors which control the sediment distribution dynamics as discussed in the following.

3.5.1. Pre-LGM (>25 ka BP)

Fig. 3.8A shows all deposits that formed prior to the Last Glacial Maximum (LGM). Those sediments were recovered in 16 cores and show deposits of Mud Facies (mF), Mixed-Sand Facies (sF_{mixed}), and Glaucony-Sand Facies (sF_{glauc}). Pre-LGM deposits are not present south of the Minho River mouth due to intensive erosion in this slightly higher elevated area during the last sea-level lowstand (Lantzsch et al., 2009).

Deposits of mF are observed at three core positions (Fig. 3.8A). At two positions (site 17 in Fig. 3.1; Core 11014-2 in Fig. 3.3A) these deposits represent relicts of fine depocentres which remained preserved over the last sea-level cycle. The third core position (site 15 in Fig. 3.1) shows an overconsolidated deposit which is interpreted as palaeosol. A comparable deposit was found at site 19 (Fig. 3.1) which does not belong to the mF. Four samples were retrieved from this soil section and the FCM reveals two transitional samples as well as two samples belonging to the sF_{glauc} due to the content of glaucony. Therefore, the FCM on palaeosols delivers no consistent classification and shows exemplarily the need of a detailed core description. In any case, the observed palaeosols provide evidence for former shelf exposure. A radiocarbon age of 36 ka BP above these deposits in Core 11015-2 (site 15 in Fig. 3.1) indicates that this exposure took place long time before the LGM. Deposits of sF_{mixed} at six positions show that this facies type was already present prior to the LGM (Fig. 3.8A). This facies type is not restricted to a certain water depth or to a defined position on the shelf. Hence, the sF_{mixed} had, most probably, a widespread occurrence. However, a proof of this statement would require more extensive recovery of pre-LGM deposits. The composition of sF_{mixed} represents a mixture of marine biogenic material and terrigenous sands derived by fluvial input. An additional contribution by reworking of older deposits is indicated by the partial occurrence of well-rounded, mature quartz grains and heavily-worn carbonate fragments.

The occurrence of major sF_{glauc} sediments within the pre-LGM time slice (Fig. 3.8A) indicates that large amounts of glaucony formed prior to the LGM. This pattern is in agreement to observations of Odin and Lamboy (1988). These authors investigated the glaucony in surface samples of the NW Iberian shelf and proposed that large portions already formed during Miocene and Pliocene.

3.5.2. LGM (25–18 ka BP)

During LGM, large areas of inner and mid-shelf were exposed due to a 123-m lower global sea level than present (mbsl; Hanebuth et al., 2009). Hence, intensive erosion prevailed due to a lower base level and large amounts of terrigenous material were transported across the entire exposed shelf towards the shallow waters on the outermost shelf (Figs. 3.8A and 3.9A). Coarse material was instantly deposited at the shoreface.

Radiocarbon dates on deposits of the Gravel Facies (gF) in Core 11005-2 (21 ka BP; Fig. 3.3B), Core 11010-2 (19 ka BP; site 10 in Fig. 3.1) and Core 11028-2 (20 ka BP; Fig. 3.3C) as well as two other age dates directly above the gF bed (18 ka BP at site 51; 20 ka BP at site 16; Fig. 3.1) show that the gF developed at these locations within the time frame of the LGM (Fig. 3.8B). The material of both sub-groups of gF – shoreface deposits and event beds – was deposited above the storm-wave base. Nevertheless, the sources and

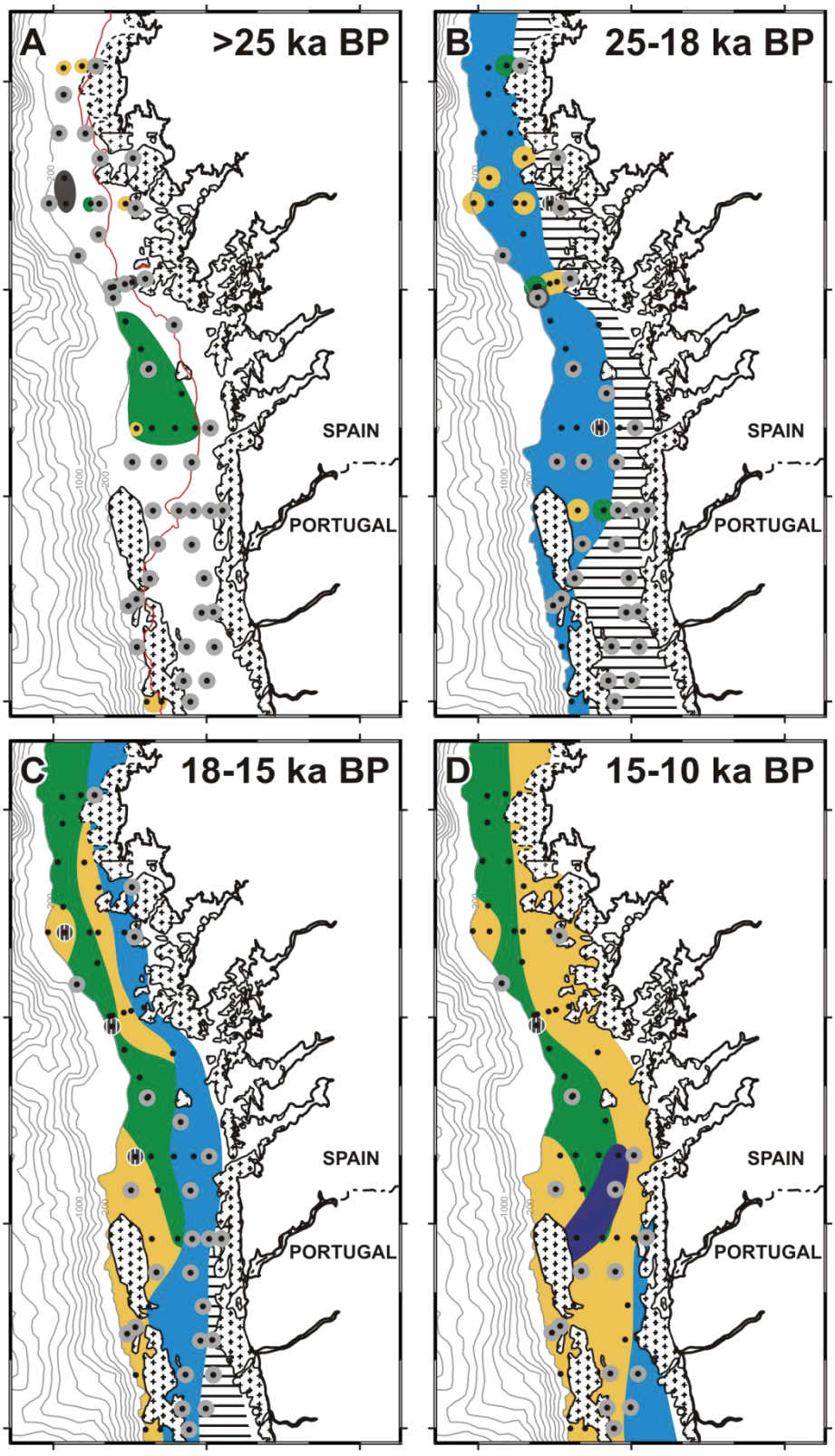

Fig. 3.8. Schematic map of the facies evolution within time slices. A = pre-LGM (>25 ka BP); B = LGM (25–18 ka BP); C = early deglaciation (18–15 ka BP); D = late deglaciation (15–10 ka BP); E = early Holocene (10–6 ka BP); F = late Holocene (6–0 ka BP). The red line in map A indicates 120-m water depth below modern sea level.

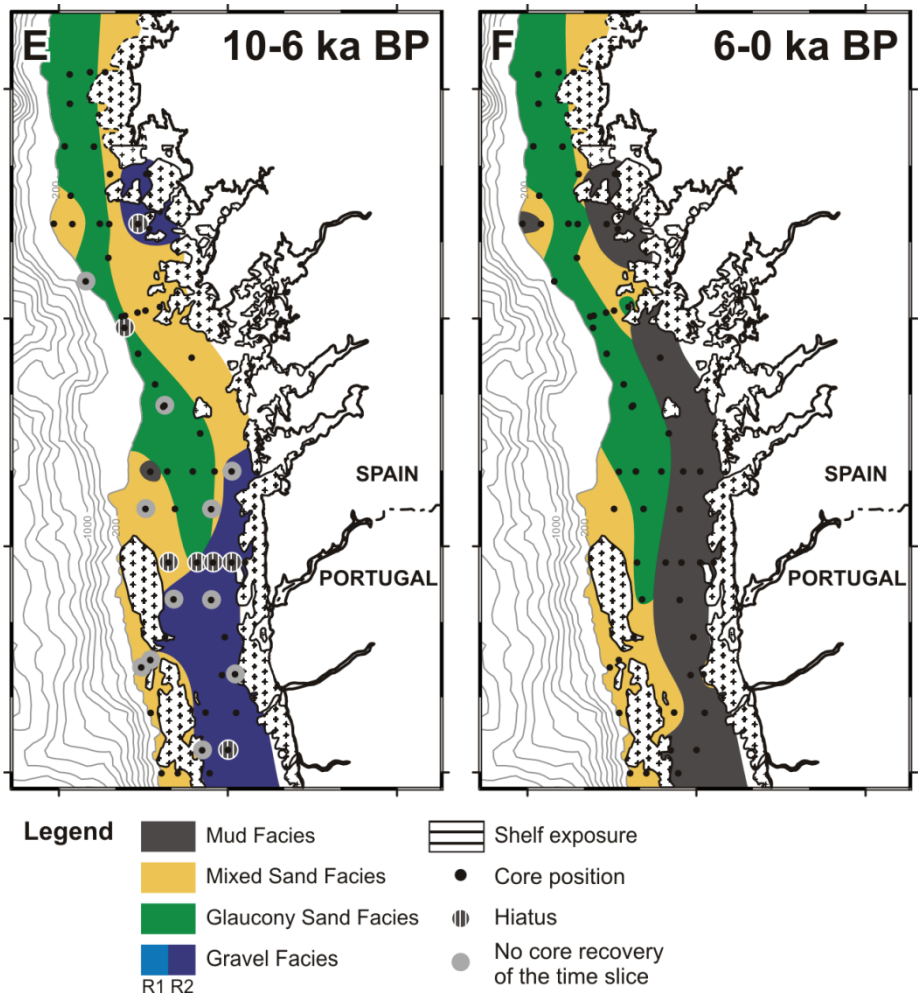

Fig. 3.8 *(continued)*.

processes controlling the sediment distribution of these sub-types differ largely. Three mechanisms of material contribution to the gF *shoreface deposits* are conceivable, (1) shallow-water production of macrobenthic carbonate shells, (2) a direct supply of coarse-grained fluvial material, and (3) recycling of material gained by erosion at the shoreline. The latter could be the dominant process as indicated by the common occurrence of heavily-altered shell fragments. However, the main processes responsible for the distribution patterns of this material are related to the strong impact of coastal currents and waves. These forces lead to the contribution and enrichment of coarse material due to coastal erosion and sorting effects, respectively. Additionally, fines are winnowed and coarse particles are rounded. The material of the gF *event beds* stems from the reworking of older coarse-sandy and gravelly shelf deposits also comprising the erosion and redeposition of shoreface deposits. The main process controlling the distribution of this sub-facies type is, therefore, the redeposition of material by high-energy events such as large winter storms. Waves, which are induced by such storms, may cause significant sediment remobilisation even in 200 m water depth (Huthnance et al., 2002). Both gF shoreface deposits and event beds are characterised by an erosional base, which is interpreted as the transgressive ravinement surface.

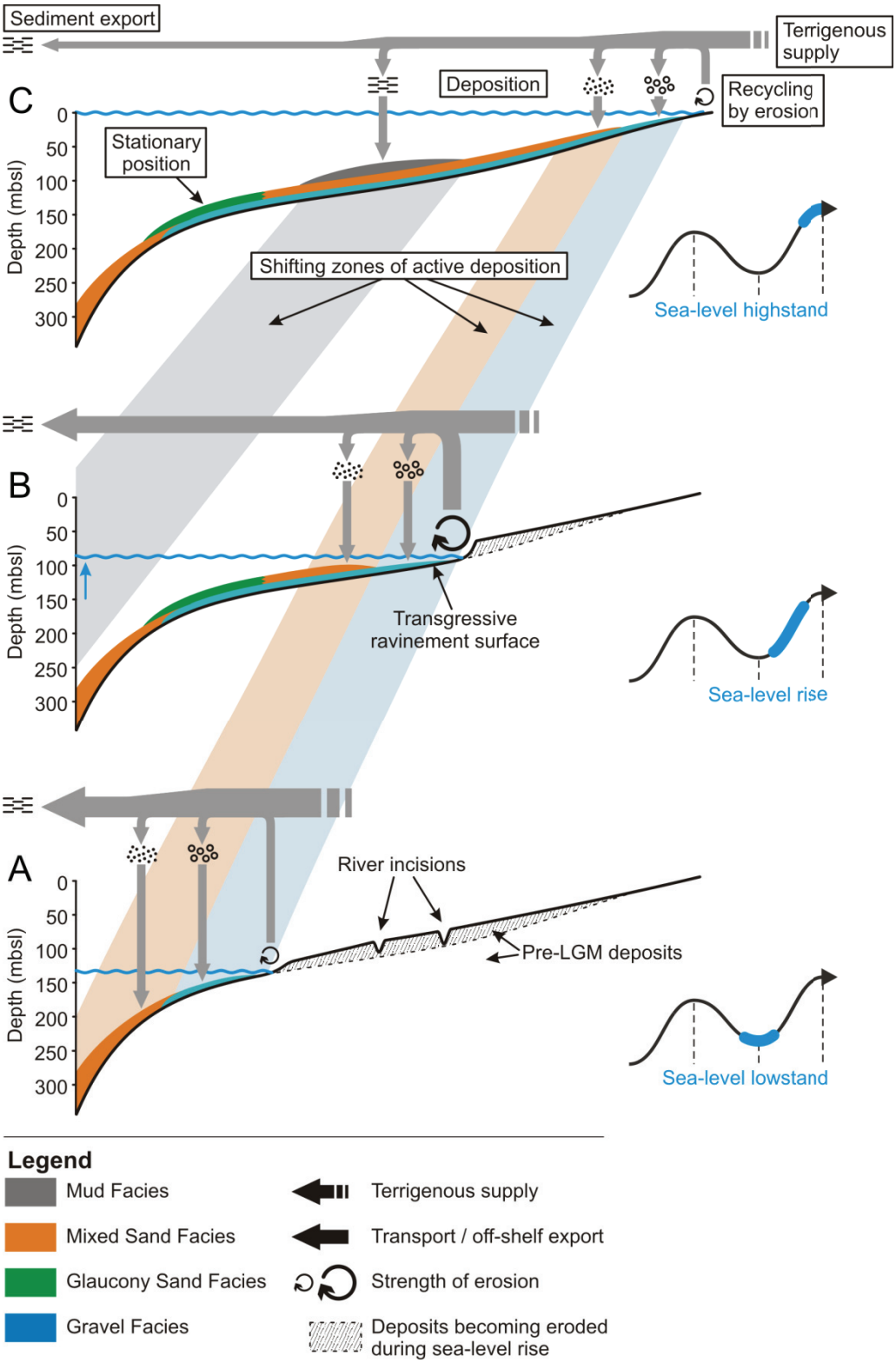

Fig. 3.9. Schematic shelf evolution model showing the distribution of the classified facies types, the landward shift of the Gravel Facies, Mixed-Sand Facies, and Mud Facies, and the decreased off-shelf export of fines as well as reduced terrigenous supply due to sea-level rise. Real thickness of the units and supply of sediments by biogenic production are not displayed. Deposits of the Glaucony-Sand Facies stem from recycling of older glaucony-containing deposits.

However, the subdivision of gF into storm gravel beds and shoreface deposits provides no consistent pattern which would allow a further subdivision of the gF within the individual time slices of Fig. 3.8. The reason could be that the interpretation of these layers is sometimes ambiguous due to the reworking and redeposition of previous shoreface sediments during storm events. This redistribution and the time-transgressive evolution of the gF point to a multi-stage evolution of these deposits.

Radiocarbon ages on sF_{mixed} and sF_{glauc} sediments in several cores (e.g., Cores 13089-2 and 11027-2 in Figs. 3.3A, C; Fig. 3.8B) indicate that the initial deposition of these facies types took already place during the LGM (Fig. 3.9A). Hence, gF beds which were formed during the LGM became subsequently covered by deposits of sF_{mixed} as well as sF_{glauc} (Fig. 3.8B). However, the shelf-wide accumulation of sF_{mixed} and sF_{glauc} sands was hindered by generally stronger hydrodynamic conditions due to the lower sea level and related lower wave base.

Fines of the mF were preferentially exported off-shelf at this time, an assumption which is supported by significantly higher sedimentation rates of slope deposits during glacial times (Baas et al., 1997; Fig. 3.9A). Nevertheless, a core from the outer shelf (130205-2; site 205 in Fig. 3.1) shows the deposition of mF during the LGM. This remarkable deposition of fines during the low sea-level of the LGM could be related to a morphological depression at this shelf position which most probably provided lower hydrodynamic conditions and acted, thus, as sediment trap along the export pathway of fines. The general mechanism for the off-shelf transport of fines might have been comparable to the modern situation in which fines are frequently resuspended by strong winter storms and partly exported via the enhanced bottom nepheloid layer during seasonal downwelling.

3.5.3. Early deglaciation (18–15 ka BP)

During early deglaciation global sea level rose to ~100 mbsl (Peltier and Fairbanks, 2006). Hence, only parts of the higher-elevated southern study area remained exposed (Fig. 3.8C). Younger radiocarbon dates on gF beds (~17 ka BP) in landward direction (Core 11012-2 in Fig. 3.3A; Core 11004-2 in Fig. 3.3B) indicate a time-transgressive development of this layer. The proceeding flooding of the shelf led to coastal retrogradation as well as to an associated landward shift of the storm-wave base. Deposition of gF sediments is restricted to this high-energy zone (Fig. 3.9B). Strong erosion within this zone might have contributed material to the gF as well as to sF_{mixed} and sF_{glauc} which show a further expansion in deeper waters on the outer shelf where lower hydrodynamic conditions already prevailed (Fig. 3.8C). However, sediments of the mF are not present during the early deglaciation due to either a general low preservation potential of these muddy deposits or, more conceivable, the continuing off-shelf export of fines and related bypassing across the shelf.

The occurrence of sF_{glauc} during the early deglaciation might be explained by large-scale redepositions of older glaucony-rich deposits. Indications for such major redepositions are (1) the Miocene to Pliocene glaucony ages in surface deposits (Odin and Lamboy, 1988), and (2) age reversals within sF_{glauc} in Cores 11004-2 (Fig. 3.3B), 11013-2 (Fig. 3.3A), and 11020-2 (site 20 in Fig. 3.1). Thus, an internal reflector at the position of Core 11013-2 within U2 in Profile A might represent an erosional surface caused by large-scale redeposition related to a major storm event (Fig. 3.2A). Hence, the formation of sF_{glauc}

seems to depend on the presence of older glaucony-containing deposits. The availability of such deposits is shown by the presence of the sF_{glauc} in the pre-LGM time slice (Fig. 3.8A). According to Odin and Lamboy (1988), the glaucony of Miocene/Pliocene origin shows no indications for burial processes which might point to frequent remobilisation since that time. Furthermore, a long history of authigenic glaucony contribution was reported by Odin and Lamboy (1988).

3.5.4. Late deglaciation (15–10 ka BP)

During the continuing sea-level rise of the late deglaciation from ~100 to ~30 mbsl (Peltier and Fairbanks, 2006) gF deposits shifted most probably towards the inner shelf as indicated by (undated) shoreface deposits at site 37 (Figs. 3.1 and 3.9B). Previous gF deposits of the LGM and early deglaciation became covered by sF_{mixed} and sF_{glauc} sediments (Fig. 3.8D) which show a maximum thickness of 15 m in the southern study area. This significant deposition of sF_{mixed} and sF_{glauc} on the shelf contradicts the common assumption that deposition during the deglacial sea-level rise is mainly restricted to the formation of a thin transgressive lag (Posamentier and Allen, 1999; Catuneanu, 2002). The relatively thick transgressive deposits on the NW Iberian shelf could be explained by large-scale erosion in shallow waters due to the rising sea-level, subsequent transport to deeper environments and redeposition of this material under moderate hydrodynamic conditions. Another indication for such massive erosion is the absence of river incisions of the last-glacial sea-level fall and LGM in seismic profiles which was emphasised by (Lantzsch et al., 2009). Additionally, these authors reported a scarce appearance of internal structures within sediments of the sea-level rise, which could be explained by the intense redistribution of sediments in the run of the rising sea-level (Fig. 3.9B). The terrigenous sediment supply to the NW Iberian shelf most probably decreased during the sea-level rise (Fig. 3.9B) due to the progressive flooding of the deep Rías Baixas and increased marine influence within river estuaries leading to a retention of fluvial material within river basins (Drago et al., 2006; Vis et al., 2008).

The widespread distribution of the homogenous sF_{mixed} deposits might be explained by the deglacial flooding of the shelf which resulted in moderate hydrodynamic conditions on outer and mid-shelf, favouring the deposition of sands (Fig. 3.9B). In contrast to the sF_{mixed}, the sF_{glauc} shows no landward shift but remained restricted to a water depth of below 120 m (Figs. 3.8D and 3.9B). This limitation could be due to (1) a non-presence of older glaucony-containing deposits above 120 mbsl and, therefore, a missing sediment source, or (2) low terrigenous sedimentation in this area. The latter could be caused by an overall low terrigenous supply or oceanographic effects such as stronger currents on the outer shelf as well as internal waves leading to a winnowing of fines. This low terrigenous supply would have favoured the authigenic production of glaucony and/or prevented the dilution of the glaucony content. At least in the area south of 42°N, the absence of older glaucony-containing deposits is obvious due to the complete erosion of pre-LGM sediments (Lantzsch et al., 2009). The authigenic formation of glaucony in this area was most probably hindered by a higher sediment input due to the contribution of terrigenous material by the Minho River during the lower sea level of the deglaciation. Hence, the main factors for sF_{glauc} deposition on the NW Iberian shelf are (1) a strong hydrodynamic regime and related reworking of older glaucony-rich deposits (Fig. 3.9B), and (2) the authigenic production of

glaucony due to low sedimentation rates. The broader extension of the sF_{glauc} in front of the Rías Baixas is most probably related to the gently dipping shelf geometry (Fig. 3.2B).

Subordinate gF deposits with a maximum thickness limited to only 0.2 m appear as intercalation in sF_{mixed} and sF_{glauc} deposits (e.g., in Core 11013-2; Fig. 3.3A). These coarse layers represent locally restricted late-transgressive lag deposits and storm event beds. A gF layer showing a more extensive spatial distribution is observed in cores on the mid-shelf (R2 in Figs. 3.3 and 3.8D, E). A radiocarbon age of 12 ka BP in Core 11003-2 above this horizon (Fig. 3.3B) and the measured age of 11 ka BP within these deposits by González-Álvarez et al. (2005; close to site 39; Fig. 3.1) indicates an initial deposition of this gF bed during the late deglaciation in water depths around 130 m between the Rías Baixas and the Minho River mouth (Fig. 3.8D). The deposition of such a coarse bed points to generally persistent conditions of occasional reworking dynamics suppressing any deposition or long-term preservation of finer sediments. These conditions could explain the non-presence of the mF during the deglacial sea-level rise. The overall terrigenous supply is expected to decrease rapidly during this time due to the rise of base-level. An even stronger decrease in terrigenous supply to the shelf was related to the progressional flooding of estuaries and drowning of the Rías, which led to trapping of major amounts of material (Drago et al., 2006; Lantzsch et al., in press).

3.5.5. Early Holocene (10–6 ka BP)

The early Holocene is characterised by a strong deceleration in global sea-level rise (Peltier and Fairbanks, 2006). The sF_{glauc} and sF_{mixed} remain relatively stationary on the outer shelf (Fig. 3.8E). However, this stabilization is not mirrored by the gF deposits. The aforementioned late-transgressive gF bed (R2 in Figs. 3.3 and 3.8D, E) shows a further shift towards shallower waters as indicated by a radiocarbon age of 12 ka BP below this layer in Core 11030-2 (Fig. 3.3C). These deposits occur in the northern study area (in front of Ría de Muros) as well as in the southern part (Fig. 3.8E), whereas cores from the middle part are characterised by the occurrence of an erosional surface without deposition of gF material (sites 1 and 10 in Fig. 3.1). The reason for the widespread occurrence of the gF in the southern study area is the higher elevation of this area and, therefore, stronger hydrodynamic conditions due to a shallower water depth (Figs. 3.1 and 3.8E).

Early Holocene deposition of sF_{mixed} and sF_{glauc} above gF deposits is restricted to exceptional positions on the mid-shelf (Fig. 3.8E). There, the late-transgressive gF beds became covered by sF_{mixed} and sF_{glauc} sands which show a continuous transition towards mF sediments (Cores 13046-2, 11002-3, and 13041-2 in Fig. 3.3). Such a gradual change was proposed to be a general pattern for the evolution of Holocene mud depocentres in the NW Iberian shelf system (Lantzsch et al., in press).

The deposition of mF sediments on top of Core 11007-2 (Figs. 3.3B and 3.8E) most probably took place during the early Holocene. The exact age of these sediments is unknown but a radiocarbon age of 13 ka BP in the same core, 70-cm below these deposits, displays the maximum age (Fig. 3.3B). Regardless of the exact age, these deposits represent an exceptional occurrence of preserved mF material on the outer shelf.

3.5.6. Late Holocene (6–0 ka BP)

The modern sea-level was established between 6 and 5 cal ka BP and remained more or less stable since then (Peltier and Fairbanks, 2006). This Holocene sea-level stabilisation provided the basis for extended mud deposition on the NW Iberian mid-shelf (Lantzsch et al., in press). In contrast to the aforementioned continuous change towards mud deposition in exceptional positions, most of the cores showing Holocene mF deposits are characterised by a well-defined hiatus between mud deposit and underlying late-transgressive gF beds (Fig. 3.3). Hence, whereas fines of the mF were mainly exported off-shelf prior to the Holocene highstand, this situation changed obviously with the stabilisation of the sea level (Fig. 3.9C; Lantzsch et al., in press). The formation of the Holocene mF is dominantly controlled by (1) fluvial input of terrigenous fines, (2) repeated resuspension of this material due to high-energy winter storms, and (3) subsequent deposition due to the relatively weak hydrodynamic regime in mid-shelf position (Drago et al., 1998; Dias et al., 2002). The shelf morphology plays a minor role for mF distribution. Its influence is mainly restricted to the trapping of fines in front of the Ría de Muros and in the most southern part of the study area (Lantzsch et al., in press). In contrast to unexpected thick deposits related to the deglacial sea-level rise, mF deposits of the sea-level highstand show a maximum thickness of 4 m on the NW Iberian shelf. This pattern is contrasting the expectation of comparably thick, aggrading and prograding deposits due to a higher base level and increased accommodation space during sea-level highstand (Posamentier and Allen, 1999; Catuneanu, 2002). Reasons for the reduced thickness of these deposits on the NW Iberian shelf are, most probably, the high-energy hydrodynamic conditions in combination with a low overall sediment contribution by the rivers within the study area, and, in case of the Galicia Mud Belt, the large distance to the Douro River as main source of terrigenous sediment supply.

The modern deposition of coarser terrigenous material, i.e. sF_{mixed} and gF, is restricted to the littoral zone as reported by Dias et al. (2002). sF_{mixed} and sF_{glauc} on outer and mid-shelf represent, most probable, relict deposits which are partially covered by mid-shelf mud deposits (Fig. 3.8F). Nevertheless, a late Holocene expansion of sF_{glauc} is indicated by surface samples, for instance in Cores 11007-2 and 11027-2 (Figs. 3.3A, B). This expansion could be either due to (1) an ongoing authigenic contribution of glaucony or (2) seasonal, non-permanent deposition of glaucony-containing material. This seasonal deposition could be also the reason for the occurrence of the mF in the surface sample of Core 13089-2 (Fig. 3.3A). Most probably, these surface deposits will be reworked once again during strong winter storms.

3.6. Conclusions

Four facies types were observed on the NW Iberian shelf, which represent the broad range of sediments on this high-energy, low-accumulation system. These are the Gravel Facies, Mixed-Sand Facies, Glaucony-Sand Facies, and Mud Facies. The spatial and temporal evolution of these facies types shows the general development of the shelf in response to the deglacial sea-level rise.

During the LGM, large areas of the shelf were exposed. Coarse material of the Gravel Facies became deposited in shallow waters of the outer shelf. There, the strong hydrodynamic regime led to enrichment of coarse material in the shoreface zone, extensive storm

redeposition as well as winnowing and bypassing of mud and sands, which were preferentially exported off-shelf.

The deglacial sea-level rise also shows a persistent export of fines, although sands of the Mixed-Sand Facies and Glaucony-Sand Facies show widespread deposition due to large-scale erosion and recycling of older deposits. The Mixed-Sand Facies developed as a mixture of terrigenous and marine biogenic sands under moderate hydrodynamic conditions. The distribution of the Glaucony-Sand Facies is strongly controlled by the large-scale redeposition of older glaucony-containing deposits, and authigenic glaucony formation contributes material in areas of low terrigenous supply. The locality of Gravel-Facies deposition shifted landward with the rising sea level. During the late deglacial sea-level rise, the drowning of river systems resulted in a decreased supply of terrigenous sands due to entrapment of major amounts of material within the river basins. The deposition of sands became restricted to the littoral zone.

Finally, the Holocene sea-level stabilisation and related weaker hydrodynamic conditions on mid-shelf favoured the deposition of the Mud Facies on the shelf. The off-shelf export of fines significantly decreased and confined Holocene mud depocentres formed in mid-shelf position. Areas of the outer shelf remained mainly bare of recent sediments.

Hence, this study shows in a comprehensive way and corroborated by numerous well-dated sediment cores that the deglacial sea-level rise resulted in a complete reconfiguration of the NW Iberian sedimentary shelf system. Moreover, the facies-type evolution in this high-energy, low-accumulation regime displays (1) the importance of large-scale sediment recycling during the sea-level rise, and (2) the effect of low terrigenous supply on the restricted sediment deposition during the sea-level highstand.

Further studies with comprehensive coring programs are needed to reveal in a comparative way the spatial and temporal evolution of sedimentary shelf systems characterised by different configurations in terms of, for instance, volume and type of sediment supply, strength of the hydrodynamic conditions, and shelf morphology. This should increase the knowledge on the general mechanisms controlling the sediment distribution and would represent an important step towards the explanation of the high sedimentary variability of these systems.

Acknowledgements

We are thankful to Dave Heslop for his support with the cluster analysis and his helpful comments on dealing with compositional data. We also wish to thank Sebastian Krastel-Gudegast, Christoph Vogt, and Vera B. Bender for their contribution to this project. Special thanks go to Captain Michael Schneider and his complete crew on *RV Poseidon* for their outstanding support. This work was funded through DFG-Research Center/Cluster of Excellence “The Ocean in the Earth System”.

References

Abrantes, F., Lebreiro, S., Rodrigues, T., Gil, I., Bartels-Jónsdóttir, H., Oliveira, P., Kissel, C., Grimalt, J.O., 2005. Shallow-marine sediment cores record climate variability and earthquake activity off Lisbon (Portugal) for the last 2000 years. Quaternary Science Reviews 24 (23-24), 2477-2494.

Aitchison, J., Barceló-Vidal, C., Martín-Fernández, J.A., Pawlowsky-Glahn, V., 2000. Logratio analysis and compositional distance. Mathematical Geology 32 (3), 271-275.

Baas, J.H., Mienert, J., Abrantes, F., Prins, M.A., 1997. Late Quaternary sedimentation on the Portuguese continental margin: climate-related processes and products. Palaeogeography, Palaeoclimatology, Palaeoecology 130 (1-4), 1-23.

Bahr, A., Wong, H.K., Yim, W.W.S., Huang, G., Ludmann, T., Chan, L.S., Thomas, W.N.R., 2005. Stratigraphy of Quaternary inner-shelf sediments in Tai O Bay, Hong Kong, based on ground-truthed seismic profiles. Geo-Marine Letters 25 (1), 20-33.

Bard, E., Arnold, M., Hamelin, B., Tisnerat-Laborde, N., Cabioch, G., 1998. Radiocarbon calibration by means of mass spectrometric Th-230/U-234 and C-14 ages of corals: an updated database including samples from Barbados, Mururoa and Tahiti. Radiocarbon 40 (3), 1085-1092.

Bartels-Jónsdóttir, H.B., Knudsen, K.L., Abrantes, F., Lebreiro, S., Eiríksson, J., 2006. Climate variability during the last 2000 years in the Tagus Prodelta, western Iberian Margin: benthic foraminifera and stable isotopes. Marine Micropaleontology 59 (2), 83-103.

Bedzek, J.C., Ehrlich, R., Full, W., 1984. The fuzzy c-means clustering algorithm. Computers & Geoscience 10, 191-203.

Bernárdez, P., González-Álvarez, R., Francés, G., Prego, R., Bárcena, M.A., Romero, O.E., 2008. Late Holocene history of the rainfall in the NW Iberian peninsula – evidence from a marine record. Journal of Marine Systems 72 (1-4), 366-382.

Blair, T.C., McPherson, J.G., 1999. Grain-size and textural classification of coarse sedimentary particles. Journal of Sedimentary Research 69 (1), 6-19.

Brooks, G.R., Doyle, L.J., Davis, R.A., DeWitt, N.T., Suthard, B.C., 2003. Patterns and controls of surface sediment distribution: west-central Florida inner shelf. Marine Geology 200 (1-4), 307-324.

Buck, K.F., C. Olson, H., Austin, J.A., 1999. Paleoenvironmental evidence for latest Pleistocene sea-level fluctuations on the New Jersey outer continental shelf: combining high-resolution sequence stratigraphy and foraminiferal analysis. Marine Geology 154 (1-4), 287-304.

Catuneanu, O., 2002. Sequence stratigraphy of clastic systems: concepts, merits, and pitfalls. Journal of African Earth Sciences 35 (1), 1-43.

Corredeira, C., Araújo, M.F., Gouveia, A., Jouanneau, J.M., 2005. Geochemical characterization of sediment cores from the continental shelf off the western rias area (NW Iberian Peninsula). Ciencias Marinas 31 (1B), 319-325.

Dekkers, M.J., Langereis, C.G., Vriend, S.P., Van Santvoort, P.J.M., De Lange, G.J., 1994. Fuzzy c-means cluster analysis of early diagenetic effects on natural remanent magnetisation acquisition in a 1.1 Myr piston core from the Central Mediterranean. Physics of the Earth and Planetary Interiors 85, 155-171.

Dias, J.M.A., Nittrouer, C.A., 1984. Continental shelf sediments of northern Portugal. Continental Shelf Research 3 (2), 147-165.

Dias, J.M.A., Gonzalez, R., Garcia, C., Diaz-del-Rio, V., 2002. Sediment distribution patterns on the Galicia-Minho continental shelf. Progress in Oceanography 52 (2-4), 215-231.

Díaz, J., Nelson, C.H., Barber, J.H., Giró, S., 1990. Late Pleistocene and Holocene sedimentary facies on the Ebro continental shelf. Marine Geology 95 (3-4), 333-352.

Drago, T., Oliveira, A., Magalhães, F., Cascalho, J., Jouanneau, J.M., Vitorino, J., 1998. Some evidences of northward fine sediment transport in the northern Portuguese continental shelf. Oceanologica Acta 21 (2), 223-231.

Drago, T., Freitas, C., Rocha, F., Moreno, J., Cachao, M., Naughton, F., Fradique, C., Araujo, F., Silveira, T., Oliveira, A., Cascalho, J., Fatela, F., 2006. Paleoenvironmental evolution of estuarine systems during the last 14,000 years – the case of Douro estuary (NW Portugal). Journal of Coastal Research 1, 186-192.

Ferrín, A., 2005. Cenozoic seismic stratigraphy of the SW Galician continental shelf. Comparative study with the Canterbury shelf (SE New Zealand) during the Quaternary. Ph.D. thesis, Facultad de Ciencas del Mar, Departmento de Geociencias Marinas y Ordenación del Territorio, Universidad de Vigo, Spain.

González-Álvarez, R., Bernárdez, P., Pena, L.D., Francés, G., Prego, R., Diz, P., Vilas, F., 2005. Paleoclimatic evolution of the Galician continental shelf (NW of Spain) during the last 3000 years: from a storm regime to present conditions. Journal of Marine Systems 54 (1-4), 245-260.

Grossman, E.E., Eittreim, S.L., Field, M.E., Wong, F.L., 2006. Shallow stratigraphy and sedimentation history during high-frequency sea-level changes on the central California shelf. Continental Shelf Research 26 (10), 1217-1239.

Hanebuth, T.J.J., Stattegger, K., Bojanowski, A., 2009. Termination of the Last Glacial Maximum sea-level lowstand: The Sunda-Shelf data revisited. Global and Planetary Change 66 (1-2), 76-84.

Huthnance, J.M., Humphery, J.D., Knight, P.J., Chatwin, P.G., Thomsen, L., White, M., 2002. Near-bed turbulence measurements, stress estimates and sediment mobility at the continental shelf edge. Progress in Oceanography 52 (2-4), 171-194.

Jouanneau, J.M., Weber, O., Drago, T., Rodrigues, A., Oliveira, A., Dias, J.M.A., Garcia, C., Schmidt, S., Reyss, J.L., 2002. Recent sedimentation and sedimentary budgets on the western Iberian shelf. Progress in Oceanography 52 (2-4), 261-275.

Lantzsch, H., Hanebuth, T.J.J., Bender, V.B., in press. Holocene evolution of mud depocentres on a high-energy, low-accumulation shelf (NW Iberia). Quaternary Research doi:10.1016/j.yqres.2009.07.009.

Lantzsch, H., Hanebuth, T.J.J., Bender, V.B., Krastel, S., 2009. Sedimentary architecture of a low-accumulation shelf since the Late Pleistocene (NW Iberia). Marine Geology 259 (1-4), 47-58.

Maldonado, A., Swift, D.J.P., Young, R.A., Han, G., Nittrouer, C.A., DeMaster, D.J., Rey, J., Palomo, C., Acosta, J., Ballester, A., Castellvi, J., 1983. Sedimentation on the Valencia Continental Shelf: preliminary results. Continental Shelf Research 2 (2-3), 195-211.

Martins, V., Dubert, J., Jouanneau, J.-M., Weber, O., da Silva, E.F., Patinha, C., Alveirinho Dias, J.M., Rocha, F., 2007. A multiproxy approach of the Holocene evolution of shelf-slope circulation on the NW Iberian Continental Shelf. Marine Geology 239 (1-2), 1-18.

Muñoz, A., Acosta, J., Uchupi, E., 2003. Cenozoic tectonics on the Galicia margin, northwest Spain. Geo-Marine Letters 23 (1), 72-80.

Naughton, F., Bourillet, J.F., Fernanda, M., Goñi, S., Turon, J.L., Jouanneau, J.M., 2007. Long-term and millennial-scale climate variability in northwestern France during the last 8850 years. Holocene 17 (7), 939-953.

Odin, G.S., Matter, A., 1981. De glauconiarum origine. Sedimentology 28 (5), 611-641.

Odin, G.S., Lamboy, M., 1988. Glaucony from the Margin off Northwestern Spain. In: Odin, G.S. (Ed.) Green Marine Clays. Developments in Sedimentology 45, Elsevier, Amsterdam, Oxford, New York, pp. 249-275.

Ogston, A.S., Cacchione, D.A., Sternberg, R.W., Kineke, G.C., 2000. Observations of storm and river flood-driven sediment transport on the northern California continental shelf. Continental Shelf Research 20 (16), 2141-2162.

Okyar, M., Ergin, M., Evans, G., 2005. Seismic stratigraphy of Late Quaternary sediments of western Mersin Bay shelf, (NE Mediterranean Sea). Marine Geology 220 (1-4), 113-130.

Oliveira, A., Rocha, F., Rodrigues, A., Jouanneau, J., Dias, A., Weber, O., Gomes, C., 2002. Clay minerals from the sedimentary cover from the Northwest Iberian shelf. Progress in Oceanography 52 (2-4), 233-247.

Oliveira, I., Valle, A., Miranda, F., 1982. Litoral problems in the portuguese west coast. Proceedings of the 18th Coastal Engineering Conference 3, 1951-1969.

Pawlowsky-Glahn, V., Egozcue, J.J., 2006. Compositional data and their analysis: an introduction. Geological Society, London, Special Publications 264 (1), 1-10.

Peltier, W.R., Fairbanks, R.G., 2006. Global glacial ice volume and Last Glacial Maximum duration from an extended Barbados sea level record. Quaternary Science Reviews 25 (23-24), 3322-3337.

Posamentier, H.W., Allen, G.P., 1999. Siliciclastic sequence stratigraphy: concepts and applications. Society of Economic Paleontologists and Mineralogists, Concepts in Sedimentology and Paleontology 7, Tulsa.

Rey Salgado, J., 1993. Relación morfosedimentaria entre la plataforma continental de Galicia y las Rías Bajas y su evolución durante el Cuaternario. Publicaciones Especiales, Instituto Español de Oceanografía 17, 1-233.

Sammon, J.W., 1969. A non-linear mapping for data structure analysis. IEEE Transactions on Computers C18, 401-409.

Stuiver, M., Reimer, P.J., Bard, E., Beck, J.W., Burr, G.S., Hughen, K.A., Kromer, B., McCormac, G., Van der Plicht, J., Spurk, M., 1998. INTCAL98 radiocarbon age calibration, 24,000–0 cal BP. Radiocarbon 40 (3), 1041-1083.

Vis, G.-J., Kasse, C., Vandenberghe, J., 2008. Late Pleistocene and Holocene palaeogeography of the Lower Tagus Valley (Portugal): effects of relative sea level, valley morphology and sediment supply. Quaternary Science Reviews 27 (17-18), 1682-1709.

Vitorino, J., Oliveira, A., Jouanneau, J.M., Drago, T., 2002a. Winter dynamics on the northern Portuguese shelf. Part 1: physical processes. Progress in Oceanography 52 (2-4), 129-153.

Vitorino, J., Oliveira, A., Jouanneau, J.M., Drago, T., 2002b. Winter dynamics on the northern Portuguese shelf. Part 2: bottom boundary layers and sediment dispersal. Progress in Oceanography 52 (2-4), 155-170.

Vriend, S.P., van Gaans, P.F.M., Middelburg, J., de Nijs, A., 1988. The application of fuzzy c-means cluster analysis and non-linear mapping to geochemical datasets: examples from Portugal. Applied Geochemistry 3 (2), 213-224.

4. Holocene evolution of mud depocentres on a high-energy, low-accumulation shelf (NW Iberia)

Hendrik Lantzsch, Till J.J. Hanebuth, Vera B. Bender

Quaternary Research, in press, corrected proof, doi:10.1016/j.yqres.2009.07.009

Quaternary Research xxx (2009) xxx–xxx

Contents lists available at ScienceDirect

Quaternary Research

journal homepage: www.elsevier.com/locate/yqres

Holocene evolution of mud depocentres on a high-energy, low-accumulation shelf (NW Iberia)

Hendrik Lantzsch *, Till J.J. Hanebuth, Vera B. Bender

MARUM — Center for Marine Environmental Sciences, and Faculty of Geosciences, University of Bremen, P.O. Box 330440, 28334 Bremen, Germany

ARTICLE INFO

Article history:
Received 9 April 2009
Available online xxxx

Keywords:
Holocene
Shelf sedimentation
Mud belt
Radiocarbon dating
Sediment dispersal
NW Iberian Peninsula

ABSTRACT

The high-energy, low-accumulation NW Iberian shelf features three confined Holocene mud depocentres. Here, we show that the evolution of such depocentres follows successive steps. The flooding of inner shelf zones and river catchment areas by the late deglacial sea-level rise provided the precondition for shelf mud deposition. Following this, the Holocene deceleration of the sea-level rise caused a rapid refill of the accommodation space within river valleys. Subsequently, the export of major amounts of fines was initiated. The initial onset and loci of shelf mud deposition were related to deposition-favouring conditions in mid-shelf position or to the presence of morphological highs, which act as sediment traps by providing protection against stronger hydrodynamic energy. The detailed reconstruction of the Holocene depocentre evolution shows for the first time that the expansion of such shelf mud deposits cannot only occur by linear growth off the associated sediment source. Rather, they might develop around centres that are fully disconnected from the source of original sediment supply, and expand later into specific directions. Based on these differences and on the connection of the individual mud depocentres to the material source we propose a conceptual subdivision of the group "mid-shelf mud depocentres".

Introduction

Clastic shelf systems represent a major sink for both terrestrial and marine materials on the sediment pathway from the coast to the continental slope. The very dynamic nature of shelves finds its geological expression in a large lateral and stratigraphical variability of the sedimentation patterns that is usually attributed to external forcing by changes in sea level, tectonics, climate, and terrigenous input. However, shelf systems show considerable self-organization by the interaction of bathymetry, wave and current regimes. During the Holocene sea-level highstand, this interplay results particularly in deposition of mud on continental shelves. In recent years, those mud deposits became of major interest due to their role in material budgeting (Durrieu de Madron et al., 2000; Lesueur et al., 2001; Jouanneau et al., 2002; Sommerfield and Wheatcroft, 2007) and as high-resolution climate archives (Martins et al., 2007; Naughton et al., 2007b; Bernárdez et al., 2008; Hanebuth and Lantzsch, 2008; Hanebuth and Henrich, 2009).

The challenge of coring the base of mud belts due to frequently occurring basal sandy lag deposits led to a general lack of knowledge concerning (1) the precise timing of growth initiation, (2) spatial and temporal sedimentary evolution of these highstand depocentres, and (3) role of the forces controlling this development. Closing these gaps should provide a new view on the dominant forces controlling the overall sediment distribution, and on the interpretation of climatic fluctuations within this framework.

We present new data from the NW Iberian shelf including a grid of 1300 km shallow-seismic profiles, 15 sediment cores, and 30 radiocarbon dates. This study (1) analyses the mechanisms for the spatial and temporal Holocene mud deposition, and (2) provides a concept of mid-shelf mud depocentres on high-energy, low-accumulation shelf systems.

Regional settings

Morphology and geology

The NW Iberian shelf is generally narrow with a maximum extension of 50 km in front of the Douro River (Fig. 1). The shelf break occurs in water depths of 160 to 180 m (Dias et al., 2002) and is cut by the Porto submarine canyon at the northern Portuguese continental shelf at 41°20′N. The outer shelf is characterised by basement outcropping south of 42°00′N (Rey Salgado, 1993; Dias et al., 2002; Oliveira et al., 2002; Fig. 1). In contrast, on the inner shelf, plutonic and metamorphic bedrock is present north of 41°30′N (Fig. 1).

Most prominent features of the Spanish coast are the four deep Rías Baixas (Muros, Arosa, Pontevedra, Vigo), which represent Tertiary river valleys, drowned during the last deglacial sea-level rise (Rey Salgado, 1993; Oliveira et al., 2002). In contrast, the Portuguese coastline is smoothened and characterised by the estuaries of the Minho, Lima, Cávado, Ave and Douro Rivers (Fig. 1).

* Corresponding author. Fax: + 49 421 218 65219.
E-mail address: lantzsch@uni-bremen.de (H. Lantzsch).

0033-5894/$ – see front matter © 2009 University of Washington. Published by Elsevier Inc. All rights reserved.
doi:10.1016/j.yqres.2009.07.009

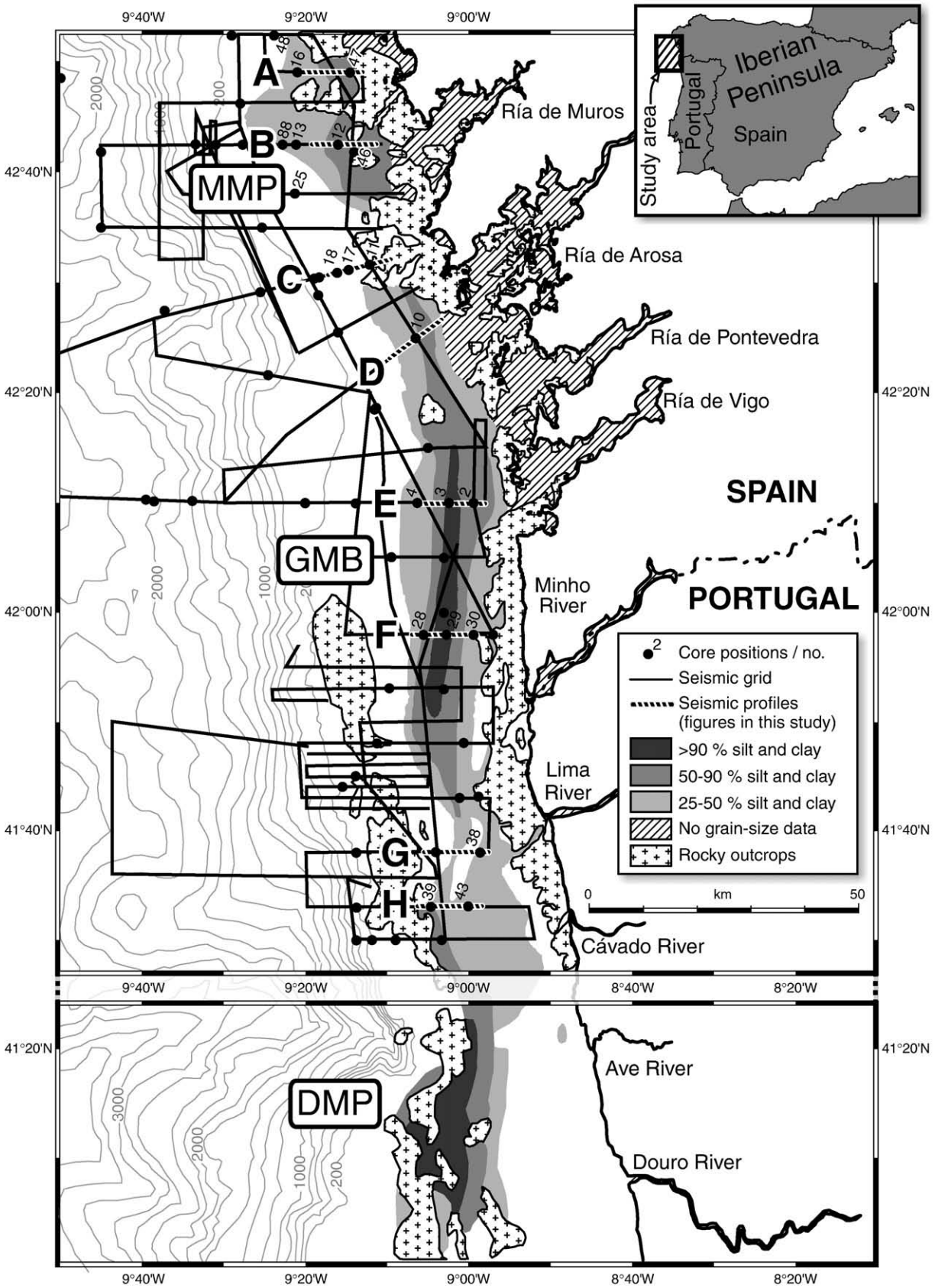

Figure 1. Map of the study area and the adjacent southern part including the position of the Douro River. The shelf surface geology is adopted from Dias et al. (2002). No grain-size measurements are applied to the Rías and river valleys. The Muros Mud Patch (MMP), Galicia Mud Belt (GMB) and Douro Mud Patch (DMP) are displayed in grey. Black lines represent the seismic profiles obtained during Cruise P342. Characters A to H represent seismic profiles shown in Figures 2 and 3. Core positions of Cruises P342 and P366/3 are marked by black dots. Cores used in this study are labelled in short form with 11002-3 being position 2 (P342), for instance and 13046-2 being position 46 (P366/3).

Please cite this article as: Lantzsch, H., et al., Holocene evolution of mud depocentres on a high-energy, low-accumulation shelf (NW Iberia), Quat. Res. (2009), doi:10.1016/j.yqres.2009.07.009

Table 1
List of the GALIOMAR sediment vibrocores of this study.

Core no. (GeoB)	Latitude (N)	Longitude (W)	Water depth [m]	Recovery [m]
11002-3	42°10.00	8°59.24	111	4.34
11003-3	42°10.00	9°02.24	129	4.54
11010-2	42°25.00	9°06.28	119	4.10
11011-2	42°31.38	9°12.07	100	4.85
11012-2	42°42.29	9°16.00	119	4.28
11017-2	42°31.10	9°14.40	120	4.88
11018-2	42°30.54	9°16.04	125	4.00
11028-2	41°57.59	9°05.29	127	4.59
11029-2	41°57.59	9°02.42	114	4.88
11030-2	41°58.00	8°59.24	94	4.60
11038-2	41°38.03	8°58.27	78	4.88
11039-2	41°33.03	9°04.38	99	4.28
11043-2	41°33.05	9°00.03	84	4.51
13046-2	42°41.80	9°14.00	106	2.41
13047-2	42°49.00	9°14.47	94	4.85

Oceanography

The NW Iberian margin is characterised by strong seasonal variations between winter and summer regimes (Dias et al., 2002; Vitorino et al., 2002). The summer situation is dominated by an equatorward directed along-shelf current, low-energy conditions, and occasional wind-driven upwelling. In contrast, highly energetic hydrodynamic conditions during the winter season result in (1) a poleward-directed current on the mid-shelf, (2) intensified river runoff due to both, generally increased precipitation and episodic river floods after storms, and (3) a shelf-wide wind-driven downwelling cell. These winter conditions are proposed to control the modern sediment distribution on the shelf (Dias et al., 2002; Vitorino et al., 2002). Therefore, we consider the NW Iberian shelf as being a high-energy sedimentary shelf system. The described oceanographic pattern is suggested to have been persistent at least over the past 4700 calibrated years before present (cal yr BP in the following; Bernárdez et al., 2008).

The sedimentary system

The Douro River is considered as the main source of fine sediments on the shelf (Araújo et al., 2002; Dias et al., 2002). In contrast, the export from the Rías Baixas is suggested to be negligible (Rey Salgado, 1993). Fine-grained fluviogenic sediments are frequently re-suspended by winter storms and transported to the north by the poleward-flowing bottom current (Dias et al., 2002). This availability of fine sediments leads to the development of well-defined areas of mud deposition in around 100 to 120 m modern water depth (Dias et al., 2002; Oliveira et al., 2002). Here, we use the term "Galicia Mud Belt" (GMB), as introduced by Lantzsch et al. (2009), due to its elongated shape running contour-parallel in mid-shelf position. The Muros and Douro mud depocentres are patch-shaped with minor elongation compared to the GMB and are, therefore, addressed as "Muros Mud Patch" (MMP) and "Douro Mud Patch" (DMP).

Due to relict sands and massive glauconite formation on the outer shelf (Dias and Nittrouer, 1984; Odin and Lamboy, 1988), and relatively low sedimentation rates (Jouanneau et al., 2002), the NW Iberian shelf is considered to represent a low-accumulation sedimentation system (Lantzsch et al., 2009). In contrast to conditions on a fully sediment-starved shelf, which is bare of any remarkable modern sedimentation (e.g. the New Jersey shelf; Goff et al., 2005), such a low-accumulation regime is characterised by the presence of confined sediment bodies as a result of persistent Holocene sedimentation.

Materials and methods

Geophysical profiling

Sediment-acoustic data were collected by means of a Boomer system during the GALIOMAR (Galician Ocean Margin Expedition) cruise in 2006 with the German research vessel POSEIDON (P342; Hanebuth et al., 2007). The frequency band of the Boomer was between 500 Hz and 10 kHz with a main frequency of around 2–3 kHz. The Boomer was shot every second with a two-second break every six shots for firing an airgun. The vertical signal resolution of the Boomer system is about 0.5 m. In total, about 1300 km of shallow-seismic lines were collected (Fig. 1).

Sediment coring

Overall, 66 sediment cores (up to 5 m long) were collected on the NW Iberian shelf and, to a minor extend, at the continental slope during the two GALIOMAR cruises P342 in 2006 and P366/3 in 2008 (Fig. 1; Table 1). A vibrocorer (VKG-6; Thomas Schmidt, Rostock, Germany) was used to recover sandy sediments from up to 230 m water depth. At greater water depths, sediment was retrieved using a gravity corer. The modern sediment surface was sampled by a giant box corer at each core location. In this study, the stratigraphic

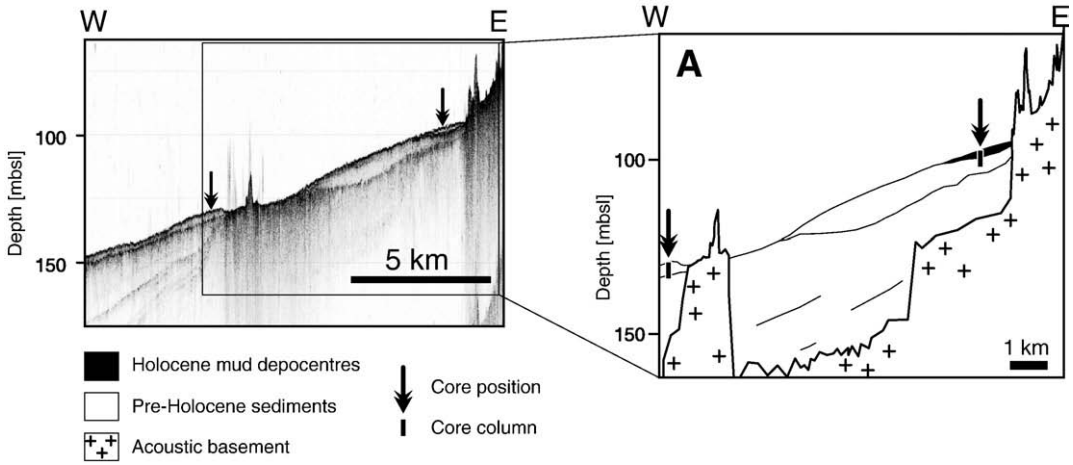

Figure 2. Boomer profile A of the respective seismic profile A shown in Figure 1 and interpretation of the architectural units following the work of Lantzsch et al. (2009). Black arrows indicate sediment-core positions. Depth on *y*-axis is given in metres below modern sea level (mbsl). The uninterpreted Boomer profiles A–H are displayed in the report of Cruise P342 (Hanebuth et al., 2007) and the interpretation of Profiles B and E–G is shown in Lantzsch et al. (2009).

Please cite this article as: Lantzsch, H., et al., Holocene evolution of mud depocentres on a high-energy, low-accumulation shelf (NW Iberia), Quat. Res. (2009), doi:10.1016/j.yqres.2009.07.009

interpretation of the mud deposits is based on Boomer profiles and 15 sediment vibrocores, and follows the late Quaternary subdivision of the NW Iberian stratigraphic shelf architecture as recently established by Lantzsch et al. (2009; Fig. 2).

Analyses in the lab

Core samples from the mud deposits are investigated in 10-cm intervals. The coarse fraction (>63 μm) was separated from the fine fraction (<63 μm) by wet sieving. The coarse fraction was then sonic-sifted into grain-size subfractions. The sediments have been classified according to their grain size using the scheme of Blair and McPherson (1999) and the results were used to corroborate the visual core description.

The selection of material for radiocarbon dating requires special care on continental shelves. Only delicate material of fresh preservation was measured in order to avoid age biasing due to re-deposition of older material. Monospecific samples were preferably selected. However, due to the lack of such a material in some samples, a selection of foraminifers and mollusc shells was necessary. As a result, 30 radiocarbon dates on 13 cores are displayed in this study (Table 2). Radiocarbon measurement was carried out by the Leibniz Laboratory in Kiel (Germany), and the Poznań Radiocarbon Laboratory (Poland). The raw ^{14}C ages were corrected using a standard marine reservoir effect of 400 yr, and converted into 1-sigma calibrated ages with the Calib 5.0.1 software (Stuiver et al., 1998). Dates with a conventional age older than 22 ka were calibrated with the function of Bard et al. (1998).

Results

The NW Iberian shelf mud deposits represent the uppermost acoustic unit in the Boomer profiles and show a sheet-like to wedge-shaped appearance (Figs. 2 and 3). Sediment cores, which were taken on these seismic profiles, show a wide range of sedimentary facies types. The cores are mainly composed of homogenous fine sands, but distinct layers of shell-fragment and siliceous gravels, and mud appear in nearly all cores as well (Fig. 3). The mud deposits are generally characterised by more than 25% fine fraction and overlie homogenous fine sands or gravels with mostly less than 10% mud contents (Fig. 3). Generally, the boundary between mud and underlying coarser sediments is sharp. Only Cores 11003-3 and 13046-2 show a different sedimentation pattern with a gradual fining-upward trend from pure sandy deposits towards mud deposition (Figs. 3B, E).

17 radiocarbon dates were measured on the gravels and fine sands underlying the mud deposits and display ages between 33,860 and 6460 cal yr BP (Table 2; Fig. 3). Two radiocarbon ages are older than 42,000 ^{14}C yr BP, i.e. beyond the limit of the radiocarbon method (Fig. 3C). Eleven radiocarbon measurements on the NW Iberian shelf mud deposits reveal ages between 5388 and 458 cal yr BP (Fig. 3). Most of these samples were taken at the base of the mud depocentres and show a considerable age offset between central and marginal core positions.

Three confined mud depocentres are observed on the NW Iberian shelf — the Muros Mud Patch (MMP), the Galicia Mud Belt (GMB), and the Douro Mud Patch (DMP). The *MMP* represents the northernmost of the mud deposits and occurs down to about 120 m water depth according to the sediment cores and surface samples in our study. The Boomer profiles of the MMP show a transparent acoustic facies, and a slightly decreasing thickness from 1.5 m to about 1 m in seaward direction, which is corroborated by the similarly seaward-thinning trend of the mud deposits in Cores 13047-2, 13046-2, and 11012-2 (Figs. 3A, B). Moreover, a grain-size coarsening is observed in the cores and surface samples in seaward direction (Fig. 3B). As a result, mud contents go generally below 25% towards the outer shelf (Sites 13, 16, 25, 48 and 88 in Fig. 1). Comparably low mud contents are also

Table 2
Radiocarbon dates and age calibration.

Lab no.[a]	Core no. (GeoB)	Depth in core (cm)	Material[b]	Age (^{14}C yr BP)	Age (cal yr BP, 1σ)[c]
KIA 33665	11002-3	250	bF	2715 ± 35	2455–2342
KIA 33664	11002-3	435	bF, bv pieces, gp	4955 ± 45	5388–5249
Poz-24670	11003-3	240	bF	7840 ± 50	8370–8260
Poz-22923	11003-3	360	bF	10,770 ± 50	12,320–12,100
Poz-24771	11003-3	399	bF	13,080 ± 70	14,810–15,110
Poz-22946	11010-2	377	*E. crispum*	15,540 ± 80	18,690–18,220
Poz-22925	11012-2	100	bF	3995 ± 35	4068–3949
Poz-22948	11012-2	320	*E. crispum*	14,820 ± 80	17,550–17,070
KIA 33677	11017-2	130	*E. crispum*	21,390 ± 200	25,540–24,910
KIA 33683	11017-2	247	*E. crispum*	28,520 ± 480	33,860–32,790[d]
KIA 33684	11017-2	417	*E. crispum*	>42,090	Uncalibrated
KIA 33685	11017-2	486	bF	>44,990	Uncalibrated
KIA 33693	11018-2	153	*E. crispum*	20,420 ± 230	24,280–23,690
KIA 33695	11018-2	399	*E. crispum*	22,030 ± 220	26,200–25,690[d]
Poz-21470	11028-2	140	bF	2555 ± 30	2290–2184
Poz-21471	11028-2	416	*E. crispum*	16,780 ± 80	19,760–19,440
Poz-22950	11028-2	429	*E. crispum*	17,310 ± 190	20,240–19,860
KIA 33687	11029-2	103	bF	850 ± 30	503–458
Poz-24772	11029-2	360	bF	2910 ± 35	2737–2669
Poz-27847	11029-2	400	bF	4300 ± 35	4490–4385
KIA 33689	11029-2	488	Echinoderm pieces	12,740 ± 80	14,480–14,080
Poz-21472	11030-2	220	bF	2940 ± 35	2749–2693
Poz-21473	11030-2	460	bF, bv	10,740 ± 50	12,260–12,040
Poz-22951	11038-2	120	bF	3165 ± 35	3013–2888
Poz-22952	11038-2	460	bF, gp	16,880 ± 90	19,800–19,500
KIA 33709	11039-2	178	bF, bv, gp	6110 ± 70	6630–6460
KIA 33714	11039-2	310	bv, gp	18,480 ± 150	21,810–21,180
Poz-26858	13046-2	135	bF	4135 ± 35	4260–4135
Poz-26856	13046-2	210	bF	8750 ± 50	9480–9390
Poz-26859	13047-2	136	bF, pF, gp	4900 ± 40	5297–5135

[a] Radiocarbon laboratory: KIA = Leibniz Laboratory in Kiel (Germany); Poz = Poznań Radiocarbon Laboratory (Poland).
[b] Material: bF = benthic foraminifers; *E. crispum* = *Elphidium crispum* (monospecific sample); bv = bivalve; gp = gastropod.
[c] For reservoir correction, the conventional age of 400 years is applied using CALIB 5.0.1. (Stuiver et al., 1998).
[d] Age calibration is based on the function of Bard et al. (1998).

Please cite this article as: Lantzsch, H., et al., Holocene evolution of mud depocentres on a high-energy, low-accumulation shelf (NW Iberia), Quat. Res. (2009), doi:10.1016/j.yqres.2009.07.009

observed in surface samples and cores of the area between MMP and GMB (Fig. 3C). Radiocarbon samples of the MMP show ages between 5297 and 3949 cal yr BP (Table 2; Figs. 3A, B). In Core 13046-2, mud contents of more than 25%, defining the MMP, are reached between 9480 cal yr BP and 4135 cal yr BP (Fig. 3B). In contrast, mud deposition in Core 11012-2 has started at 4068–3949 cal yr BP (Fig. 3B), which indicates a later onset of mud deposition in seaward parts of the MMP.

The *GMB* shows an elongated shape and stretches parallel to the coast in mid-shelf position between Ría de Arosa and Lima River. The central part of the GMB, characterised by more than 90% fine fraction, is situated in around 120 m water depth between the Ría de Pontevedra and the mouth of the Minho River (Fig. 1). A wedge geometry and distinct internal stratification are observed in the Boomer profiles in areas with a maximum thickness of 4 m (Figs. 3E, F). Marginal parts, i.e. in seaward and landward direction as well as to the north and to the south, show a decreasing thickness (Figs. 3D, G), which is corroborated by a cored mud thickness of down to 1.2 m in marginal positions (Figs. 3D–G). The contact between GMB and DMP is transitional and characterised by a limited thickness and coarser grain size compared to the well-defined centres of GMB and DMP (Figs. 1 and 3G). Radiocarbon ages of the GMB display a range between 5388 and 458 cal yr BP (Table 2; Figs. 3D–F). In the cores of Profile E, mud contents of more than 25% are reached between 8370 and 5249 cal yr BP (Fig. 3E). Similar to the radiocarbon dates from the MMP, the base of the GMB shows younger ages towards the margin of the depocentre. This is most obvious in Profile F (Fig. 3F) where marginal cores show a later onset of mud deposition (2290–2184 cal yr BP in Core 11028-2, 2749–2693 cal yr BP in Core 11030-2) than the central core (4490–4385 cal yr BP in Core 11029-2). In addition, an age range of 3013–2888 cal yr BP indicates a later initial deposition of mud in the marginal southern part (Fig. 3G).

The *DMP* is located in mid-shelf position in front of the Douro River and shows a slightly elongated extension towards the north (Fig. 1). In contrast to the GMB, the DMP is characterised by a transparent acoustic facies, and its distribution is related to the occurrence of rocky outcrops at a water depth of around 100 m (Fig. 1). The modern DMP centre is situated slightly southward of the study area. Although the surface mud contents of the DMP within the study area indicate a relatively homogenous distribution (Fig. 1), Boomer Profile H, and respective sediment cores 11039-2 and 11043-2 show that the thickness of the DMP is not distributed equally (Fig. 3H). Two areas of increased thickness are recognisable which are connected with each other by a thin blanket. The area east of the basement elevations on the outer shelf shows a maximum thickness of about 1.5 m, thinning eastward. Further landward, a maximum thickness of about 3 m is reached, finally gradually thinning towards the inner shelf (not shown).

Mud-depocentre evolution

Initial onset of mud deposition

According to the radiocarbon dating on sediments of the Muros Mud Patch (MMP) and Galicia Mud Belt (GMB), the first onset of major mud deposition is defined by a transition from pure fine sands towards mud contents of more than 25%. This transition marks the initial onset of the MMP between 9480 and 4135 cal yr BP (Figs. 3B and 4A) and of the GMB between 8370 and 5249 cal yr BP (Figs. 3E and 4A). Hence, this gradual pattern can be considered as a general mechanism of mud-belt initiation on the NW Iberian shelf. The initial accumulation of significant amounts of fine sediments, recorded by an increasing mud content in cores of the central MMP and GMB was most probably related to the drowning of the inner shelf zone during the late phase of deglacial sea-level rise and the establishment of the quasi-modern oceanographic conditions. Subsequently, the latest postglacial sea-level rise has resulted in the flooding of river valleys. Since the Douro River is considered as being the main source for the mud deposits on the NW Iberian shelf (Araújo et al., 2002), the initial evolution of these mud depocentres should be closely related to the development of this estuary. Drago et al. (2006) observed a change from a continental sedimentary facies towards marine conditions inside the Douro River valley related to this early Holocene flooding from ~9800 to ~6000 cal yr BP. Afterwards, the deceleration in Holocene sea-level rise has caused a shift in the balance between rate of sea-level rise and sediment supply, which led to a gradual refilling of the Douro estuary as documented by Drago et al. (2006) and Naughton et al. (2007a). Observations by other authors (Dabrio et al., 2000; Boski et al., 2002; Sommerfield and Wheatcroft, 2007; Vis et al., 2008) show a similar mechanism of estuarine infill. According to Long (2001), the available accommodation space within most of the worldwide estuaries was largely filled between ~7800 and ~4400 cal yr BP, which resulted in increased terrigenous export to the shelf. This enhanced export can be considered as one main reason for the initiation and further expansion of shelf mud depocentres.

Expansion of the mud depocentres

The detailed stratigraphic analysis of the NW Iberian shelf mud deposits on the base of Boomer profiles, sediment cores, and radiocarbon dates elucidates here for the first time that the evolution of such mid-shelf fine depocentres on a low-accumulation, high-energy shelf is not uniform but unexpectedly complex. The initial onset of the *MMP* is marked by a measured age of 5297–5135 cal yr BP in the northern part (Fig. 3A), and a gradual transition from pure fine sand to mud between 9480 and 4135 cal yr BP (Site 46 in Fig. 1; Fig. 3B). A basal age of 4068–3949 cal yr BP further seaward (Fig. 3B) indicates a temporal and spatial expansion of the MMP in offshore direction (Figs. 4A, B). This quasi-concentric and continuous broadening hints to the point that, although the Rías Baixas are considered to act mainly as sediment traps (Rey Salgado, 1993), the Ría de Muros is the main source for the muddy sediments of the MMP. An additional contribution of fines from the adjacent northern bay between Ría de Muros and Cape Finisterre is indicated by the northward extension of the MMP (Site 47 in Fig. 1; Fig. 3A). Consequently, the MMP does not represent a northward extension of the GMB as was suggested by previous studies (Dias et al., 2002; Oliveira et al., 2002) but rather represents an individual depocentre. Further indications for this source connection are the decrease in the MMP thickness towards the mid-shelf and the coarser grain size in seaward direction (Figs. 1 and 3A, B). The contribution of mud from the Ría de Muros to the shelf is most probably restricted to the autumn–winter period when (1) the continental runoff is enhanced, and (2) the expansion of river plumes reaches its maximum extension towards the shelf during upwelling conditions (Álvarez-Salgado et al., 2000; Otero et al., 2008).

The location of the MMP is controlled by several factors. According to McCave (1972) and Hill et al. (2007), for instance, the dominant forces influencing the distribution of mid-shelf mud belts are sediment input and the hydrodynamic conditions on the shelf (i.e. the effect of waves and shelf currents). Other authors (Edwards, 2002; Hanebuth and Lantzsch, 2008) additionally emphasised the influence of morphological features, such as structural highs and morphological steps, on the formation of mud deposits. Considering the low sediment export from the Rías Baixas, the interplay of morphological features and hydrodynamic conditions should be the key factor for the MMP formation. Hence, rocky outcrops in the inner to mid-shelf region have most probably strong influence on the shape of the MMP by trapping material due to a sheltering of sediments against stronger hydrodynamic energy. Therefore, those morphological features are considered as being the dominant parameter enabling MMP deposition. Otherwise, a sandy inner shelf would be expected in such a high-energy environment, as it is the case for the area in front of the Douro River mouth, for instance (Fig. 1).

Please cite this article as: Lantzsch, H., et al., Holocene evolution of mud depocentres on a high-energy, low-accumulation shelf (NW Iberia), Quat. Res. (2009), doi:10.1016/j.yqres.2009.07.009

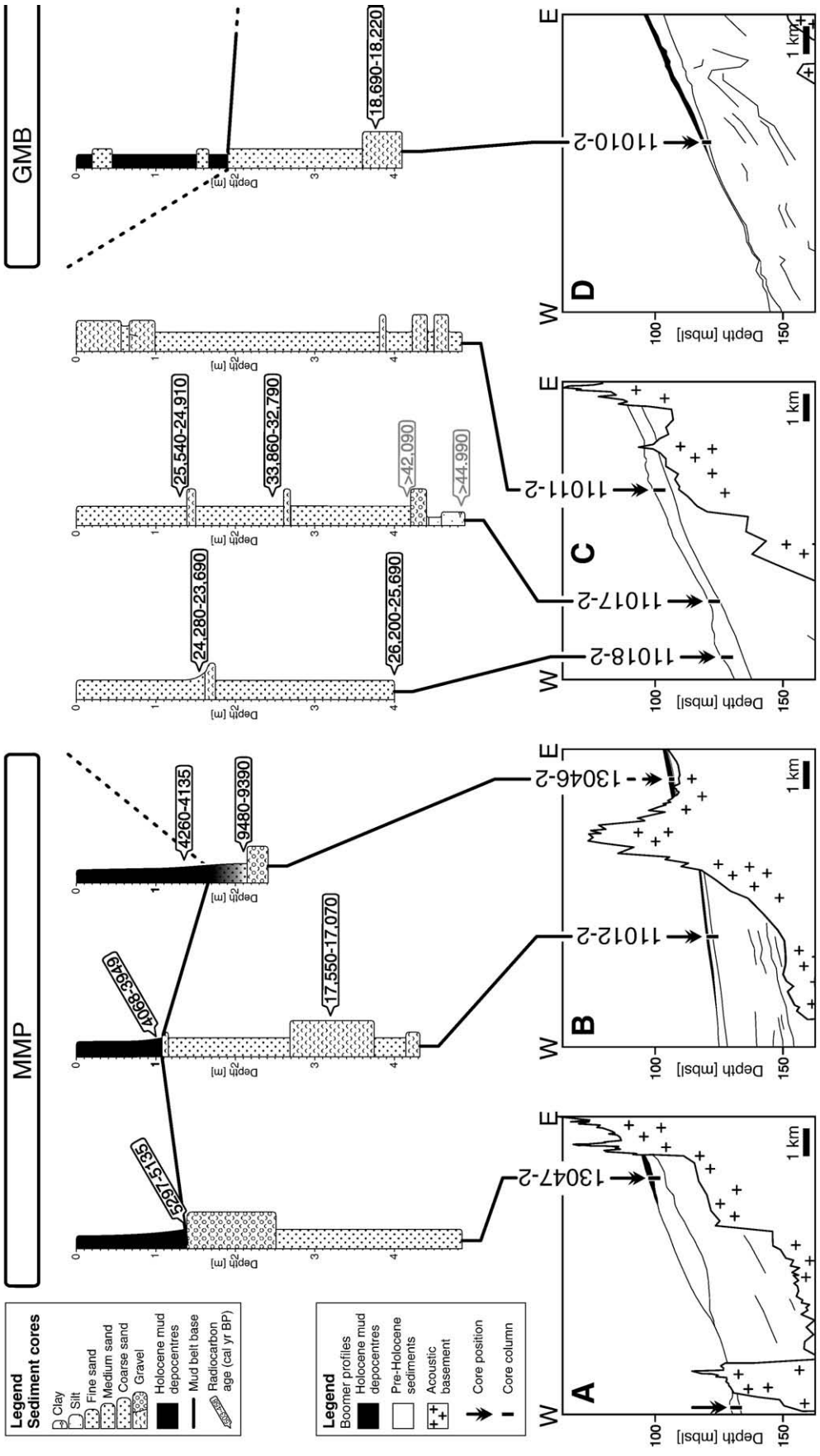

Figure 3. Interpretation of the Boomer profiles A to H and respective sediment-core records taken on these profiles. Lithology, grain size and radiocarbon ages are shown in the sediment-core columns. The locations of Profiles A–H are shown in Figure 1. Black arrows in the Boomer profiles indicate sediment-core positions. Unlabelled arrows indicate sediment cores not displayed in this study. MMP: Muros Mud Patch, GMB: Galicia Mud Belt, DMP: Douro Mud Patch. See Figure 1 for the exact position of Core 13046-2 (placed slightly southward of Profile B).

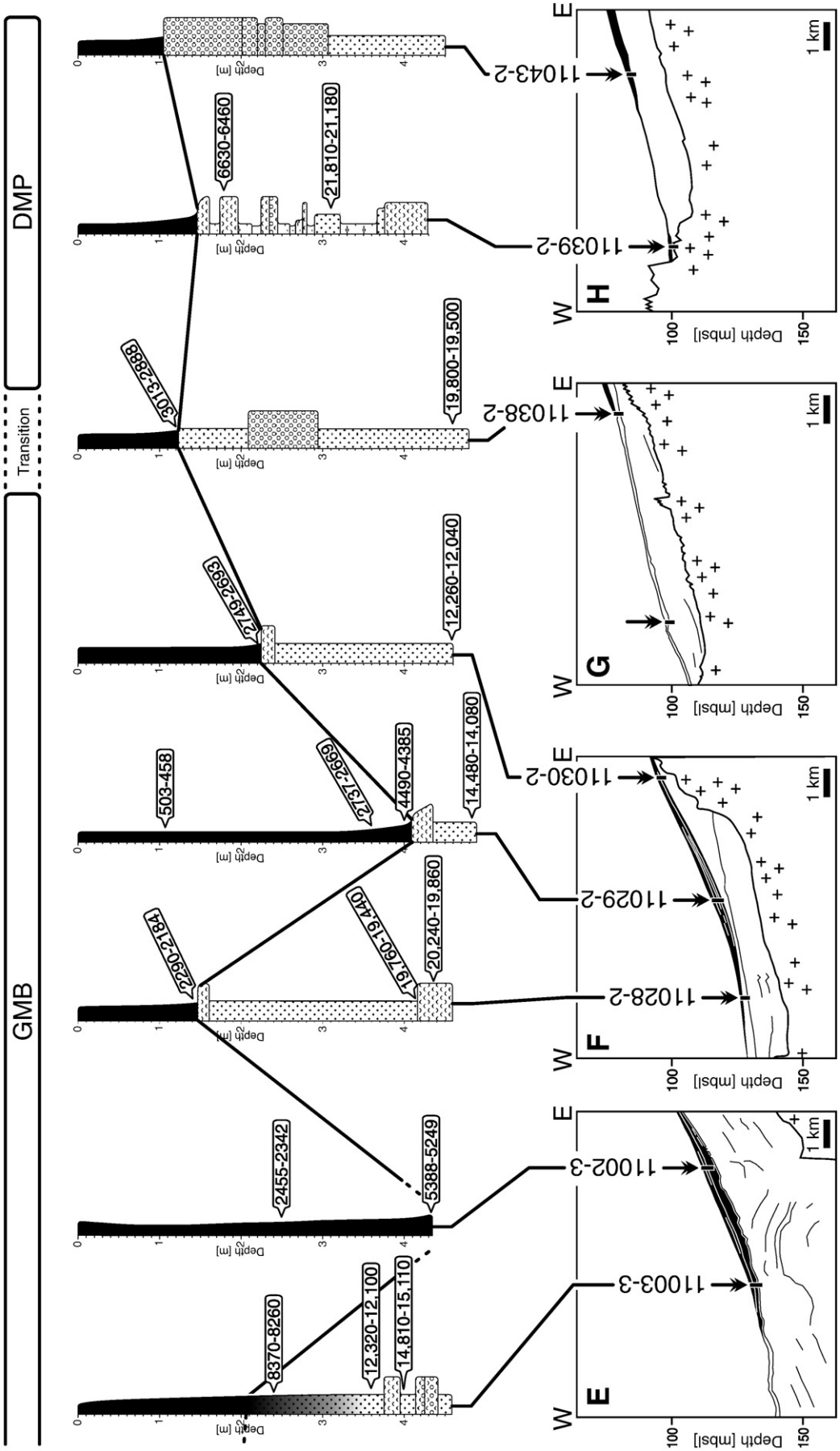

Figure 3 (*continued*).

Please cite this article as: Lantzsch, H., et al., Holocene evolution of mud depocentres on a high-energy, low-accumulation shelf (NW Iberia), Quat. Res. (2009), doi:10.1016/j.yqres.2009.07.009

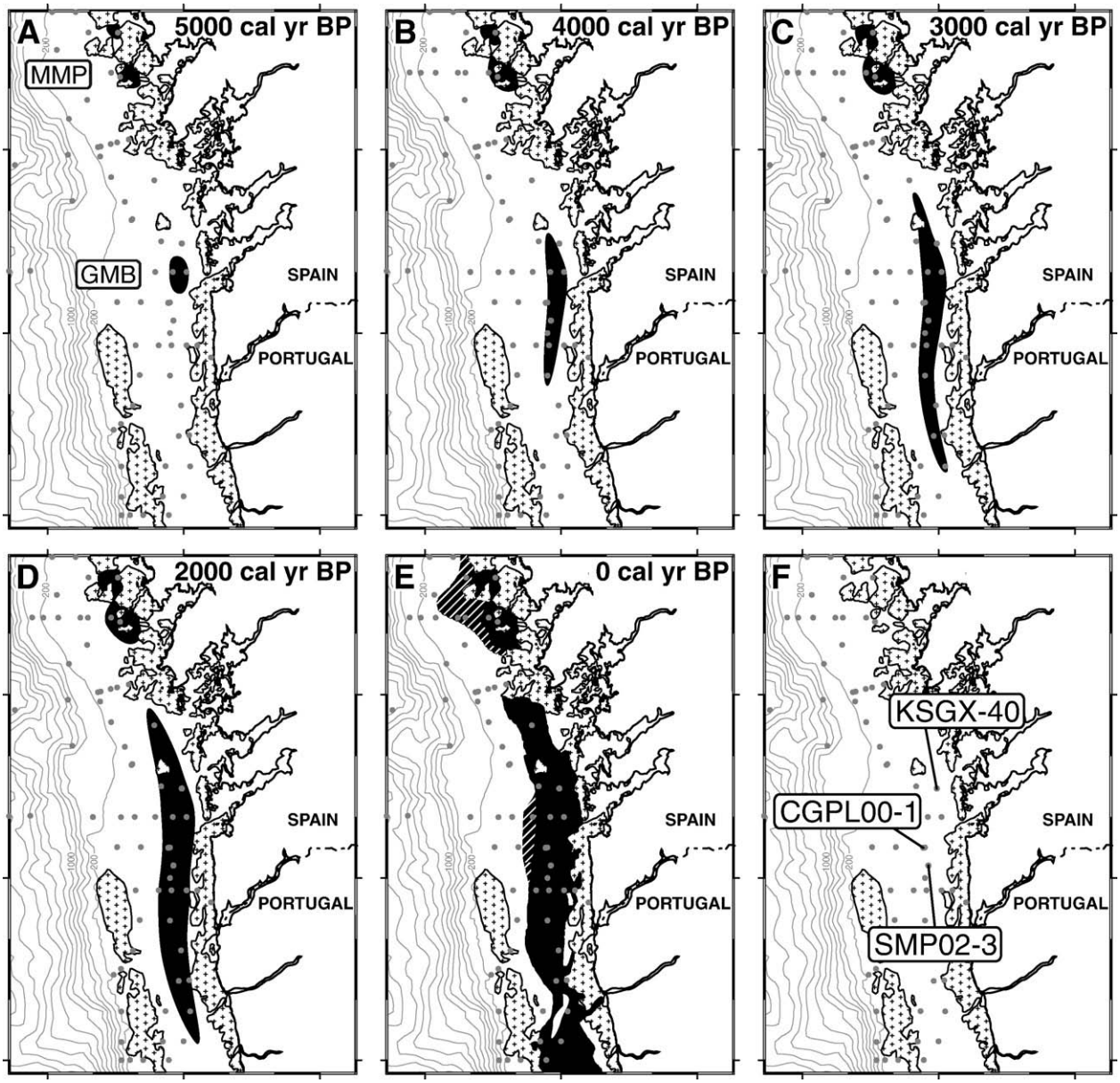

Figure 4. Initial onset and further expansion of the Muros Mud Patch (MMP) and the Galicia Mud Belt (GMB). Black areas indicate mud contents >25%. Core positions of this study are indicated by grey dots and core locations of other studies are displayed in box F (CGPL00-1: González-Álvarez et al., 2005; KSGX-40: Martins et al., 2007; SMP02-3: Bernárdez et al., 2008). The present-day mud-belt distribution in box E is adopted from Dias et al. (2002). Streaked areas indicate discrepancies between the study of Dias et al. (2002) and the own grain-size measurement on surface samples.

Mud-belt sediments in the area between MMP and GMB are neither detected in the cores and surface samples of our study (Figs. 3C and 4E), nor mapped by Dias et al. (2002; Fig. 1). Although we cannot exclude some trapping of fine sediments in shallower water depths, the reason for this particular non-deposition should be found in the pronounced northern rim of the Ría de Arosa, which is characterised by rocky outcrops extending far across the mid-shelf (Dias et al., 2002; Fig. 1). These outcrops seem to act as a sediment barrier due to either (1) their high elevation preventing sediment transit, or (2) enhanced hydrological energy in this area caused by reflection of incoming waves and/or (3) deflection of the poleward shelf current, which might result in an off-shelf export of fine sediments at the southern rim of this barrier. However, mud contents below 25% are also found in our study at Sites 13, 16 and 88 in the MMP (and Site 4 in the GMB; Fig. 1). This pattern is contrasting the mud distribution mapped by Dias et al. (2002; Fig. 4E), which might point to a strong influence of either seasonal or annual variations in the extent of the modern margins of the main mud depocentres. Above all, frequently appearing storm events might lead to intensive re-mobilisation (Vitorino et al., 2002) and, thus, margin re-shaping in these areas.

The formation of the *GMB* did not take place continuously over the whole area but in successive steps. The initial onset of the GMB is displayed by a gradual development from fine sands towards mud deposition between 8370 and 5249 cal yr BP in the region of Profile E (Figs. 3E and 4A). However, the onset of the GMB varies largely across the shelf. Martins et al. (2007) reported deposition of >25% mud in front of the Ría de Vigo (KSGX-40; Fig. 4F) from ~2500 cal yr BP. This age indicates a northward contour-parallel expansion of the mud belt (Figs. 4A, B). The extension of the Galicia Mud Belt, however, did not only appear into northward direction alone. Profile F further south displays mud deposition starting at 4490–4385 cal yr BP and deposition of fines in Profile G is recorded not earlier than 3013 cal yr BP (Figs. 3G, F and 4A, B). In addition, Bernárdez et al. (2008)

Please cite this article as: Lantzsch, H., et al., Holocene evolution of mud depocentres on a high-energy, low-accumulation shelf (NW Iberia), Quat. Res. (2009), doi:10.1016/j.yqres.2009.07.009

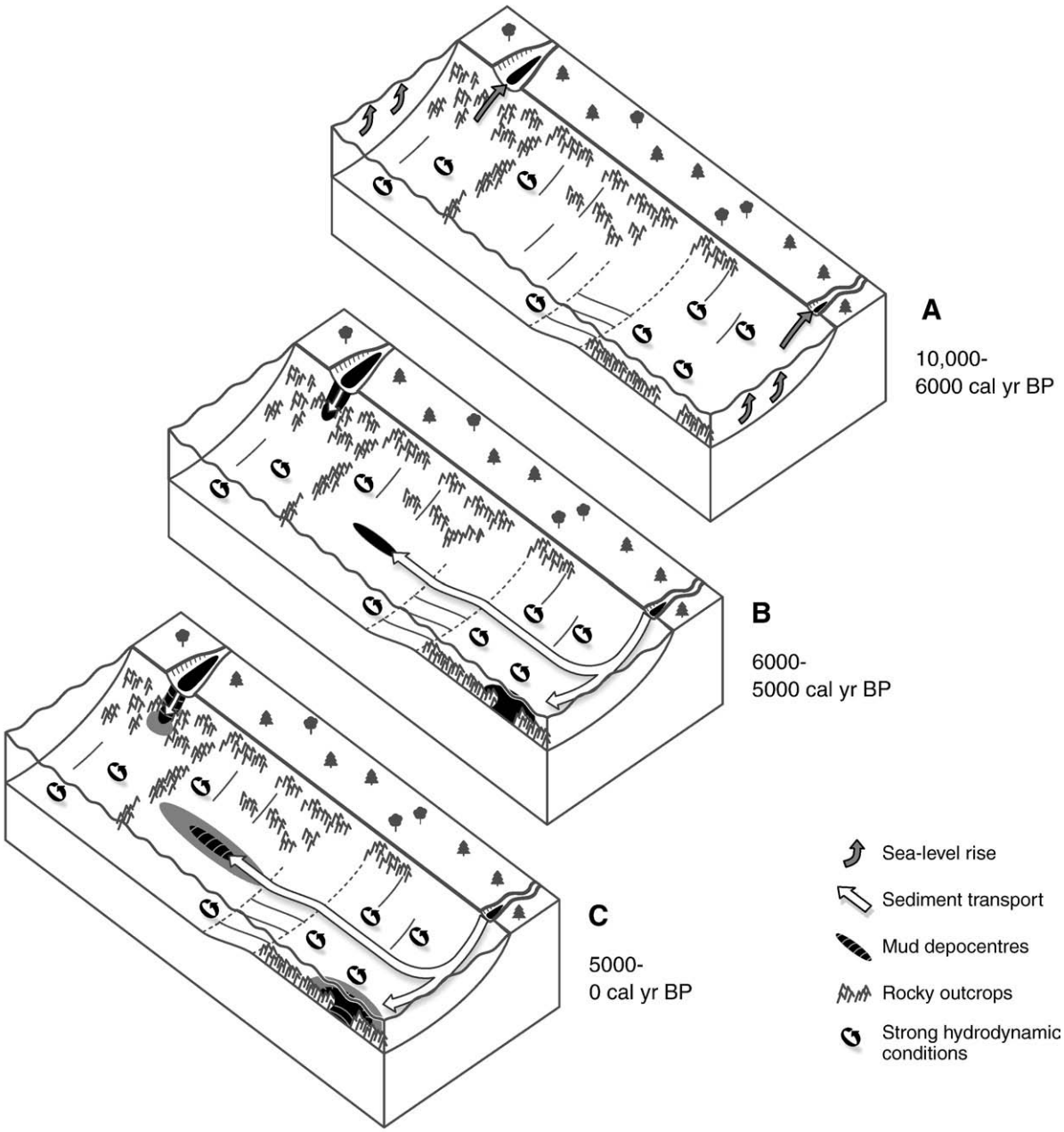

Figure 5. Schematic block diagram showing (A) the flooding of the Rías and estuaries due to the deglacial/early Holocene sea-level rise, (B) the onset of major mud deposition on the NW Iberian shelf, and (C) the further expansion of these fine-grained depocentres.

recently published an increasing mud content in fine sands between ~4700 and ~3300 cal yr BP (SMP02-3; Fig. 4F). The lateral expansion of the GMB was not only restricted to N–S direction paralleling the bathymetry. For instance, cores in Profile F directly display the extension history in W–E direction (Fig. 3F). Mud deposition started at 4490–4385 cal yr BP in Core 11029-2, which is located in the central part of the modern mud belt. In contrast, Cores 11028-2 and 11030-2 from marginal positions show an onset of the mud belt after 2290 and 2749 cal yr BP, respectively (Figs. 4D, E). In addition, González-Álvarez et al. (2005) reported the initiation of mud at ~2800 cal yr BP in the marginal part of the GMB (CGPL00-1; Fig. 4F). Hence, the detailed reconstruction of the GMB evolution shows that this mud belt started to develop in the area of Profile E, and all marginal parts around the GMB main centre, parallel to the bathymetry as well as in seaward and landward directions, show a successively later time of initiation (Fig. 4). This non-linear extension from a centre points to a development of the GMB detached from the sediment source in the south.

The location of the GMB is related to the deposition-favouring environment in mid-shelf position in contrast to stronger hydrodynamic conditions on inner and outer shelf as previously stated by McCave (1972) and Hill et al. (2007). Hence, the shelf bathymetry and water depth, respectively, determine the position of mid-shelf mud deposition, and the coarsening of GMB sediments towards marginal parts is related to a stronger wave impact towards the inner shelf and intense currents on the outer shelf. The delayed onset of mud sedimentation in the south and generally coarser deposits (muddy fine sands) in the transitional area between GMB and Douro Mud Patch (DMP) should then be related to the elevated bathymetry of this area relative to the centre of the GMB leading to stronger hydrodynamic conditions. In contrast to the MMP, pronounced basement elevations are of minor influence on the GMB distribution.

The modern DMP centre is located slightly south of the study area. Sediment cores have been retrieved from the northern branch of the DMP and a radiocarbon date of 6500 cal yr BP was measured beneath

Please cite this article as: Lantzsch, H., et al., Holocene evolution of mud depocentres on a high-energy, low-accumulation shelf (NW Iberia), Quat. Res. (2009), doi:10.1016/j.yqres.2009.07.009

the DMP deposits in Profile H (Fig. 3H). Consequently, the extension of the DMP towards the north took place later than 6630–6460 cal yr BP. In addition, one single age of 495–677 cal yr BP was recently published by Burdloff et al. (2008) from the central part of the DMP. However, the age of the mud base is not known. Therefore, the spatial and temporal development of this depocentre remains speculative. Nevertheless, the detailed reconstruction of the MMP and the GMB evolution, as examined in this study, illustrates that the modern centres of fine deposition correspond well with the location of the initial onset of mud deposition. In analogy, the initiation of the DMP is suggested to have also started at the position of the modern fine centre and, therefore, clearly detached from the sediment source. This detached development is supported by the mechanism, which controls the DMP formation. The highest sedimentation rates of the DMP are found immediately east of rocky outcrops in about 100 m water depth. Hence, Drago et al. (1999) have suggested a relation of the DMP origin to the topographic relief which might provide a weak hydrodynamic environment on the one hand. On the other hand, these rocks lead to sediment trapping by acting as a barrier within the flow direction of the bottom nepheloid layer. Consequently, the sediments are hindered to move further offshore. Hence, these sediment-protecting and -catching morphological features represent the dominant parameter responsible for DMP deposition. Non-deposition of mud in front of the Douro River might be related to the absence of such pronounced morphological features favouring sediment bypassing and winnowing of fines by winter storms.

As a summary, the evolution of the NW Iberian shelf mud deposits has taken place in succeeding steps. This development is schematically reconstructed in Figure 5. First, the flooding of major estuaries during the late Pleistocene to early Holocene sea-level rise led to accumulation of fine sediments inside the river valleys (Fig. 5A). The export of terrigenous material to the shelf was then initiated by a shift in the balance between rate of sea-level rise and amount of terrigenous sediment supply. Hence, Holocene sea-level stabilisation and decreasing accommodation space within the Douro estuary gave rise to the deposition of larger amounts of fine sediments on the NW Iberian shelf at around 6000–5000 cal yr BP (Drago et al., 1999; Lantzsch et al., 2009; Fig. 5B). This initiated export of sediments provided the prerequisite for the sedimentation of mud on the shelf. Mid-shelf zones are characterised by deposition-favouring hydrodynamic conditions, and the occurrence of morphological features has additionally strongly controlled the location of the initial onset (Fig. 5B) and further extension of the mud depocentres (Fig. 5C). The relatively steady position of the mud deposits on the NW Iberian shelf suggests that no major changes of the general oceanographic setting took place during the Holocene. Consequently, the effect of the hydrodynamic regime and the influence of morphological features essentially control the general mud distribution. Within this framework, Holocene climatic changes cause internal grain-size fluctuations in the sediment cores (González-Álvarez et al., 2005; Martins et al., 2007; Bernárdez et al., 2008).

Conceptual subdivision of mid-shelf mud depocentres

The NW Iberian mud deposits represent mid-shelf mud belts according to the classification of McCave (1972). Nevertheless, these depocentres show considerable differences regarding their overall shaping and loci of formation. Those differences reveal the dominant forces controlling the mud-belt distribution. This study shows that reduced hydrodynamic conditions in mid-shelf environments are not the exclusive mechanism for the formation of mud belts, but that the role of morphological features might be of similar importance. Therefore, we propose a conceptual subdivision here concerning the characteristic distribution of mud deposition. Two main types are observed.

Type 1 mud deposits are attached to the associated sediment source and show an expansion from this sediment source towards the mid-shelf (Fig. 6). Additionally, sediment coarsens and thickness decreases with distance to the source. Type 1 can be further subdivided concerning the dominant forces, which control the distribution of fines. The common *Type 1a*, though not developed on the NW Iberian shelf, is closely related to the deposition-favouring hydrodynamic conditions in mid-shelf position (Fig. 6). In contrast to this mid-shelf mud, large areas of inner and outer shelf are typically characterised by sand draping due to the impact of storm wave activity and strong shelf currents (McCave, 1972). Nevertheless, the

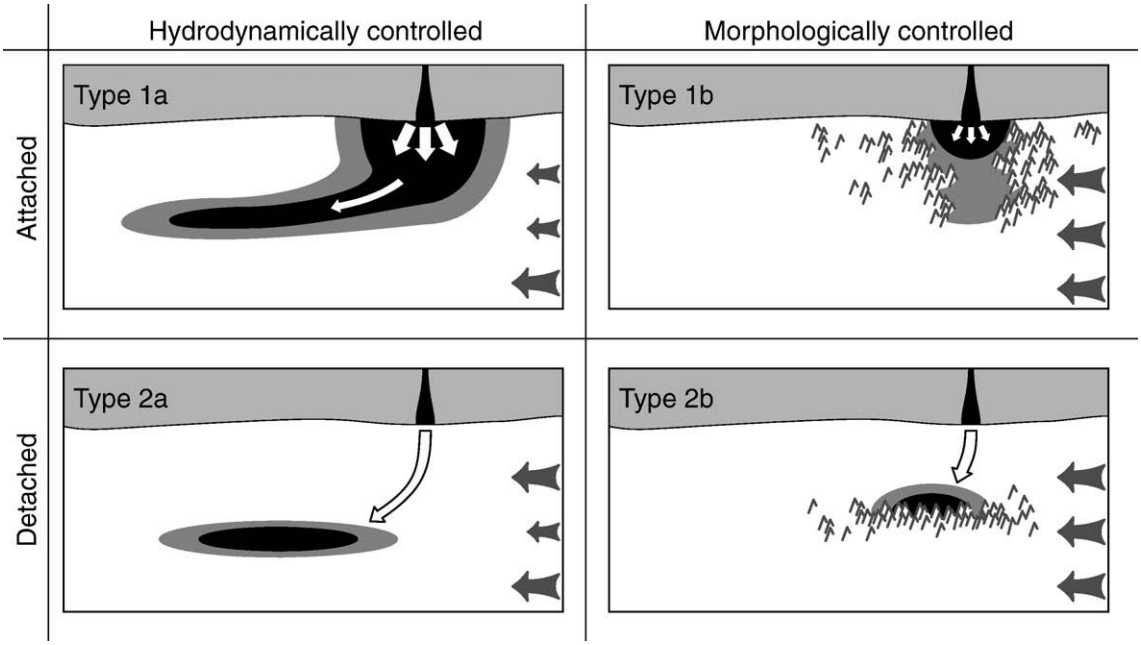

Figure 6. Types of Holocene mud depocentres. Type 1 is attached to the sediment source, Type 2 is detached. The sediment distribution of Types 1a and 2a is related to the deposition-favouring hydrodynamic conditions in mid-shelf position, whereas Types 1b and 2b are strongly controlled by the occurrence of morphological features. White arrows indicate sediment input and transport, grey arrows the strength of the hydrodynamic regime on inner, mid-, and outer shelf.

Please cite this article as: Lantzsch, H., et al., Holocene evolution of mud depocentres on a high-energy, low-accumulation shelf (NW Iberia), Quat. Res. (2009), doi:10.1016/j.yqres.2009.07.009

Type 1a depocentre is attached to the sediment source. Hence, either higher sediment input or a weak hydrodynamic regime close to the source favour mud deposition on the inner shelf. Therefore, this type does not occur under the low-accumulation, high-energy setting of the NW Iberian shelf. Examples for Type 1a are the mud belt off SW Africa (Meadows et al., 2002), the Gulf of Lions mud belt (Durrieu de Madron et al., 2000), and the Ebro mud belt (Díaz et al., 1996). In these cases, the sediment input by a major river leads to the development of a prodelta and of a connected adjacent, elongated mid-shelf mud belt. Hence, mud belts, which are in contact with a prodelta, are typical representatives of Type 1a. *Type 1b*, in contrast, shows an influence of morphological features (Fig. 6), as it is the case for the MMP. There, deposition is related to rocky outcrops on the inner and mid-shelf. Those elevations act as sediment traps and shelter the sediments against strong hydrodynamic conditions which prevent as well an extended deposition of mud on the shelf, as it is the case for Type 1a. By now, other examples for Type 1b from literature are, to our knowledge, not known, what might be due to generally few publications dealing with such small-scale mud entrapments. In addition, Type 1b represents a special morphological setting, which should be restricted to high-energy, low-accumulation shelves. An absence of such morphological barriers would cause non-deposition and erosion of fines.

The most characteristic feature of *Type 2* mud deposits is their development detached from the sediment source (Fig. 6). Those areas are characterised by extensive sand draping on inner and outer shelf due to strong hydrodynamic conditions. Therefore, this type should be typical for low-accumulation and high-energy shelf regimes. As for Type 1, a further subdivision can be applied. The distribution of *Type 2a* mud belts is strongly dependent on weak hydrodynamic conditions, which are usually located in mid-shelf position (Fig. 6). On inner and outer shelf, the impact of the wave base and strong currents, respectively, prevents a deposition of fines. Therefore, Type 2a represents the textbook-style example of a mid-shelf mud belt as defined by McCave (1972). The GMB shows all of these characteristics and various other examples fulfilling these criteria have been reported in literature such as the mud belt off the Russian River in northern California (Demirpolat, 1991), the Grande Vasiere Mud Belt in the Bay of Biscay (Lesueur et al., 2001), and the Huksan Mud Belt in the southeastern Yellow Sea (Lee and Chu, 2001). In all these cases, pronounced morphological features are either absent or of minor importance for the distribution of these mud deposits. This morphological influence becomes the dominant control in *Type 2b* mud belts, which represents, again, a special depositional setting on a high-energy, low-accumulation shelf system. Those mud deposits are formed due to the occurrence of morphological features (Fig. 6). The water depth is of subordinate importance and Type 2b mud belts might occur divergently from the optimal water depth that would be characterised by the weakest hydrodynamic conditions in case of an absence of morphological elevations. The DMP represents a well-suited example for Type 2b. However, examples from literature for the influence of morphological features on the mud depocentre distribution are scarce. Edwards (2002) reported north of Monterey Bay (California) topographic highs on the mid-shelf to act as barriers for fine sediments and to lead to sediment ponding. Jouanneau et al. (2008) observed sediment trapping related to rocky outcrops on the Basque shelf (Bay of Biscay). Nevertheless, the influence of these morphological features is of minor importance for the general sediment distribution, and a dominant influence such as reported by Drago et al. (1999) for the NW Iberian shelf system is not present in those shelf settings.

Conclusions

The Holocene mud deposits on the NW Iberian shelf provide a new view on the evolution of mid-shelf mud depocentres in high-energy, low-accumulation sedimentary shelf regimes. The observed differential lateral onset and dynamic of expansion reveal exemplarily the major controls on the development of such mud depocentres.

The deceleration in early Holocene sea-level rise was conducive to the deposition of fines on the shelf. This initial mud deposition is marked by a transition of fine sands towards mud in sediment cores from the central Muros Mud Patch between 9480 and 4135 cal yr BP and from the Galicia Mud Belt between 8370 and 5249 cal yr BP. The detailed analysis of the mud-depocentre evolution reveals that the Galicia Mud Belt started to develop in a main centre detached from the coastal source of original sediment supply. The succeeding development of this mud belt was surprisingly non-linear. The expansion towards the sediment source as well as towards the north following the current direction is contrasting the linear development of the Muros Mud Patch which took indeed place from the sediment source towards the mid-shelf as generally expected for shelf mud deposits.

The location of the initial onset of these depocentres and their further expansion was most probably determined by the deposition-favouring hydrodynamic conditions in mid-shelf position, and the occurrence of morphological features, which act as sediment traps.

Following these characteristics, two main types of fine depocentres can be defined. Type 1 is attached to the associated sediment source and shows an expansion from this source towards the mid-shelf. The distribution of Type 1a is dominantly controlled by the deposition-favouring hydrodynamic conditions in mid-shelf position. In contrast, the position of Type 1b deposits is strongly influenced by the occurrence of morphological features such as local elevations in basement, which trap sediments by sheltering the deposits against stronger hydrodynamic conditions.

Type 2 mud deposits emplace in detachment from the sediment source. Reason is either low sediment input or strong hydrodynamic conditions along inner shelf and shore zone. This detached evolution is proposed to be a characteristic feature of low-accumulation sedimentary shelf systems in contrast to input-dominated shelves where excessive supply overshadows the effect of other forces. Similar to Type 1, Type 2 can be further subdivided. Whereas the distribution of Type 2a is dominantly controlled by the hydrodynamic conditions related to water depth, Type 2b is largely influenced by defined morphological features.

Further studies should focus on the initial onset and development of other mud belts to get a deeper insight into the evolution of such depocentres and further support the proposed conceptual subdivision by a well-dated stratigraphy.

Acknowledgments

Special thanks go to Sebastian Krastel and Hannes Riepshoff for their contribution to this project. We also wish to thank Captain Michael Schneider and his complete crew on RV POSEIDON for their outstanding support. We are thankful to Rüdiger Henrich for providing the opportunity to conduct this study. This work was funded through DFG-Research Center/Excellence Cluster “The Ocean in the Earth System“.

References

Álvarez-Salgado, X.A., Gago, J., Míguez, B.M., Gilcoto, M., Pérez, F.F., 2000. Surface waters of the NW Iberian margin: upwelling on the shelf versus outwelling of upwelled waters from the Rías Baixas. Estuarine, Coastal and Shelf Science 51 (6), 821–837.

Araújo, M.F., Jouanneau, J.M., Valério, P., Barbosa, T., Gouveia, A., Weber, O., Oliveira, A., Rodrigues, A., Dias, J.M.A., 2002. Geochemical tracers of northern Portuguese estuarine sediments on the shelf. Progress in Oceanography 52 (2–4), 277–297.

Bard, E., Arnold, M., Hamelin, B., Tisnerat-Laborde, N., Cabioch, G., 1998. Radiocarbon calibration by means of mass spectrometric Th-230/U-234 and C-14 ages of corals: an updated database including samples from Barbados, Mururoa and Tahiti. Radiocarbon 40 (3), 1085–1092.

Please cite this article as: Lantzsch, H., et al., Holocene evolution of mud depocentres on a high-energy, low-accumulation shelf (NW Iberia), Quat. Res. (2009), doi:10.1016/j.yqres.2009.07.009

Bernárdez, P., González-Álvarez, R., Francés, G., Prego, R., Bárcena, M.A., Romero, O.E., 2008. Late Holocene history of the rainfall in the NW Iberian peninsula — evidence from a marine record. Journal of Marine Systems 72 (1–4), 366–382.
Blair, T.C., McPherson, J.G., 1999. Grain-size and textural classification of coarse sedimentary particles. Journal of Sedimentary Research 69 (1), 6–19.
Boski, T., Moura, D., Veiga-Pires, C., Camacho, S., Duarte, D., Scott, D.B., Fernandes, S.G., 2002. Postglacial sea-level rise and sedimentary response in the Guadiana Estuary, Portugal/Spain border. Sedimentary Geology 150 (1–2), 103–122.
Burdloff, D., Araújo, M.F., Jouanneau, J.M., Mendes, I., Monge Soares, A.M., Dias, J.M.A., 2008. Sources of organic carbon in the Portuguese continental shelf sediments during the Holocene period. Applied Geochemistry 23 (10), 2857–2870.
Dabrio, C.J., Zazo, C., Goy, J.L., Sierro, F.J., Borja, F., Lario, J., González, J.A., Flores, J.A., 2000. Depositional history of estuarine infill during the last postglacial transgression (Gulf of Cadiz, Southern Spain). Marine Geology 162 (2–4), 381–404.
Demirpolat, S., 1991. Surface and near-surface sediments from the continental shelf off the Russian River, Northern California. Marine Geology 99 (1–2), 163–173.
Dias, J.M.A., Nittrouer, C.A., 1984. Continental shelf sediments of northern Portugal. Continental Shelf Research 3 (2), 147–165.
Dias, J.M.A., Gonzalez, R., Garcia, C., Diaz-del-Rio, V., 2002. Sediment distribution patterns on the Galicia-Minho continental shelf. Progress in Oceanography 52 (2–4), 215–231.
Díaz, J., Palanques, A., Nelson, C.H., Guillén, J., 1996. Morpho-structure and sedimentology of the Holocene Ebro prodelta mud belt (northwestern Mediterranean Sea). Continental Shelf Research 16 (4), 435–456.
Drago, T., Araújo, F., Valério, P., Weber, O., Jouanneau, J.M., 1999. Geomorphological control of fine sedimentation on the northern Portuguese shelf. Boletín Instituto Español de Oceanografía 15 (1–4), 111–122.
Drago, T., Freitas, C., Rocha, F., Moreno, J., Cachao, M., Naughton, F., Fradique, C., Araujo, F., Silveira, T., Oliveira, A., Cascalho, J., Fatela, F., 2006. Paleoenvironmental evolution of estuarine systems during the last 14,000 years — the case of Douro estuary (NW Portugal). Journal of Coastal Research 1, 186–192.
Durrieu de Madron, X., Abassi, A., Heussner, S., Monaco, A., Aloisi, J.C., Radakovitch, O., Giresse, P., Buscail, R., Kerherve, P., 2000. Particulate matter and organic carbon budgets for the Gulf of Lions (NW Mediterranean). Oceanologica Acta 23 (6), 717–730.
Edwards, B.D., 2002. Variations in sediment texture on the northern Monterey Bay National Marine Sanctuary continental shelf. Marine Geology 181 (1–3), 83–100.
Goff, J.A., Austin, J.J.A., Gulick, S., Nordfjord, S., Christensen, B., Sommerfield, C., Olson, H., Alexander, C., 2005. Recent and modern marine erosion on the New Jersey outer shelf. Marine Geology 216 (4), 275–296.
González-Álvarez, R., Bernárdez, P., Pena, L.D., Francés, G., Prego, R., Diz, P., Vilas, F., 2005. Paleoclimatic evolution of the Galician continental shelf (NW of Spain) during the last 3000 years: from a storm regime to present conditions. Journal of Marine Systems 54 (1–4), 245–260.
Hanebuth, T., Bender, V., Bujan, S., Elvert, M., Frederichs, T., Kockisch, B., Krastel-Gudegast, S., Lantzsch, H., Mena Rodríguez, Á., Schmidt, F., Strozyk, F., Wagner Friedrichs, M., 2007. Report and first results of the Poseidon cruise P342 GALIOMAR, Vigo — Lisboa (Portugal), August 19th–September 06th, 2006. Distribution pattern, residence times and export of sediments on the Pleistocene/Holocene Galician Shelf (NW Iberian Peninsula). Berichte, Fachbereich Geowissenschaften, University of Bremen 255, 203 pp.
Hanebuth, T.J.J., Henrich, R., 2009. Recurrent decadal-scale dust events over Holocene western Africa and their control on canyon turbidite activity (Mauritania). Quaternary Science Reviews 28 (3–4), 261–270.
Hanebuth, T.J.J., Lantzsch, H., 2008. A Late Quaternary sedimentary shelf system under hyperarid conditions: unravelling climatic, oceanographic and sea-level controls (Golfe d'Arguin, Mauritania, NW Africa). Marine Geology 256 (1–4), 77–89.
Hill, P.S., Fox, J.M., Crockett, J.S., Curran, K.J., Friedrichs, C.T., Rockwell Geyer, W., Milligan, T.G., Ogston, A.S., Puig, P., Scully, M.E., Traykovski, P.A., Wheatcroft, R.A., 2007. Sediment delivery to the seabed on continental margins. In: Nittrouer, C.A., Austin, J.A., Field, M.E., Kravitz, J.H., Syvitski, J.P.M., Wiberg, P.L. (Eds.), Continental Margin Sedimentation — From Sediment Transport to Sequence Stratigraphy. Blackwell Publishing, International Association of Sedimentologists Special Publication 37, Malden, Oxford, Carlton, pp. 49–98.
Jouanneau, J.M., Weber, O., Drago, T., Rodrigues, A., Oliveira, A., Dias, J.M.A., Garcia, C., Schmidt, S., Reyss, J.L., 2002. Recent sedimentation and sedimentary budgets on the western Iberian shelf. Progress in Oceanography 52 (2–4), 261–275.
Jouanneau, J.M., Weber, O., Champilou, N., Cirac, P., Muxika, I., Borja, A., Pascual, A., Rodríguez-Lázaro, J., Donard, O., 2008. Recent sedimentary study of the shelf of the Basque country. Journal of Marine Systems 72 (1–4), 397–406.
Lantzsch, H., Hanebuth, T.J.J., Bender, V.B., Krastel, S., 2009. Sedimentary architecture of a low-accumulation shelf since the Late Pleistocene (NW Iberia). Marine Geology 259 (1–4), 47–58.
Lee, H.J., Chu, Y.S., 2001. Origin of inner-shelf mud deposit in the southeastern Yellow Sea: Huksan Mud Belt. Journal of Sedimentary Research 71 (1), 144–154.
Lesueur, P., Jouanneau, J.M., Boust, D., Tastet, J.P., Weber, O., 2001. Sedimentation rates and fluxes in the continental shelf mud fields in the Bay of Biscay (France). Continental Shelf Research 21 (13–14), 1383–1401.
Long, A., 2001. Mid-Holocene sea-level change and coastal evolution. Progress in Physical Geography 25 (3), 399–408.
Martins, V., Dubert, J., Jouanneau, J.-M., Weber, O., da Silva, E.F., Patinha, C., Alveirinho Dias, J.M., Rocha, F., 2007. A multiproxy approach of the Holocene evolution of shelf-slope circulation on the NW Iberian Continental Shelf. Marine Geology 239 (1–2), 1–18.
McCave, I.N., 1972. Transport and escape of fine-grained sediment from shelf areas. In: Swift, D.J.P., Duane, D.B., Pilkey, O.H. (Eds.), Shelf Sediment Transport: Process and Pattern. Dowden, Hutchinson and Ross, Inc., Stroudsburg, pp. 225–244.
Meadows, M.E., Rogers, J., Lee-Thorp, J.A., Bateman, M.D., Dingle, R.V., 2002. Holocene geochronology of a continental-shelf mudbelt off southwestern Africa. Holocene 12 (1), 59–67.
Naughton, F., Goñi, M.F.S., Drago, T., Freitas, M.C., Oliveira, A., 2007a. Holocene changes in the Douro estuary (Northwestern Iberia). Journal of Coastal Research 23 (3), 711–720.
Naughton, F., Bourillet, J.F., Fernanda, M., Goñi, S., Turon, J.L., Jouanneau, J.M., 2007b. Long-term and millennial-scale climate variability in northwestern France during the last 8850 years. Holocene 17 (7), 939–953.
Odin, G.S., Lamboy, M., 1988. Glaucony from the Margin off Northwestern Spain. In: Odin, G.S. (Ed.), Green Marine Clays. Developments in Sedimentology, 45. Elsevier, Amsterdam, Oxford, New York, pp. 249–275.
Oliveira, A., Rocha, F., Rodrigues, A., Jouanneau, J., Dias, A., Weber, O., Gomes, C., 2002. Clay minerals from the sedimentary cover from the Northwest Iberian shelf. Progress in Oceanography 52 (2–4), 233–247.
Otero, P., Ruiz-Villarreal, M., Peliz, A., 2008. Variability of river plumes off Northwest Iberia in response to wind events. Journal of Marine Systems 72 (1–4), 238–255.
Rey Salgado, J., 1993. Relación morfosedimentaria entre la plataforma continental de Galicia y las Rías Bajas y su evolución durante el Cuaternario. Publicaciones Especiales, Instituto Español de Oceanografía 17, 1–233.
Sommerfield, C.K., Wheatcroft, R.A., 2007. Late Holocene sediment accumulation on the northern California shelf: oceanic, fluvial, and anthropogenic influences. Geological Society of America Bulletin 119 (9–10), 1120–1134.
Stuiver, M., Reimer, P.J., Bard, E., Beck, J.W., Burr, G.S., Hughen, K.A., Kromer, B., McCormac, G., Van der Plicht, J., Spurk, M., 1998. INTCAL98 radiocarbon age calibration, 24,000–0 cal BP. Radiocarbon 40 (3), 1041–1083.
Vis, G.-J., Kasse, C., Vandenberghe, J., 2008. Late Pleistocene and Holocene palaeogeography of the Lower Tagus Valley (Portugal): effects of relative sea level, valley morphology and sediment supply. Quaternary Science Reviews 27 (17–18), 1682–1709.
Vitorino, J., Oliveira, A., Jouanneau, J.M., Drago, T., 2002. Winter dynamics on the northern Portuguese shelf. Part 2: bottom boundary layers and sediment dispersal. Progress in Oceanography 52 (2–4), 155–170.

Please cite this article as: Lantzsch, H., et al., Holocene evolution of mud depocentres on a high-energy, low-accumulation shelf (NW Iberia), Quat. Res. (2009), doi:10.1016/j.yqres.2009.07.009

5. Conclusions and future perspectives

This thesis represents the first detailed study to unravel the sedimentary evolution of a high-energy, low-accumulation shelf system and to reveal the forces controlling spatial and temporal sediment distribution patterns. The research of this thesis follows a comprehensive approach from (1) the establishment of a general stratigraphic framework of the NW Iberian shelf, over (2) the reconstruction of sedimentary buildup and facies evolution of this high-energy, low-accumulation shelf system to (3) the detailed identification of mechanisms controlling the evolution of Holocene depocentres.

In a first step, extensive hydroacoustic profiling in combination with 47 sediment cores and a large set of 61 radiocarbon dates reveals the late-Quaternary stratigraphy of the NW Iberian shelf. The spatial and temporal sediment distribution of the main stratigraphic units is primarily controlled by the impact of sea-level changes. Within this superimposed framework, both tectonically induced differences in the elevation of the basement, and hydrodynamic conditions have strong impact on the sedimentary buildup of high-energy, low-accumulation shelf regimes. Although sufficient amount of sediment supply is essential for the sediment deposition, the volume of sediment supply is, in contrast to high-accumulation shelf systems, not overwhelming the effect of morphology and hydrodynamics.

The excellent shelf coverage by numerous well-dated sediment cores enabled the detailed observation of the sedimentary evolution within the stratigraphic framework. Individual facies types are defined by combining results of visual core description, grain-size analysis, X-ray diffraction measurement, and microscopic component analysis in combination with statistical calculations. These facies types reveal individual depositional environments as a result of local hydrodynamic situation, morphological influences, and the dominant type of sediment supply (terrigenous input, biogenic production, sediment recycling). Their detailed sedimentary distribution patterns within various time slices of the latest Quaternary and the temporal changes of these distribution scenarios display the response to varying shelf configurations such as

(1) widespread shelf exposure, intensive erosion, and enhanced outer-shelf deposition during the last-glacial sea-level lowstand,

(2) rapid time-transgressive shifting of facies zones, ravinement processes, and large-scale sediment recycling in the run of the deglacial sea-level rise, and

(3) development of locally confined mid-shelf mud deposition due to the Holocene sea-level stabilisation.

The deposition of a thick transgressive system during deglacial sea-level rise, and, in contrast, accumulation of a thin unit during the Holocene sea-level highstand display the direct opposite of the expected configuration. These findings emphasise the importance of large-scale recycling during sea-level rise and low terrigenous supply in the Holocene. From the results of this study it can be concluded that the detailed description of sedimentary facies types and their spatial and temporal occurrence provides a very efficient tool to reveal the forces controlling sediment distribution and partitioning in the highly-dynamic environment of shelf systems.

Moreover, the NW Iberian shelf represents an ideal area to study the spatial and temporal appearance of Holocene mud depocentres due to the existence of three distinct mid-shelf sediment bodies which share in two cases the same coastal source of original sediment supply. Numerous radiocarbon dates at the base of these mid-shelf depocentres provide the exceptional chance to investigate the mechanisms of initial emplacement and further expansion dynamics of such depocentres in detail. The results show that the initial onset of such depocentres can be detached or attached from the associated source of terrigenous supply. Furthermore, the detailed observation of the further expansion reveals for the first time that mud depocentres may expand from a centre disconnected from the sediment source. The results provide evidence that this expansion from a centre could be a general mechanism for the emplacement of mid-shelf mud belts, and contradict the common assumption of a general linear development starting from the source of sediment supply and expanding in direction of sediment transport. Hence, the localised nuclei of growth onset and following expansion reveal the forces which have governed the development of Holocene mud depocentres on a high-energy, low-accumulation shelf. The spatial and temporal distribution of such depocentres is dominantly controlled by the availability of sediment input and the interplay of hydrodynamic conditions and morphological features. The degree of influence of these forces and the relation to the sediment source allowed a conceptional subdivision of these types of mid-shelf mud depocentres increasing the knowledge and understanding on the mechanisms behind emplacement and evolution of such depocentres.

This study shows exemplarily that, within the framework of sea-level variations, the sediment deposition in a high-energy, low-accumulation shelf system is restricted to confined areas where the balance between the three main forces (sediment supply, hydrodynamics, morphology) provides favourable conditions. Thus, morphological features may, on one hand, act as both sediment traps and source but, on the other hand, may lead to deflection and focussing of currents favouring sediment export and erosion, respectively. The spatial and temporal variability in the local hydrodynamic conditions such as enhanced wave impact in shallow waters and seasonal shelf currents, determines not only the general grain-size distribution and loci of deposition but leads to significant differences in sediment facies compositions. Hence, this thesis provides a new view on the forces which govern the spatial and temporal sediment partitioning as well as the response of sediment distribution patterns to varying shelf configurations, and can be seen as a case study on the sedimentary evolution of a high-energy, low-accumulation shelf.

Hence, an important task for future research will be to compare the results of this thesis to shelf systems which are characterised by different configurations in terms of, for instance, local hydrodynamic conditions and morphology. This would reveal similarities and differences in the sedimentary evolution, and in the intensity of response of the sedimentary system to varying shelf configurations. Thus, further investigations would increase our general understanding on sediment distribution patterns and should stimulate further research by providing a solid framework for more specialised studies on continental shelf systems.

Moreover, further comprehensive studies are needed to close the still-existing gap in the sedimentary connection of shelf and continental slope. These studies should provide new insight in, for instance, the volume and timing of sediment off-shelf export. The observation of individual material transformations on the sedimentary pathway from the

coast to the deep sea would lead to a more comprehensive understanding of the related processes.

Further work is also required on the combined effect of small-scale sedimentary processes such as, for instance, flocculation, disaggregation, and sorting of fines by near-bed hydraulic processes as well as on the impact of these processes on the depositional patterns in contrasting shelf environments. Although such research would require extensive *in-situ* observations to understand modern processes in detail, it provides the chance to corroborate theoretical implications by measurements in natural environments and represents an important step towards establishing comprehensive sedimentation models and explaining the large variability of shelf systems. However, the basis for all these future tasks is the detailed knowledge of the shelf architecture and its spatial and temporal sedimentary partitioning patterns.

Appendix 1: A Late Quaternary sedimentary shelf system under hyperarid conditions: Unravelling climatic, oceanographic and sea-level controls (Golfe d'Arguin, Mauritania, NW Africa)

Till J.J. Hanebuth[1], Hendrik Lantzsch[1]

[1] *MARUM – Center for Marine Environmental Sciences and Faculty of Geosciences, University of Bremen, P.O. Box 330 440, 28334 Bremen, Germany.*

Marine Geology, 2008, 256, 77–89

Abstract

The sedimentation on the Mauritanian shelf off the western Saharan desert is strongly influenced by dust supply and is investigated in this study by combining surface mapping, shallow-acoustic profiling and the analysis of sediment cores. Coarse-grained carbonates dominate wide areas of the open shelf at places where the shelf is exposed to the Atlantic Ocean. The sheltered Golfe d'Arguin, in contrast, is characterized by muddy shoals in its inner area, and locally restricted and wedge-shaped muddy depocenters which extend contour-parallel in mid-shelf settings. In both cases, cross-shelf currents control sediment distribution and accumulation, not location or amount of primary eolian input. A major discontinuity on the outer shelf is located in 85–110 m water plus sediment depth and is refilled by a sedimentary facies succession of shoreface, tidal and open-shelf deposits. This succession has formed during temporary lower sea levels along the last overall regression (MIS-4 and MIS-3), the Last Glacial Maximum, and during the past deglacial sea-level rise.

Significant sediment deposition and preservation is limited to very restricted areas. Concerning the overall shelf architecture, sea level was the main factor enabling or suppressing deposition in terms of 1) creating local erosional swales which have favored subsequent trapping and preservation of sediments; 2) determining the type of sedimentary facies refilling these depressions under a variety of nearshore conditions; 3) interacting with the seafloor morphology and, by this, controlling timing of initiation and growth geometry of mud wedges. These mud wedges have formed since ca. 9 cal. ka under a continuous sedimentation regime. These bodies must have formed in hydraulic equilibrium but they are detached from a defined sediment point source which is in contrast to common mudbelt formation on shelves.

In general, sediment storage on shelves under hyperarid conditions seems to be very limited due to comparably low sediment input, strong ravinement activity during changing sea levels, significant bypassing and winnowing processes, and a low preservation potential of the non-cohesive materials. These conditions lead to the development of almost sediment-starved systems with low subsidence rates over longer geological timescales.

Appendix 2: Mud depocentres on continental shelves – a classification

Till J.J. Hanebuth[1], Hendrik Lantzsch[1], Jean Nizou[1]

[1] *MARUM – Center for Marine Environmental Sciences and Faculty of Geosciences, University of Bremen, P.O. Box 330 440, 28334 Bremen, Germany.*

Submitted to Earth Science Reviews

Abstract

Mud deposition on clastic continental shelves takes place under a range of environmental conditions which is expressed by a variety of resulting types of mud depocentres. An increasing number of three-dimensional studies of mud bodies on shelves through sediment-acoustic and sediment-coring approaches has gained the knowledge on the architecture and evolution of such deposits over recent years. To achieve a systematic comparability and to prevent confusion in the use of related terms we propose a genetically oriented classification for shelfal mud depocentres here.

Locally defined mud deposition on shelves starts at four alternative time intervals related to 1) an early stage of outer-shelf drowning, 2) wide inner-shelf inundation, 3) the maximum flooding, or 4) during sub-recent times. The subsequent expansion dynamic might occur a) omni-directional in case of a direct depocentre attachment to the fluvial sediment source, b) in terms of current-parallel or current-normal clinoform progradation, or c) in the direction of advective current transport associated with a detachment from such a source. Classical mud belts seem often to initiate around defined nuclei which's location is determined by seafloor morphology rather than by the location of the source.

Nine individual types of shelfal mud depocentres are identified and described on the base of their surface and in-depth appearance and their formation history. These defined types are prodelta, subaqueous delta, mud blanket, mud patch, mud belt *s.s.*, mud downdrift, mud entrapment, mud wedge, mud contourite drift. The types are, further, arranged in the ternary field of the major control parameters sediment input, morphology and hydrography with the aim to provide a robust classification. A lateral or stratigraphic transition from one into another type might be developed as response to a shift in environmental control forces. Further studies in modern and ancient settings are needed for a better understanding of the formation and preservation potentials on such shelfal mud depocentres.

Appendix 3: Results of microscopic component counting and fuzzy c-means cluster analysis

Core No. (GeoB)	Depth in core (cm)	Component distribution (%)							Cluster membership (%)			Assigned cluster
		Glauconу	Carb. fragm.	Quartz	Mica	Plant ibres	Biog. carb.	Others	Cluster 1 (mF)	Cluster 2 (sF_{mixed})	Cluster 3 (sF_{glauc})	
11001-2	surface	37	19	20	1	2	20	1	6	15	79	3
11001-3	20	37	27	8	1	2	22	2	12	20	68	3
11001-3	40	34	29	14	1	1	20	1	4	13	83	3
11001-3	100	52	13	9	14	2	6	5	15	36	49	0
11002-1	surface	0	5	0	12	42	41	0	95	4	2	1
11002-3	0	0	15	0	7	5	71	2	94	4	2	1
11002-3	60	0	8	0	10	22	58	1	95	3	2	1
11002-3	101	0	12	0	11	28	48	0	97	2	1	1
11002-3	160	1	14	1	19	20	45	1	100	0	0	1
11002-3	220	1	17	0	9	22	49	2	99	0	0	1
11002-3	280	3	12	0	16	20	47	1	98	1	1	1
11002-3	340	5	11	1	21	15	45	2	96	2	1	1
11002-3	380	9	13	1	5	11	58	3	84	8	8	1
11002-3	419	18	14	1	7	8	52	1	62	17	21	1
11003-2	surface	2	7	0	9	41	39	2	98	1	1	1
11003-3	0	14	11	2	5	4	63	1	50	23	27	1
11003-3	40	14	12	2	6	7	56	2	67	16	17	1
11003-3	120	18	12	2	6	5	55	2	58	20	22	1
11003-3	199	33	13	4	3	3	44	1	20	23	57	3
11003-3	240	30	13	5	3	3	41	5	31	26	43	0
11003-3	260	46	17	9	2	2	22	2	9	18	73	3
11003-3	300	59	7	15	4	2	13	0	6	17	76	3
11003-3	360	50	12	22	6	1	6	2	5	23	72	3
11003-3	399	58	16	15	7	1	2	1	3	18	79	3
11003-3	449	63	17	19	1	0	0	0	1	8	91	3
11004-1	surface	98	0	2	0	0	0	0	6	16	78	3
11004-2	60	92	2	6	0	0	0	0	1	7	92	3
11004-2	160	95	2	3	0	0	0	0	1	6	93	3
11004-2	280	84	3	3	2	0	3	5	8	24	68	3
11004-2	380	92	1	3	1	1	2	0	7	13	80	3
11005-1	surface	93	1	5	0	0	0	0	0	3	96	3
11005-2	20	81	5	14	0	0	0	0	3	14	83	3
11005-2	200	93	1	5	0	0	0	0	4	9	87	3
11005-2	295	90	2	8	0	0	0	0	0	4	96	3
11005-2	320	92	0	8	0	0	0	0	2	8	90	3
11007-1	surface	16	22	7	0	0	55	0	2	18	79	3
11007-2	20	0	27	0	42	1	30	0	91	7	2	1
11007-2	60	0	34	0	34	0	31	1	87	11	3	1
11007-2	100	2	40	2	37	0	18	1	2	94	5	2
11007-2	140	15	33	6	35	1	10	0	7	49	44	0
11007-2	200	6	43	2	33	1	15	0	11	78	11	2
11007-2	240	17	38	5	30	0	7	2	3	82	14	2
11007-2	280	26	33	8	17	3	10	3	23	43	34	0
11007-2	300	34	26	14	19	1	7	0	4	29	66	3
11007-2	320	48	31	11	4	0	5	0	0	1	99	3
11008-1	surface	89	1	9	0	0	1	0	1	4	95	3
11008-2	20	84	4	12	0	0	0	0	1	7	92	3
11008-2	120	87	1	11	0	0	1	0	5	11	84	3
11008-2	160	83	7	10	0	0	0	0	1	7	91	3
11008-2	240	87	2	10	0	0	0	0	1	7	92	3
11008-2	320	69	6	23	0	0	2	0	0	4	96	3
11009-1	surface	73	3	23	0	0	2	0	2	8	90	3
11009-2	40	82	2	15	0	0	0	1	4	14	82	3

Core No. (GeoB)	Depth in core (cm)	Component distribution (%)							Cluster membership (%)			Assigned cluster
		Glauconv	Carb. fragm.	Quartz	Mica	Plant ibres	Biog. carb.	Others	Cluster 1 (mF)	Cluster 2 (sF_{mixed})	Cluster 3 (sF_{glauc})	
11009-2	60	84	2	13	0	0	0	0	1	7	91	3
11009-2	140	78	5	16	0	0	1	0	0	5	95	3
11010-1	surface	6	27	6	4	11	45	1	69	15	16	1
11010-2	0	7	30	22	26	0	14	0	0	91	8	2
11010-2	60	11	20	6	1	4	52	6	47	23	30	0
11010-2	140	14	21	8	2	3	52	1	21	25	54	3
11010-2	158	18	37	36	8	0	1	0	1	33	66	3
11010-2	180	16	24	8	1	3	47	0	18	22	60	3
11010-2	200	16	39	33	9	0	4	0	2	29	69	3
11010-2	280	16	34	35	10	0	5	0	0	61	39	0
11010-2	340	9	12	48	29	0	2	0	2	60	39	0
11011-1	surface	20	54	25	0	0	1	0	1	10	89	3
11011-2	120	3	37	13	36	0	10	0	4	72	24	2
11011-2	200	12	45	20	18	0	6	0	1	57	41	0
11011-2	260	1	18	3	72	0	6	1	8	89	3	2
11011-2	300	3	40	12	40	0	5	0	0	98	2	2
11011-2	360	1	34	15	47	0	4	0	2	88	10	2
11011-2	400	0	23	4	67	0	5	0	17	75	8	2
11011-2	480	0	26	20	51	1	3	0	17	76	6	2
11012-1	surface	1	28	0	6	11	53	1	99	1	0	1
11012-1	0	0	33	5	18	0	42	1	18	76	6	2
11012-2	20	2	28	1	2	3	63	2	84	9	6	1
11012-2	100	1	33	1	3	2	60	1	87	8	5	1
11012-2	120	2	27	5	52	0	13	1	1	96	3	2
11012-2	140	10	42	13	27	0	8	0	2	66	32	2
11012-2	180	9	45	20	18	1	6	0	3	75	23	2
11012-2	260	16	27	22	33	0	2	0	2	58	41	0
11012-2	400	13	16	25	44	0	2	0	2	62	36	2
11013-1	surface	60	14	9	1	0	16	0	1	8	91	3
11013-2	20	59	25	13	1	0	2	0	0	6	94	3
11013-2	40	58	27	8	1	0	5	0	1	8	92	3
11013-2	60	30	32	9	14	0	16	0	2	41	58	0
11013-2	80	27	36	7	11	0	20	0	2	40	58	0
11013-2	123	10	8	3	77	0	1	0	3	80	17	2
11013-2	163	6	6	3	85	0	1	0	3	74	23	2
11013-2	204	15	14	9	61	0	1	0	1	80	19	2
11013-2	224	26	26	9	35	1	2	0	7	54	39	0
11013-2	264	15	25	9	49	0	2	0	1	84	15	2
11013-2	324	26	26	16	30	0	1	0	1	71	28	2
11013-2	364	36	24	16	23	0	0	1	6	50	44	0
11013-2	423	15	11	9	64	0	2	0	2	64	34	2
11014-1	surface	5	39	2	7	1	45	1	35	44	20	0
11014-2	0	1	31	1	11	0	55	0	7	79	14	2
11014-2	60	6	64	9	3	0	17	0	1	71	28	2
11014-2	120	6	35	3	3	0	52	0	12	47	41	0
11014-2	180	2	58	6	11	0	22	0	1	93	6	2
11014-2	220	4	51	3	11	0	30	0	11	73	16	2
11014-2	300	1	1	1	96	1	0	1	37	43	21	0
11014-2	440	0	2	0	95	2	1	0	92	6	2	1
11015-2	surface	6	56	7	8	0	22	1	1	84	15	2
11015-2	40	5	15	3	5	1	70	1	31	44	25	0
11015-2	60	5	16	4	2	1	72	2	37	32	31	0
11015-2	100	4	18	3	1	1	71	2	40	31	29	0
11015-2	140	12	61	7	3	0	17	0	2	38	60	0
11015-2	180	31	35	7	21	0	6	1	1	69	30	2
11015-2	220	34	27	8	27	0	2	1	3	60	37	0
11015-2	260	34	31	8	25	0	1	0	2	50	48	0

Core No. (GeoB)	Depth in core (cm)	Component distribution (%)							Cluster membership (%)			Assigned cluster
		Glauconу	Carb. fragm.	Quartz	Mica	Plant ibres	Biog. carb.	Others	Cluster 1 (mF)	Cluster 2 (sF_{mixed})	Cluster 3 (sF_{glauc})	
11015-2	280	64	6	25	3	0	1	0	1	10	89	3
11015-2	300	63	11	16	10	0	0	0	4	34	62	3
11015-2	340	2	12	5	78	0	2	1	2	93	5	2
11015-2	380	14	7	11	63	1	3	1	11	65	25	2
11015-2	420	37	31	12	10	0	7	1	1	36	63	3
11015-2	439	4	1	0	73	20	0	1	75	15	10	1
11015-2	479	4	3	2	78	12	1	0	71	19	10	1
11016-1	surface	4	30	3	3	0	59	0	11	42	47	0
11016-2	0	2	4	1	86	0	7	0	4	88	8	2
11016-2	80	12	16	5	62	0	4	0	1	89	10	2
11016-2	160	22	16	6	53	0	3	0	1	81	17	2
11016-2	200	21	21	13	43	0	2	0	1	78	21	2
11016-2	240	33	23	12	30	0	1	0	1	64	35	2
11016-2	280	39	18	9	33	1	0	1	6	47	47	0
11016-2	320	60	11	27	0	0	1	0	4	11	85	3
11016-2	360	18	16	9	56	0	1	0	2	60	38	0
11016-2	380	20	12	5	62	0	1	0	2	76	23	2
11016-2	437	10	12	4	70	0	3	1	2	87	11	2
11017-1	surface	11	27	9	3	0	47	3	4	59	37	0
11017-2	60	11	18	35	32	0	3	1	1	89	10	2
11017-2	140	16	21	50	12	0	1	1	1	66	33	2
11017-2	160	8	19	50	19	0	4	1	1	87	13	2
11017-2	242	6	26	42	13	1	7	5	5	77	18	2
11017-2	282	7	35	45	1	0	8	5	3	52	45	0
11017-2	342	11	40	34	6	0	9	0	1	66	33	2
11017-2	402	5	43	29	6	0	11	5	2	78	20	2
11017-2	441	0	5	1	53	36	1	3	93	5	2	1
11017-2	481	0	1	0	95	4	0	0	73	19	8	1
11018-1	surface	23	18	41	2	1	15	0	3	15	81	3
11018-2	0	7	16	52	23	0	1	0	2	80	19	2
11018-2	80	13	20	49	16	0	1	0	1	68	31	2
11018-2	140	7	17	43	30	0	1	1	1	84	15	2
11018-2	180	3	9	27	59	0	2	0	1	93	6	2
11018-2	280	7	22	44	25	0	1	0	2	64	35	2
11018-2	395	5	16	46	32	0	2	0	1	89	10	2
11019-1	surface	62	3	34	0	0	1	0	0	4	95	3
11019-2	20	48	9	41	0	0	3	0	1	5	94	3
11019-2	60	13	24	32	28	0	2	1	1	81	18	2
11019-2	200	24	20	43	9	0	4	0	1	42	57	0
11019-2	360	25	20	49	3	0	2	1	1	15	85	3
11019-2	420	57	3	17	21	0	0	1	6	40	55	0
11019-2	460	48	2	12	31	2	1	4	17	39	43	0
11019-2	480	62	2	32	3	1	0	0	9	29	61	3
11019-2	490	67	6	25	1	0	0	1	1	15	84	3
11020-1	surface	58	3	38	0	0	1	0	2	9	90	3
11020-2	0	53	10	32	1	0	4	0	0	4	95	3
11020-2	58	79	4	15	0	0	1	0	1	7	93	3
11020-2	140	22	14	9	53	0	2	0	1	79	20	2
11020-2	200	77	8	15	0	0	0	0	4	22	74	3
11020-2	240	72	8	19	0	0	0	0	2	11	87	3
11020-2	320	66	10	23	0	0	0	0	1	6	93	3
11020-2	360	75	7	17	0	0	0	0	0	4	95	3
11022-1	surface	55	11	6	5	0	23	0	2	23	75	3
11025-1	surface	3	16	7	6	0	68	0	10	48	42	0
11025-2	40	1	23	3	3	0	69	0	16	49	34	0
11025-2	120	5	22	6	8	0	58	0	10	63	27	2
11025-2	180	25	29	12	34	0	0	0	2	51	47	0

Core No. (GeoB)	Depth in core (cm)	Component distribution (%)							Cluster membership (%)			Assigned cluster
		Glauconу	Carb. fragm.	Quartz	Mica	Plant ibres	Biog. carb.	Others	Cluster 1 (mF)	Cluster 2 (sF_{mixed})	Cluster 3 (sF_{glauc})	
11025-2	240	19	26	9	45	0	0	0	4	63	33	2
11025-2	340	40	39	13	7	0	1	0	1	26	73	3
11025-2	370	7	11	3	78	0	1	0	2	86	12	2
11025-2	460	9	8	4	76	0	2	0	5	81	14	2
11027-1	surface	18	56	5	0	1	21	0	10	17	72	3
11027-2	0	10	37	2	41	5	5	0	46	35	19	0
11027-2	40 B	2	22	1	68	2	2	3	74	21	5	1
11027-2	60	4	82	3	8	0	4	0	2	72	26	2
11027-2	140	8	61	3	22	0	5	0	5	81	13	2
11027-2	240	9	83	4	0	0	3	0	3	20	77	3
11027-2	340	15	70	2	6	0	7	0	2	66	32	2
11027-2	440	37	44	2	13	0	4	0	2	41	57	0
11028-1	surface	2	6	1	4	53	34	0	72	14	15	1
11028-2	20-22	5	13	0	2	29	46	4	92	4	4	1
11028-2	120	7	21	1	0	16	53	1	67	13	20	1
11028-2	180	66	19	1	6	0	7	0	2	35	63	3
11028-2	199	34	28	5	19	0	15	0	4	34	61	3
11028-2	220	87	9	1	2	0	1	0	1	13	86	3
11028-2	300	46	29	3	12	0	9	0	2	34	64	3
11028-2	400	73	12	1	8	0	5	0	2	26	72	3
11029-1	surface	0	4	0	21	47	28	0	89	7	4	1
11029-2	0	0	2	0	7	62	23	7	94	4	2	1
11029-2	100	0	3	0	5	64	23	5	94	4	2	1
11029-2	200	0	1	0	0	15	19	64	87	8	5	1
11029-2	240	1	5	1	13	45	22	13	98	1	1	1
11029-2	300	0	2	0	1	88	7	2	95	3	2	1
11029-2	320	1	8	4	9	45	30	4	98	1	1	1
11029-2	341	2	10	6	11	28	40	3	96	2	1	1
11029-2	400	3	18	11	2	7	54	6	69	17	14	1
11029-2	460	49	10	12	26	0	3	1	1	56	43	0
11029-2	475	23	17	3	50	0	8	0	2	72	25	2
11030-1	surface	0	7	1	44	20	26	2	97	2	1	1
11030-2	40	0	12	0	31	41	13	2	95	4	2	1
11030-2	80	0	20	1	19	31	24	6	100	0	0	1
11030-2	100	1	5	0	25	54	6	9	98	1	1	1
11030-2	160	0	14	0	27	36	20	2	100	0	0	1
11030-2	198	1	15	0	29	34	18	3	100	0	0	1
11030-2	260	0	12	9	76	0	1	1	43	49	8	0
11030-2	436	0	14	11	73	0	1	0	36	56	8	0
11031-1	surface	18	23	6	1	0	52	0	2	26	72	3
11031-2	20	13	17	2	0	0	67	1	6	35	59	3
11031-2	80	31	14	3	41	0	11	0	6	44	50	0
11031-2	120	25	11	2	54	0	7	0	3	57	39	0
11031-2	180	6	29	0	47	0	18	0	25	51	23	2
11032-1	surface	1	23	2	1	0	73	1	12	62	27	2
11036-1	surface	2	83	1	1	0	13	0	4	47	49	0
11036-2	80	1	94	2	2	0	2	0	2	75	23	2
11036-2	160	1	88	1	8	0	2	0	2	86	12	2
11036-2	300	1	94	1	2	0	2	0	2	71	27	2
11037-1	surface	1	33	28	24	5	8	1	57	35	8	0
11038-1	surface	0	27	7	16	2	47	0	82	14	4	1
11038-2	20	0	34	19	13	5	27	2	80	15	5	1
11038-2	120	0	47	20	10	4	18	1	76	18	5	1
11038-2	160	1	45	44	4	0	4	2	2	87	11	2
11038-2	320	0	25	62	10	0	1	1	14	73	13	2
11038-2	460	0	34	43	22	0	1	1	13	76	11	2
11039-1	surface	0	13	0	5	46	34	1	95	3	2	1

Core No. (GeoB)	Depth in core (cm)	Component distribution (%)							Cluster membership (%)			Assigned cluster
		Glauconv	Carb. fragm.	Quartz	Mica	Plant ibres	Biog. carb.	Others	Cluster 1 (mF)	Cluster 2 (sF_{mixed})	Cluster 3 (sF_{glauc})	
11039-3	20	0	1	0	1	45	0	53	73	16	11	1
11039-3	60	0	7	0	13	67	4	8	94	4	2	1
11039-3	80	0	17	0	39	28	13	2	97	2	1	1
11039-3	100	0	53	0	3	9	33	2	94	4	2	1
11039-3	140	1	14	0	6	44	34	2	95	3	2	1
11039-3	160	1	19	0	2	74	2	2	91	5	4	1
11039-3	180	1	8	0	25	49	9	8	94	4	2	1
11039-3	200	0	13	0	80	1	5	1	89	9	2	1
11039-3	208	0	58	2	1	15	24	0	94	4	2	1
11040-1	surface	0	65	4	2	0	28	1	7	79	13	2
11040-2	0	0	53	3	33	0	11	0	21	71	8	2
11040-2	60	0	54	6	32	0	7	1	4	92	5	2
11040-2	120	0	54	4	35	0	6	0	17	75	8	2
11040-2	200	1	57	7	27	0	7	1	1	97	2	2
11040-2	300	0	61	6	27	0	5	1	18	73	9	2
11040-2	340	0	54	6	35	0	4	1	18	73	9	2
11040-2	381	0	19	3	74	1	2	2	79	17	4	1
11040-2	420	0	25	1	63	7	2	1	92	6	2	1
11040-2	480	0	7	0	91	0	1	1	76	20	4	1
11041-1	surface	0	23	2	27	10	36	1	100	0	0	1
11041-2	20	0	30	1	14	14	39	1	100	0	0	1
11041-2	100	0	28	8	7	7	48	2	94	5	2	1
11041-2	140	0	25	37	33	0	4	1	15	74	11	2
11041-2	200	0	33	31	28	0	4	3	18	70	11	2
11041-2	300	0	32	38	20	0	3	6	24	67	9	2
11041-2	420	1	34	40	20	0	0	5	6	78	16	2
11042-1	surface	0	14	8	23	18	36	1	97	2	1	1
11042-2	20	0	42	35	11	3	9	0	29	48	23	0
11042-2	80	1	20	15	58	0	2	4	13	80	7	2
11042-2	140	0	23	17	57	0	2	1	17	74	9	2
11042-2	200	0	49	36	12	0	0	2	18	63	19	2
11042-2	320	1	57	30	12	0	1	0	2	78	20	2
11042-2	380	0	53	34	12	0	1	0	11	78	11	2
11042-2	440	1	48	31	17	0	1	2	2	91	6	2
11043-1	surface	0	17	1	26	13	43	0	95	3	1	1
11043-2	4	0	26	58	6	4	6	0	47	37	16	0
11043-2	60	0	18	24	15	22	19	1	90	7	3	1
11043-2	320	0	17	21	59	1	1	1	55	37	8	0
11043-2	420	0	4	11	80	0	0	4	41	44	15	0
11044-1	surface	3	69	3	0	0	24	0	11	31	58	3
11045-1	surface	0	48	5	3	0	43	0	7	82	11	2
11046-1	surface	1	46	3	3	0	47	0	5	81	14	2
13039-5	surface	11	6	2	16	43	18	4	90	5	5	1
13041-1	surface	0	22	0	42	1	28	8	87	11	3	1
13041-2	50	0	42	0	13	16	28	1	95	3	2	1
13041-2	250	6	40	16	15	4	17	3	35	47	18	0
13043-1	surface	0	1	0	26	53	19	0	86	8	6	1
13045-1	surface	80	1	18	0	0	0	0	1	11	88	3
13046-1	surface	2	22	0	4	18	52	1	89	6	5	1
13046-2	40	1	29	0	4	8	58	0	96	2	1	1
13046-2	135	4	33	1	6	6	47	4	93	4	3	1
13046-2	210	3	45	3	2	0	46	1	5	67	28	2
13047-1	surface	0	24	1	1	34	35	4	97	2	1	1
13047-2	136	6	19	51	2	1	11	10	17	40	42	0
13047-2	300	0	17	73	9	0	1	0	3	81	17	2
13048-1	surface	32	21	24	2	1	21	0	1	7	91	3
13048-2	100	24	6	58	11	0	0	0	2	33	66	3

Core No. (GeoB)	Depth in core (cm)	Component distribution (%)							Cluster membership (%)			Assigned cluster
		Glauconу	Carb. fragm.	Quartz	Mica	Plant ibres	Biog. carb.	Others	Cluster 1 (mF)	Cluster 2 (sF_{mixed})	Cluster 3 (sF_{glauc})	
13048-2	300	15	7	36	42	0	1	0	2	70	28	2
13049-1	surface	84	5	4	0	0	7	0	4	10	86	3
13049-2	50	79	14	3	1	0	3	0	1	9	91	3
13050-1	surface	58	18	4	1	0	19	0	1	12	86	3
13050-2	50	45	20	3	1	0	29	1	5	17	78	3
13050-2	130	5	14	1	79	0	2	0	3	79	18	2
13051-1	surface	15	30	27	0	0	27	0	2	23	76	3
13051-2	40	14	27	38	1	1	16	3	5	29	66	3
13051-2	150	4	29	53	11	0	3	0	1	65	34	2
13051-2	278	10	32	53	3	0	2	0	1	30	69	3
13051-2	350	1	7	8	84	0	1	0	2	88	10	2
13052-1	surface	1	73	2	1	0	23	0	23	50	27	2
13052-2	200	1	53	4	26	0	16	0	1	95	3	2
13052-2	447	0	56	7	23	0	13	1	19	72	9	2
13088-1	surface	31	17	5	3	2	41	1	13	23	64	3
13088-2	30	57	26	8	1	0	8	0	1	10	90	3
13088-2	70	16	13	8	1	0	45	17	16	37	47	0
13088-2	120	29	36	5	3	0	26	0	1	35	64	3
13088-2	220	28	3	53	14	2	0	1	10	36	54	0
13089-1	surface	1	26	3	21	2	46	0	69	24	7	1
13089-2	98	0	63	13	5	0	18	1	18	70	12	2
13089-2	300	0	55	6	11	0	27	0	18	75	7	2
13089-2	489	0	58	14	9	0	18	1	24	69	8	2
130205-1	surface	23	5	69	0	0	3	0	0	7	93	3
130205-2	37	1	1	2	57	37	1	0	83	11	6	1
130205-2	269	13	17	22	33	9	5	0	26	41	33	0
130205-2	495	24	10	15	45	1	5	0	5	55	40	0
130207-2	surface	2	43	5	8	0	42	0	2	87	11	2
130207-3	62	0	16	0	71	6	1	6	92	6	2	1
130207-3	100	2	60	5	32	0	1	0	7	71	22	2
130207-3	200	7	62	2	29	0	0	0	3	70	28	2
130207-3	350	0	5	1	90	5	0	0	73	20	7	1
130207-3	430	2	96	1	1	0	1	0	2	54	43	0
130212-1	surface	1	34	22	9	13	21	1	79	15	6	1
130212-2	50	0	50	4	44	0	2	1	18	74	8	2
130212-2	300	7	51	2	40	0	0	0	7	63	30	2
130213-1	surface	0	6	88	2	0	4	0	3	76	22	2
130213-2	70	0	14	84	1	0	0	0	3	70	27	2
130213-2	300	0	22	72	5	0	1	0	9	75	16	2
130213-2	442	0	15	76	8	0	0	0	11	75	14	2
130216-1	surface	1	38	42	0	0	19	0	3	40	56	0
130216-2	50	0	59	35	0	0	6	0	15	66	19	2
130216-2	320	0	65	13	22	0	0	0	26	59	14	2
130216-2	450	0	7	0	87	0	4	0	80	17	3	1

Acknowledgements

First of all, I am very thankful to Till Hanebuth for his great support. Thank you for the fruitful discussions, for all the advice, for handling together the sensitive "Rüttelsusi" during three cruises, and for a new view on round edges. Thank you for the nice time!

I also wish to thank Rüdiger Henrich for the great opportunity to conduct this PhD study and for evaluating this thesis. Moreover, I am very thankful to Sebastian Krastel for the evaluation of this PhD study, and for providing the Boomer data.

Well, "many hands make light work" – There are many other people who contributed to this project and made this study possible. Muchas gracias Ángel "langsam hiefen" Mena Rodríguez for pulling the cable almost alone and retrieving 54 vibrocores, and, not to forget, for introducing me to the world of "Pimientos de Padrón" and "Orejas de cerdo"! I also wish to thank all other members of the GALIOMAR cruises as well as Captain Michael Schneider and his complete crew on RV Poseidon for making these cruises such an outstanding success. I really enjoyed the participation! Also, I am thankful to Tilo von Dobeneck for providing the chance to join the second cruise to the NW Iberian shelf. Guillermo Francés Pedraz is acknowledged for the nice cooperation and I would like to thank Francesco L. Chiocci, Francisco J. Lobo, and Domenico Ridente for the helpful comments. Moreover, I wish to thank Vera Bender for her help with the Boomer interpretation. Hannes Riepshoff is thanked for having a deep look into the gravel deposits of the NW Iberian shelf. Of course, thanks go to all members of the working group sedimentology/palaeoceanography, especially to Brit Kockisch and Helga Heilmann for the comprehensive help as well as to our student assistants Johanna, Wiebke, and Aline for their support. Dave Heslop and Christoph Vogt are acknowledged for their helpful and friendly support with cluster analysis and XRD measurements, respectively. Furthermore, I am very thankful to John Reijmer, Sven Roth, and Lars Reuning for introducing me to the world of science during my Diploma thesis. This study is an outcome of the MARUM project "Sediment partitioning and transformation on shelves". The work was funded through DFG-Research Center / Cluster of Excellence "The Ocean in the Earth System".

A lot of thanks, but there are still some really important left. "Nothing shocks me. I'm a scientist" (Harrison Ford) – Thank you Jean for being such a nice officemate and for the deep scientific discussions in the Lila Eule. Thanx James for being a native speaker…just kiddin'! Above all, thank you for sharing a nice time in Bremen but thank you as well for zee help wiz my english. By the way, many thanks go to the guys from www.leo.org and www.quickdic.de. Thank you Claudia, GM, Julien, Cyril, and Tobias for the nice time, and for surviving together the "Vegetarian Wednesdays".

Außerdem möchte ich mich bei allen Freunden bedanken, besonders bei Thomas und Ulf für die lange Freundschaft…kann man sich für sowas bedanken? Egal, schön dass es Euch gibt! Danke auch an meine lieben Mitbewohner – über die Zeit kamen so einige zusammen die mir ans Herz gewachsen sind…deswegen in alphabetischer Reihenfolge: Annika, Aron, Carlos, Flo, Hermen, Irene, Jan, Jule, Karen, Lasse, Laura und Sandra. Danke für die schöne Zeit! Danke auch an alle anderen Turbinen für die schönen Abende. Außerdem gehen auch noch ganz liebe Grüße nach Kiel, vor allem an Anna und Jenny.

So, die vielleicht wichtigsten Danksagungen kommen ganz zum Schluss: Ich möchte mich ganz besonders bei meiner Familie bedanken. Schwierig zu formulieren – "Danke für Alles!" trifft es am Besten. Es hat mir nie an etwas gefehlt. Und…wenn DOH auf EOH trifft, dann werden Wünsche war. Ganz besonderen Dank an meine kleine Freundin Geli für die Freude in schönen Zeiten und die Unterstützung in schweren Zeiten. "I love NY" und "Recreation Basketball" sind ein verdammt gutes Team! Ich freue mich auf die Zukunft!

Name: Hendrik Lantzsch Datum: 29. September 2009

Anschrift : Kornstr. 221
28201 Bremen

E r k l ä r u n g

Hiermit versichere ich, dass ich

1. die Arbeit ohne unerlaubte fremde Hilfe angefertigt habe,

2. keine anderen als die von mir angegebenen Quellen und Hilfsmittel benutzt habe und

3. die den benutzten Werken wörtlich oder inhaltlich entnommenen Stellen als solche kenntlich gemacht habe.

_____, den .....

(Unterschrift)